AALBORG UNIVERSITY
DENMARK
STUDENT REPORT

Impact Assessment of Integrating Thermostatic Loads and Plug-in Electric Vehicles in Future Low Voltage Distribution Grids

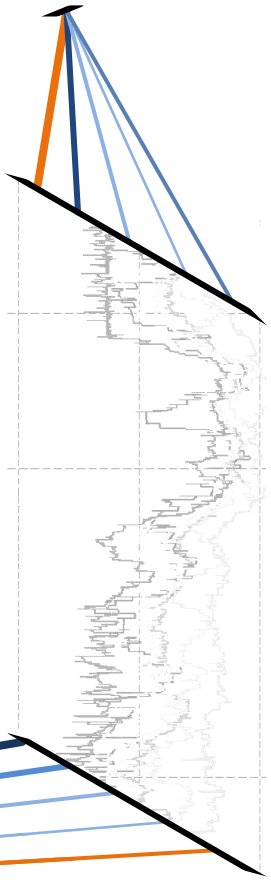

Master's Thesis

Peter Thais Bjerregaard
Ireneusz Grzegorz Szczesny

Group EPSH4-1030, Spring 2013
Board of Studies of Energy
Aalborg university

Supervisors
Iker Diaz de Zerio Mendaza
Jayakrishnan Radhakrishna Pillai

AALBORG UNIVERSITY
DENMARK
STUDENT REPORT

Title:	Impact Assessment of Integrating Thermostatic Loads and Plug-in Electric Vehicles in Future Low Voltage Distribution Grids
Semester:	3rd - 4th
Project period:	1/9-2012 – 30/5-2013
ECTS:	50
Supervisor:	Iker Diaz de Zerio Mendaza Jayakrishnan Radhakrishna Pillai
Project group:	EPSH4-1030

Ireneusz Grzegorz Szczesny

Peter Thais Bjerregaard

SYNOPSIS:

The Danish power system is expected to undergo a technically challenging evolution in the coming years and decades, caused by an increase of the wind power penetration. As the production of power will become less controllable due to weather conditions, the end consumers will need to evolve into active elements of the power system. The transformation is often referred to as demand side management. Electric vehicles and heat pumps are expected to offer a great deal of flexible consumption in the future. This master's thesis investigates the influence of implementing the units in two different LV grids in a 2025 scenario. Models of the units have been implemented in DIgSILENT PowerFactory DSL. A multi-layer control strategy has been applied, which enables the units to improve the voltage levels of weak grids and enables the future aggregators to provide balancing services to the TSO.

Copies:	3
Last page:	130
Last appendix:	C

By signing this document, each member of the group confirms that all participated in the project work and thereby all members are collectively liable for the content of the report.

Preface

This report has been written by the project group *EPSH4-1030* during the 3rd and 4th semester at Aalborg University - Board of Studies of Energy. The report is aimed at students of and stakeholders in the future smart grid. The scope of the report would be of particular interest to the distribution companies, aggregators/service-providers as well as in general, people with electro-technical backgrounds, interested in the future smart grids grids.

This report uses SI base units, derived units and prefixes as described by The International System of Units together with units outside of the SI standard. All units are written as [unit].
Sources are inserted following the Vancouver method, with a [number], which refers to the bibliography in the back of the report. Citations are written in "*italic*" followed by their source.
Appendixes are declared with an A in front of the page number and can be found in the back of the report.

Frequently used constants and abbreviations are described in the reports nomenclature, which can be found in appendix B on page A27. Additionally, a CD has been created, which features the report, sources and all programming in digital format.

Table of contents

1 Introduction

The Danish electric energy sector is planning for a technically challenging evolution of the way the power system works as a result of political short- as well as long term goals and ambitions. This chapter presents the introduction and background for this specific project, which includes the political reasoning behind the Danish energy agreements, the future smart grids as well as demand side management. The scope of objectives in the project covers load flow studies, the development of a centralized control strategy and an investigation of the flexibility capability of the units when controlled in groups. Following the objectives, the methodology employed in the project work will be introduced.

A brief introduction to the content of each chapter in the report is to be found in the outline.

1.1 Background

Danish political and socio-economic policies have focussed on a "green" direction in the Danish energy system for decades. This common direction has through the years produced increasingly ambitious energy agreements. In February 2011, the 'Energy Strategy 2050' was made public. This agreement formulates the overall objectives and tasks involved in making Denmark independent of fossil fuels by 2050 [1]. The latest agreement, 'Accelerating Green Energy Towards 2020' was presented on March 2012 and formulates the tasks which need to be accomplished in the years 2012-2020 [2]. The goal of transforming a whole country to become completely independent of fossil fuels is the first of its kind. One of the reasons behind Denmark's direction to become independent of coal, oil and gas is that the majority of these natural resources are concentrated in less and increasingly unstable countries and regions around the world [1]. Therefore, in the future Danish energy system, energy is to a higher degree supplied mostly by renewable energy sources. Furthermore, the greater part of the renewable energy will be supplied by wind turbines.

One of the major milestones in Energy Strategy 2050 is the reduction in the consumption of fossil fuels by 33% in the years 2009-2020 [1]. To reach this goal some coal-fired CHP (Combined Heat and Power) plants will be reconfigured to run on biofuel and the wind power penetration will be increased. In 2020, it is planned to supply 50% of the demand for electrical energy by wind turbines. Currently three new large contributions to wind power production are planned [2]:

- A new offshore wind farm, Horns Reef 3, of 400MW
- A new offshore wind farm, Krieger's Flak, is expected to include 600MW of wind turbine production
- New close-to-shore production will be implemented, adding 500MW
- Land based wind turbine production is planned to increase by 500MW

Since the reliability of the production in the future relies to a further degree on weather conditions there will be times, in order to balance the power system, where it is necessary to import/export power to a higher degree than known today. The import of power during low wind – high consumption conditions as well as export during high wind - low consumption periods will therefore play a greater part as the conversion from a fossil fuel based energy system towards a RE-based system proceeds. Thefore, it will be necessary to develop new- and improve the existing interconnections.

The Danish distribution grids are designed to meet the peak power demand [3]. The end-consumer as known today uses power when needed which is completely independent of when wind power is available. In the afternoon when many people get off work and arrive at their respectable households, the consumption peaks. Likewise, during the night the consumption is at its lowest. In the current power system, this is managed by increasing production or import (depending on the price of power) to match production to consumption. In the future Danish power system, the weather will be the dominant factor in deciding whether power is available or not. Hence, to a further degree, the mismatch between production and consumption will at times be higher than what is managed and overcome today. As the wind power penetration will be >50% in the future, at times it might not be possible to balance the power system by increasing-/decreasing the production by the conventional generators in Denmark. There simply will not be sufficient capacity left, as the amount of power produced by conventional generators will decrease, along with the increase in the wind power penetration. Power balancing will therefore be an increasingly challenging task. The issue could be solved in the "traditional" manner, by utilizing the full capacity of the conventional generators (which are controllable) combined with increased import/export, but would not be a proper socio-economic solution in a system with a very high wind power penetration [4]. A better solution would be to match the consumption to the production, at least to some degree. In order to do so, the end-consumers will need to be included, as an active element, in the planning of the power system. The transformation of the today passive end-consumer, into a flexible consumer in the future, is often referred to as demand side management.

The smart grids will form the link in-between the fluctuating production and flexible consumption [5]. The role of Energinet.dk, the Danish TSO, will in the future be a lot like it is today, which means that Energinet.dk will handle the import, export and overall balance of energy in the Danish electricity system as well as operating the transmission grid. The DSOs will as today handle the operation of the distribution grids as well as set the rules for how new service partners (or aggregators) will operate and interact in the LV-grids. The service partners are fairly new operators in the power system and will form a link in-between the DSOs, market and flexible consumer. The end-consumers will through contracts let the aggregators control their flexible units.

The flexible units of highest priority, when seen from a grid perspective, are the electric vehicles and the heat pumps as they will have the biggest capability of flexible consumption in terms of the shear amount of energy which can be shifted through time. In order to make a large-scale implementation of these units successful, the following items are amongst many others, of interest:

- How will the implementation of the units affect the current LV-grids and how to reduce the need for reinforcements?
- Can the aggregators control the units in order support the grids?
- How will a large-scale implementation of the units affect grid limits (voltage levels, cable loading etc.)?

This project will be driven by these questions in order to investigate the behaviour of two current LV-grids in a future with a large penetration of electric vehicles and heat pumps.

1.2 Objectives

The objectives of the project are linked to the background presented in the previous section.

The project is divided into three distinct parts.

Load flow studies
The first part of the project investigates the two grids, LV-I and LV-II, in terms of bottlenecks as well as weak- and strong points in steady state. The investigations employ static models of the heat pump and electric vehicle.

- Implementation of the two distribution grids in DIgSILENT PowerFactory
- Implementation of time dependent loads to assess grid behaviour at different times of day
- An identification of key weak points in each of the grids
- A study of various scenarios looking into the effects of implementing a large amount of EVs and HPs

Dynamic control
The second part of the project investigates the influence of a high penetration of electric vehicles and heat pumps in the time domain. The unit behaviour will be assessed through 24-hour studies. This part of the project involves the task of developing an "intelligent" centralized control-strategy for the charging of EVs and running of HPs. The control-strategy will be focused on maximizing grid utilization based on the results gained within the first part of the project.

- Design of mathematical models suitable to investigate the effects of the control of the units
- Design of the control solution for the units based upon the results gained in the first part of the project
- An assessment of the performance of the applied control through case studies

Flexibility control
The third part of the project involves adding extra functionality to the control applied in part 2. This functionality covers an extra layer of control which will enable the units to interact with the TSO, through the aggregator, by providing balancing power.

- Design of a control solution, which respects the control applied in part 2, able to act on a request of balancing power
- An assessment of the performance of the applied control through case studies

1.2.1 Limitations

This section contains an overview of limitations and assumptions made in the project work

- During the project work all loads has been considered as being 3-phase, balanced
- Short term transient behaviour has been neglected
- 24 hour simulations are assumed to be long enough to be able to reflect the general behaviour of units and control
- Losses has been not been considered unless elsewise stated
- August 11th 2012 has been randomly chosen to be a representative of a typical summer week-end day
- January 22nd 2013 has been randomly chosen to be a representative of a typical winter week day
- All communication and data-paths used by units/models/control has been assumed to be without any limitations or delays
- The one type of EV and one type of HP are assumed to be representatives of the future units
- LV-I is assumed to represent a strong LV grid
- LV-II is assumed to represent a weak LV grid
- The cost of implementing the control design with signalling paths and equipment has not been considered
- It has not been investigated if the control design will affect the security of supply in the LV grids
- The units and control have been implemented without duplicity/redundancies.
- Behaviour under hardware/software breakdowns have not been considered

Further limitations/assumptions are presented where found relevant.

1.3 Methodology

During the project work various software tools have been employed to perform calculations and studies.

The primary tool used to perform mathematical studies has been MATLAB. MATLAB has been utilized to prepare most of the input data for the modelling performed in DIgSILENT PowerFactory. Most graphs presented throughout the report have been prepared using MATLAB.

DIgSILENT PowerFactory has been the primary tool utilized throughout the project work and has served as a multi-purpose instrument. During the first part of the project work PowerFactory has been employed to perform load-flow analyses using the Newton-Raphson method. DIgSILENT includes the DSL-module which has been used to implement models of the heat pump, electric vehicle and control-algorithms. In order to assess the working of the models through time, the RMS-simulation has been used. This process is depicted in Fig. 1.1.

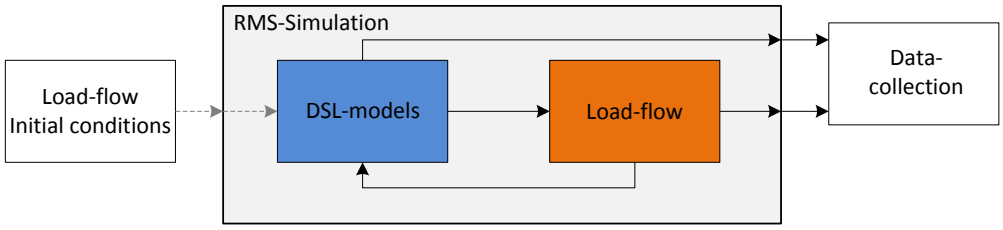

Figure 1.1: RMS-simulation

The RMS-simulation is a tool combining load-flow calculations and user defined models. The user defined models are most commonly connected to a grid in one way or another. For instance, a model could be controlling the power-demand of a specific load to meet some criteria set up in a DSL-model. To run the model some knowledge about the grid status is needed, the DSL-model controlling the power of the load might “need to know” the voltage level at the node where the load is connected in order to compute the power-demand. As such, any RMS-simulation starts out with performing a single load-flow analysis which forms the initial-conditions for the DSL-models. Hence, as the initial conditions are computed, the actual simulation can start. The RMS-simulation runs with a step time defined by the user to suit the specific needs of a study. The DSL-models create results which are used in the load-flow studies which then create results used in the DSL-models. As data for each simulation loop is saved, the behaviour and impact of a user defined model in a grid can be studied through time. Most case-studies in the project have been run for 24-hours investigating various scenarios.

Yet another feature of DIgSILENT PowerFactory has been employed during the project work, namely the possibility to implement ‘variations’. As an example, the ‘variations’ makes possible to change the load of every household in a grid from summer- to winter-consumption, with a single click of a button. An array of different variations has been implemented in DIgSILENT PowerFactory which is reflected in the case studies.

1.4 Outline

This section will briefly sum up the content of the various sections of the report.

Chapter 1 – Introduction
The introduction contains information to the background of doing the project. The political agreements presented in the last few years, the smart grid philosophy and the expectancy of a large penetration of electric vehicles and heat pumps in the near future forms the basis for doing the project. The objectives of the project are then presented along with limitations. Following the objectives, the methodology used in the project work is introduced.

Chapter 2 – State of Art
The state of art contains an extended introduction to the project work. It presents the relevance of doing the project. The Danish power system as it is today along with the wind power perspective is introduced. The consequences of combining the current capacity of the LV-grids with an increased wind power penetration will be presented. This discussion leads to why smart grids are thought of as being a package of solutions which could assist in managing the Danish energy puzzle in the coming years and decades. The smart grid will be presented along with demand side management which leads to the topic of flexible loads. The last part of the state of art will contain an introduction to flexible loads in general followed up by specifics about the heat pump and electric vehicle.

Chapter 3 – Case study description
The case study description presents various structures within distribution grid design in general. The two grids which have been used throughout this project will then be presented along with topologies, characteristics and load profiles. The input data used in the heat pump modelling and electric vehicle modelling and then be presented. The data consists of thermal demands and driving patterns.

Chapter 4 – Steady state analysis
The steady state analysis includes the assumptions made regarding the steady state implementation of the electric vehicles and heat pumps. The various seasonal dependencies and assumptions will be introduced. In order to investigate the effect of implementing the static units, methods and algorithms have been developed which assists in assuming where units will be connected in the grid. Following the introduction of the assumptions made, the results of the steady state analysis will be presented. Within the results will show the bottlenecks and limitations in the grids, simple reinforcements as well as the theoretical limit for the penetration of electric vehicles and heat pumps.

Chapter 5 - Dynamic control
This chapter presents the dynamic modelling performed in the project. First an overview and introduction to the modelling and control deign is presented. The modelling has been divided into heat pump plants, electric vehicle plants, sub-system controllers as well as the top level grid control. The sections within the chapter are closely tied to the structure of the models and control. The last part of the chapter contains the results obtained performing various case studies. The case study section is concluded by a short discussion of the results obtained.

Chapter 6 - Flexibility control
The flexibility control adds an extra layer of functionality to the dynamic control. The chapter begins with an introduction and overview of the flexibility control. Following the introduction, the modelling of the flexibility control for the heat pumps and electric vehicles is presented. The control design is verified through various case studies. The results obtained through performing the case studies will be summed up in the last section of the chapter.

Chapter 7 - Conclusions
This chapter contains the conclusions of the project as whole.

Chapter 8 - Future work
This chapter contains a presentation of the direction the project would be headed if more time would have been available.

2 State of Art

This chapter covers the technical background needed for carrying out the project, including an introduction to the smart grid concept, demand side management as well as flexible loads.

2.1 The Danish Power System

This section will give a brief introduction to the Danish power system as it is today. The power system is divided into two levels more or less based on voltage, namely the transmission system (>132kV) and the distribution system (<132kV).

2.1.1 The Transmission System

The transmission system is owned and operated by Energinet.dk, the Danish TSO. The purposes of Energinet.dk are as follows [6]:

- To ensure the security of supply in the overall Danish electric system
- To operate and develop the infrastructure needed to operate the electric system
- To develop unbiased and objective market conditions on the various energy markets and to monitor that the purposes of the market conditions meet the right objectives
- To plan the electric network in the long term to ensure proper levels of transmission system capacity and security of supply
- To propose and support research projects relevant to the development of strategies and technologies capable of assisting environmentally friendly production of electric energy

The Danish transmission system consists mainly of 400-, 150- and 132kV infrastructure with various voltage levels in-between which are suitable for specific tasks. The Danish transmission system differs from many others since it contains two regions which are not synchronously connected. The system east of the island of Funen (EDK) is a part of the Nordic energy system synchronously connected to countries like Sweden and Norway. The system west of Zealand (WDK) is synchronously connected primarily to Germany. Just recently an HVDC-connection has been implemented connecting the island of Funen to Zealand, (WDK to EDK).Fig. 2.1 shows the Danish transmission system ultimo 2012.
Interconnections are an important part of the Danish power system. It allows for import, export and transporting energy between our neighbors. WDK is synchronously connected to Germany and connected to both Sweden and Norway through HVDC. EDK is synchronously connected to Sweden and connected to WDK and Germany through HVDC. The transmission system therefore makes possible to balance the overall power system through import and export as well as increasing the competitive performance of actors in the energy markets which is socio-economically beneficial.

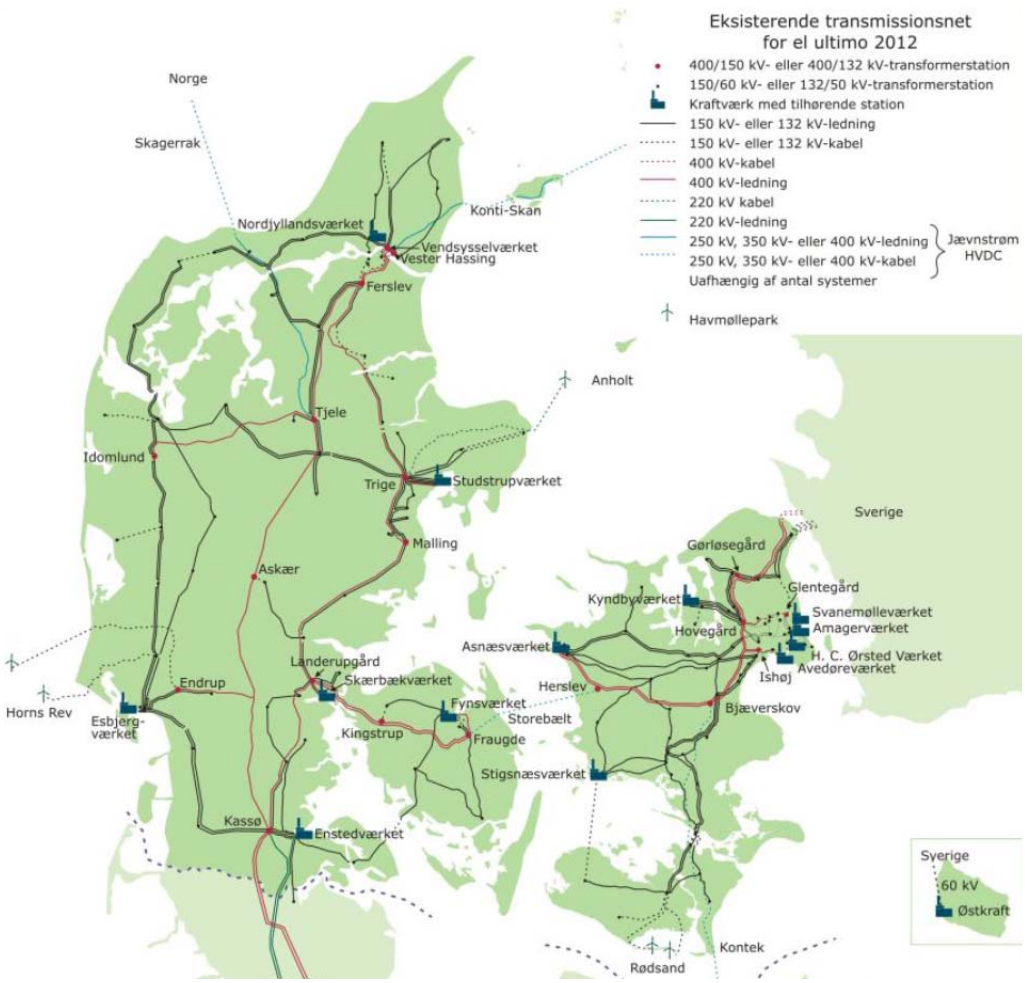

Figure 2.1: The Danish transmission system ultimo 2012 [7]

2.1.2 The Distribution System

The end-consumers of power are connected to the transmission system and producers of energy through the distribution system. The distribution system is owned and operated by the distribution system operators. These companies are monopolies in the transport of energy [8]. Both the TSO and the DSOs are bound to act within the borders of the law for supply of electricity. Within the law the purposes of the DSOs are to ensure the electric distribution system is developed and enhanced in order to meet the demands for the security of supply, socio-economics, the environment and the protection of the consumer.

The DSOs are responsible for measuring the consumption of energy at the end-consumers. They do not pay the DSO directly. The DSOs pass on the consumption-data to the traders of energy, commonly referred to as retailers, which handle the actual billing of energy consumption.

The greater volume of infrastructure in the Danish distribution network consist of voltage levels 20 kV, 10 kV and 0.4 kV. The distribution network is connected to the transmission system most commonly via a 60 kV / 50 kV connections in-between or a little less frequent directly at the 150 kV or 132 kV levels [3].

The development and planning of the distribution system is of particular interest in this project.

Until recently the DSOs have utilized much similar strategies in order to develop optimal business plans based on various load scenarios. Since improvements of existing- or development of new in electric infrastructure impose large investments, the horizon for planning and development is most commonly long. According to [3] DONG Energy internal guidelines recommend that the horizon for planning new grids should be 20 years and upgrading existing grids should be around 10 years. The long planning horizon is due to the lifetime of the infrastructure. The lifetime of an arbitrary section of a distribution system is expected to be around 40 years. The DSOs will therefore need to make good estimations of the expected consumption in the future.

Many distribution networks have been planned according to worst case scenarios which ensure that a distribution network is at all times able to transport and supply the demand for power. The distribution system therefore is dimensioned to being able to carry the maximum load.

Until recently most distribution companies did not do continuous measurements in the LV-grids [3]. Most DSOs measured the flow of power at the 10 kV radials at main transformer sites. The estimation of consumption habits has therefore been based on yearly energy sales as well as measurements at the main transformer busbars. By use of a mathematical correlation-method, specific consumption profiles for single consumers can be estimated. When the loads have been estimated it is possible to run load flow studies which help determine cable sizes. Common practice suggests that the cables should be loaded to no more than 70% of the nominal capacity under no-fault scenarios. Under n-1 scenarios the cables are allowed to be loaded by 100% of nominal capacity [8].

The voltage limits must be in compliance with relevant grid codes. For the distribution system the grid code EN 50160 is highly relevant. This standard states that the voltage levels always must be within ±10% for 95% of the time [9].

2.2 Wind Power in Denmark

As mentioned in section 1.1, Denmark has planned to increase the already large wind power penetration in the coming years and decades. Denmark started implementing wind turbines into the power system around 1990. Fig. 2.2 shows the wind power penetration from 1970 to 2011 [10].

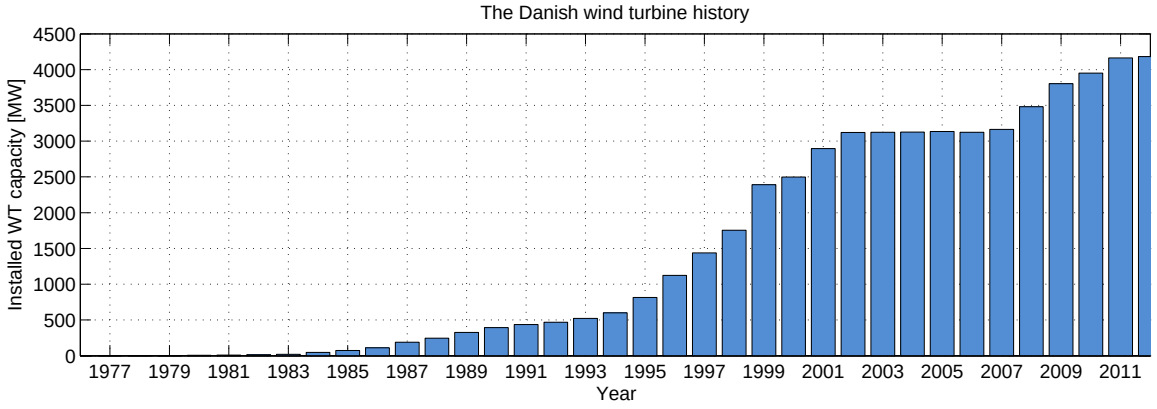

Figure 2.2: The Danish wind turbine history

The Danish venture in wind turbines is the main reason for carrying out this project. Without the goal of becoming independent of fossil fuels and implementing wind turbines as replacements the perspectives in the Danish power system would look a lot different. The main driving force behind

demand side management is simply put, the conversions from production-facilities which are controllable to production facilities which are somewhat uncontrollable due to the weather-reliability of wind turbines.

The most recent political agreement [7] has finalized the plan to add 1.45GW wind turbine production capacity to the Danish power system. The new wind farms are all planned to be generating before 2020.
The offshore wind farm, Kriegers Flak, is planned to contain 600 MW of wind turbine production.
The area, Horns Reef, contains at present time two offshore wind farms of roughly 200 MW each. It is planned to add another wind farm, the so-called Horns Reef 3. Horns Reef 3 is planned incorporate 400 MW of wind turbine capacity.
In addition to the planned enhancement in terms of the two major contributions to wind power, it is also planned to build 500 MW of near-shore wind turbines before 2020. According to [7] these are to be placed at eight different locations.
Besides the three before mentioned contributions, some land wind turbines and will be decommissioned and new will replace them, in total adding up to the abovementioned 1.45 GW which when fully implemented will supply roughly 50% of the total power demand [7].
Present day, Anholt offshore wind farm, of 400 MW installed capacity is just about finished and is planned to go into full production during 2013.
Since wind turbines are inherently uncontrollable, the large wind power penetration will give rise to situations where the wind turbine production capacity will exceed the demand for power.
Such a scenario is presented in Fig. 2.3. The figure shows en example of how production and demand could behave in the 2nd quarter of 2025.

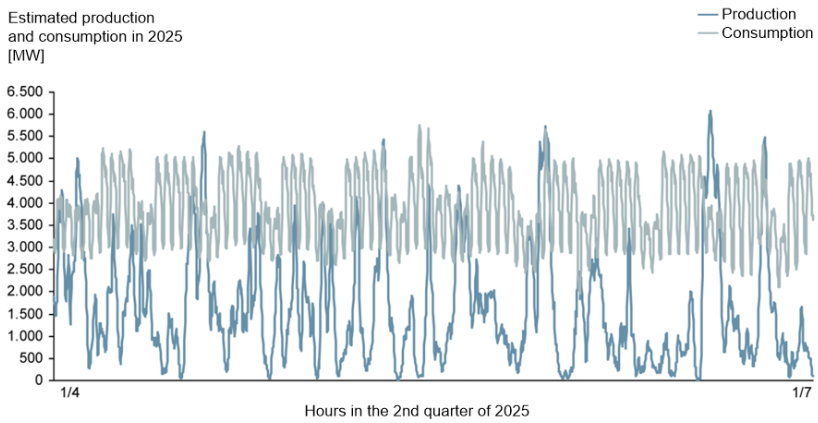

Figure 2.3: Example – Danish Production and consumption in 2025 [11]

Fig. 2.3 shows periods where the wind power production capacity exceeds the power demand. In such scenarios there are various solutions. In order not to supply more than demanded, thereby raising the system frequency, the wind turbine production can be reduced. If the occurrence of this scenario would happen frequently it would severely limit the socio-economic perspective of implementing the wind turbines to the degree planned. Most likely though, a surplus of power would be sold on the energy markets and exported. The possible means of reducing the amount of periods with an overflow of production are presented in section 2.5 and 2.6.

2.3 The Energy Markets

The energy markets tie together the consumers and producers with the retailers as middlemen. The primary energy market of the Nordic countries is the Nord Pool market. The Nord Pool market can be divided into two sections, namely the Spot (day-ahead) market and the Elbas (intra-day) market. Yet another service of interest to this project is regulating power, which is a direct exchange of services between retailers/producers and their respective TSO. In order to understand the need for multiple markets, it is needed to look into when it is possible to interact with the respectable markets. Fig. 2.4 depicts the time of which it is possible to trade on the Nord Pool markets and directly with the TSO.

It is possible to trade on the Elspot market until 12-24 hours before the power is delivered.

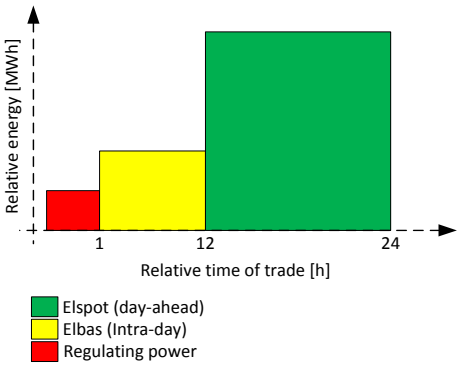

Figure 2.4: Time of interaction with the various energy markets

Any changes in demand or production occurring in-between the time where the trade on Elspot has taken place and time of delivery, will need to be balanced out on the intra-day market. Trades on the Elbas market close one hour before time of delivery and are made in order to support the Elspot trades to assist power system balance. The last layer of trading happens directly between the TSO and producer/retailer within the hour of consumption.

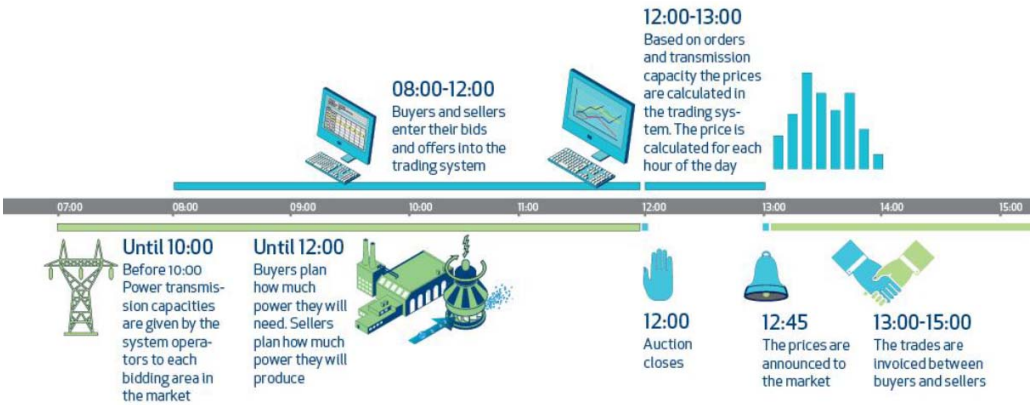

Figure 2.5: Daily rutine on the Elspot market [12]

Nord Pool is the primary market for energy in the northern part of Europe. 77% of the Nordic power consumption is traded on the Nord Pool Elspot market [12]. Fig. 2.5 represents the daily routine on the Elspot market.

The spot market contains three central elements. The energy demand traded by aggregators, the available energy traded by producers and the available capacity in the transmissions systems (and interconnections) which is announced by the respective TSOs. The actual prices are calculated separately for each hour of the coming day. Fig. 2.6 shows how the prices are calculated.

The producers decide how much power they are able and willing to sell at which price. At Fig. 2.6 this is represented as the orange curve. Less power is available in the low end of the price scale and more in the high end of the scale as would be expected. The blue curve represents the power demand. The aggregators (or retailers) announce the power demand and which price they are willing to pay for some amount of energy. The aggregators are of course most interested in buying the greater amount of power at the lowest cost. The intersection of two lines represents the Elspot price for a specific hour. The price of power also depends on the area where to the power is to be delivered, which is why the TSOs need to announce the free capacity for each hour. If the there is a large free capacity in a specific area of the transmission system the price for transmitting the power would be relatively low. Similarly, if power is to be transmitted through heavily loaded parts of the transmission system, the price would be higher.

Figure 2.6: Elspot price calculation

When the Elspot market closes, the day before consumption, retailers and producers have made specific deals for the trade of power in terms of amount of power and time of delivery. Between the time where the Elspot auction closes and the day of consumption, changes in the power demand or production capacity could occur. For instance a block at a power plant could be shut down due to unforeseen issues or a wind farm could produce more than expected due to better wind conditions than forecasted. This is where the Elbas market supports the Elspot market. The Elbas or intra-day market allows for trading of energy to match production to consumption within the day of operation. At the Elbas market, actors can trade energy up to one hour before the power is consumed. The combination of the Elspot and Elbas markets therefore is able to match production to consumption very closely; however, trades on the Elbas market will therefore always be lagging the hour of consumption by one hour.

Imbalances within the hour of consumption therefore need to be dealt with in a different manner. The TSO has made arrangements with various actors in the power system to help ensure the power system balance. Hence, these actors have the responsibility to make power for up- or down regulation available to the TSO when needed. The TSO is therefore able to pay large actors to reduce consumption, reduce production or increase production depending of the status of the power system. Figure 2.7 shows the time range of regulating power agreed upon by the European TSOs through ENTSO-E (European Network of Transmission System Operators for Electricity).

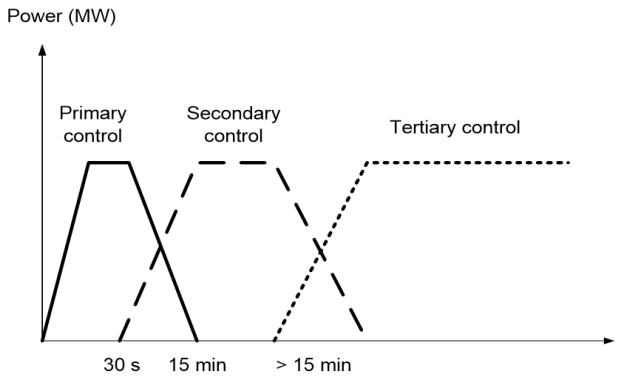

Figure 2.7: Regulating power

The primary control is commonly referred to as frequency control. The ENTSO-E guidelines/agreements state that the frequency control should be activated if the frequency deviates from the pre-set 50Hz by more than ±20mHz. The frequency control should be fully operational within 30 seconds of a deviation greater than 20mHz. The need for regulating power is rather limited in terms of the amount of power needed.

The secondary control (or Load Frequency Control) is utilized to support and relieve the primary control. The secondary control reserves must be active no later than30 seconds after a deviation has occurred and the deviation in frequency must be within the limits no sooner than 15 minutes [13] after the regulation has begun.

The tertiary control covers the activation of manual reserves which are activated if the system unbalance is not restored for the hour of consumption.

The regulating power is an interesting topic when looking into flexible consumption and demand side management. The flexible units covered in this project, namely the EV and HP, are both capable of interacting with the balancing-market and assisting when in need for regulating power. The EVs will be able to directly and actively assist with both up- and down regulation of power, by consuming power or delivering power back to the grid (V2G). The HPs will also be able to assist, but in a more passive role than the EVs. The HPs will be able to stop consumption for some amount of time when there is a power deficiency as well as consuming when there is a surplus of energy in the grids.

Wind turbine production usually represents a low price in the markets since wind power production is supported by taxes paid for by the end-consumers. As a fictitious example to illustrate the system, assume the following:

- The cost for producing 1 MWh by use of a traditional generator is 1€
- The cost for producing 1 MWh by use of a wind turbine is 2€
- The owner of the wind turbine receives a tax-support of 1.2€ per produced MWh

These simple statements reveal two interesting details. With the focus on green energy in Denmark, it has become less lucrative to produce power by conventional methods since the competitive position of the traditional generators has been artificially decreased. On the other hand it has become more lucrative to produce energy by green alternatives such as wind turbines due to the tax-support. The

second detail concerns the price of power on the energy markets. As wind turbine power is supported by taxes it will be put for sale at artificially low prices at the Nordpool markets. This means that a high wind power penetration will be reflected as a lower price of energy.
The actual tax paid by the end-consumers in Denmark is the so-called PSO-tariff. The collected PSO-money is used by Energinet.dk to promote RE-technologies on behalf of the government.

2.4 Consequences

When adding up the statements in the previous two sections it seems to be clear that the need for environmentally friendly energy brings forth challenges in the planning of the future energy system. Based on the current political plans for the future power system Energinet.dk has presented how the energy system could look like in 2030. Much could happen, but the overall tendency will be that the transmission system will be enhanced to support more import/export as well as a greater wind power penetration. An estimation of the setup of the power system in 2030 can be seen in Fig. 2.8.

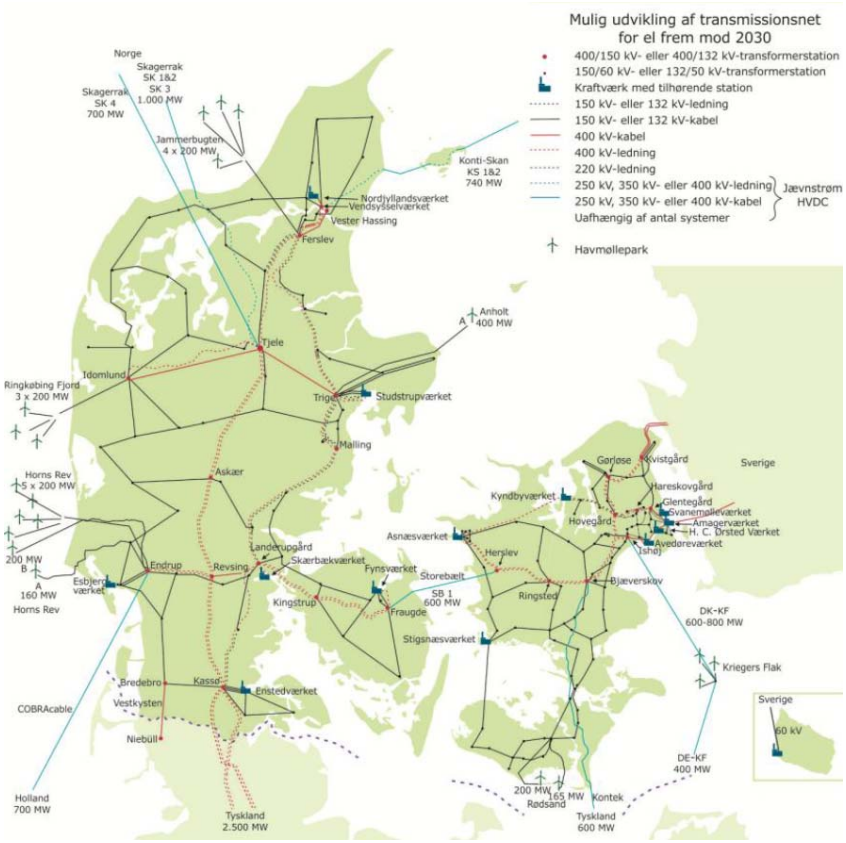

Figure 2.8: Possible setup of the Danish electric energy system i 2030

An investment in strong interconnections plays a vital role in the socio-economic perspective of having a WT-dominated base of production. The strong interconnections will enhance the security of supply as well as improve the possibility of being able to act in a smart manner on the energy markets. Energinet.dk estimates that additional 2.000 MW of capacity will need to be added by 2020 [7].

The energy agreement Accelerating Green Energy Towards 2020, from March 2012 imposes the so-called “wholesale-model”. This model employ changes to the law for supply of electricity which makes the electricity-traders (or aggregators) become the only traders of energy in the retail market.

As mentioned previously the DSOs have monopolies within their branch. This means that the competitiveness in the market could possibly be degraded. As such the new wholesale-model prohibits the direct interaction between DSO and costumer [7]. The aggregators will in the future become a completely necessary layer in the power system. The aggregators will in the future offer a full package of products covering electricity-, network-, and system services. Thereby, to promote competitiveness, the aggregators will be billing the end-consumers and the DSOs will be billing the aggregators.

To handle the great amount of fluctuating production the end-consumers will need to be able to interact in a flexible manner with the aggregators. The end-consumers are expected to invest in heat pumps, electric vehicles and other electric units capable of flexible consumption in the coming years. It is estimated that by 2025 one of four consumers will own an electric vehicle and one of two consumers not living in an area supplied with district heating will use a heat pump for hot water and/or heating demands [4]. As such the future distribution system will carry a much higher amount of energy when compared with today. If the flexible loads are controlled in an poor manner, their consumption could add to the peak which happen in the hours 17-20. Such a scenario is shown in Fig. 2.9. Without any control the following could happen. When the end-consumers get off work, they come home and start charging their EVs the moment they arrive at their house. Without any control the heat pumps could in the worst case be running at the same time.

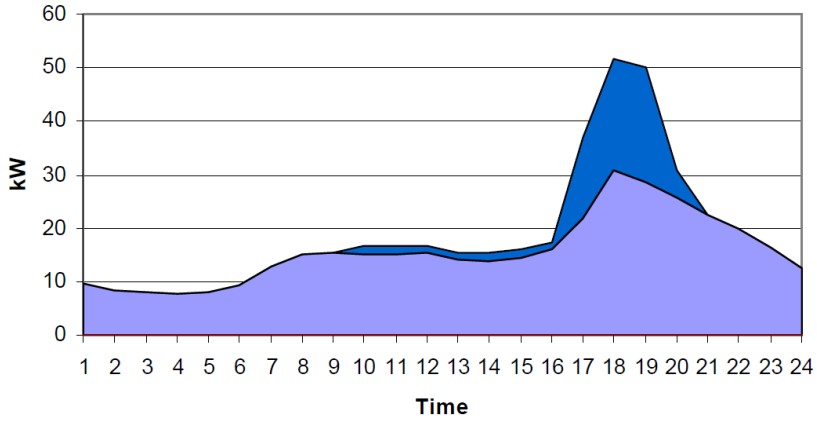

Figure 2.9: Poor control of the flexible units [8]

The ambition is to be able to reach a scenario which resembles the scenario shown at Fig. 2.10. This shows that the consumption is shifted to periods with lesser consumption. For instance most EVs would be charged during the night along with the heat pumps consumption. Appliances like dishwashers and washing machines could run in off-peak periods as well.
Peak-shaving is only one of many goals one could set-up for the control of the flexible units. Peak shaving is all about reducing the need for grid reinforcements by flattening the consumption profile. Peak-shaving therefore maximizes grid utilization.
Yet another control-approach could be to maximize the consumption when there is a high wind power production. In this scenario Fig. 2.9 could actually show a good control-approach if a high wind power production occur in the hours between 17:00 and 20:00. This scenario is commonly referred to as load following.
The chosen control approach therefore defines the success-criteria for demand side management.
Even if some perfect control-approach were to be implemented, the addition of more electrical loads will increase the overall loading of the electric system including the MV and LV parts. This means that the DSOs will need to upgrade existing networks based on smart consumption at least to some degree. This makes the traditional approach to load estimation much less useful. Fig. 2.11 shows the

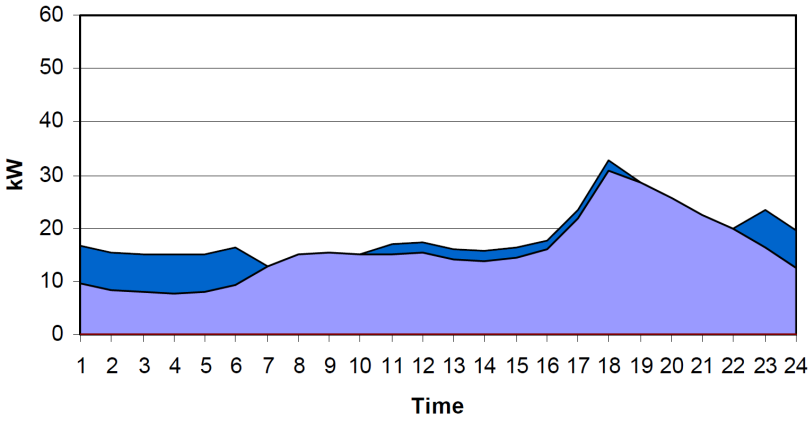

Figure 2.10: Smart control of the flexible units [8]

results of an estimation of cable loading in 2025 [11]. The study shows the loading of 148 0.4kV cable sections with a loading scenario from 2010 and compares it to a load estimation for 2025 without any grid reinforcements.

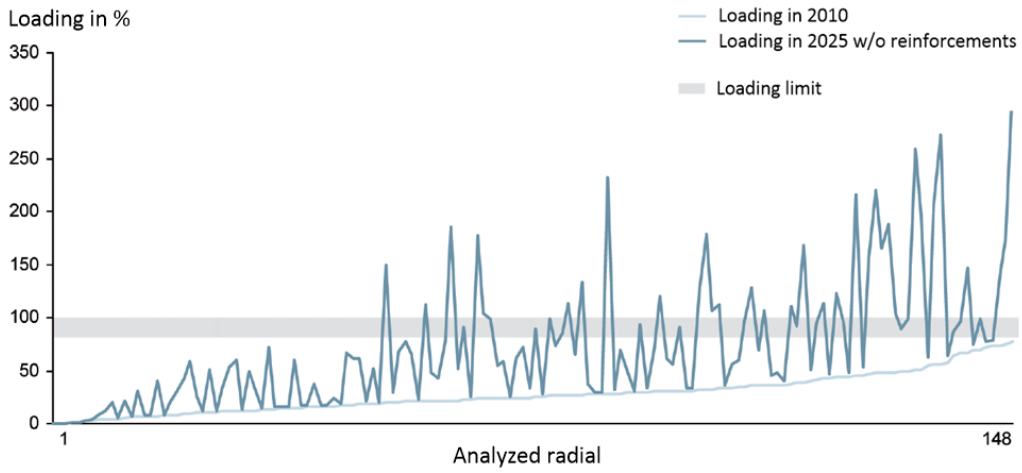

Figure 2.11: Analysis of the loading of 148 0.4 kV radials [11]

It is very clear that the cable sections need heavy reinforcement in the coming years to cope with the additional load introduced by the flexible loads.

2.5 Smart Grids

The previous section has covered some of the challenges which will show in the future Danish energy system. A proposed solution to cope with some of these challenges is so-called smart grids. The smart-grid concept contains various elements which when combined, will contain a package which could support the conversion from a fossil-fuel based electricity system to a renewable energy based system. Fig. 2.12 shows a representation of the smart concept [11].
The figure presents the Danish power system of the future. Research projects and experiments have been in the works for years and laws and legislation are being implemented in order to implement the system step by step. The smart grids will establish the framework to be able to offer services designed to stabilize the electric system. It will reduce the need for grid reinforcements by making flexible consumption a possibility. It will assist in the usage of energy when offered cheap. It will lower the

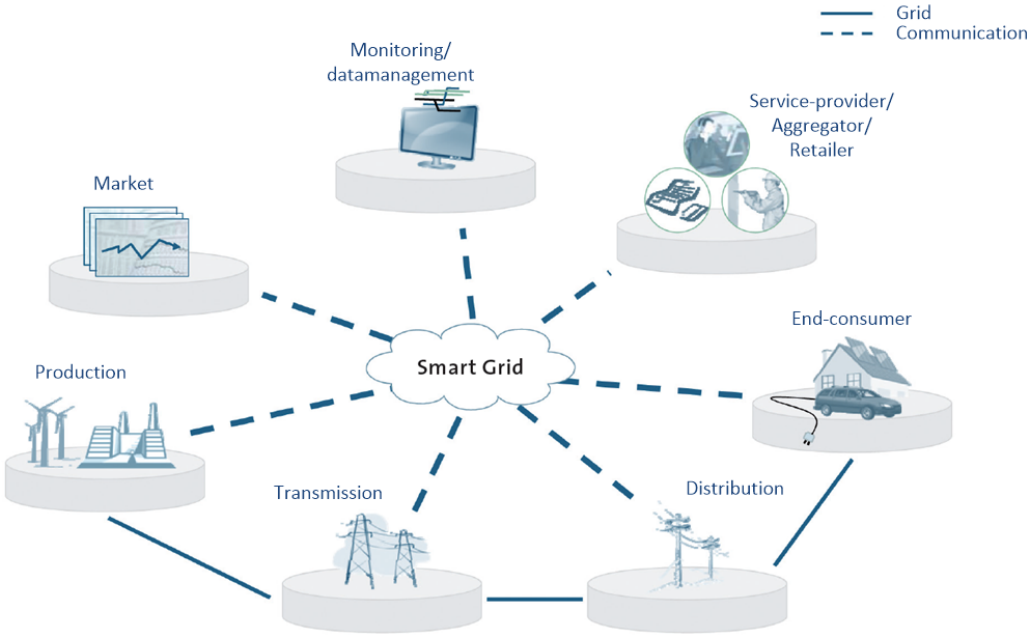

Figure 2.12: The smart grid concept [11]

relative consumption of energy by increasing the consumption of electric energy in an intelligent manner. The system is designed to bring forth socio-economic benefits as well as bring savings to the end consumer.

The energy produced in the future will as previously mentioned be of a more fluctuating character as to what is known today. Apart from the production within the country itself the development in the various energy markets and the generally larger interconnections between countries means that it will be useful for the Denmark as well as for the Danish end-consumer to consume when the price of electric energy is low. The smart grids will in reality not differentiate between cheap energy produced at hydro power plants in Norway or Sweden and the energy produced on a windy day from wind turbines in Denmark. The driving force of the flow of energy will be the price.

The transmission system will as mentioned before, much as today, transport the greater amount of power the greater distances. The difference is that the energy in the future to a greater degree will flow across borders to be supplied to consumers within the country. As consumers pay for using the electric infrastructure transporting energy from producer to consumer enhancing the interconnections between countries bring forth socio-economic benefits in long term.

The distribution systems will need reinforcements in the future in order to be able to handle the great amount of electric consumption brought forth by the large scale conversion of fossil-fuel fired product to products running on electricity. The amount of reinforcements needed rely on success of demand side management [14].

Most people neither know nor care where the energy comes from, as long as it is present at the end of the power cord, connecting their TV to the power outlet in the wall. The reason for this is first of all that the security of supply in Denmark is very high making power availability a trivial concern to the end-consumer. Secondly the consumer has no interest in thinking of when to consume, since no matter how he/she acts and when he/she consumes power makes no difference when the electricity

bills are due. In the future the same costumer might have an electric vehicle charging in the garage, a heat pump providing hot water and uses his/her appliances late night. This consumer will be happy on windy days and behave differently under different market conditions since his/her behaviour will be reflected when the bills are due.

The role of the DSOs will be reduced in the future. Until recently it was common practice that a distribution company would be the owner, operator as well as the unity billing end-consumers for the services provided. In the future DSOs will be companies which have licenses with the government to own and run the distribution networks. The trade of energy between end-consumer and DSO will be handled with a fairly new layer in-between as electric traders or aggregators. Based upon legislation, need for flexibility and general market terms the aggregators will offer services to the end-consumers and ensure competitiveness on the market, securing the end-consumers. Fig. 2.13 shows how the roles and responsibilities will be divided in the smart grid.

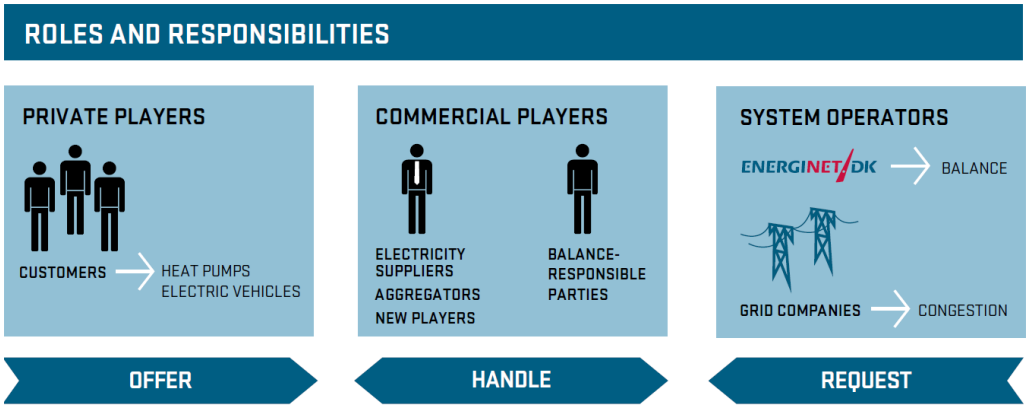

Figure 2.13: Roles and responsibilities [5]

In order for the smart grid concept to be successful intelligent control of all loads capable of acting flexible will be necessary. In order to be able to react and adapt the control to various scenarios measuring equipment will need to be rolled out on a large scale. For instance a radial in a LV-grid could be overloading. The control could in such a scenario reduce the charging power of some electric vehicles in the problem area or shut down some heat pumps provided that there is a surplus of energy in the heat pump system. During fault scenarios the electric vehicles would be able to assist in stabilizing the grid for a limited amount of time. In these cases it is vital to know the amount of electric vehicles connected to the grid.

The driving force of the whole system will be the energy markets. The energy traders will buy and sell energy through various energy markets. The price of energy will be heavily influenced by weather conditions. The end-consumers will react to the prices set via the aggregators which, through competitiveness with other aggregators, will offer fair prices for energy supplied to the end consumers. The behaviour of the end-consumer will therefore in the end be adapted to the overall power system conditions. In the service agreements between aggregator and end-consumer clauses will make sure that the DSOs can utilize some flexibility under rare operating conditions. In cases with voltage dips the DSOs could for instance interfere through the aggregators by artificially increasing the price or taking more or less direct control of units.

Fig. 2.14 shows a more detailed view of what at the moment is thought of as being the future smart grid. Part one shows the link between Nord Pool, the TSO, DSOs, aggregators and other market rele-

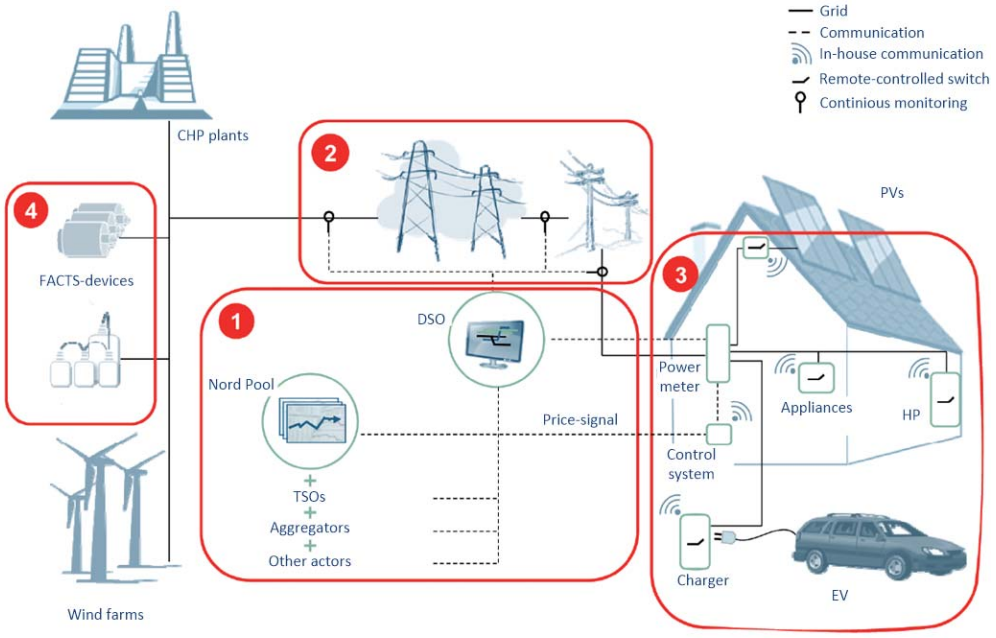

Figure 2.14: Smart grid in detail [11]

vant entities. The TSO and DSOs especially will be the market actors in need of flexibility in order to limit the need for grid reinforcements and balancing the grids. The Nord Pool market will as today be the primary market in the Nordic region. The prices of energy at the Nord Pool markets and the need for flexibility will form the prices seen at the end-consumers.

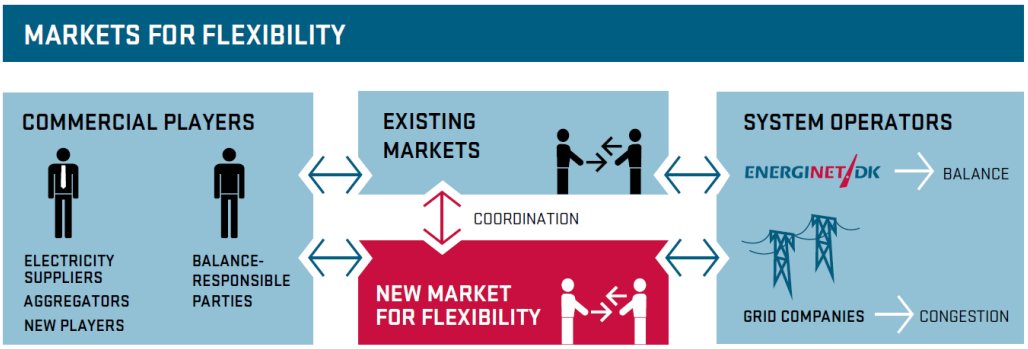

Figure 2.15: New market for flexibility [5]

In the future energy system a new market will appear where commercial players will be able to offer flexibility as a commodity. The interactions between actors on the market are shown in Fig. 2.15 [5]. The Smart Grid 2.0 report gives an example of how the aggregators in the future could behave. For instance a costumer has invested in a heat pump. He makes a deal with an aggregator to take control of the consumer's heat pump. For instance the consumer the consumer agrees to conditions that ensure between 20-22°C during the day and between 16-18°C at night. The heat pump without the control from the aggregator would consume energy for 6.000 DKK per year. The aggregator would control the heat pump within the comfort limits for 5.500 DKK. Since the aggregator now has access to the flexibility of the heat pump, these services would be sold on the new market for flexibility gaining some earnings by doing so.

Part two at Fig. 2.14 represents the need for real-time measurements in the distribution grids in order not to violate grid constrains. It full it infrastructure needs to be implemented capable of handling this huge amount of data from different sources. The point of having the measurements is also to help the consumers act flexible in order to meet the consumers' demands without them loosing comfort.

Part three represents the changes on the household level. Every household containing units capable of flexible loading will need to have smart-meters which can read and send data back and forth between aggregators (the price-signals), record the consumption as well as the status of various appliances and units. The measurement and communication systems are of importance first of all to unit control, the same control which will in the end assist consumer comfort and generate savings for the end-consumer while assisting the grid. This part also contains the concept of demand side management..

Part four represents the new equipment needed to ensure system stability. In some cases the produced wind power would be so high that the CHP plants would shut down since the possible gains from producing would be too low. In these cases the short circuit levels in the grid would be heavily reduced leaving the grid very vulnerable to power quality issues or in worst cases black-outs. In order to maintain system stability in these cases it planned to compensate for the low short circuit capacity by adding new units to the grid. The plan for what needs to be implemented is not ready yet, but for now it is planned to add synchronous condensers to inertia and short circuit power and FACTS-devices to improve voltage levels by reactive power compensation [11].

2.6 Demand Side Management

Demand side management is a popular term covering the control of flexibility at the end-consumers. In this project only households, not larger consumers, are of interest which will be reflected in this section.

As covered in previous sections the wind power penetration is increasing steadily, but Denmark is not the only country implementing wind power. An increase in wind power penetration seems to be a trend in all of Northern Europe. This fact influences the power system in Denmark, since a high wind power production in Denmark will usually also mean a high wind power production in the neighbouring countries. As such, the interconnections will not necessarily assist in selling more energy when a surplus production exists. Demand side management is going to be a part of the solution to this issue. DSM will support a high socio-economic efficiency from the wind turbine production.

Energinet.dk emphasizes heat pumps and electrical vehicles when looking for flexible loading in the future demand side management [4]. Energinet.dk published the report "Effective use of electric energy from wind turbines in Denmark[1]" in March 2009. The calculations made in this report use estimated values for the number of heat pumps and electric vehicles implemented in 2025. The same values will be used as a reference in this project and are as follows [4]:

- It is estimated that 25% of the transportation needs by car is covered by electric vehicles
- It is estimated that 50% of the heating demands in regions outside the district heating sector is covered by heat pumps

[1] Title translated to English. Original title: "Effektiv anvendelse of vindkraft baseret el i Danmark"

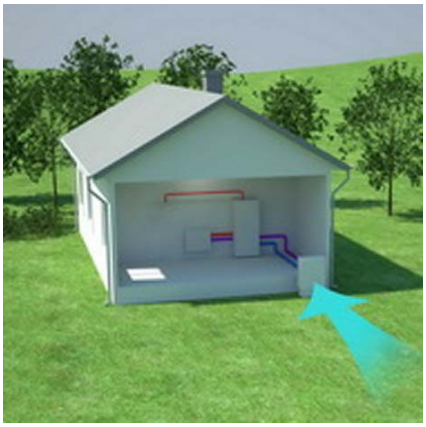

Figure 2.16: Air-source heat pump [15]

Figure 2.17: Ground-source heat pump [15]

2.6.1 Heat Pumps

Heat pumps are interesting to the future electric system for various reasons. First of all they are energy efficient, some types more than others. They remove the need for the consumption of fossil fuels for individual heating demands by running on electricity. The heat pumps, with their interconnected tank, can store energy for some time and "spend" the energy gradually, allowing them to act flexible. Not only the heat pump system allows for flexibility. Since many heating systems deliver the heat as floor heating, the house and pipe-system will act as an additional buffer-layer.

Various types of heat pumps exist. Based on their cost, functionality and efficiency various types are better suited than other for specific tasks.

Air-air source heat pumps are rather common in Denmark, especially in vacation homes around the country. It absorbs the energy in the surrounding air and delivers it through one or multiple fans inside a building. This type of heat pump is commonly dimensioned for being able to deliver roughly 70% of the heating demand of a household [4]. The remaining heating demand will need to be supported by for instance a resistive heating element which has a low efficiency compared to the heat pump itself. The power consumption of this type of heat pump follows the inside temperature of the building where it is connected closely, since the delivering mechanism is through the air which has a low time constant, when compared to delivering the energy through a system of pipes in the floor. This means that this type of heat pump unfortunately will not be of much use in terms of flexibility. There simply put is no means of storing energy in longer periods of time in such a system.

A better approach with flexibility in mind is the air-water or ground-water type of heat pump system. These types both have in common that they deliver the produced heat to a system of pipes flowing through the floors of the households usually with an accumulation tank of some size in-between. The pipes flowing in the floors of the building will dissipate the heat at a much slower pace than the air-air heat pump. This means that the heat pump can accumulate energy simply by the specific manner of dissipation. What is more interesting by the specific heat pumps systems in question is that they allow the possibility to utilize an interconnected water tank for extra storage. This is most commonly the case. The slow dissipation of heat as well as the storage tank makes water based heat pump systems well suited for flexible consumption. Fig. 2.16 and Fig. 2.17 show the two heat pump sources.

A good way to operate the heat pumps with flexibility in mind is to stop the consumption of power in high priced periods and consume power in low priced periods. During the winter season the air

source heat pumps will be running for most of the time to keep up with the high heating demand while being less effective due to the low outside temperatures [4]. There is no dispute that the ground source heat pump has a better year-round efficiency than the air source heat pump. The ground stays warmer than the air in the winter season which means that the efficiency of the heat pump will be better. The ground source heat pump therefore has better characteristics in terms of flexible consumption in the winter time than the air-source heat pump. As usual, nothing comes for free. Since digging is involved, the ground source heat pump system is more expensive to install than an air-source system.

An investigation carried out in [4] shows that the surplus energy from wind turbine production in 2025 would be 90 GWh/year in a scenario without any heat pumps. By intelligent use of the flexibility of heat pumps assuming 50% penetration for individual heating outside the district heating sector and 15% inside the district heating sector the surplus was reduced to 9 GWh/year which is quite some difference. This study clearly shows the impact the heat pumps can have if controlled intelligently.

The intelligent control means acting in order to earn savings for the end-consumer as well as acting in order to limit the peak consumption in the grid. Since the heat pumps add consumption to grids at in some points the grids will need to be reinforced. If controlled intelligently the need for grid reinforcements can be limited to a smaller amount than would be needed using no control. The conclusions of the report [4] published by Energinet.dk is that the large-scale implementation of heat pumps will assist the future energy system as well as being a good socio-economic investment when combined with fluctuating production.

M. Akmal presents in [16] an investigation of, the impact of implementing heat pumps on a large scale in the LV-grids. The investigation has shown that even with soft starters the heat pumps which are powered with induction motors will draw high starting currents. The study has shown that the soft starter only reduces the start-up current to approximately twice the nominal current. This current gives rise to transient voltage dips which in the case presented in the paper was of sizes violating grid codes during worst case scenarios.
J. Curtiss Fox presents in [17] that HPs can give rise to flicker-issues. In the future with a HP-penetration greater than 50%, a control structure where many HPs could be turned on within a very short time period could cause severe flicker issues. The turn-on off multiple units in the short time frame is not unrealistic and could be a product of HP price control. A sudden dip in price, would encourage multiple units to turn on simultaneously.

Heat pumps represent somewhat large loads in the ranges, for a common household, 0.8-5kW. As such the heat pumps when implemented in 50% of the households will add a large amount of power consumption to a grid. Therefore it is expected that the shear amount of added consumption could give rise to voltage drops when multiple units run simultaneously.

G. Papaefthymiou has in [18] investigated the potential for HPs to increase wind power utilization by intelligent control. The idea utilized in the paper is to utilize the load-shifting potential of the HPs to consume power when the prices are low and stop consumption when prices are high. The generalized control approach used in [18] can be seen in Fig. 2.18.
The paper concludes that the control approach brings significant savings for the end-consumers when compared to a no-control scenario. As the wind power production reduces the market price of energy due to the PSO-tariff, using low price energy is linked to using wind power (See section 2.3). Fig. 2.18 shows that the control utilizes the temperature bands of the water tank to add flexibility to the system. As long as the control stays within some predefined limits, the consumer comforts will

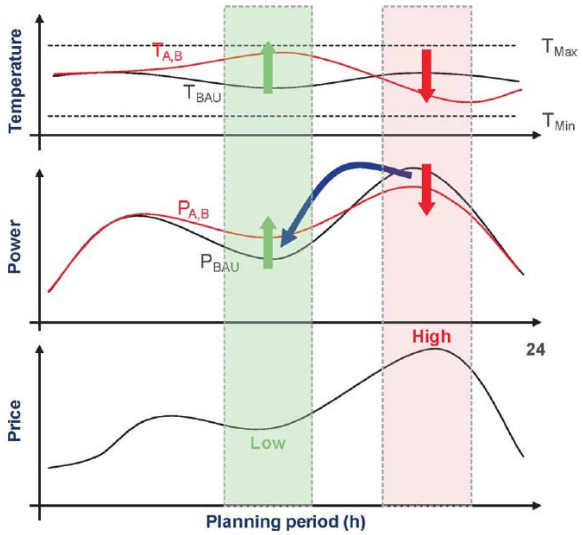

Figure 2.18: Heat pump control approach from [18]

not be affected noticeably.

This project looks into dynamic control of the HPs and will therefore not look into a load scheduling control-approach.

2.6.2 Electric Vehicles

The report from Energinet.dk [4] is, as mentioned previously, used as a reference for the amount of electric vehicles implemented in 2025. The report assumes that every one of four vehicles for personal transportation in Denmark in 2025 will run on electricity. The assumption for the EV-penetration requires that the EVs become a better overall competitor to the conventional car in market for transportation than they are today. The net consumption from all types of electric vehicles (including commercial vehicles and busses) is assumed to amount to 600.000-900.000 electric vehicles which in total will consume about 2.6 TWh/year [4]. It is assumed that the vehicles are a mix between vehicles running solely on electricity and hybrids. The charging patterns of the electric vehicles are of great importance when investigating the effects these units have in relation to demand side management. Various patterns have been investigated in [4]. The worst case and best case scenarios has been linked to the socio-economic perspective of having a high wind power penetration. Charging only in the peak periods is used as a worst case scenario and charging solely outside peak periods as the best case scenario (See section 2.4). By charging the EVs by the worst case scenario, the surplus energy produced by the wind turbines over a full year, would be reduced from 90 GWh/year to 85 GWh/year which is a very small reduction. As this scenario would add extra loading during the peak period, it would contribute to the need of massive reinforcements of the grids. By intelligent changing of the EVs in off-peak periods, the surplus energy per year would be completely non-existing [4]. This means that the socio-economic benefits from implementing wind power would be at its maximum. The report presumes that with the off-peak control, the need for grid reinforcements would be limited, when only looking at the EV consumption for 2025.

L. Dow has in [19] amongst other looked into the difference between intelligent control and no-control and compared it to a no-EV scenario. The findings are shown in Fig. 2.19 which shows multiple characterizes. When comparing the scenario with no EVs to the scenario with EVs without control it is seen that the non-controlled EVs add a considerable amount of loading of the grid all day round.

Worst part is that the load from 17-20 is increased, which in Denmark is the peak period. As such, this scenario would not be socio-economically desirable. Investments would need to be made on grid reinforcements, since not being able to use the wind power optimal since the flexibility of the EVs is not utilized. This further consolidates the statements of [4] which shows the importance of intelligent control.

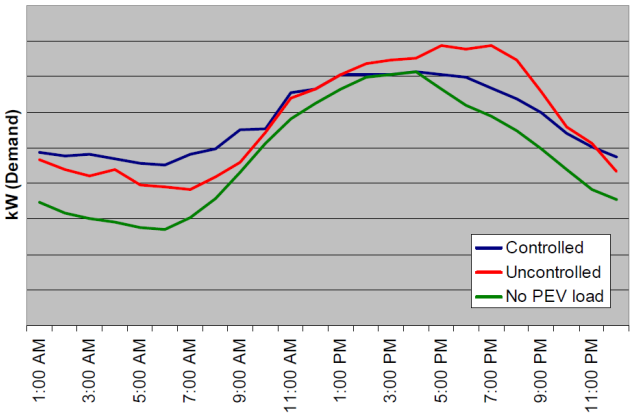

Figure 2.19: EV charging control from [19]

As EVs represent large electrical loads when implemented in the LV-grids it, is assumed that the presence of a high EV-penetration will affect voltage levels. J. R. Pillai has in [20] investigated the possibility of improving transformer utilization in three different LV-grids, two of which are the same as the ones investigated in this project. The paper concludes that voltage drops are the central technical constraint limiting transformer utilization. The paper investigates the grids LV-I, LV-II and LV-III where LV-I and LV-III are the strongest grids and LV-II is characterized as being rather weak. The findings in [20] show that the possibility of adding more EVs into the grid relies heavily on the actual load conditions in the grid. Maximum and minimum demand happens during summer and winter. Fig. 2.20 shows a bar plot from [20] which shows the theoretical EV-penetration possible when considering technical constraints as voltage drops, cable loading and transformer loading.

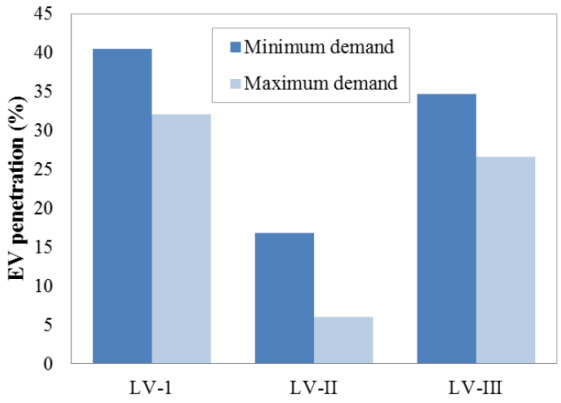

Figure 2.20: Possible EV penetration in 3 different grids from [20]

For LV-I, the strong grid, the technical constraint hit is the transformer loading which is actually fully loaded in Fig. 2.20. LV-II and LV-III are limited due to voltage drops in the feeders.

Another interesting property of electric vehicles is the possibility to deliver energy back into the grid.

This property is commonly referred to as vehicle to grid or simply V2G. Energinet.dk is responsible for keeping the system balanced continuously, by buying or selling energy. This task is performed in order to keep the frequency at 50 Hz. The V2G concept can help in assisting the frequency by charging during surplus energy scenarios or delivering power to the grid during a energy deficiency scenario. The V2G-concept will rely on clusters of EV-owners selling the flexibility of their EV to an aggregator who on a larger scale will sell power for up- or down regulation to the TSO. The EV-batteries are very interesting in the balancing power aspect since they, unlike conventional generators, do not have startup- or shutdown costs [21]. Yet another interesting item relating the V2G concept is the fact that the need for balancing power over time will have a net value close to zero. This means that over time the energy "spend" to up-regulate and energy "gained" by down regulation will more or less even out. This implies that the payments involved are paid for the available capacity for regulation rather than the actual amount of energy traded with the power system [21]. The aggregator and the balancing responsible will therefore make a contract specifying the amount of power available for up- and down regulation. This arrangement brings yet another interesting topic in play. The EV-batteries will not be able to provide any capacity for up-regulation if fully charged. Therefore, the batteries will need to be charged to some specified upper limit (fx. SOC $\leq$ 90%) to ensure capacity for balancing needs. This will have a direct and visible impact on the end-consumer. If assumed that some arbitrary EV has a range of 200km when fully charged, the end-consumer would see a reduction in range of 20km due to the "need" for balancing power. As the end-consumers will invest in EVs to cover transportation needs (and not to assist the power system) it is of vital concern that this side-effect is limited.

C. Zhou has investigated the wear of batteries in relations to the V2G concept in [22]. The study shows that V2G will reduce the expected life time of EV-batteries. The two major factors influencing the wear of the batteries are the depth of discharge as well as the ambient temperature at the point when the battery will deliver power to the grid. Lithium-ion batteries are by far the best choice for V2G applications and will wear down at at rate approximately four times slower than lead-acid- or NiMH batteries if all subject to the same V2G patterns. The paper compared the wear of the batteries for V2G applications in China and the UK. The batteries would be degraded approximately 50% faster in China due to the higher temperature. The usefulness of the V2G concept therefore relies on the ratio between the cost of battery-wear compared to the possible earnings by selling a balancing service to a balancing responsible operator.

3 Case Study Description

This chapter will introduce the work carried out prior to starting any actual modelling or simulations.

A brief introduction to various grid topologies will be presented in the first section leading to the topologies of the two LV-grids used during the project work. The two LV-grids (LV-I and LV-II) been used as a base for every case study carried out through the report. At the surface the grids seem similar, but actually show very different properties.

The next section introduces the household energy consumption, covering electrical- as well as heating demands. It has been needed to estimate the hourly energy consumption of every household during different seasons to be able to perform simulations showing the performance of the two grids at different times of day as well as year. The calculations and estimations done in this regard will be presented in sub-section 3.3.1.

In chapter 5 the dynamic control of the EVs and HPs will be presented. In order to run the dynamic HP models, the space heating- and domestic hot water demands will need to be specified. The data used within this project is presented in sub-section 3.3.2.

Likewise, the behaviour of the EV models will be defined by the driving patterns adopted in the project. The generation of driving patterns will be presented in section 3.4.

3.1 Distribution Grid Topologies

The distribution system makes up a large part of the electrical power system. It is connected with the transmission system and provides a continuous service of supplying end-consumers with electricity. In order to provide the end-consumers with a high quality power supply the networks must be reliable, robust and efficient parts of the power system. The Danish distribution grids mostly consist of underground cable systems since they offer a high reliability and allows for supplying power in a less visible manner in highly populated residential areas.

Three widely used grid topologies are introduced in this section. Table 3.1 contains a rough comparison between the topologies. In reality though, distribution systems consist of a wide range of combinations between various topologies due to varying consumer density, consumer types and load distribution across the supplied area.

Typically distribution grids in low populated regions are supplied using the radial distribution topology as it is relatively cheap and simple to implement. Usually with this configuration, a centrally located power source which commonly is a higher voltage level transformer, supplies a busbar. The power from the busbar is fed by only one string to cable boxes from where it is delivered to the end-consumers. To decide if this topology is applicable in a specific scenario an engineer would need

	Radial	Ring	Mesh
Reliability	*	**	***
Cost	***	**	*
Simplicity	***	**	*
Short circuit capacity	*	**	***

Table 3.1: Distribution grid topologies (***: Better, *: Worse)

to look into the downsides to simplicity and cost as it comes with a price. Any faults happening to this single line structure would cause a complete power outage until the fault is cleared, making the reliability low. The single line structure could also be vulnerable to overloading scenarios if the capacity of the feeder would be close to the maximum load of the consumers connected at the feeder. In multi-feeder systems, this scenario would cause the high load current to run via multiple feeders therefore reducing the risk of experiencing a severe overload. The reliability of the radial topology can be improved by implementing redundancy in form of a passive parallel secondary feeder, which is only connected in cases of maintenance of or faults in the primary feeder. Fig. 3.1 and 3.2 show the two varieties of the radial topology.

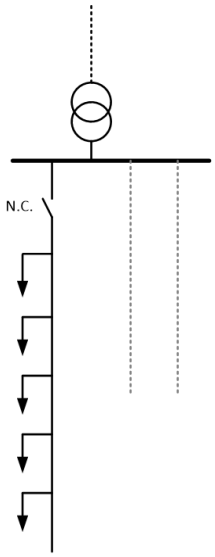

Figure 3.1: Radial grid topology

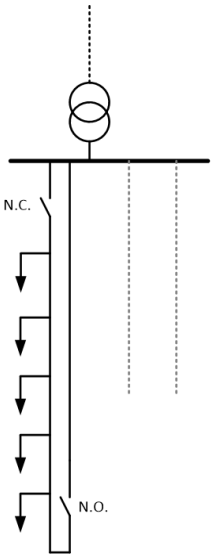

Figure 3.2: Radial grid topology with parallel backup

A ring configuration allows for supplying one single feeder from both ends. In case one of the supply lines is out of service, another should be able to carry the load temporarily. For this to work, the feeders which could be acting as backups, need to be dimensioned for the extra load. The ring system therefore offers a higher reliability than the radial topology. The ring topology is shown in Fig. 3.3.

The mesh grid is most reliable and complex grid type. Such a system consists of more than one primary loop, with interconnection between nodes, and several power supplies. This network topology provides the highest continuity of service and tolerates line breakdowns without significant interruptions of consumer service. The topology is usually designed for high density municipal zones. An example of the mesh grid topology is seen in Fig. 3.4.

The overview of the topologies shows examples of how designers / engineers can choose to approach a specific network design task. Most commonly the distribution networks in Denmark are designed using a combination of the various topologies. This will be seen in the next section where the two

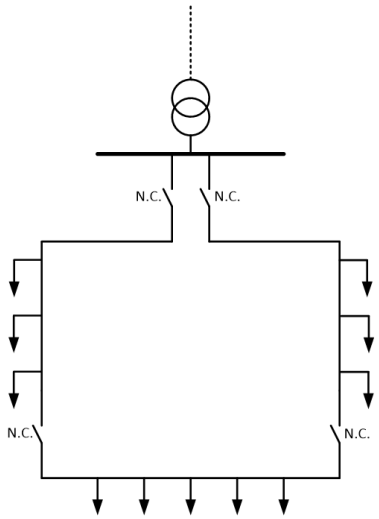

Figure 3.3: Ring grid topology

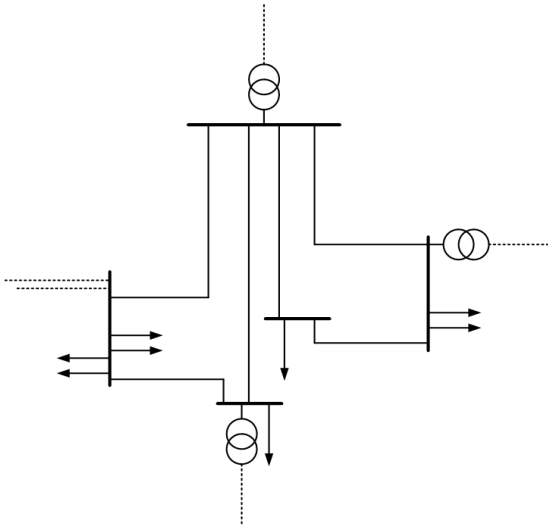

Figure 3.4: The mesh grid topology

studied low voltage grids will be presented.

Common for the Danish power system in general is also that it is designed with a high security of supply in mind.

3.2 The Investigated Low Voltage Grids

The full circuit models of the two studied low voltage grids (LV-I & LV-II) has been modelled in DIgSILENT PowerFactory. Along with the modelling of the grids, the data for the household consumption through time has been implemented as well. In order to implement the specific consumption data needed during the project work, some data manipulation has been needed to be carried out prior to doing any simulations. The data made available to the group has been used in [20]. The actual calculations made regarding the household consumption profiles are presented in 3.3.1. Both grids are located near Broenderslev, Jutland.

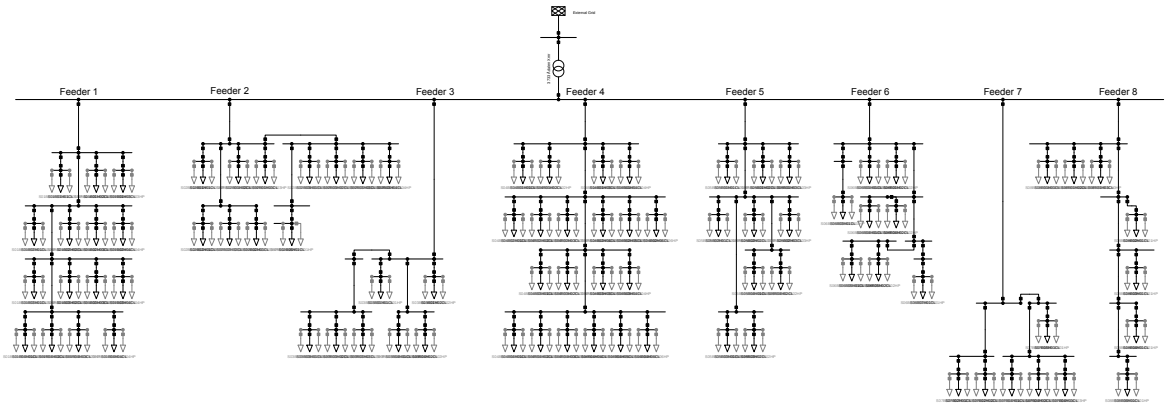

Figure 3.5: Single-line diagram of LV-I (From DIgSILENT PowerFactory)

The first low voltage grid, LV-I, is supplied from a 10kV network through a 400 kVA transformer which supplies 84 individual households. The grid layout from DIgSILENT PowerFactory is seen in Fig. 3.5. LV-I represents the radial topology as briefly described in the previous section. The transformer is

connected directly to the main busbar. The primary busbar connects the secondary winding to eight separated strings, also called feeders. Each of the strings is supplying individual households through cables.

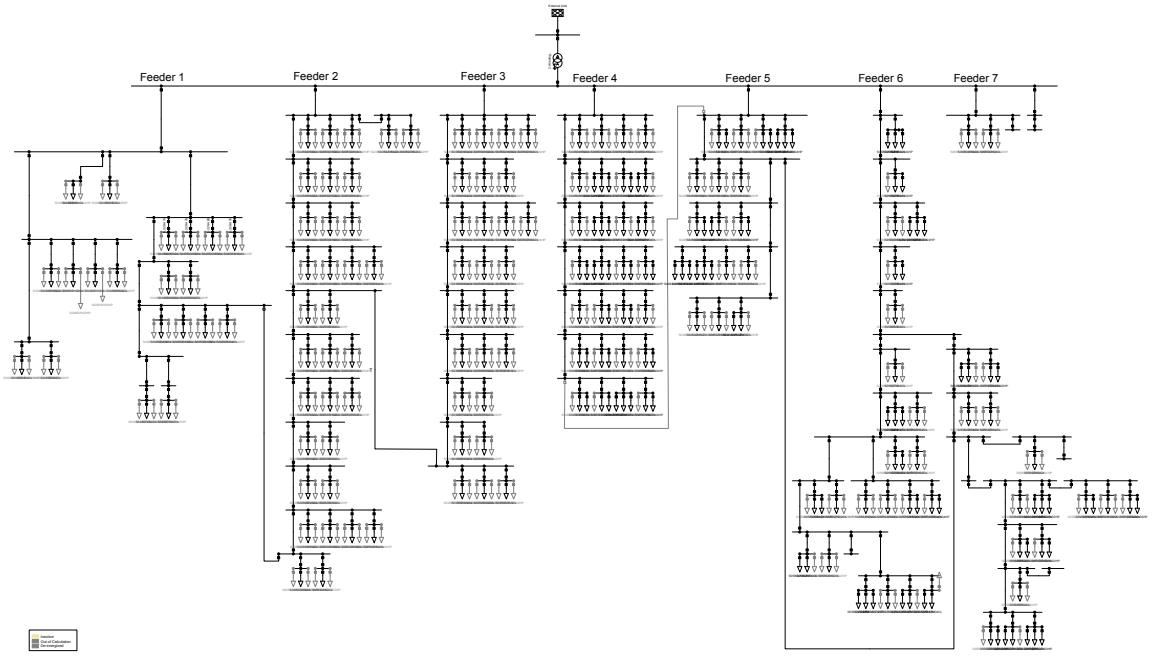

Figure 3.6: Single-line diagram of LV-II (From DIgSILENT PowerFactory)

LV-II is the second low voltage grid analysed in this project. The system is supplied from a 10kV medium voltage network through a 630kVA transformer supplying 166 individual households divided between 7 feeders. The grid topology of LV-II grid is also a radial configuration. However, every string is equipped with an additional cable, connecting it to an adjacent feeder, which means that during emergencies or maintenance, the affected feeders can be operated in an open ring configuration. In general, the tie points are out of service, except during these abnormal conditions. The entire system is built with underground cables. A single line diagram of LV-II is seen in Fig. 3.6.
Information regarding the transformers, the grids as well as consumers in the grids are to be found in tables 3.2, 3.3 & 3.4.

	LV-I	LV-II
Topology	Dyn5	Dyn5
Voltage Rating [kV]	10 / 0.4	10 / 0.4
Rated Power [kVA]	400	630

Table 3.2: Transformer parameters for LV-I & LV-II

	LV-I	LV-II
Topology	Radial	Radial /w tie-points
Short circuit capacity [MVA]	636	873
Number of feeders	8	7

Table 3.3: Grid parameters for LV-I & LV-II

All loads are assumed to be balanced 3-phase. The loads per radial point in Table 3.4 lists the number of consumers per feeder starting with the leftmost feeder in each of the low voltage grids.

	LV-I	LV-II
Sum of loads	84	166
Loads per radial	15 11 7 20 10 8 6 7	20 33 27 28 17 39 2
Load furthest from transformer [m]	894 (feeder 6)	865 (feeder 1)

Table 3.4: Load parameters for LV-I & LV-II

3.3 Household Energy Consumption

The energy consumption of a household can be divided into two groups:

- Electricity demand
- Heating demand

The electricity demand does of course cover the running of all household appliances consuming power, such as fridges, TVs, electric kettles etc.. The heating demand covers the need for having a certain temperature inside the house. As the desired temperature within a household, for most of the year in Denmark, is higher than the outside temperature, energy losses to the ambient will occur. These losses are more or less continuously covered by adding some amount of energy (ambient temperature dependent), in form of added heat, thereby keeping the inside temperature fixed to a user-specified temperature-range. The heating demand also covers the need for having hot water available in the various tabs around the household.

This section will present the energy demands for the individual households in LV-I and LV-II.

3.3.1 Household Load Profiles

Original consumption profiles for the households in the two low voltage grids has not been available during the project work. Therefore, the consumption profiles presented in this section, are based upon the actual data available combined with various assumptions.

The annual electricity consumption of a household in LV-I varies between 0-13450 kWh/year. The consumption of a household in LV-II varies between 421-15615 kWh/year. The average electricity consumption is equal to 3929 kWh for LV-I and 4036 kWh for LV-II. Fig. 3.7 shows an example of the transformer loading of LV-II during a winter day.

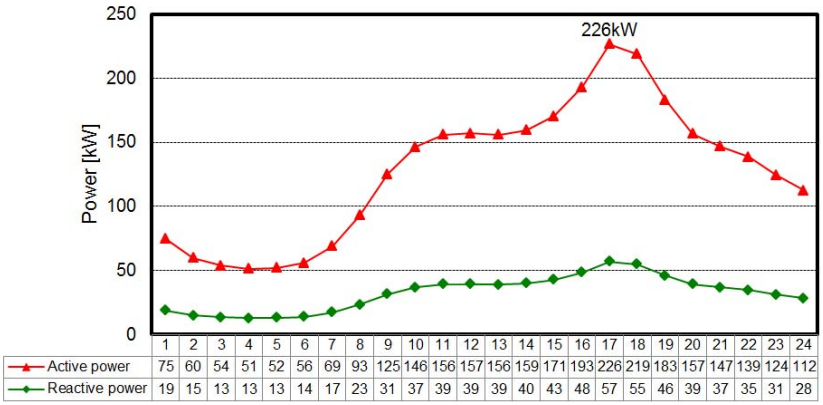

	1	2	3	4	5	6	7	8	9	10	11	12	13	14	15	16	17	18	19	20	21	22	23	24
Active power	75	60	54	51	52	56	69	93	125	146	156	157	156	159	171	193	226	219	183	157	147	139	124	112
Reactive power	19	15	13	13	13	14	17	23	31	37	39	39	39	40	43	48	57	55	46	39	37	35	31	28

Figure 3.7: LV-II: Transformer loading during a winter day

According to a report published by the International Energy Agency in 2009 [23], the annual electricity demand in Western European varies significantly. The average peak demand during summer is roughly 30-35% of the average winter peak demand. The day-by-day electricity consumption is also highly diverse.

For LV-II the peak demand, present at 17:00, is roughly four times greater than the average electricity demand at 4:00. As an example from the LV grids used in this project, the power demand in LV-II during a winter work day at 17:00 is approximately six times greater than during summer weekend day at 4:00.

These numbers represent the fact that the maximum amount of EVs and HPs possible to supply in the future grids without reinforcements, will be highly dependent of the seasons. The technical limits, such as voltage levels as well as cable- and transformer loading, define the grid capacity. The statistics therefore relate the seasons to the free capacity at a specific time of year.

The power factor of a common household vary in the range of 0.95 lagging to 0.95 leading [24][25]. During the project work an equivalent household power factor, valid for all households, of 0.97 lagging has been assumed.

The area wherein LV-I and LV-II are located is supplied by district heating. This has a few implications to the project. First of all, the grids are not dimensioned for electrical heating which will be added in a large scale. Secondly, the heat pump models will need a heating demand input.

The first implication means that implementing the heat pumps will add load in the grids which most likely would not be present in a future reality since district heating is assumed to be cheaper and more reliable than any individual heating source. A similar implication though, would have been seen in a grid located in an area heated purely by oil-fired boilers, which would be a grid where a scenario with a large future heat pump penetration would make sense. Therefore the implementation of the heat pumps in LV-I and LV-II is presented as a viable future case study.

As for the second implication, data for household heating demands for 25 individual households, has been presented in [26]. This data has been used and manipulated in order to provide the 83 different heating demand profiles needed for the heat pumps in LV-II and 42 heat pumps in LV-I. The data and manipulations are presented in 3.3.2.

Multiple approaches to load profile estimation are available in literature [3][27][28]. Since each house is characterized by its own load curve, none of the methods are able to reflect an exact load profile. However, in order to analyse and estimate the grid capability of LV-I and LV-II it has been found acceptable to base the load profiles upon a correlation method.

The correlation method used to estimate the daily consumption profiles has been defined in [27]. It presents a method which utilizes the annual electricity demand to identify seasonal maximum peak demands for single households. The methodology presumes, that if each of the households consume a similar amount of energy per year, a load factor (LDF) can be expressed in terms of annual energy consumption and maximum power demand [27][29].

$$LDF(N) = \frac{e(N)}{8760 \cdot D(N)} \quad [-] \quad (3.1)$$

where,
LDF(N): Seasonal load factor for N households
e: Annual electricity consumption for N households [kWh]
8760: Number of hours within a year [hour]
D(N): Average daily maximum power demand per N households [kW]

According to [29] the load profile of the daily consumption of an individual house can be determined based on an annual energy consumption measured at the house terminals. In order to calculate the maximum peak demand of a single individual house, the expression for LDF is transformed to the final form:

$$D = \frac{e}{8760 \cdot LDF} \quad \text{[kW]} \quad (3.2)$$

The LDF coefficient determines the scale of the daily maximum power demand. It has been decided to create profiles for the two extremes which are a summer weekend day as well as a winter week day. In Table 3.5 the LDF coefficients for summer weekend days and winter working days are shown. These values are based on [20].

	LV-I	LV-II
Summer LDF	0.805	0.739
Winter LDF	0.372	0.347

Table 3.5: LDF values for LV-I & LV-II

Daily peaks allows for creating daily load profiles of each individual house. In order to match the data measured at the transformer, the peak demand is taken as the reference point. The reference point is then projected on the transformer loading characteristic. This allows for scaling down the transformer characteristic to match a single household and estimating the 23 remaining hours of the profiles.

As an example, one of the households in LV-II has an annual consumption equal to 15615 kWh. The transformer peak value of a certain day during winter is equal to 226kW.
The peak demand, D, during winter is equal to:

$$D = \frac{e}{8760 \cdot LDF} \Rightarrow \quad \text{[kW]} \quad (3.3)$$
$$D = \frac{15615}{8760 \cdot 0.347} = 5.14\text{kW}$$

where,
D: Average daily maximum power demand of a single household [kW]

The sum of estimated peak demands needs to match the peak demand of the transformer. Thus, the transformer load profile shown earlier in Fig. 3.7 is scaled down to the peak point D, in order to reach the same shape for a household profile as the transformer load profile. According to Fig. 3.7 the peak of the total grid consumption appears at 17:00 with a value of 226kW (red line). The peak demand of the household appears at the same time and is equal 5.14kW.
In next step, the remaining points of the household consumption profile are estimated. The relationship, shown below allows for calculating the power demand at a certain hour, h.

$$P_{hh}(h) = \frac{D \cdot P_t(h)}{P_{t,max}} \quad \text{[kW]} \quad (3.4)$$

where,
$P_{hh}(h)$: Estimated average hourly consumption of a single household [kW]
$P_t(h)$: Average hourly consumption at the transformer [kW]
$P_{t,max}$: Maximum hourly consumption at the transformer [kW]

To continue the example, at 16:00 the power is therefore equal to

$$P_{hh}(16) = \frac{5.14 \cdot 192.95}{226} = 4.39\text{kW} \quad (3.5)$$

Now, two values in a load profile for a single household has been calculated. The process then is continued in order to find the remaining 22 values of the full daily profile. This process has been carried out for every household in LV-I and LV-II. The calculations have been made using MATLAB. Examples of the estimated load profiles during a summer and a winter scenario are shown in Fig. 3.8. The profile with the greater values represents the consumption of the household with the highest annual energy consumption during winter time. The dots illustrate the previously calculated values P(17) = 5.14kW and P(16) = 4.39kW.

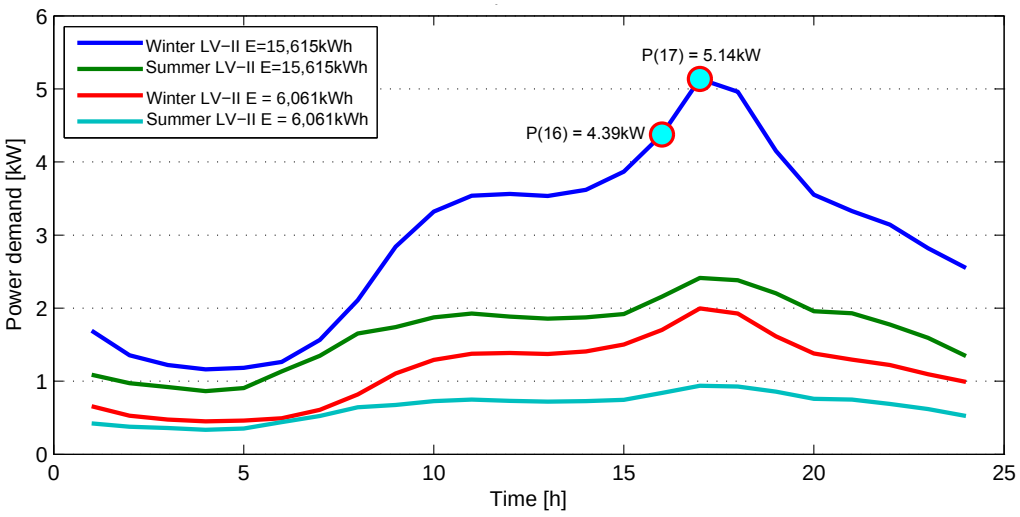

Figure 3.8: Examples of household load profiles for LV-II during summer/winter

In Fig. 3.8 The profile with the greater values represents the load profile for a house with an annual electricity consumption of E = 15,615kWh during a winter week day. The green line represents the same household consumption but during a summer weekend day. The blue line and the red line with lesser consumption illustrate the daily profiles of household with an annual consumption of E = 6,061kWh.

Load profiles for two different households in LV-I are shown in Fig. 3.9. The upper blue line represents the load profile for the largest annual electricity consumption of a single household of E = 13,450kWh.

The used approach to estimate the consumption profiles guarantees that the estimated load profiles when summed up, matches the measurements taken at the transformer substation. The reason for

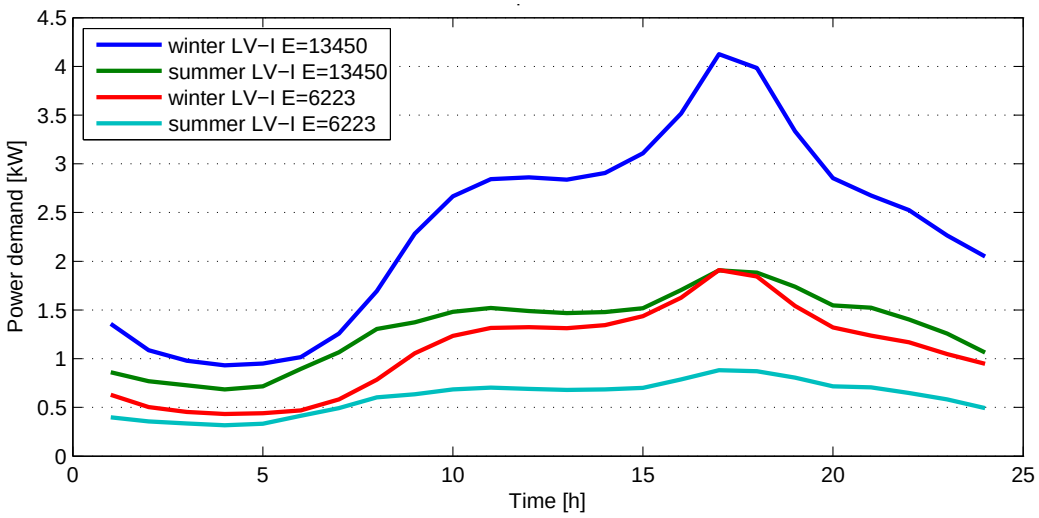

Figure 3.9: Examples of household load profiles for LV-I during summer/winter

this is simply that in the process of creating the profiles the household consumption is projected onto the transformer loading curve. However, the real household profiles do not necessarily have a peak demand at the same exact moment as shown in figure 3.8 and 3.9. The calculated peak is most probably slightly shifted in time. This error is considered to be negligible for the further project work.

3.3.2 Space Heating Demand and Hot Water Consumption

The majority (≈60%) of the individual households in Denmark are supplied with district heating. District heating is supplied from the thermal power plants (usually co-generation plants). In CHP plants, the high pressure- and temperature water is a by-product from the conventional electricity generation process. Waste heat is also produced in some of the large industries, which as a side product to their main business sell the waste heat, converted to hot water, generated by their primary processes. As large co-generation plants and industries are located around the country, the heating demands of many domestic areas are met as a consequence of the waste heat to hot water conversion.

The domestic heating demand can be divided in two:

- The *space heating demand* which cover the heat supplied to the household in order to keep the proper temperature in the living space
- The *hot water demand* which cover the heating energy supplied to cover basic humans needs i.e. cooking, washing

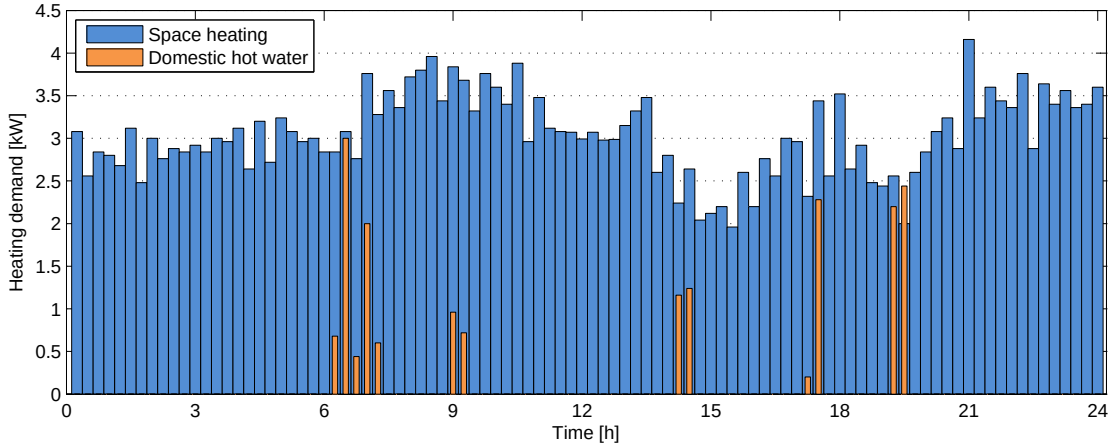

Figure 3.10: Single household - typical winter day heating demand

Since measurements of heat consumption (district heating) in the studied area are not available, the project has adopted the data set used in the project presented in [30]. This data-set consists of values measured in 25 Danish households during a full year. The measurements are presented as 15 minute averages of space heating and hot water consumption separately. The heat pump model will be the application in need of the data and will be described in detail in chapter 5. As an example typical winter day consumption profile for a single household is shown in Fig. 3.10.
On Fig. 3.10 it is seen that the space heating demand is continuous, contrary to the hot water demand which occurs during specific periods. This reflects reality in the sense that the space heating demand is present primarily due to cover the heat loss from household to ambient which is assumed to be fairly constant. The hot water demand is present only at times where hot water consumption actually occurs. This could for instance be for showering or doing the dishes.

As only one type of heat pump (P=3.1kW) is implemented in chapter 5, three heating profiles has been disregarded due to the demand being too high for the heat pump to support the need. In reality, the households would have needed bigger heat pumps implemented.

Both LV grids will receive the same input profiles for the heat pump operation, LV-I less than LV-II though. LV-II would ideally need 83 heat pumps due to the desire to implement a heat pump in 50% of the households in the grid. The heat pumps will be operating in systems of heat pumps 12 in DIgSILENT PowerFactory. LV-II has 9 heat pump groups implemented, not all operating though. Therefore at least 108 heating profiles will be needed.

As only 22 (25 minus 3 disregarded) profiles has been available, every profile could be used for five different heat pumps or the profiles could be manipulated to create the remaining profiles needed to grant every heat pump an individual profile. It was decided to create five profiles from each original profile (original included) to gain a higher degree of randomization of the operational behaviour of the heat pump.

As chapter 5 will look into the behaviour of the HPs through the seasons, two sets of consumption profiles have been created, one for January 22^{nd} and one for August 11^{th}. Fig. 3.11 shows the average heating demand of the two data sets.

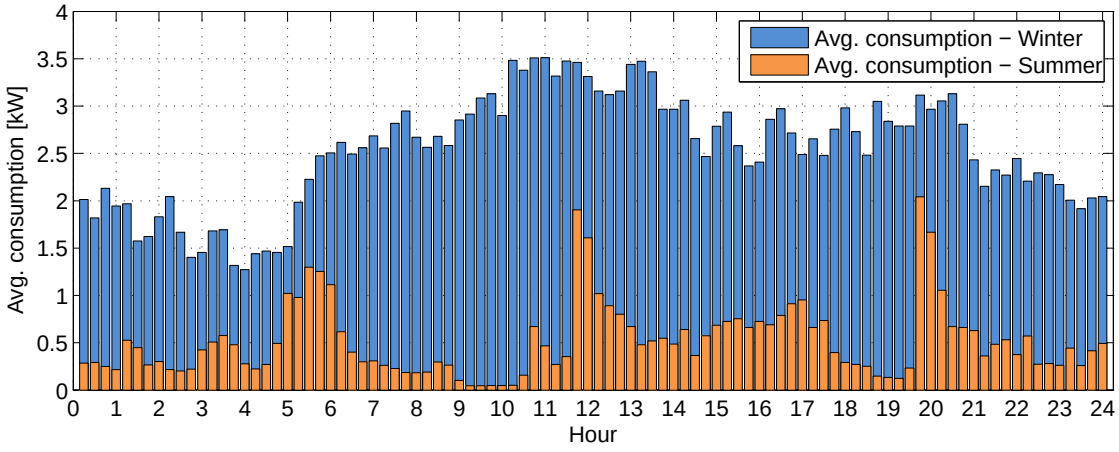

Figure 3.11: Average heating demand - summer/winter

Each original profile has been manipulated with regards to the following parameters:

- Amplitude increased by 10%
- Amplitude decreased by 10%
- Consumption shifted one hour ahead of "real time"
- Consumption shifted one hour behind "real time"

An example of the generation of the additional profiles is shown in Fig. 3.12. The figure shows an arbitrary eight hour snip of an original profile during winter time with its four appurtenant manipulated profiles.

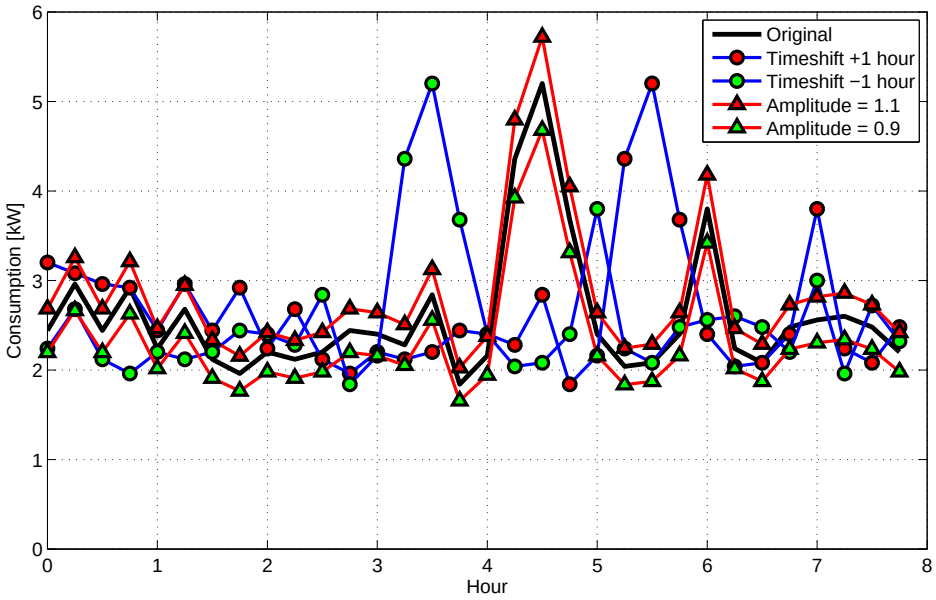

Figure 3.12: Example of the generation of four additional profiles per original

3.4 Driving Patterns

The driving patterns of the electrical vehicles highly influence their ability to contribute to load flexibility. Therefore, within this section, individual driving habits are analysed which leads to the generation of driving habit profiles used by the dynamic EV models implemented in DIgSILENT PowerFactory (Chapter 5/6). It has been decided to prepare 100 different profiles which includes the time of which the EVs are available at the households as well as the driving distance covered while away.

The first task is the preparation of an EV operation schedule for 100 units, 24 hours. The schedule needs to contain the daily driving distance, time spent on the road (unavailable) and time not spent on the road (available). The driving distance will provide knowledge about the energy status of the battery after the distance has been covered. The time not spent on the road implies a period where the EV is available for charging and supporting the grid and time spent on the road specifies a period where the EV is not available for charging or assisting the grid.

Prior work in this field has been performed in [31]. The article defines driving distances and time periods where EVs are unavailable (on the road). The data presented is based on statements gathered from Danish car owners. The entire data-set has been created by The Danish National Transport Survey during more than 15 years. The data is based on more than 100,000 responders.

In order to estimate the battery state of charge (SoC) as an EV arrives at home, it is necessary to estimate the power consumption per driven distance. This information allows for relating the driven distance to electrical power consumption and thereby depth of discharge of the EV battery. In [31] the power demand is determined to be within the range of 120-180Wh/km, depending on the EV performance and dimensions. If no information regarding the EV energy consumption is available, it is recommended to use an average power demand of 150Wh/km. The article estimates the overall daily driving distance of a regular Danish car to be ≈29.5km. The variation in the driving distance within week days, weekend days and holidays is also provided in the paper. It is shown that during week days the driving distances do not change significantly from the overall average. The week day average driving distance is ≈30km as well. During week days, 38% to 43% of the cars drive less than 10km/day.

During holiday- and weekend days, 50% to 60% of the cars drive less than 10km/day and the average driving distance is 26km/day. The lowest average distance of just 18.9km/day occurs during holidays.

In case the planing procedure does not require a distinction between week days, holidays or weekend days, [31] provides an average distance distribution which is illustrated in Fig.3.13. The vertical axis represents the driving distance ranges while the horizontal axis represents the driving distance contribution in percentage of the total sample number of 134,756 samples. As an example, the first bar from the bottom of Fig. 3.13 indicates that 45.31% of the 134,765 cars drive a distance between 0km and 10km per day.

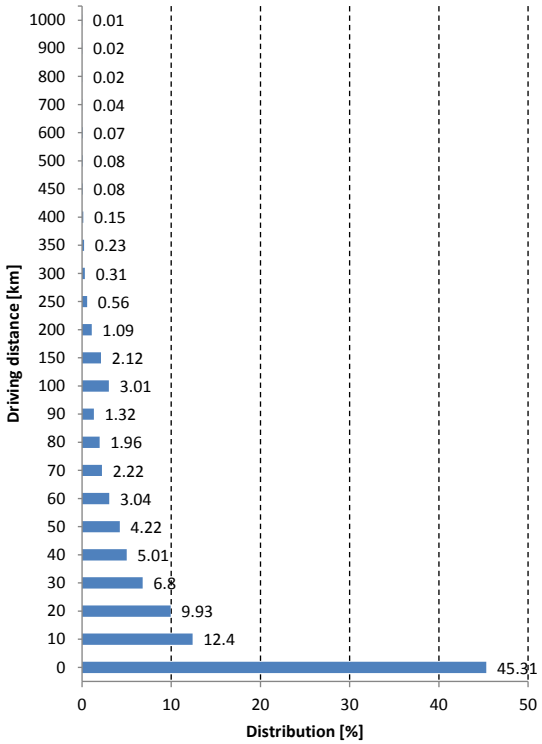

Figure 3.13: Individual driving distance distribution

The article also establishes the availability of the cars in percentage. A car is available when it is not driving (EV connected to the grid) and unavailable when it is on the road. In Fig. 3.14 it is seen that the availability varies between 94.35% and 97.29% of the total number of cars. The minimum availability is observed at 8:00 and at 17:00. The maximum availability appears at night between 23:00 and 4:00. The "shape" of the availability is similar for different working days due to similar car user habits. In the morning, the majority of the car users leave their homes around 8:00 and drive off to work, school etc.. Later, the majority of the cars users arrive home between 16:00 and 17:00. During weekends and holidays the lowest availability appears around 11:00 and the highest appears during night time. The overall availability distribution, seen in Fig. 3.14 represents the hourly car availability without distinguishing between weekend-, holiday- or week days. Fig. 3.14 shows in which time periods the majority of the EVs will be available and when they will be unavailable. However, this approach does not distinguish between the point of connection due the assumption that EVs are possible charge anywhere they park.

This project only looks into the charging of EVs at home. Hence, time periods when the cars are available at home needs to be clearly defined. For this reason the availability data has been reconstructed according to [32]. In the article, the daily overall availability is divided into two normal distribution

functions. The first defining time of leaving, where the EVs are leaving their households, and the second defines when the EVs are arriving at home. Both distribution functions are represented by the 'Normal'-distribution. The "leaving"- and "coming" distribution functions, fitted to the availability data are shown in Fig. 3.14.

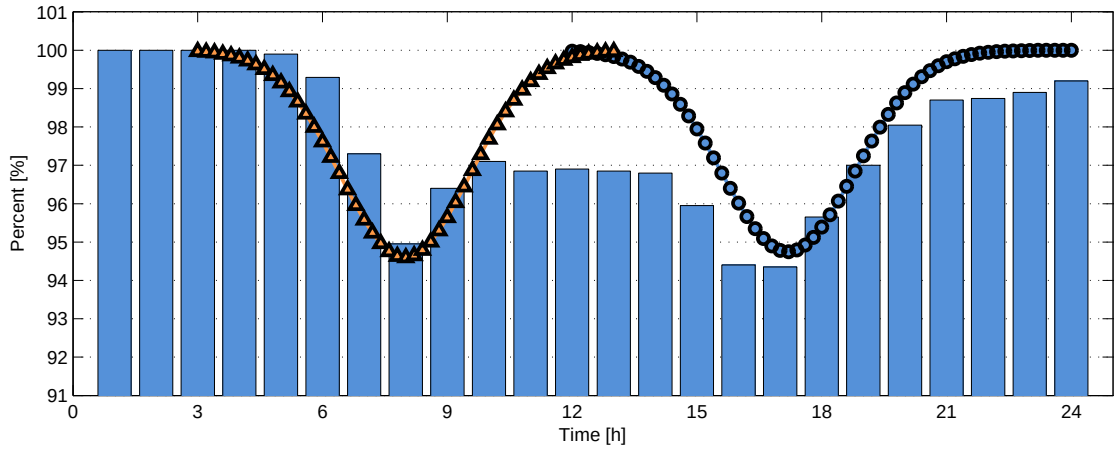

Figure 3.14: Overall EV hour availability data

The driving pattern generation approach has been to create a script in MATLAB capable of representing the data presented in [31]. In order to being able to get a good fit between the generated data and the true data, a sample pool of 20,000 EVs has been made. In the end 100 samples with driving distances less than 200km will be picked from the 20,000 samples generated, representing the true data. The 200km limit is due to the EV battery size which currently does not support longer distances according to [33].

In the first step, the driving distance has been extracted from Fig. 3.13. In order to build the distance sample-pool reflecting the data obtained from Fig. 3.13, a random number generator has been applied in MATLAB. The generator creates a specific number of samples within a defined range of values corresponding to the numbers presented in Fig. 3.13.

As an example of the sample generation procedure, the generation of data corresponding to the lowest bar of Fig. 3.13 is presented. The total number of samples which should be included in the driving distance range (0km to 10km) is equal 45.31% of 20000 equal to 9062 samples. The MATLAB algorithm generates random numbers in the range 0 and 10km until it reaches 9062 samples. Afterwards, the algorithm jumps to the next driving distance range and repeats the procedure until it reaches the new sample pool equal to 12.4%. The remaining samples are generated in the same manner. The entire process allows for the creation of the distance distribution histogram shown in Fig. 3.15.

Fig. 3.15 shows a clear difference between the number of cars driving 10km and 11km per day. This phenomena is presumed to be a side-effect of the data-collecting procedure employed by The Danish National Transport Survey, and does not necessarily represent reality very well. It is believed to be the effect of questions such as "*do you drive between 0-10km/day or 11-20km/day...*". Hence, it has been decided to modify the original data pool according to some distribution function that will reduce the presumed "error". The procedure has been to find an adequate distribution function which fits fairly good to the data shown in Fig.3.15 and thereby flatten the impact of the large steps between different distance ranges. Simply put, the resolution of the data has been increased.

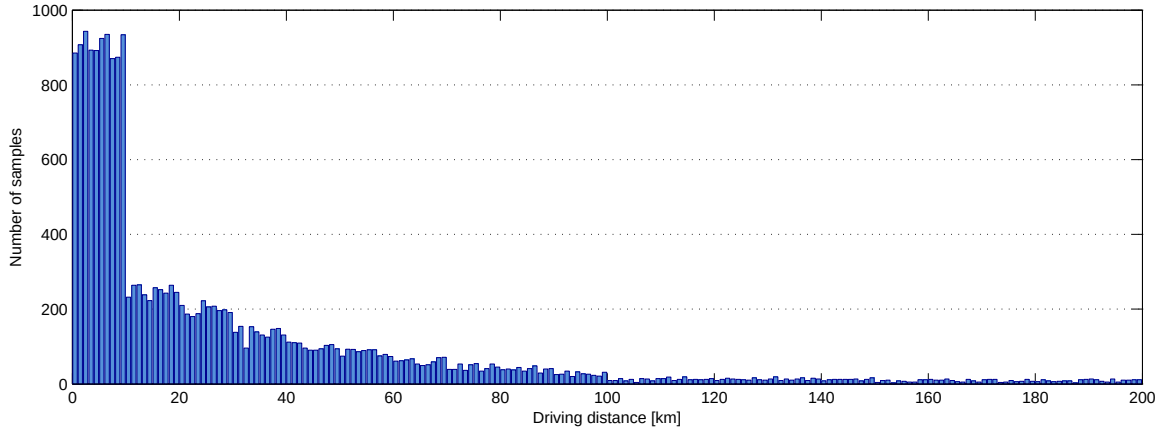

Figure 3.15: Estimation of individual driving distances

In order to obtain a smooth distribution shape, different distribution functions are matched to the original by using MATLAB's fitting function *fitdist* and then compared to the original distribution. The most suitable function will be used create a new sample pool with a higher resolution. The comparison is made with respect to the mean and variance of the original data set and estimated distribution function. Table. 3.6 shows the mean and variance of the various distributions tested. The first row represents the mean and variance of the distribution function shown in Fig. 3.15. The most accurate fit function should have the closest mean and variance values to the original distribution.

Some of the more important code is presented in Appendix A.2.2.

Distribution function	Mean	Variance
Original	28.33	1318.40
Beta	30.43	1104.35
Birnbaum-Saunders	25.85	2368.10
Exponential	28.66	780.67
Gamma	28.12	1077.71
Inverse Gaussian	31.29	11101.70
Kernel	28.71	1404.32
Logistic	19.82	997.22
Loglogistic	45.20	35639.49
Lognormal	37.85	7575.15
Nakagami	31.96	1058.75
Normal	29.72	1255.76
Rayleigh	39.88	425.62
t Location Scale	-79.92	5918674.98
Weibull	28.32	1098.29

Table 3.6: Distribution functions comparison

Table 3.6 shows that a few of the analysed distribution functions represents the original data significantly better than others. These distribution functions are the Gamma-, Kernel-, Normal and Weibull distributions. By using MATLAB's random function, four data pools have been generated with respect to the chosen distribution functions. Each data pool consists of 20000 distance samples. The histograms showing samples for the original data and fitted distribution function are presented in Appendix A.2.2. The most accurate fit is obtained by using the Kernel distribution function shown in

the lower graph in Fig. 3.16. The upper graph shows the histogram of the original data estimation.

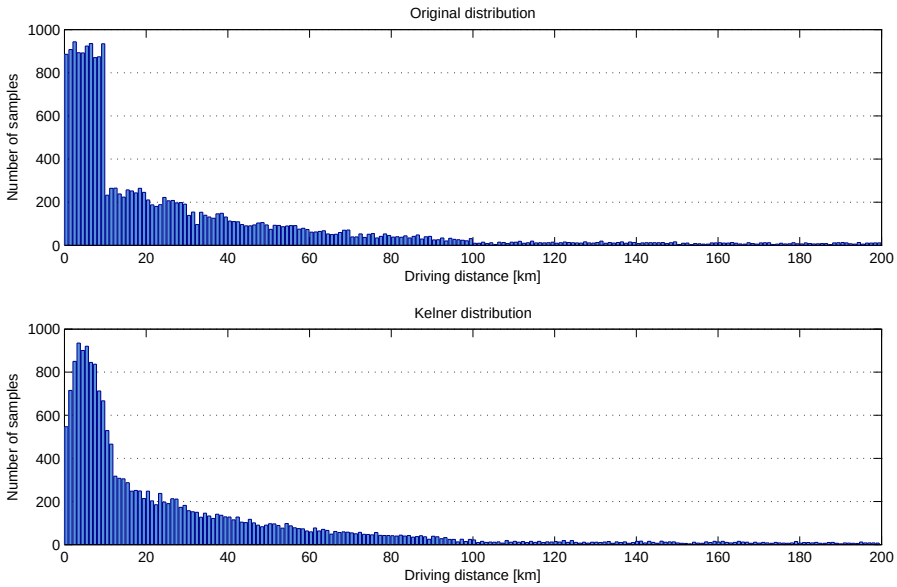

Figure 3.16: Individual driving distances

In the next step, 100 driving distances are picked from the Kernel distribution pool. These samples are shown in Fig. 3.16. The results exhibit the same properties as the original data. Most of the driving distances are in the 0-40km distance range. The lowest value is 0km and the highest 160km. In order to provide energy to drive 160km, the EV battery capacity has to be at least 24kWh. In case the battery of the car, supposed to drive 160km does not have enough capacity, the car will require an additional charging away from home or needs to be charged twice at home during the day.

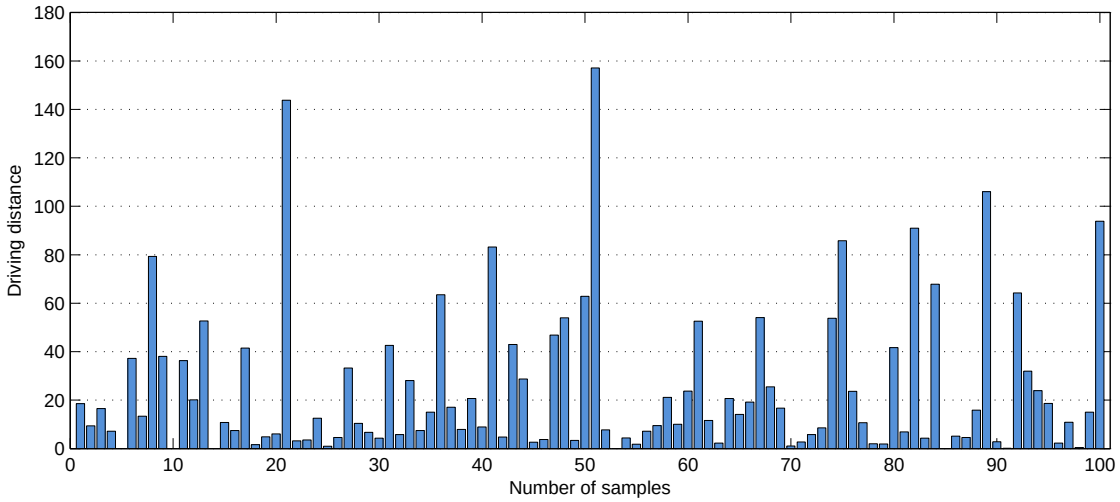

Figure 3.17: Estimated driving distances

Now the driving distance of 100 EVs has been obtained. The next step is to estimate when the EV are available at the household and when away. The data available only states when the cars are driving and not which does not correspond very well with the needs for the project driving patterns. It is needed to know exactly when the EVs arrive to- and leave the household. This issue has been solved by making the assumption that an EV only leaves the household once a day as well as arrives at the household only once a day. This procedure does not reflect reality completely, but is assumed to be

an assumption which fits the objectives of the project and DSL models sufficiently well.

Two normal distribution functions has been fitted to match the curvature of Fig. 3.14 in order to generate the time instants for when the cars leave the houses and when cars come back. An additional assumption concerns the unavailability time which must match the respective distance estimated previously. This means the car is not able leave home at 9:00 and come back at 10:00 and drive 150km. In such cases the time of arrival has been delayed.

The leaving and coming functions are estimated according to following parameters:

- Leaving distribution: Mean value equal to 8 (implies 8:00) with variance equal to 1.5h
- Coming distribution: Mean value equal to 17 (implies 17:00) with variance equal to 1.5h

By using the MATLAB random function with the two normal distributions, 100 different time instants for leaving and 100 time instants for coming events have been prepared which are shown in Fig. 3.18. The horizontal axis illustrates the time intervals where the EVs leave house(blue bars) or come back (orange bars). The vertical axis illustrates the number of cars that leave or come within a particular time interval. The additional two lines illustrate the ideal distribution functions to compare the achieved distribution with the patterns.

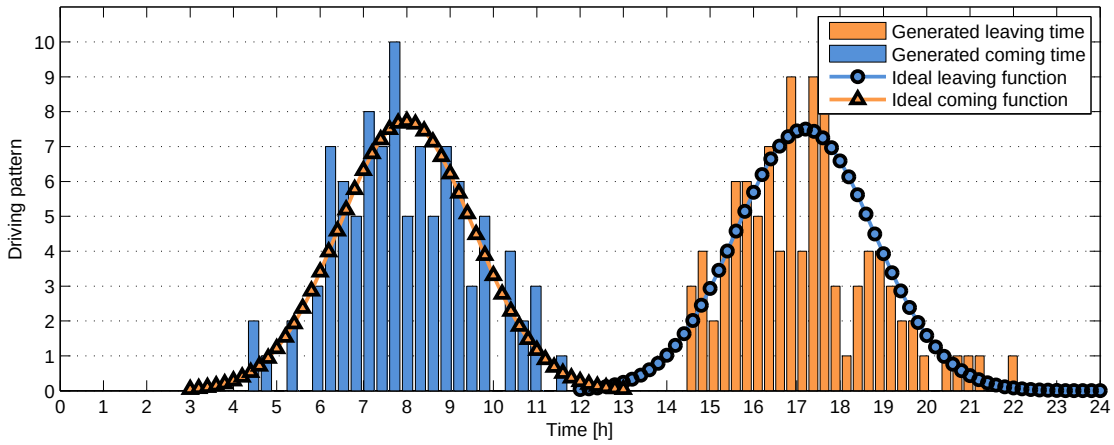

Figure 3.18: EV availability functions

Combination of the obtained driving distances with the leaving and coming instants allows to build the final 100 different driving patterns. These are shown in Fig. 3.19. The orange bars represent the time where the EVs are unavailable and the blue bars represent times where the EVs are available. This data-set will provide the base for the study cases conducted in chapter 5 and 6.

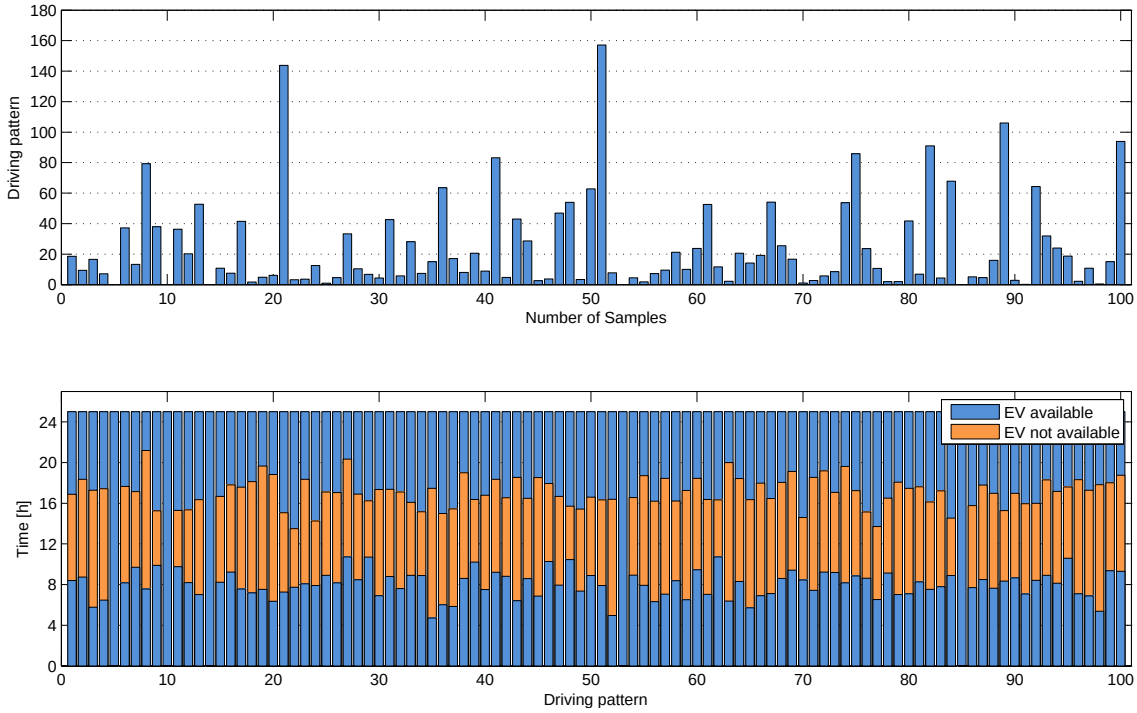

Figure 3.19: Driving patterns

4 Steady State Analysis

This chapter will contain a study of the behaviour of LV-I and LV-II in a future scenario with a high penetration of electric vehicles and heat pumps.

The objectives of the steady state analysis are as follows:

- A diagnose of weak as well as strong points in the LV grids
- An investigation of the maximum possible grid utilization using static HP and EV models
- An investigation of the improvements in grid utilization by closing the tie-point in LV-II

The first section of the chapter will present the behaviour of the grids as they are today without additional loads implemented. This special case will be used as a reference to be able to have a scale for the gained results in coming sections and chapters.

The second section will present the static models of the heat pump and electric vehicle as well as how the models are implemented in DIgSILENT PowerFactory, which is where the load flow analysis has taken place.

The behaviour of the grids are highly dependent upon the seasonal variance in the household power consumption. As the grids are affected, this also affects the amount of electric vehicles and heat pumps which are able to be implemented before reaching technical constraints. The seasonal variances are presented in the third section.

A somewhat thorough presentation of the implementation methodologies will follow the seasonal dependency. The term implementation methodology covers the algorithms developed in order to implement the static models of the EVs and HPs in the grids following specific methods designed to reflect various scenarios.

As the last section, the results of steady state analysis are presented. The results are divided into two sub-sections, namely the identification of grid bottlenecks and a presentation of the maximum possible grid utilization. The term maximum grid utilization covers the quantification of how many of the new large loads can be accommodated into the LV grids without violating technical limits and without implementing any grid reinforcements.

4.1 Current Grid Utilization

This section illustrates the results of load flow studies with zero EV and HP penetration. This study has been performed in order to have a reference for the further studies in the project. Specifics about

single feeders, cable cross-sections etc. is to be found in section 4.4.

The bar-plots presented in Fig. 4.1 and 4.2 represent the loading of the grid seen from the 10/0.4kV supply transformers. The blue bars represent the loading throughout the day during winter. The red bars represent a summer scenario.

As the consumers of LV-I and LV-II are supplied by district heating the bar-plots represent only electric loading.

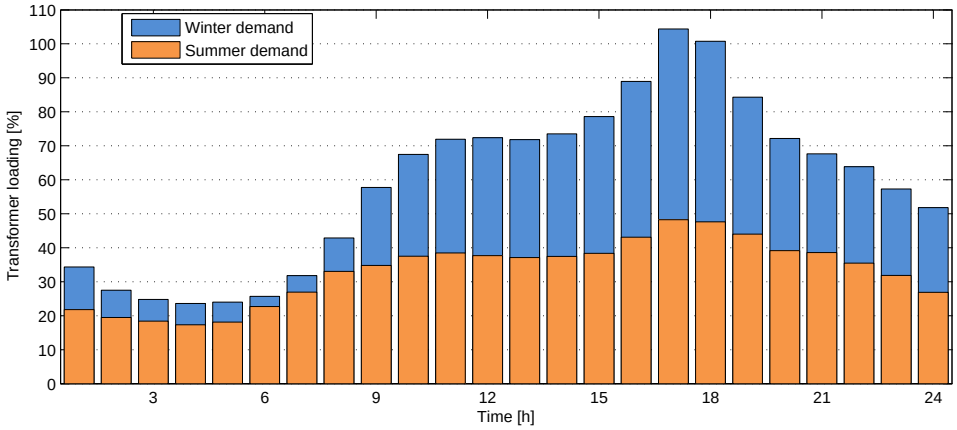

Figure 4.1: LV-I Transformer loading - Winter - No units

As presented in section 3.2, LV-I is supplied by a 400kVA transformer. Fig. 4.1 shows that during summer, the transformer is loaded by roughly 10% of nominal capacity. During winter this transformer is loaded by roughly 20% of maximum capacity.

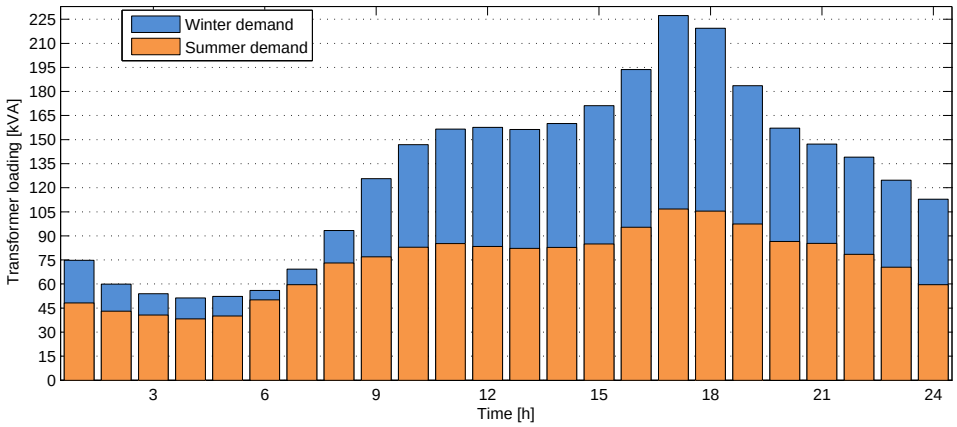

Figure 4.2: LV-II Transformer loading - Winter - No units

LV-II is supplied by a 630kVA transformer since it supplies roughly the double amount of loads than LV-I. Fig. 4.2 shows that during summer, the transformer is loaded by roughly 15% of nominal capacity. During winter this transformer is loaded by roughly 20% of maximum capacity.

Both grids therefore have free transformer capacity available for the implementation of additional loads in form of HPs and EVs. The primary limiting factor for the implementation of additional units is the node voltages in specific feeders. This topic will be discussed in detail during the chapter.

The difference between night and day consumption can be divided into two large groups. Namely the base consumption which occurs at night and the day-time consumption. The base consumption consists primarily of the consumption from cold appliances (freezers/fridges) as well as stand-by consumption (TV, radio etc.) [34]. The day-time consumption is harder to define explicitly. Basically the day time consumption occurs due to the active use of electric appliances within the household. The day time consumption is affected of the time of day though. As people in general get off work during the afternoon, the consumption is bound to rise as they arrive at home. Dinner has to be prepared, clothes needs to be washed etc.. The varying day time consumption is therefore hard to define, except for tendency that the more people are home and awake, the higher the consumption will be.

The seasons also clearly has an influence on the transformer load profiles presented in Fig. 4.1 and 4.2. Yet again, many factors influence the great difference between winter and summer consumption. A quite interesting fact is that the night time consumption does in-fact not differ much between summer and winter. As the night time consumption roughly equals the base consumption mentioned in the previous paragraph, the similar night time consumption does make sense.

The lower day-time consumption during summer is a product of a multiple of reasons. One factor is the lighting demand difference between winter and summer. The lighting demand during winter is roughly 50% higher than during summer [35]. Another factor is that a greater amount of outside activities take place during summer which limit the amount of people at their homes.

4.2 Static Models

In order to investigate the impact of a high penetration of electric vehicles and heat pumps in the future Danish distribution systems, models of a 3.1kW heat pump with a power factor of 0.98 [36] along with an 11kW electric vehicle charger with unity power factor have been implemented in the models of LV-I and LV-II in DIgSILENT PowerFactory. The actual implementation of the units has been carried out in an unconventional manner in order to ease the investigation process. Fig. 4.3 shows an example of an arbitrary grid containing two households connected at a busbar.

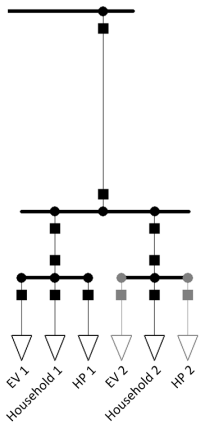

Figure 4.3: Implementation of static loads

Fig. 4.3 shows two households, *Household 1* and *Household 2*. These two loads exist in the grids

as they are today. In the models of the future grids, used in this chapter as well as in the following chapters, all households of LV-I and LV-II has been extended to contain an EV and a HP. In order to implement a specific amount of HPs and EVs, all the units was put *Out of Service* using an in-built function of PowerFactory and hereafter put back into service where needed. In Fig. 4.3 *EV 1* and *HP 1* are in service contrary to *EV 2* as well as *HP 2*, which are out of service. Units which are out of service are greyed out.

4.3 Implementation Methodology

One of the primary goals of this chapter to estimate the amount of free LV grid capacity possible to utilize for accommodating heat pumps and electric vehicles before violating technical limits. Three different algorithms have been developed in order to meet the objectives stated in the beginning of this chapter. The algorithms are designed in order to investigate the following scenarios:

- The effects of a plain and even distribution of units (*the uniform algorithm*)
- The effects of a close-to worst case distribution of units (*the adverse algorithm*)
- The effects of an absolute worst case distribution of units (*the bottleneck algorithm*)

The bottleneck algorithm is increasing the EV and HP penetration one by one with respect to a pre-set sequence until the weakest node violates one of the technical limitations. The unit list represents the order by which the units are implemented. The unit list is an array containing the sequence of EVs and HPs implemented. An example of the unit list is shown in Table 4.1.

N	Unit
1	HP
2	EV
3	HP
4	HP
5	EV
6	HP
7	HP
8	EV
9	HP
...	...

Table 4.1: The unit list sequence

The unit list is designed with respect to meet two criteria. The first being the ratio of 2:1 between HPs and EVs respectively. The ratio is given by the assumption that in 2025 50% of households not covered by district heating will have a heat pump and 25% of households will have an EV. In a (somewhat unrealistic) scenario where no grid constraints would be reached, the unit list would ensure that the percentages are reached and kept with respect to each other. The list starts with a HP followed by an EV. This is not a coincidence. In a (bottleneck) scenario a specific node in a grid could be so weak, that a HP (3.1kW) could be implemented, but not an EV (11kW). Therefore, by starting the list with a HP the possibility of obtaining a greater resolution in the gained results is reached.

The two other algorithms reach the same goal in another manner which will be presented in their respective sub-sections.

All of the algorithms has been implemented using a one hour step size and has adopted the technical constraints listed in Table 4.2

Target	Limit
Voltage [pu]	1 ± 0.06
Current [A]	$I \leq I_{max}$
Power [P]	$P \leq P_{max}$

Table 4.2: Technical constraints

4.3.1 The Bottleneck Algorithm

The bottleneck algorithm will be used to run the absolute worst case scenario. The algorithm will run a load flow simulation, identify the weakest node (bottleneck), add a unit to the weakest node and repeat the process until a technical limit is reached. A graphical representation of the working of the bottleneck algorithm is represented by the flow chart presented in Fig. 4.4.

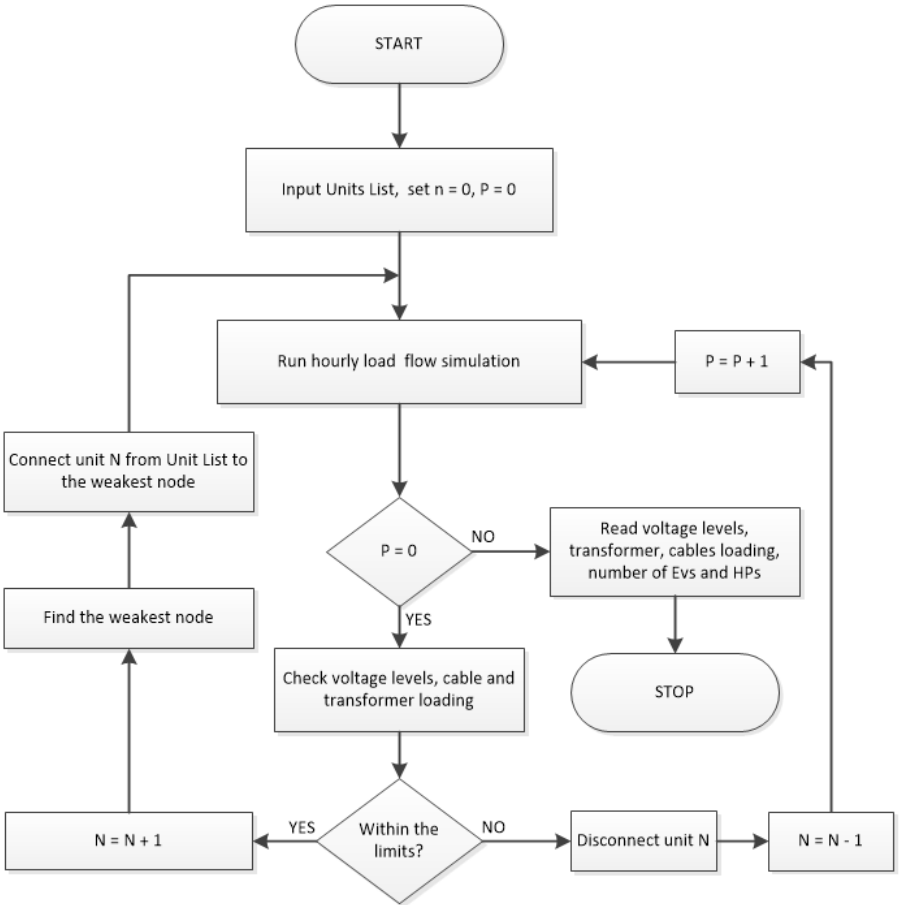

Figure 4.4: Bottleneck algorithm flowchart

In accordance with Fig. 4.4, the algorithm starts by setting the number N = 0 (EVs + HPs = 0). Hereafter, the process checks the current status of the grid, hence the load flow simulation. If the grid constraints

from Table 4.2 are not violated, the process continues into the left-side loop. At this stage number of units is increased to N = N + 1 = 1 and the first load from the priority list is connected to the weakest node. Each of the loops entail running a load flow analysis in order to verify the grid status and identify the weakest node. In case the transformer, a node or a cable is not in compliance with the technical limits, the algorithm disconnects the last connected unit (N = N - 1), runs a final load flow simulation and returns the results. The *P* variable therefore controls when to stop the process and the *N* variable represents the N'th unit of the unit list.

4.3.2 The Adverse Algorithm

The second algorithm, named adverse, has been designed with focus on identifying the weakest and strongest feeders in the grids. It does so by adding a single unit to the furthest node from the transformer in the string with the lowest unit penetration. The adding of units will keep on going until a technical limit is violated.

The number of EVs, HPs and households have been multiplied by 10. The reason for doing so, is to be able to choose the feeder containing the most households, which is where the first unit should be implemented. This concept will become more clear throughout the sub-section.

In order to present the algorithm, an overview of notations and variables will be given:

- Var (*notation*): Variable
- x (*notation*): Feeder number
- P (*variable*): Used in the algorithm to stop the process

  P = 0 (continue), P = 1 (stop)
- NEV (*variable*): Denotes 10 times the number of EVs in the grid

  The actual number of EVs is the rounded value of NEV / 10

  Ex. NEV = 31 equals 3 EVs
- NHP (*variable*): Denotes 10 times the number of HPs in the grid
- UP (*variable*): Denotes an artificial unit penetration per household in a feeder

  UP equals NEV + NHP divided by the number of households in the feeder times 10

In the next part of this sub-section Fig. 4.5 and Table 4.3 are presented. The figure represents the flowchart of the adverse algorithm. The table represents the L-matrix for LV-II wherein the parameters, post initialization of the adverse algorithm process, are presented followed by two iterations of the algorithm.

According to Fig. 4.5, the algorithm starts with the initialization of P = NHP = 0 and NEV = 1. The initialization of NEV = 1 is carried out in order to initialize the UP-value. If NEV = 1 had not been set, all UP-values would be zero and the process would break down. NEV = 1 therefore ensures that the block in the left side loop containing the following statement

- *Go to the L-matrix and choose feeder x containing the lowest UP-value*

will pick the correct feeder during the first loop.

Following the initialization, a load flow analysis is run in order to check the grid status, to decide if to go to the left side loop (*continue*) or the right side loop (*stop*).

The left side loop updates the L-matrix with the values from the initialization (or previous iteration), picks the feeder x with the lowest UP-value and read NEV and NHP of feeder x.

The decision-block containing

- *NHP(x) / NEV(x) < 2*

performs a similar job to the unit list presented (Table 4.1) in the previous section. It ensures a high resolution by always starting by implementing a HP followed by an EV as well as ensuring the ratio 2:1 between HPs and EVs.

Depending on the unit connected, NEV(x) or NHP(x) will be increased by 10 (one unit). The sum of NEV(x) and NHP(x) will be exported to the L-matrix during the following loop and used to calculate the new UP(x) value.

The UP-values ensure that the ratio, unit per household, is kept close for every feeder. This ensures that the goal of comparing the strength of the feeders to each other is met.

When a violation of a technical limit occurs, the process will enter the right side loop (the stop-loop). The stop-loop removes the last load added in the grid to prepare the output of the results. The L-matrix is then updated with the final values, P is set to P = 1 (stop command), the process reads and outputs all relevant values and stops the process.

Table 4.3 serves two purposes. It presents the L-matrix as well as an example of how the L-matrix is updated throughout two iterations. Important cells are highlighted using bold text.

Iteration	Var	Feeder 1	Feeder 2	Feeder 3	Feeder 4	Feeder 5	Feeder 6	Feeder 7
	NEV	1	1	1	1	1	1	1
-	NHP	0	0	0	0	0	0	0
	UP	1/200	1/330	1/270	1/280	1/170	**1/390**	1/20
	NEV	1	1	1	1	1	1	1
1	NHP	0	0	0	0	0	10	0
	UP	1/200	**1/330**	1/270	1/280	1/170	**11/390**	1/20
	NEV	1	1	1	1	1	1	1
2	NHP	0	**10**	0	0	0	10	0
	UP	1/200	**11/330**	1/270	**1/280**	1/170	11/390	1/20

Table 4.3: The L-matrix with initialization (-) and two iterations (1)(2)

Either one of the rows (-, 1 or 2) represents a single snapshot of the L-matrix after receiving an update from one of the two update-blocks.

During the initialization (-), NEV is set to NEV = 1. It is seen that performing this task gives the UP-values a value of 1 divided by by the number of loads in the feeder multiplied by 10. By doing so it is possible to differentiate the unit penetration in the strings even at the point where no units have been

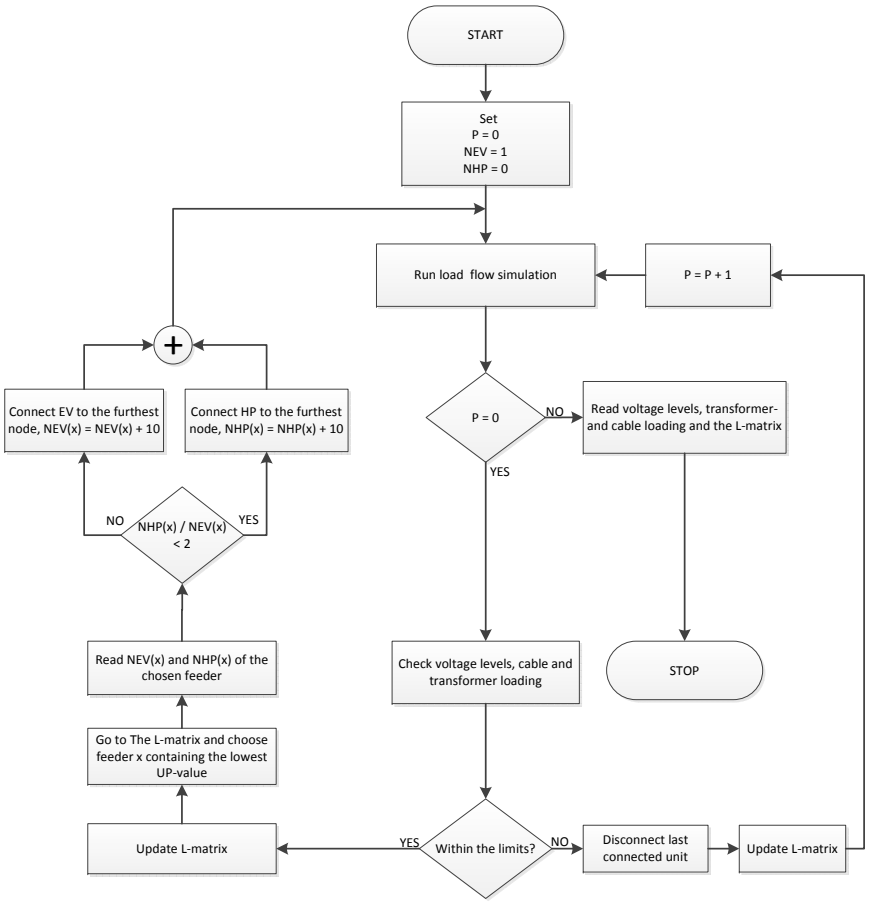

Figure 4.5: Adverse algorithm flowchart

added. Feeder 6 has the lowest UP-value after initialization.

During the first iteration, the process is adding a HP to the end of feeder 6 since UP(6) had the lowest value.

During the second iteration, UP(2) has the lowest value and therefore a HP is added in the end of feeder 2.

The process continues adding units to the feeders according to the method presented above, until a technical limit is violated.

4.3.3 The Uniform Algorthm

This sub-section will present the uniform algorithm. The goal of the algorithm is to implement a scenario where the units are spread out in a uniform manner. This distribution is assumed to represent the most realistic scenario of the three algorithms presented.

The uniform algorithm is similar to the adverse algorithm presented in the previous subsection, but represents a very different scenario. Much of the information given in the previous sub-section will therefore be much alike the information presented during this sub-section.

The uniform algorithm will choose the feeder with the lowest unit penetration and add a unit in the middle of the string. The process will keep adding units in the middle of the feeders until a feeder has six (or a multiple of six) units (two EVs, four HPs). At this point, the six units will be removed from the middle of the feeder, and three units (one EV, two HPs) are moved to the end closest to the main busbar and three moved furthest from the busbar. The units are therefore spread out across the feeder.

The approach of adding and splitting units has, through manual load flow analysis, been found to represent the uniform methodology nicely. The manual load flow analysis showed that the lowest voltage in a specific feeder remained *more or less* constant before and after the split.

The uniform algorithm therefore adds units in a manner which represents an even distribution of units across the feeders.

In order to present the algorithm, an overview of notations and variables will be given:

- Var (*notation*): Variable
- x (*notation*): Feeder number
- P (*variable*): Used in the algorithm to stop the process

  P = 0 (continue), P = 1 (stop)
- NEV (*variable*): Denotes 10 times the number of EVs in the grid

  The actual number of EVs is the rounded value of NEV / 10

  Ex. NEV = 31 equals 3 EVs
- NHP (*variable*): Denotes 10 times the number of HPs in the grid
- D (*variable*): Counter for HPs and EVs.

  Implemented since NEV and NHP is reset by the algorithm.

  D = 1: Represents two EVs and four HPs

  D = 2: Represents four EVs and eight HPs
- UP (*variable*): Denotes an artificial unit penetration per household in a feeder

  UP equals NEV + NHP + 60D divided by the number of households in the feeder times 10

In the next part of this sub-section Fig. 4.6 and Table 4.4 are presented. The figure represents the flowchart of the uniform algorithm. The table represents the L-matrix for LV-II wherein the parameters after the initialization are presented. The L-matrix for the uniform algorithm is slightly different than the L-matrix for the adverse algorithm as it also contains the *D* variable.

According to Fig. 4.6, the algorithm starts with the initialization of D = P = NHP = 0 and NEV = 1. The initialization of NEV = 1 is carried out in order to initialize the UP-value. If NEV = 1 had not been set, all UP-values would be zero and the loop would break down. NEV = 1 therefore ensures that the block in the left side loop containing the following statement

- *Go to the L-matrix and choose feeder x containing the lowest UP-value*

will pick the correct feeder during the first loop.

Following the initialization a load flow analysis is run in order to check the grid status to decide if to go to the left side loop (*continue*) or the right side loop (*stop*).

The left side loop updates the L-matrix with the values from the initialization (or previous iteration), picks the feeder x with the lowest UP-value and read NEV and NHP of feeder x.

The decision-block containing

- *NHP(x) / NEV(x) < 2*

performs a similar job to the unit list presented (Table 4.1) in the previous section. It ensures a high resolution by always starting by implementing a HP followed by an EV as well as ensuring the ratio 2:1 between HPs and EVs.

Depending on the unit connected, NEV(x) or NHP(x) will be increased by 10 (one unit). The following block

- *NEV + NHP = 61?*

will check the sum of NEV(x) and NHP(x). If the sum of 61 has been reached, six units have been added in the middle of the feeder. If the statement is true, the units in the middle of the feeder will be disconnected, split into two identical groups and reconnected at the beginning and end of the string. Following a split NEV and NHP are re-initialized and D = D + 1.
The UP-values ensure that the ratio, unit per household, is kept close for every feeder. This ensures that the goal of of achieving a uniform distribution is met.

When a violation of a technical limit occurs, the process will enter the right side loop (the stop-loop). The stop-loop of the uniform distribution offers the possibility of closing tie-points, if the results gained are not deemed to be satisfying. The stop-loop can therefore exit the loop if the possibility to close tie-points exists and is desirable. Every time the process enters the stop loop, the results will be read and a tie-point (if possible, and not all tie-points has already be closed already) will be closed, restarting the process, or the process will stop.
Table 4.4 presents the L-matrix of the uniform distribution. The values in the table are presented for LV-II after initialization of the process.

Iteration	Var	Feeder 1	Feeder 2	Feeder 3	Feeder 4	Feeder 5	Feeder 6	Feeder 7
	D	0	0	0	0	0	0	0
-	NEV	1	1	1	1	1	1	1
	NHP	0	0	0	0	0	0	0
	UP	1/200	1/330	1/270	1/280	1/170	1/390	1/20

Table 4.4: The L-matrix for LV-II after initialization for the uniform algorithm

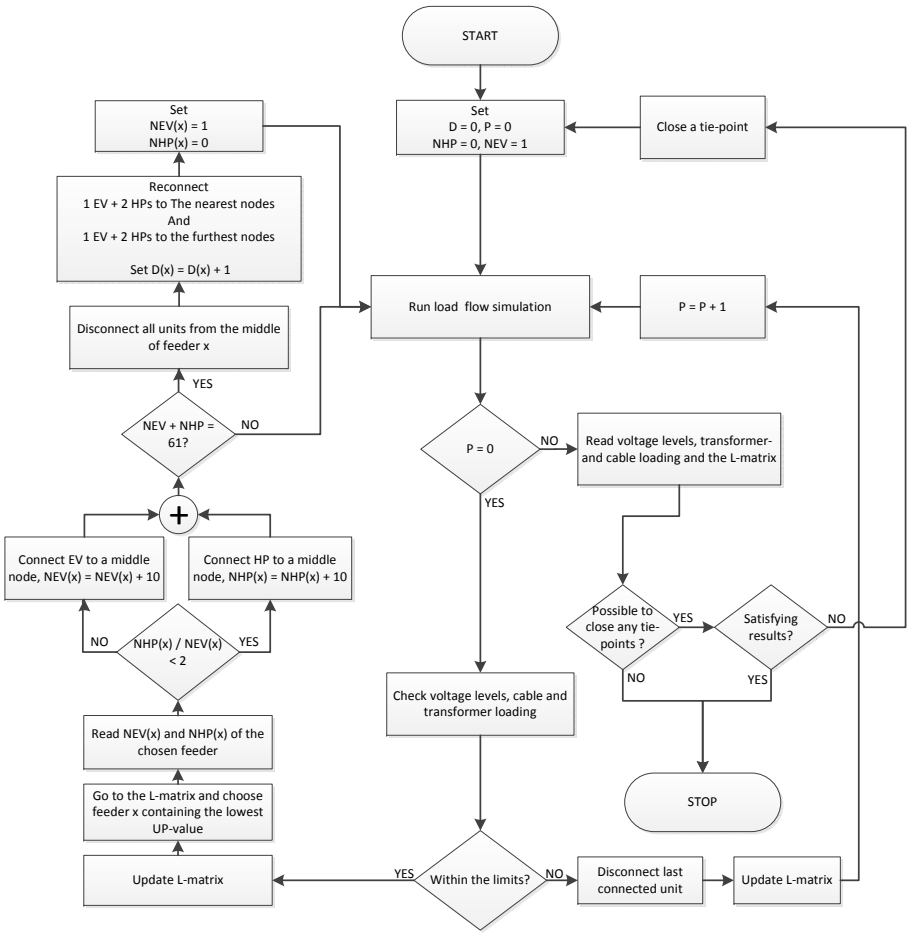

Figure 4.6: The uniform algorithm

4.4 Results

This section presents the results gained by use of the three algorithms presented in the previous section.

The first sub-section will present the worst case performance of the two LV-grids.

The second sub-section will present the maximum possible amount of units which can be run simultaneously seen from a steady-state perspective. The maximum grid utilization will be tested with both the adverse- (worst-case) and uniform algorithm. The steady-state maximum grid utilization results will be relevant to the further work as they show the amount of units which can be run simultaneously at some given point of time.

Finally, the conclusions of each case will summed up and presented as whole in the last sub-section.

4.4.1 Absolute Worst Case Performance

This sub-section presents the results of the absolute worst case scenario for each of the two grids. In order to achieve the worst possible conditions, the bottleneck algorithm will be used. The household

load scenario will be a winter work day at 17:00 which is when the peak consumption occurs.

The results will be presented, according to the algorithm, as the amount of units possible to implement before the technical limits are violated. The technical limits of interest is the transformer- and loading as well as the voltage level. The voltage level is the bottleneck of the grid performance in both grids and has been the parameter which has constrained the possibility of adding more units during all simulations. The cable loading has not exceeded 80% during any simulations.

Table 4.5 presents the results gained by using the above-mentioned procedure. Three cases are presented. First, a reference scenario, where no units has been implemented. The second and third cases are performed utilizing two different voltage limits to investigate the effects it has on the results. The highest cable loading on the table covers the 3 most heavily loaded cables in the grid when the process stops.

The the bottleneck algorithm started adding units at the end of feeder 6 in LV-II and in the end of feeder 4 in LV-I.

LV Grid	**Scenario**	**Lowest voltage**	**Highest cable loading**	**Transformer load**	**EVs**	**HPs**
-	-	pu	%	%	-	-
LV-I	No units	0.98	10-14	25.3		
LV-II	No units	0.93	46-49	35.4		
LV-I	V > 0.94	0.94	36-41	37.9	3	5
LV-II	V > 0.94	0.93	46-49	35.4	0	0
LV-I	V > 0.90	0.9	60-75	50.8	5	11
LV-II	V > 0.90	0.9	59-61	39.5	1	1

Table 4.5: Absolute worst case results for LV-I and LV-II

Table 4.5 shows that LV-I in general is much stronger than LV-II. The reasons for this are multiple.

Generally speaking, the feeders in LV-II are longer than the feeders of LV-I. Therefore the effective mean value resistance between consumer and transformer is higher for LV-II than for LV-I. Common practice in LV grid feeders is to have high cross-section cables close to the main busbar and lower cross-section cables further from the busbar in order to match the cable capacity to the cable loading. In LV-II the "switch" from higher-to-lower cross-section cables in general occur closer to the busbar than in LV-I. This further increases the difference in the effective mean value resistance between consumer and transformer in the two grids.

As LV-II has roughly twice the consumers of LV-I, divided between a similar amount of feeders, the loading of the feeders in LV-II is roughly twice as loaded as LV-I. Twice the loading coupled with a high mean value effective resistance makes LV-II a much weaker grid than LV-I.

The results also show that LV-II during a winter day at 17:00 will have a very limited capacity of running HPs or charging EVs in the end of string 6. LV-I has way better properties regarding the running of units during worst place and worst time scenarios.

4.4.2 Feeder Comparison

This sub-section will contain the results obtained by using the adverse and uniform algorithms. The algorithms have been utilized in order to identify strong and week feeders which is presented in the

beginning of the subsection.

Table 4.6 and 4.7 present the results of the feeder identification. The results presented in the tables have been obtained by carrying out the following studies for a winter- and a summer scenario for both grids:

- No-unit grid performance
- Adverse algorithm grid performance (unit implementation farthest from transformer)
- Uniform algorithm grid performance (unit implementation evenly distributed across feeders)

Carrying out and comparing the various studies have been done in order to increase the validity of the gained results.

Table 4.6 shows the results of the feeder comparison of LV-I.

Scenario	**Season**	**Time**	**F1**	**F2**	**F3**	**F4**	**F5**	**F6**	**F7**	**F8**
			V	V	V	V	V	V	V	V
		h	pu	pu	pu	pu	pu	pu	pu	pu
No units	Winter	17:00	0.98	0.98	0.98	0.98	0.98	0.98	0.99	0.98
Adverse algorithm	Winter	17:00	0.95	0.96	0.96	0.94	0.96	0.97	0.98	0.94
Uniform algorithm	Winter	17:00	0.95	0.95	0.97	0.94	0.95	0.96	0.97	0.95
No units	Summer	04:00	0.99	0.99	0.99	0.99	0.99	0.99	0.99	0.99
Adverse algorithm	Summer	04:00	0.96	0.96	0.96	0.94	0.96	0.97	0.98	0.95
Uniform algorithm	Summer	04:00	0.96	0.95	0.96	0.94	0.96	0.97	0.97	0.95

Table 4.6: Identification of strong and weak feeders, LV-I

The applied methodology has shown that feeder 4 is the weakest feeder when compared to the remaining feeders. This result does not imply that LV-I is a weak grid though.

In reality it is difficult to distinguish between the weak and strong feeders in LV-I by use of common load flow analysis. During a winter work day (without any units added), the maximum voltage drop in the entire grid is only 0.02 pu and the highest cable loading only 14%. Such numbers usually represent a grid of high strength.

When looking at the raw grid data (cross-sections and length of cables, distribution of loads between feeders etc.), it is quite difficult to locate issues or abnormalities within the LV-I grid-design. The feeders approximately have the same length, use similar cables and the loading is more or less evenly distributed which is what makes the voltage profile across the feeders much alike and therefore the grid performance very uniform.

The aspect that makes feeder 4 weaker compared to the others strings, is therefore the number of consumers. Feeder 4 supplies 20 households through 150mm^2 cables. All other feeders are equipped with the same 150mm^2 cable but are supplying a, in some cases, quite noticeably less number of consumers.

By use of the argument of consumers per feeder, the strongest strings are feeder 6 and 7 which only supply only 8 and 6 households respectively. This statement is supported by results shown in table 4.6.

When combined, the study of the raw grid data and the feeder identification show that even the weakest feeder of LV-I relatively seen is rather strong and definitely capable of adopting additional loads, even under worst case conditions.

Table 4.7 shows the results of the feeder comparison of LV-II.

Scenario	**Season**	**Time**	**F1**	**F2**	**F3**	**F4**	**F5**	**F6**	**F7**
			V	V	V	V	V	V	V
		h	pu	pu	pu	pu	pu	pu	pu
No units	Winter	17:00	0.96	0.96	0.97	0.97	0.97	0.93	0.99
Adverse algorithm	Winter	17:00	0.96	0.96	0.97	0.97	0.97	0.93	0.99
Uniform algorithm	Winter	17:00	0.96	0.96	0.97	0.97	0.97	0.93	0.99
No units	Summer	04:00	0.99	0.99	0.99	0.99	0.99	0.99	0.99
Adverse algorithm	Summer	04:00	0.95	0.96	0.97	0.97	0.97	0.94	0.99
Uniform algorithm	Summer	04:00	0.96	0.96	0.98	0.97	0.97	0.94	0.99

Table 4.7: Identification of strong and weak feeders, LV-II

Table 4.6 shows that feeder 6 is by far the weakest feeder of LV-II. The bad performance is represented by the high voltage drop seen at the furthest nodes of the feeder. The feeder is not even able to stay above the voltage limit of 0.94 pu even without the addition of any units. Within the winter work day, the measured node voltages cross the adopted voltage limit [20] of 0.94 pu. This has the effect that, if the voltage limit were to be respected, LV-II as whole would not able to adopt any furthers loads than the ones currently existing.

The primary reason for the significant voltage drop, is the relatively high loading of the five first cables of feeder 6 which are connected in series to the main busbar. The average loading of those cables is approximately 43% up to a maximum of 49% while the transformer loading is only 37%. The distance between the main busbar and the end of the five first cables is only half of the total distance between transformer and the furthest nodes. At the end of the five first cables, the voltage is approximately 0.95 pu. The voltage drop present in the beginning of feeder 6 is therefore the primary reason for the voltage drop equal to 0.93 pu at the furthest nodes. The cables in question are depicted in Fig. 4.7

The voltage drop indicates that the cross-section of the first five cables installed closest to the main busbar is too small. The first 300 meters of cable in feeder 6, carrying the full load from 33 consumers, has a cross-section of only 50mm^2. As a comparison, the strongest feeder of LV-II (feeder 3) supplies 28 households by 160 meters of 150mm^2 cables followed by 95mm^2 cables. The distance between transformer and the furthest consumer is roughly 600 meters in both feeder 3 and 6 but due to the difference in cable cross-sections, the maximum voltage drop is less than 0.03 pu in feeder 3. During the winter day the maximum cable loading cable loading is no more than 12%.

The comparison clearly shows the difference in the effective mean value resistance from load to transformer between feeder 6 and feeder 3. If taking all the previous statements into account, the differences between the feeders makes up for a high contrast between the performance of feeder 6 and 3 which is also reflected by the results presented in table 4.7. Feeder 6 is not capable of handling any additional loads, but due to the cross-sections of the cables and the fact that the feeder is already supplying roughly the double amount of loads than some of the stronger feeders, this were to be expected. This indicates a somewhat improper grid-design which does not allow for a higher transformer utilization due to the weakness of one single feeder. The remaining feeders are in general

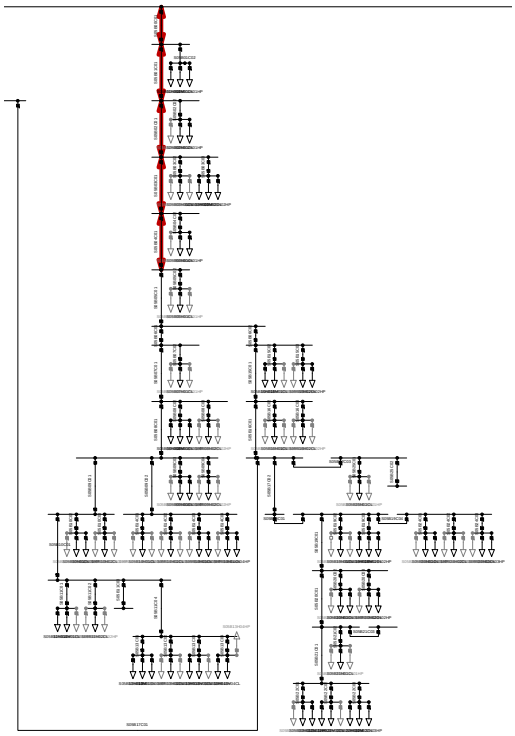

Figure 4.7: Low cross-section cables of LV-II, feeder 6

relatively strong and able to adopt further loads.

4.4.3 Maximum Grid Utilization

This sub-section contains a presentation of the results gained by investigating the maximum possible amount of units possible of running simultaneously throughout a day during different seasons.

The studies have been carried out using the adverse- and uniform algorithm in order to present results from a worst case perspective and a somewhat more realistic perspective, respectively.The uniform algorithm is therefore used in order to obtain results corresponding to the more realistic future scenario where the running of units will be spread out somewhat evenly across the grid. The adverse algorithm is used to represent the scenario, of lesser occurrence, where the units running unfortunately could be consuming power at the weakest nodes of the grid simultaneously.

The studies has been carried out with the ability to change various parameters such as the following:

- Grid (*LV-I* / *LV-II*)
- Season (*Summer* / *Winter*)
- Tie-point position (*Open* / *Closed*)

  Only applicable for LV-II

The scenarios presented in this sub-section are the following:

- LV-I - Winter - Uniform algorithm (Fig. 4.8)
- LV-I - Winter - Adverse algorithm (Fig. 4.9)
- LV-II - Winter - Uniform algorithm - Tie points open (Fig. 4.10)
- LV-II - Winter - Uniform algorithm - Tie points closed (Fig. 4.11)
- LV-II - Winter - Adverse algorithm - Tie points closed (Fig. 4.12)

Appendix A.1 contains the corresponding results of the summer time studies.

All graphs are divided into an upper and lower section. The upper section represents the transformer utilization, which reflects the grid utilization. The red line represents the utilization without the addition of any units. The blue line represents the utilization with the maximum amount of loads implemented in the grid as the voltage limit of 0.94 pu [20] is reached. The notation *CL* (Common Load) represents the load present due to the regular consumers in the grids. The difference between the blue and red curves can be looked upon as being the free capacity of the grid at the particular hour of the day.

The lower section represents the amount of units possible to run simultaneously during a specific hour of the specific case study. The blue bars represent the number of HPs running and the red bars represent the amount of EVs running.

The first two cases present a winter time scenario at 17:00 in LV-I using the uniform and adverse algorithms.

Fig. 4.8 shows the LV-I winter scenario investigated using the uniform algorithm. The results show that the loading present in the grid due to existing consumers loads the grid only lightly. Therefore, a great amount of EVs and HPs are possible to run simultaneously throughout the whole day. It is seen

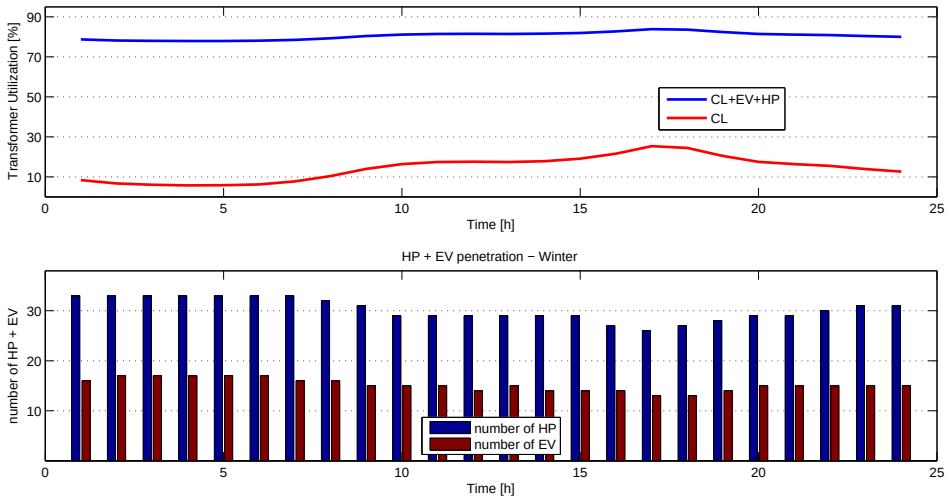

Figure 4.8: Maximum grid utilization: LV-I - Winter - Uniform algorithm

in the upper part of the figure, that the transformer utilization is at roughly is 20% without units and 80% with units. Due to the uniform and strong grid-design of LV-I, the utilization of the grid with the addition of the maximum possible amount of units therefore is very high. Roughly 30 HPs and 15 EVs would be able to run simultaneously throughout the whole day assuming that the load from the units are spread out evenly across the grid.

Fig. 4.9 shows again the winter scenario for LV-I, this time carried out using the adverse algorithm. This algorithm represents a worst case scenario as discussed earlier in the report. A comparison of the results obtained by using the uniform algorithm to the results gained by use of the adverse algorithm shows only small differences. The uniformity of feeders, high cross-section cables, few consumers per feeder and overall strength of LV-I makes possible for the grid to perform well even during bad operating conditions.

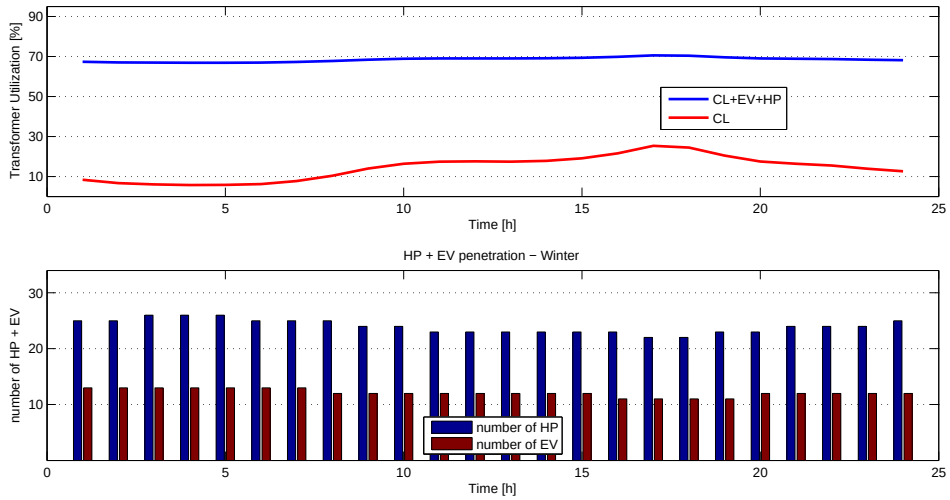

Figure 4.9: Maximum grid utilization: LV-I - Winter - Adverse algorithm

Ideally, assuming the desire of a 50%/25% HP-/EV penetration in 2025, LV-I needs to be able to adopt the load from approximately 40 HPs and 20 EVs. The results presented in Fig. 4.8 and 4.9 suggests

that the desired unit-penetration could possibly be reached without having to reinforce the grid considerably.

Fig. 4.10 shows the LV-II (open tie-points) winter scenario investigated using the uniform algorithm. As the tie-points are open, this scenario represents the operation of LV-II as it is in real life today. The uniform algorithm represents the uniform distribution of units which is the better-case distribution considering the alternative algorithms designed in this project.

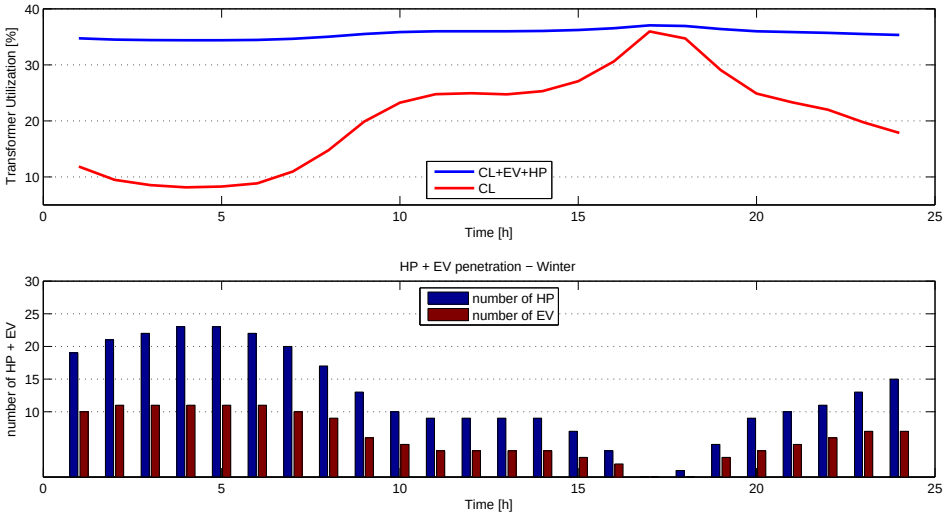

Figure 4.10: Maximum grid utilization: LV-II (tie-points open) - Winter - Uniform algorithm

It is seen that the transformer utilization is poor throughout the day, and only half of the performance of LV-I during the same scenario. As the transformer utilization is presumed to be linked with the overall grid utilization, the results further underline the fact that LV-II is indeed a weak grid. The possibility for LV-II to adopt any loads throughout a winter day varies a lot. During the lesser loaded periods of the day, the grid is able to support up to roughly 20 HPs and 10 EVs. During the heavier loaded periods of the day, the grid is only capable of supporting a very limited amount of units or none at all.

The reason behind the poor performance is the very weak feeder 6 which severely constrains the possibility of adopting units in the grid as whole. Ideally, assuming the desire of a 50%/25% HP-/EV penetration in 2025, LV-II would need to be able to adopt the load from approximately 80 HPs and 40 EVs. Even though all units would not be running simultaneously, when interpreted, the results makes the desired unit penetration seem unlikely to be able to reach.

As such, the further investigations of LV-II will allow for the closing of the tie-points between the feeders. Fig. 4.11 shows the LV-II (closed tie-points) winter scenario investigated yet again using the uniform algorithm. The examination of the upper part of the figure shows that the transformer utilization with closed tie-points has increased by more than 25% to 45%. Therefore, the closing of the tie-points has a very positive effect on the possibility of adding adding additional units in LV-II. The closing of the tie-points especially increases the voltage level in feeder 6 which is one of the reasons behind the increase in the amount of simultaneously running units. The upper limit for the running of units has increased by roughly 10 HPs and 5 EVs during the lesser loaded periods. Just as interesting, the minimum amount of units possible to run, which occurs during the heaviest loaded hours, has increased from none to at least 10 HPs and 5 EVs.

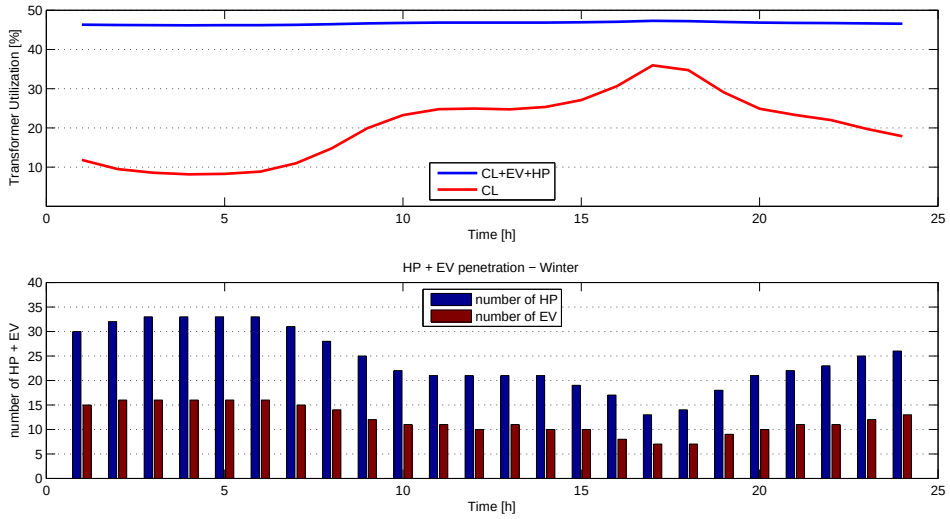

Figure 4.11: Maximum grid utilization: LV-II (tie-points closed) - Winter - Uniform algorithm

Fig. 4.12 shows the winter scenario for LV-II, still with closed tie-points, this time carried out using the adverse algorithm. The results obtained by use of the adverse algorithm further underlines the improvement in the grid utilization during the heavily loaded hours. The grid is still able to support the running of units during all hours of the day. Unfortunately the results also show a low grid utilization represented by the low transformer utilization. The grid utilization is even worse than the scenario with open tie-points carried out using the uniform algorithm. This shows that a scenario where units are turned on at the weaker parts of the grid will affect the grid performance severely.

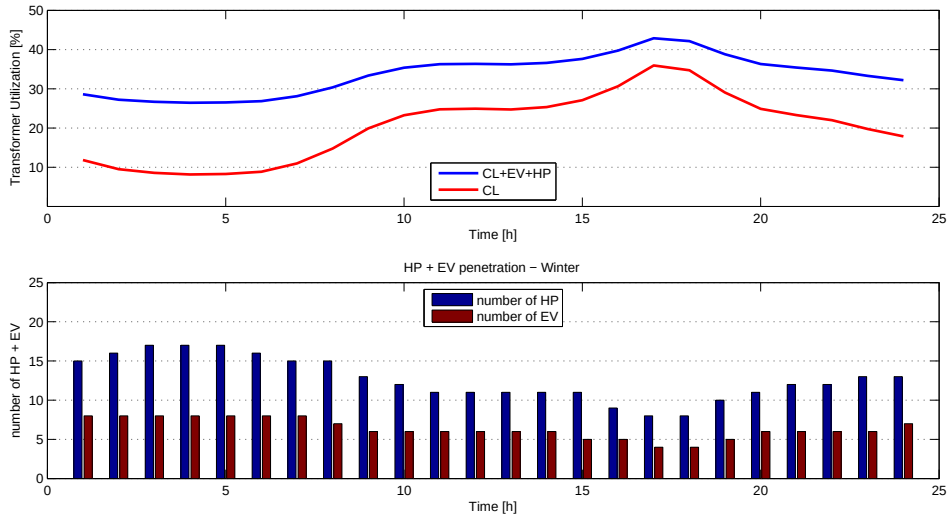

Figure 4.12: Maximum grid utilization: LV-II (tie-points closed) - Winter - Adverse algorithm

When combining the results of the maximum possible grid utilization scenarios for LV-II, it seems unlikely that the grid will be able support the desired amount of units which is roughly 80 HPs and 40 EVs, without undergoing reinforcement of the weaker parts of the grid, such as feeder 6.

In order to obtain a better understanding of the influence of adding a large amount of units into typical LV grids in the future, the remaining part of the project and report will look into the dynamic

behaviour of the units and investigate their effects through time.

5 Dynamic Control

This chapter presents the dynamic studies carried out in order to investigate the effects of adding 50% heat pumps and 25% electric vehicles in households of typical Danish LV grids in 2025.

The steady state analysis presented in chapter 4 revealed that the voltage level in both LV grids was the primary bottleneck limiting the overall grid utilization. Therefore the control-strategy applied will be focussed upon improving the voltage level and thereby increasing the grid utilization.

The chapter will start out presenting an overview of the system design from the top-layer control (Grid Control) to the unit plants (HP ,EV).

All modelling has been carried out using DIgSILENT PowerFactory's DSL-interface coupled with RMS-simulations (See section 1.3, page 5). Input data has been prepared using MATLAB. An overview of the DSL models are to be found in appendix A.3. The full models are included on the project CD found at the last page of the report.

The heat pumps have been implemented using various assumptions as well as simplifications in order to ease the process of a full-scale implementation of the units. These will be presented along with the various functions built into the models in order to replicate their behaviour and represent the control-structure. The household heating consumption, which functions as an input for the heat pumps, has been presented in sub-section 3.3.2, page 37.

The electric vehicles have been modelled as a charger with a battery, connected or disconnected to/from the grid at specific times of day. The behaviour of the electric vehicles is highly dependent upon the chosen driving patters. A driving pattern covers the time of which the car is available at the household as well as the depth of discharge the EV has at arrival. The driving patterns used in this project has been presented in section 3.4, page 40.

Clusters of units, of maximum 6 EVs and 12 HPs, are connected to a sub-system controller. The sub-system controller amongst other, performs the task of communicating with the individual units connected. The sub-system controller receives data such as the state of charge of batteries, energy level in heat pump water tanks as well as voltage levels at all nodes where units are connected. The controller sends back for instance the lowest measured voltage to the HPs and a signal which controls charging power for the EVs.

The sub-system controllers also communicate with the top layer control, *Grid Control*. The grid control defines which sub-systems need to be prioritized based upon the average energy stored in the HP water tanks and EV batteries.

As the modelling has been introduced, the results obtained from various case studies will be pre-

sented in the last part of the chapter.

5.1 Overview

This section will present an overview of the system and the overall modelling.

A fundamental part of the modelling has been the desire to treat every consumer within a grid equally. With the implemented control strategy, this goal has been possible to reach within the constraints of sub-systems. Within the grid as whole, complete equality between users have proven to severely limit grid utilization. This phenomena will be discussed in detail in the coming sections.

As a simple example, in the beginning of a feeder (close to the primary busbar), the voltage is inarguably higher than in the end of the same feeder (further from the primary busbar). As such, a consumer with an EV living electrically closer to the beginning of the feeder could be able to charge his EV faster than the consumer connected near the end of a feeder. This phenomena has been eliminated within the sub-systems. Instead, it has been decided to charge the EVs prioritizing the EV(s) with the lower SoC. Therefore, an EV with a lower SoC than the average SoC of the sub-system will be permitted to charge with higher power than the EVs at or above the mean value SoC. Implementing such a strategy within a limited section of the grid, the grid utilization is not decreased by "much". Implementing a similar strategy for the full grid, would cause a large drop in the grid utilization. In its simplest form, an example could be that an EV connected at a very strong node of a grid would not be allowed to utilize the good conditions to charge with nominal power, due to an EV charging a lot slower, connected at a very weak node of the grid.

Fig. 5.1 shows a simplified overview of the control system implemented in DIgSILENT PowerFactory.

The notations used in the figure are as follows:

- $S_{power,lim}$: Signal which limits the power consumption of the sub-systems as needed [-]
- $E_{SoC/E,mean}$: Average energy stored per unit of the sub-system [pu]
- SoC: Battery state of charge [pu]
- SoE: Heat pump water tank energy level [pu]
- V_{node}: Voltage at the node where the unit is connected [pu]
- V_{low}: Lowest measured voltage in the sub-system [pu]
- S_{charge}: Charging signal for the EVs [-]

Fig. 5.1 shows three distinct layers of the model. Each layer combines the information received from upper and lower layers in order to make decisions based upon equations in order to improve various parameters (i.e. increase voltage levels/increase charging power etc.).

The *Grid Control* act as the top layer of the models. The control-strategy implemented allows for the grid controller to add capacity (the possibility to increase power) in individual sub-systems by limiting the capacity of others. Every sub-system of a grid sends the average energy per unit (EV/HP) to the *Grid Control* continuously. Based on the average energy per unit in the sub-systems, the grid control will act to even out the average energy per unit in the grid by limiting the power consumption

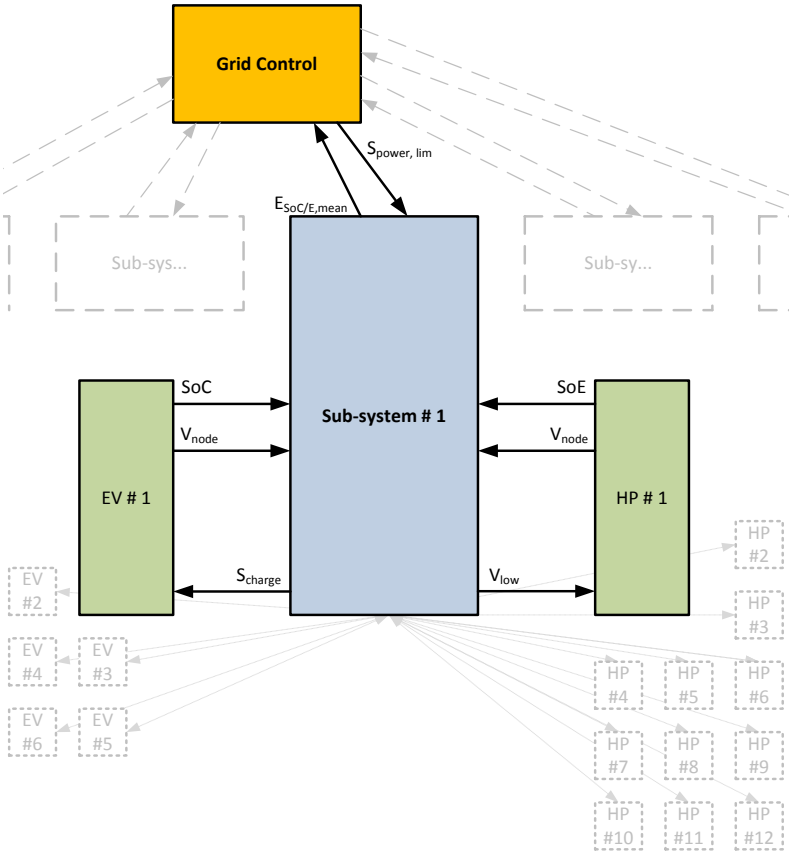

Figure 5.1: Dynamic control - Simplified overview

possible by the units in sub-systems with a higher than average mean value energy level. By limiting the consumption of the units in one sub-system an increase of the voltage at the main busbar will occur. As such, the power in other sub-systems is possible to increase. The tuning of the top layer parameters has been an interesting task perform. If the grid control is tuned to act very aggressively, the grid utilization will be severely decreased. If acting too passive, the mean value energy in the sub-systems would float independently of the other sub-systems.

The *Sub-system* controller has a wider range of responsibilities than the grid control. It receives the state of charge and voltage at connection nodes from EVs as well as state of energy (resembles water tank temperature) and voltage at connection nodes from heat pumps. By knowledge of how many EVs are connected in the sub-system as well as their respective SoC, the controller sends a signal which directly controls by how much power an EV is able to charge. The controller creates a list of the EVs connected and prioritizes the EV(s) with lower SoC. Thereby, by increasing the charging power of low SoC EV(s), the EVs ideally are fully charged at the exact same time. By knowledge of the voltage levels within the sub-system, the controller is able to utilize the section of the grid wherein the controller is connected, up till maximum capacity as it increases the total power of the units until a grid violation is present. Therefore the sub-system controller will always charge the EVs as fast as the grid allows for while respecting the grid limits.

The *Sub-system* controller also affects the functionality of the individual heat pumps, but in a much less invasive manner than for the EVs. The HPs has an in-built control function which makes them act if a voltage limit violation within the sub-system has been present for some amount of time. If the violation is severe enough, the HPs will act by turning off, if running when the emergency-mode op-

eration starts. The trigger for the emergency-mode operation is based upon the lowest voltage level in the sub-system.

The modelling and control of the single units will be presented in their respective sections within this chapter. Following the individual units, the sub-system controller and grid control will be presented in-depth.

5.2 Heat Pumps

This section presents all modelling concerning the heat pumps. The figures and methodology presented relating to the heat pump modelling does not necessarily reflect the specific modelling carried out in DIgSILENT PowerFactory. The modelling in PowerFactory has been carried out in a practical fashion which replicates the operation presented within this section completely. The primary reason behind doing so, has been the full-scale implementation of the units in the grids. A very large amount of signals, blocks, equations etc., has been implemented in DSL. In order to be able to make changes within the models, without spending more time than necessary, where possible, blocks and equations has been grouped.

The very basic idea behind the heat pump model implemented in the project work is based upon the work presented in [37].The heat pump model will represent the operation of an air-source heat pump with an interconnected water tank.

Most commonly the control of a HP will be based on the water temperature within the interconnected water tank of the system. If the water temperature of the water tank drops below a pre-set lower limit, the heat pump is turned on and increases the water temperature in the tank. When the temperature reaches a pre-set upper limit, the heat pump is turned off. This type of control is commonly referred to as dead-band control or simply ON-/OFF control.

Some heat pumps also include speed-control of the heat pump compressor in order to be able to produce a constant output temperature. As the compressor speed is varied within the ON-period, the power consumption of the heat pump varies as well. The heat pump model implemented in this project neglects the varying power consumption.

The heat pump power and COP is based upon [38]. The heat pump has a nominal (electrical) power of 3.1kW. The power factor has not been provided in [38]. Therefore, an assumption has been made which is based on the presumption that LV grids in 2025 could have a HP penetration >50%. As the HPs are rather large loads, the presumption is that the authorities will regulate the power factor of the HPs to reduce the need for producing and transmitting exceptional amounts of reactive power in the future power system. The power factor has been assumed to be 0.98 lagging. Furthermore, the heat pump is assumed to be powered by an induction motor.

The heat pump of [38] is recommended to have an interconnected water tank of either 300L or 500L. The size of the water tanks influence how flexible a heat pump system is able to act as larger tanks will be able to prolong the need for power for a longer time as well as store a larger amount of energy if needed. Therefore both sizes of water tanks have been implemented in the models with the ratio 1:1.

Fig. 5.2 represents an overview of the HP plant.

The HP model has been designed for the purpose of representing the energy consumption from - as well as energy contribution to the water tank. The water tank energy consists of the following energy contributions:

$$E_{TANK,ABS} = E_{initial} + E_{HP} - E_{DHW} - E_{loss} \quad \text{[kWh]} \quad (5.1)$$

where,
$E_{TANK,ABS}$: Energy stored in the water tank [kWh]
$E_{initial}$: Initial energy stored in the tank as the model is initialized [kWh]

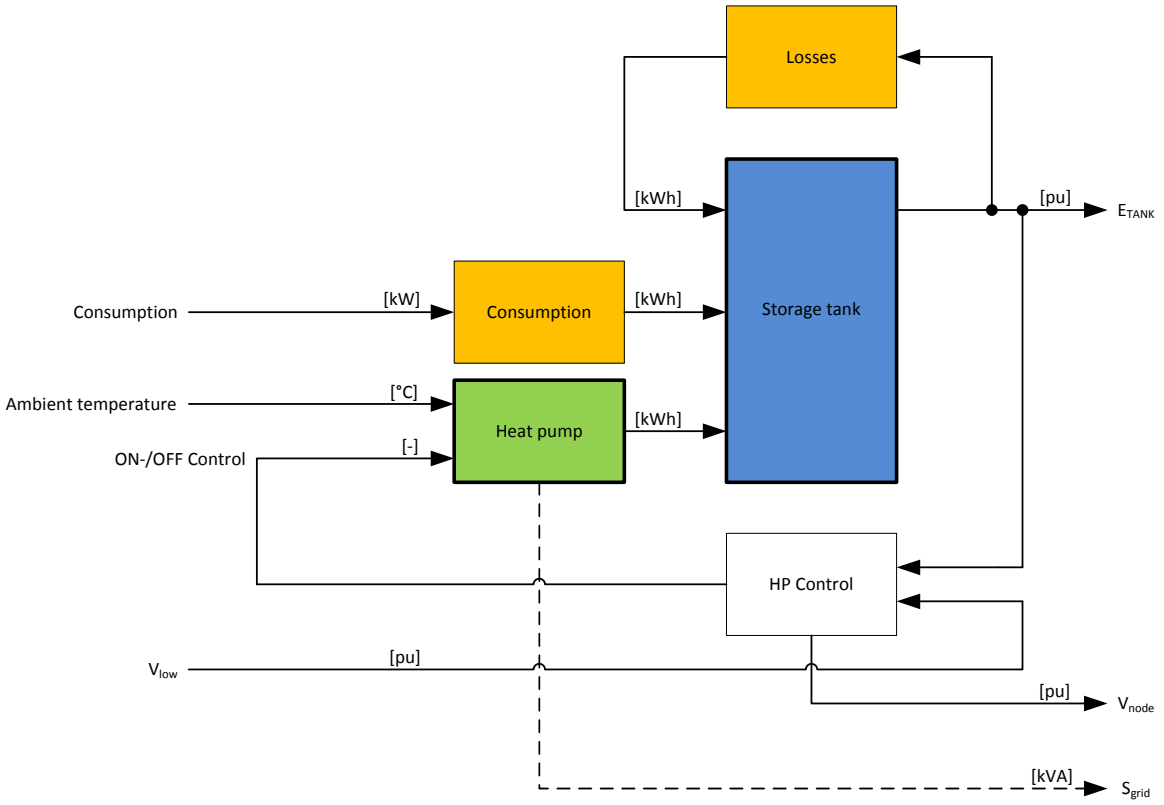

Figure 5.2: The heat pump plant overview

E_{HP}: Energy added from the heat pump [kWh]
E_{DHW}: Energy removed due to the user consumption of DHW [kWh]
E_{loss}: Energy removed due to losses from tank to ambient [kWh]

As seen in Fig. 5.2, the output from the *Storage tank* block is in pu. The conversion from a true value into a pu-value is based upon the assumption, that the water tank is energy-less if the water temperature drops below 55°C. Similarly, the water tank is considered as being fully charged if the water temperature exceeds 70°C. By use of these assumptions the usable energy in the water tanks has been calculated as follows:

$$E_{range} = V_{TANK} \cdot C_p \cdot \Delta T \cdot K_C \Rightarrow \quad \text{[kWh]} \quad (5.2)$$
$$E_{range,300} = 5.25\text{kWh}$$
$$E_{range,500} = 8.75\text{kWh}$$

where,
E_{range}: Energy difference between two temperatures [kWh]
C_p: Specific heat capacity of water [kJ/kg°C]
ΔT: Temperature difference (55-70°C) [°C]
K_C: Conversion factor between J and kWh [-]

Therefore by combination of Eq. 5.1 and 5.2, the tank energy has be defined as a per unit value of 0 when energy-less and 1 when fully charged:

$$E_{TANK} = \frac{E_{TANK,ABS}}{E_{range}} \quad \text{[pu]} \quad (5.3)$$

The *Consumption* block of Fig. 5.2 handles the integration of the household heating demand which is input from an external file and read as a continuous power demand updating every 15 minutes. The energy consumption due to the heating demand is calculated as follows:

$$E_{DHW} = K_N \int P_{DHW}(t)\, dt \quad \text{[kWh]} \quad (5.4)$$

where,
K_N: Normalization factor (hours to seconds) [h/s]
$P_{DHW}(t)$: Heating demand [kW]

The *Losses* block of Fig. 5.2 represents the losses present due to the temperature difference between the water tank and the temperature of the room wherein the water tank is placed. As the losses are dependent upon the temperature of the water inside the tank, the tank energy is converted into a temperature. The losses are calculated as follows:

$$T_{TANK} = (E_{TANK} \cdot \Delta T) + T_{min} \quad [^\circ C] \quad (5.5)$$

$$E_{loss} = (T_{TANK} - T_{room}) \cdot U \cdot A_{TANK} \cdot K_C \quad \text{[kWh]} \quad (5.6)$$

where,
T_{TANK}: Temperature of the water stored inside the tank [°C]
ΔT: Operational dead-band range (55-70°C) [°C]
T_{min}: Temperature where: $E_{TANK} = 0$ [°C]
U: Overall heat transfer coefficient [W/°C]
A_{TANK}: Surface area of the water tank [m^2]
T_{room}: Temperature of room where the water tank is placed [°C]

The surface areas used have been approximated from dimensions presented in [39][40]. The 300L water tank has a surface area of $\approx 8m^2$. The 500L water tank has a surface area of $\approx 10m^2$.

The *Heat pump* of Fig. 5.2 represents the heat pump operation and behaviour. The heat pump receives two inputs - the ambient temperature and the ON-/OFF signal from the control-block.

Most commonly, when a heat pump is turned on it will draw cold water from the bottom of the interconnected water tank, heat it and send it back to the top of the water tank. This statement is only valid for water-based heat pump systems, obviously. At the instance when the heat pump is turned on, the heat pump only slightly heats the temperature of the water, which has the consequence, that the water temperature of the top-layer of the water tank gets cooled. As the heat pump runs for longer time, the output water temperature increases to some maximum. According to [41], this process (for the heat pump investigated in [41]) takes roughly 15 minutes. It has been decided to try to resemble this effect and implement it into the heat pump model as it affects the time it takes to increase the water tank temperature. As a consequence of this effect the heat pumps will be running for a longer time.

This effect seems as if it will decrease the energy of the water tank until the moment where the heat pump output temperature equals the water tank top layer temperature. This is not the case. If assumed that the heat pump does not heat the water at all during the first few seconds of running, it

does not add any energy to the water. As it does not remove any energy either, the energy stored in the water flowing through the heat pump stays unaltered. Therefore, as the heat pump extracts water from the (cold) water tank bottom layers and adds it to the water tank top layers, the heat distribution in the water tank becomes more even.

The effect has been implemented by ramping the heat pump energy supply as it turns on. The ramping of the energy supply is described as follows:

$$\text{HP, on}: \quad K_E(t) = 1/900$$
$$\text{HP, off}: \quad K_E(t) = -\infty$$
$$E_{supply} = \int K_E(t)\, dt\,, \quad 0 \le E_{supply} \le 1 \qquad \text{[pu]} \quad (5.7)$$

where,
$K_E(t)$: Integration factor dependent upon the state of the HP (ON/OFF) [-]
E_{supply}: Heat pump energy supply [pu]

Fig. 5.3 shows an arbitrary example of the heat pump energy supply. The figure shows from top to bottom, the tank energy, control signal and heat pump energy supply implemented according to Eq. 5.7.

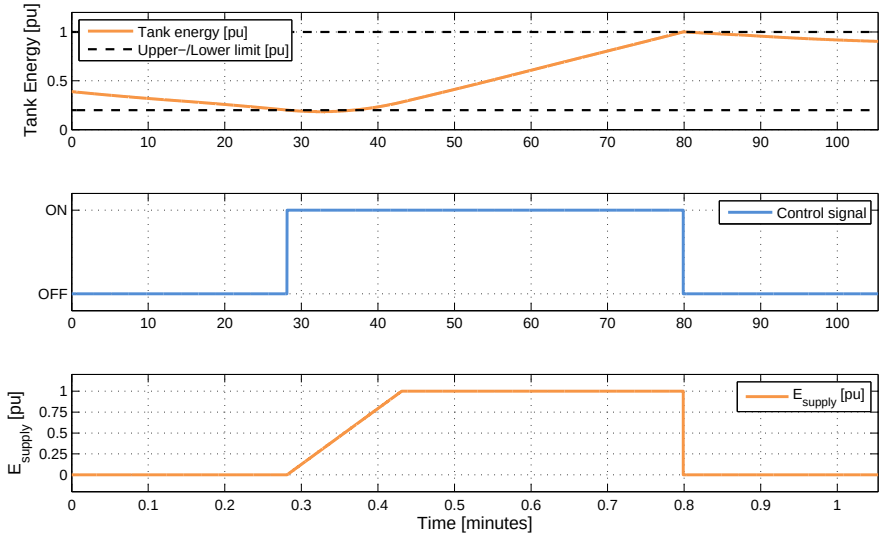

Figure 5.3: Arbitrary example of the heat pump energy supply

Fig. 5.3 shows that as the control turns on the HP, the energy of the tank keeps decreasing due to the consumption and losses, until the heat pump energy supply becomes high enough for the HP input to match, and as time increases, exceed the consumption whereby the energy stored in the tank increases.

The heat pump model has been equipped with a temperature dependent coefficient of performance, COP. The COP has been derived from a graph presented in [38]. In order to utilize the temperature dependent COP within the models an interpolation of the data has been made. Fig. 5.4 and Eq. 5.8 show the plot and function of the interpolation carried out using the MATLAB function, *cftool*.

$$COP(T_{amb}) = (0.078 \cdot T_{amb}) + 2.791 \qquad [-] \quad (5.8)$$

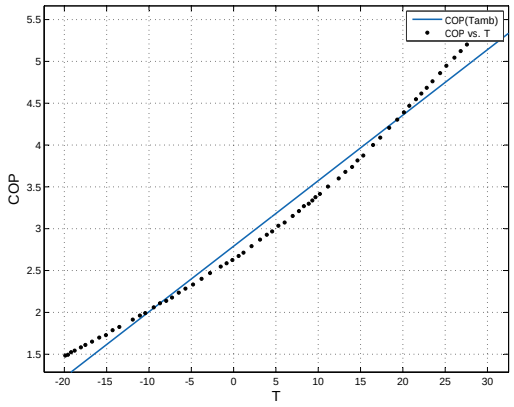

Figure 5.4: Curve fitting of the COP of NIBE F2026

where,
$COP(T_{amb})$: Heat pump coefficient of performance [-]
T_{amb}: Ambient temperature [°C]

The heat pump is connected to the grid in PowerFactory. This means that the DSL model sends the consumption data from the HP model to a specific load in LV-I or LV-II. The connection between the DSL-model and the grid is carried out in another manner than reflected by Fig. 5.2 due to the desire for limiting the amount of signals in DSL.

All heat pumps have been equipped (modelled) with a soft-starter, since the HP model is assumed to be powered by an induction motor. The main purpose of the soft starter is, as the name implies, to limit the starting current which in some cases can reach high values (5 to 7 times I_{nom}). The soft starter functionality implemented into the HP model is based on a measurement of the start up current of a 3-phase HP presented in [16]. The implementation of the soft starter has been done by manipulation of the start-up power of the heat pump. The power is represented in the following manner:

$$A = 0.2 \quad [-]$$
$$\text{if} \quad t_{start} \geq 2s \quad B = 0.2 \quad \text{else} \quad B = 0 \quad [-]$$
$$\text{if} \quad t_{start} \geq 4s \quad C = 1.6 \quad \text{else} \quad C = 0 \quad [-]$$
$$\text{if} \quad t_{start} \geq 5s \quad D = 1.0 \quad \text{else} \quad D = 0 \quad [-]$$

$$P_{HP} = (A + B + C - D) \cdot P_{nom} \quad [\text{kW}] \quad (5.9)$$

where,
A, B, C, D: Timed constants [-]
P_{nom}: Heat pump nominal power [kW]
P_{HP}: Heat pump model power sent to grid [kW]

Fig. 5.5 shows the functionality of Eq. 5.9. The C→D period last roughly three times longer than presented in [16]. This is due to the step-size of 1000ms of the RMS simulations in PowerFactory. Lowering the step-size additionally, would cause the simulations to become too time consuming to run.

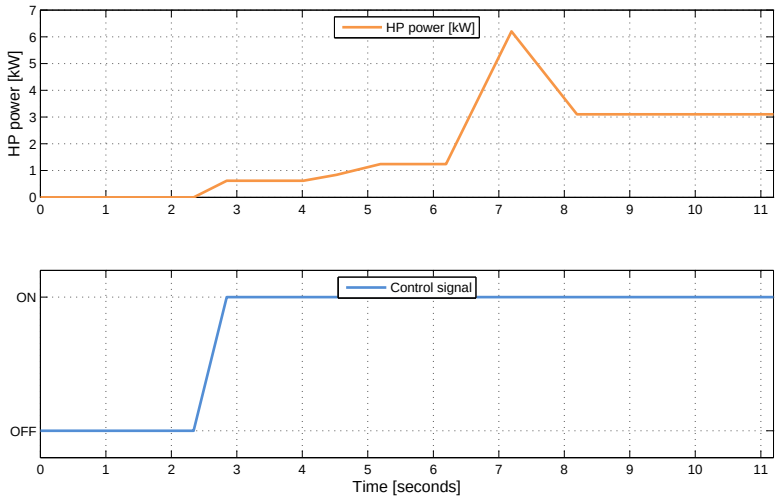

Figure 5.5: Example of the HP softstarter implemented in PowerFactory

The *Control* block of Fig. 5.2 represents the control of a single heat pump. The control block decides when the heat pump is turned on and off by use of common ON-/OFF control. The ON-/OFF control works in the manner that if the water tank energy drops to a pre-set lower limit, the HP is turned on and stays on until the energy reaches a pre-set upper limit. The ON-/OFF control can be manipulated by controlling the upper- or lower band of the dead-band. Basically, the HP can be turned on ahead of time by increasing the lower band sufficiently as well as turned off by lowering the upper band sufficiently.

The control approach for the heat pumps is highly influenced by the heat pump energy supply effect presented in Fig. 5.3 and Eq. 5.7. The overall energy supply of the heat pump system is decreased the more often the unit is turned on. Therefore, the HP control is focused on being able to assist the grid, if and only if, an emergency-situation occurs.

The heat pump control consists of the basic ON-/OFF control with a fixed dead-band as well as an emergency control which is activated by use of manipulation of the dead-band.

The ON-/OFF control has been implemented by use of the *picdro* and *flipflop* functions of PowerFactory. In order to present the functionality the common if-loop will be used where Eq. 5.10 represents *picdro* and Eq. 5.11 represents *flipflop*.

$$\begin{aligned} &\text{if} \quad E_{TANK} < E_{min} \quad \Rightarrow \quad K_{ON} = 1 \quad \text{else} \quad K_{ON} = 0 \\ &\text{if} \quad E_{TANK} > E_{max} \quad \Rightarrow \quad K_{OFF} = 1 \quad \text{else} \quad K_{OFF} = 0 \end{aligned} \tag{5.10}$$

$$\begin{aligned} \text{if} \quad & K_{ON} = 1 \ \wedge \ K_{OFF} = 0 \quad \Rightarrow \quad C_{HP} = 1 \\ \text{else if} \quad & K_{ON} = 0 \ \wedge \ K_{OFF} = 1 \quad \Rightarrow \quad C_{HP} = 0 \\ \text{else} \quad & C_{HP} \text{ stays unaltered} \end{aligned} \tag{5.11}$$

where,
E_{min}: Lower limit for the tank energy [pu]
E_{max}: Upper limit for the tank energy [pu]
K_{ON}: Variable which turns 1 when the lower limit is violated [-]

K_{OFF}: Variable which turns 1 when the upper limit is violated [-]
C_{HP}: Heat pump ON-/OFF signal [-]

The basic functionality is depicted in Fig. 5.3 presented previously in the section.

The heat pump control also includes an "emergency" voltage control. This control is based on the input, lowest voltage of the sub-system, which is provided by the sub-system controller.

Heat pumps are inherently uncontrollable for longer periods of time, at least for grid improvement purposes. If aggressive control is applied, turning on and off the heat pumps frequently, the average heat pump energy supply is lowered, and therefore is not an option. As such, the heat pumps are not able to actively support the voltage. The heat pumps can basically perform two operations. Consume ahead of time or delay consumption (provided that some surplus of energy is available in the tank).

Due to these factors, it has been decided to equip the heat pumps with a function which will reduce the heat pump power consumption if an under-voltage scenario is deemed severe enough. The severity of the under-voltage is assessed by the amplitude of a voltage drop combined with how long the voltage drop has been present in the grid.

In order to ensure that the heat pumps are able to stop consuming for some amount of time, without causing consumer discomfort, the lower band (E_{min}) of the regular ON-/OFF control is set at 0.2 pu. Therefore, ≈20% of the water tank capacity is reserved for the emergency voltage support.

When an emergency scenario occurs, the control will lower both the upper- and lower limit of the dead-band. Lowering the upper limit has the effect that HPs running will be turned off according to Eq. 5.10 and 5.11. Lowering the lower band ensures that the heat pumps will be able to delay time of consumption, ideally until the under-voltage scenario has been cleared.

The lower voltage limit of the grids is throughout the rest of the report assumed to be 0.94 pu. The voltage assessment, deciding if an under-voltage scenario is considered severe, is explained mathematically by Eq. 5.12 assisted by Fig. 5.6.

$$\begin{aligned} &\text{if} \quad V_{low} < V_{lim} \quad K_v(t) = -K_n \cdot (1 - ((V_{lim} - V_{low}) + 1)^n) \\ &\text{else} \qquad\qquad\quad K_v(t) = K_k \end{aligned} \tag{5.12}$$

$$K_{vs} = \int K_v(t)\ \mathrm{dt}\ , \quad -1 \leq K_{vs} \leq 0$$

$$\begin{aligned} \text{if} \quad K_{vs} < -0,5 \quad &\text{emergency} \\ \text{else} \qquad\quad &\text{no emergency} \end{aligned}$$

where,
V_{low}: Lowest voltage recorded in the sub-system [pu]
V_{lim}: Voltage limit [pu]
$K_v(t)$: Integration factor [-]
K_n: Linear gain (higher value → increased emergency sensitivity) [-]
n: Exponential gain (higher value → increased emergency sensitivity) [-]
K_k: Linear gain (higher value → faster emergency clear time) [-]

K_{vs}: Voltage severity factor [-]

In the project K_{vs} has been tuned to react to an under-voltage of 0.935 pu in roughly 10 minutes and an under-voltage of 0.9 in less than 10 seconds using the parameters presented in Table 5.1.

Parameter	Value
K_n	0.001289
n	100
K_k	0.001667

Table 5.1: Parameters for Eq.5.12 used in the project

By use Eq. 5.12 and the values for the gains presented in Table 5.1 the heat pumps recognise an emergency as presented in Fig. 5.6.

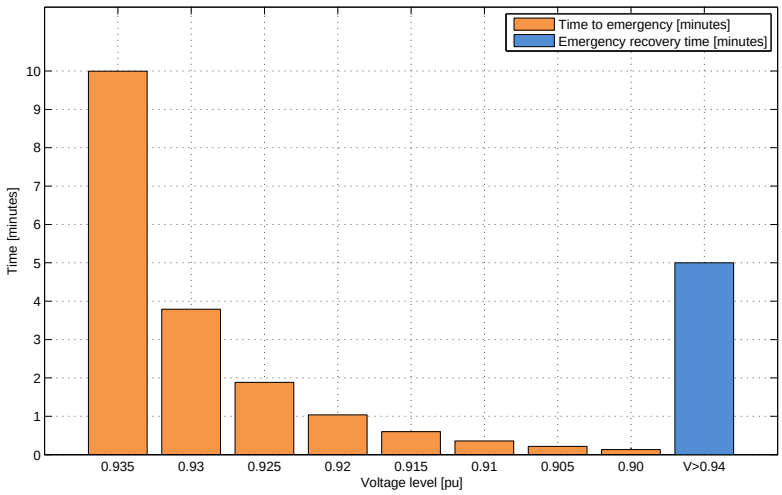

Figure 5.6: HP emergency scenario timing

The heat pumps therefore utilize an adaptive delay to determine when to operate and act during under-voltage scenarios.

If an emergency scenario is detected, the upper- and lower band of the heat pump ON-/OFF control is modified. The lower band drops instantaneous from $E_{min} = 0.2$ to $E_{min} = 0$. The upper band is gradually lowered from $E_{max} = 1$ to $E_{max} = 0.4$ since then, the heat pumps ideally will be turned off one by one until the under-voltage scenario is cleared, or the lower limit of the upper band is reached. The functionality when entering the emergency operation is described by Eq. 5.13.

$$\begin{aligned} &\text{if} \quad K_{vs} < -0.5 \quad K_{max}(t) = -1/60 \\ &\text{else} \qquad\qquad\quad K_{max}(t) = \infty \end{aligned}$$

$$E_{max} = \int K_{max}(t)\ \mathrm{dt}\ , \quad 0.4 \leq E_{max} \leq 1 \qquad \text{[pu]} \quad (5.13)$$

where,
$K_{max}(t)$: Slope-controlling integration factor of the upper band [-]

When the under-voltage at some point is cleared, it takes up to 5 minutes before the upper band jumps back to normal operation, due to the setting of K_{vs}.

When leaving an emergency scenario, the lower band (E_{min}) will be increased from 0 to 0.2 pu. The HP tank energy could, with a high probability, be in the range of 0 - 0.2 pu when the under-voltage scenario is cleared. Therefore, this operation is crucial, as it will most likely turn on a lot of the heat pumps in the sub-system. If not carried out in a smart manner, 12 heat pumps *could* turn on at the exact same point of time, causing start-up currents to coincide. This undesirable effect is a product of the control applied. In order to soften the transition phase, the increase of the lower band is ramped up rather than stepped up, in order to turn on the heat pumps one by one. Eq. 5.14 represents the control of the lower band.

$$\begin{aligned} &\text{if} \quad K_{vs} > -0.5 \quad K_{min}(t) = 1/60 \\ &\text{else} \qquad\qquad\quad K_{min}(t) = -\infty \end{aligned}$$

$$E_{min} = \int K_{min}(t)\ \mathrm{dt}\ , \quad 0 \leq E_{min} \leq 0.2 \qquad \text{[pu]} \quad (5.14)$$

where,
$K_{min}(t)$: Slope-controlling integration factor of the lower band [-]

Fig. 5.7 shows the emergency control at work. During the arbitrary scenario presented, the voltage drops below the limit of 0.94 pu. As the under-voltage is present for more than 10 minutes, the emergency parameter ($K_{vs} < -0,5$) is crossed and the dead-band is manipulated according to Eq. 5.13 and Eq. 5.14.

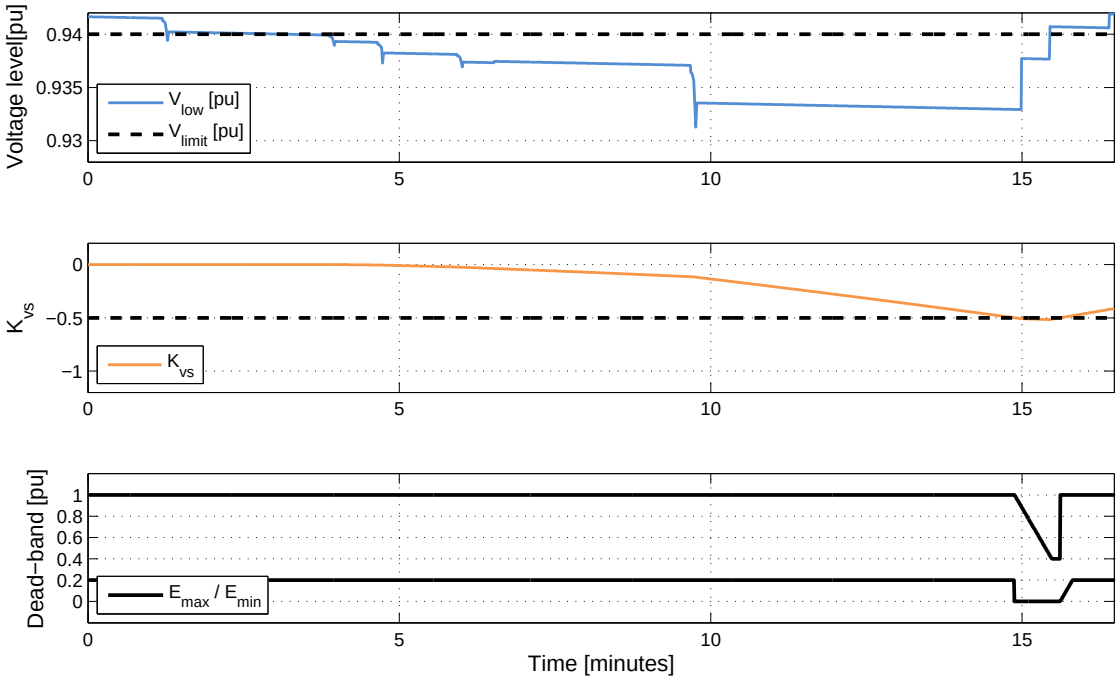

Figure 5.7: HP emergency control - example

As seen, it takes a very long time before the HP control reacts to the under-voltage. This is desired as the under-voltage is not deemed very severe. In the scenario presented, it is seen that as the upper band is reduced, two large jumps in the voltage occurs. This is due to two heat pumps being switched off. As the voltage is yet again greater than 0.94 pu, the system returns to normal operation.

The upper band jumps directly back to the upper limit, where the lower band is ramped up in order not to turn back on all HPs instantaneously.

5.3 Electric Vehicles

The following section presents the implementation of an EV model capable of representing the behaviour and grid impact of EVs in long term simulations. A model overview is shown in Fig. 5.8.

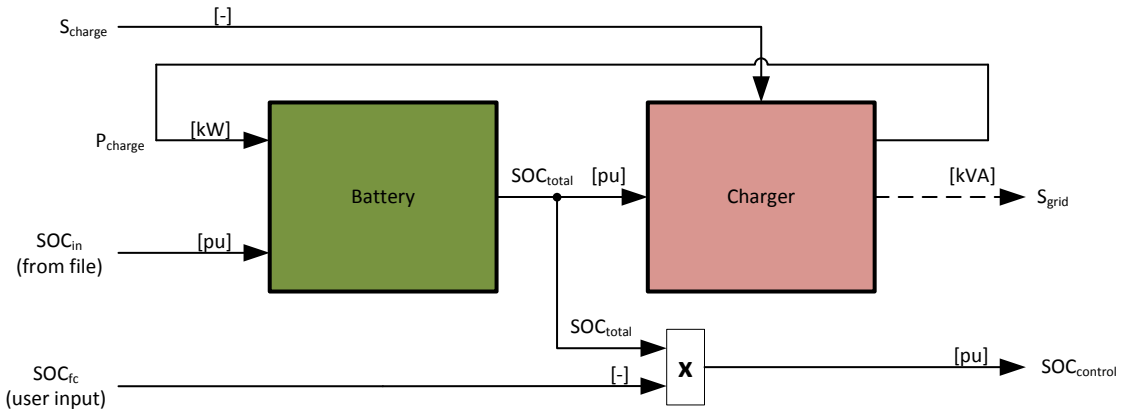

Figure 5.8: The electrical vehicle overview

As seen in Fig. 5.8, the charger block receives two input signals. The SOC_{total} signal continuously informs the charger about the current state of charge of the connected battery. Continuous measurements of the SoC supports control according to the current battery status and prevent overcharging. If the signal reaches a certain value, the charging process stops. S_{charge} is a signal which each individual charger receives directly from the sub-system controller (presented in the next section). This is responsible for the charging power control P_{charge} and is therefore highly important to the charger operation. The actual signal is a square wave with variable positive and negative amplitude and variable duty cycle. The amplitude primarily depends on the current SoC of plugged-in battery while the duty cycle depends on the grid capacity which is reflected by voltage and current limits.

Fig. 5.9 depicts the dependencies between P_{charge}, feeder capacity as well as state of charge. The figure is divided into 3 plots. The upper plot represents the influence the relative SoC has on the charging signal. A lower than average SoC will increase the control signal amplitude and vice versa. The middle plot represents the influence the feeder capacity has on the charging signal. The control will adapt the duty cycle of the signal to the grid conditions. This means that if the grid violations occur, the duty cycle will be decreased until the EV power consumption no longer violates the grid limits. The lower plot shows the effect the two upper plots have on the charging power through time. The example is purely made to illustrate the quantities affecting the power consumption. In reality the charging signal is a product of the two upper plots.

The control of the EV power is further explained in section 5.4.

$$P_{charge} = \int S_{charge}(t)\ dt\ , \quad 0 \leq P_{charge} \leq P_N \qquad \text{[kW]} \quad (5.15)$$

where,
P_N: Nominal charging power [kW]

The charger block also contains two output signals. The first one is the output charging power P_{charge}, explained by Eq. 5.15. P_{charge} is directly connected to the battery input and varies between 0 and rated charging power. The signal S_{grid}, represents the input power of the charger, which is sent to the

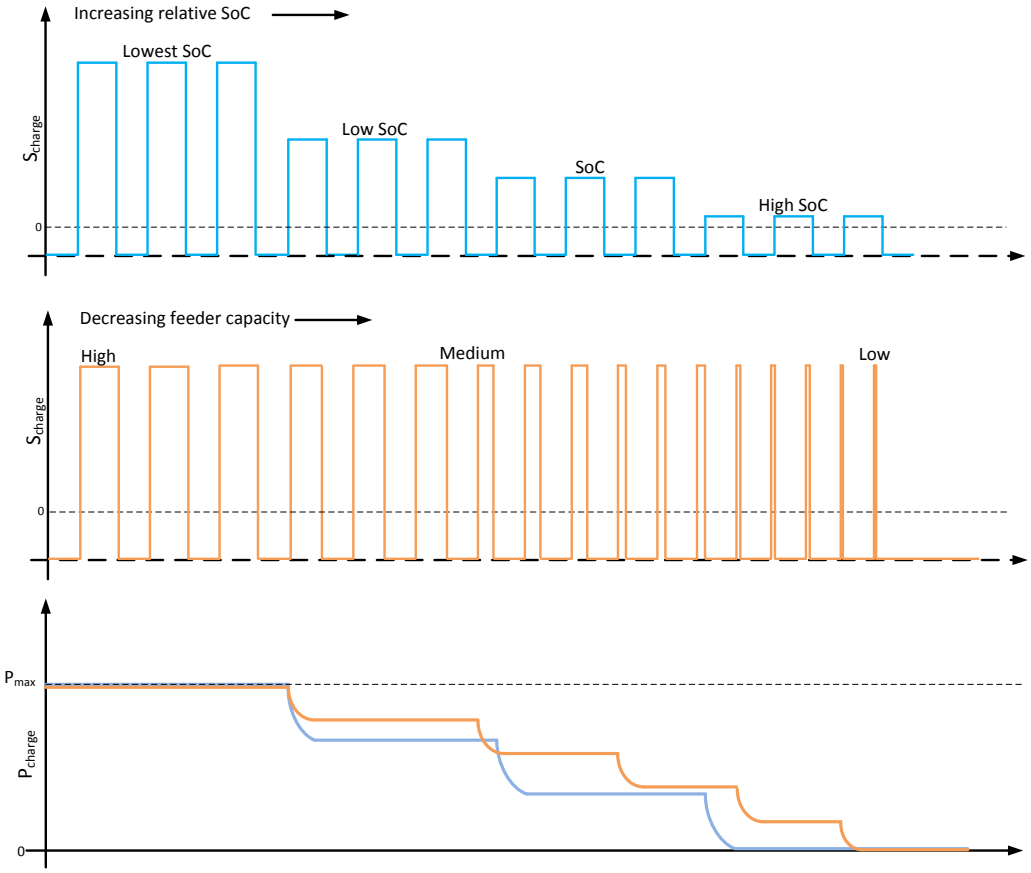

Figure 5.9: Charging power dependency

load in the LV grid. The battery shown in Fig. 5.8 as the green block, receives the output power from the charger and converts it to energy by following Eq. 5.16

$$SOC_{charge} = \int P_{charge}(t)\ dt\ , \quad 0 \leq SOC_{charge} \leq SOC_{max} \qquad \text{[kWh]} \quad (5.16)$$

where,
SOC_{max}: maximum battery capacity [kWh]

The input signal, SOC_{in}, represents the energy stored in the battery as the charging process starts. The energy stored in the batteries are based upon the driving patterns estimated in section 3.4.

$$SOC_{total} = SOC_{in} + \frac{SOC_{charge}}{SOC_{max}} \qquad \text{[pu]} \quad (5.17)$$

where,
SOC_{total}: Actual battery SoC [pu]
SOC_{in}: Battery SoC initial value [pu]
SOC_{charge}: SoC added by the charger [kWh]
SOC_{max}: Battery maximum SoC [kWh]

The sum of the initial value and added energy by the charger produces SOC_{total} which refers to the actual state of energy stored in the battery. SOC_{total} is monitored by the charger. When the value

reaches a certain limit, the charging process stops. Between the battery and the charger, the signal SOC_{total} is split into two signals. One of these is connected to the charger and the other is multiplied by a fast charging factor, SOC_{fc}, after which it is sent to the sub-system controller. The factor, SOC_{fc}, represents that the EV owner has requested fast charging which means that the user, by assuming extra costs, is prioritized for the highest possible charging power. Basically, the owner could be in need of a fully charged battery as fast as possible. By activating the fast charging request, K_{fc} switches from 0 to 1 and according to the relations shown in Eq. 5.18, $SOC_{control}$ decreases which makes the sub-system controller see an EV which has very low SoC and thereofre must be prioritized.

An example of the fast charging event is shown in Fig. 5.10.

$$\begin{aligned} &\text{if} \quad K_{fc} = 1 \quad \wedge \quad SoC_{total} < SoC_{max} \quad \Rightarrow \quad SoC_{fc} = 0.001 \\ &\text{else} \qquad\qquad\qquad\qquad\qquad\quad \Rightarrow \quad SoC_{fc} = 1 \end{aligned}$$

$$SoC_{control} = SoC_{fc} \cdot SoC_{total} \quad \text{[pu]} \tag{5.18}$$

where,
K_{fc}: User fast charging request [-]
SoC_{fc}: Fast charge gain [-]
$SoC_{control}$: SoC value sent to sub-system controller [pu]

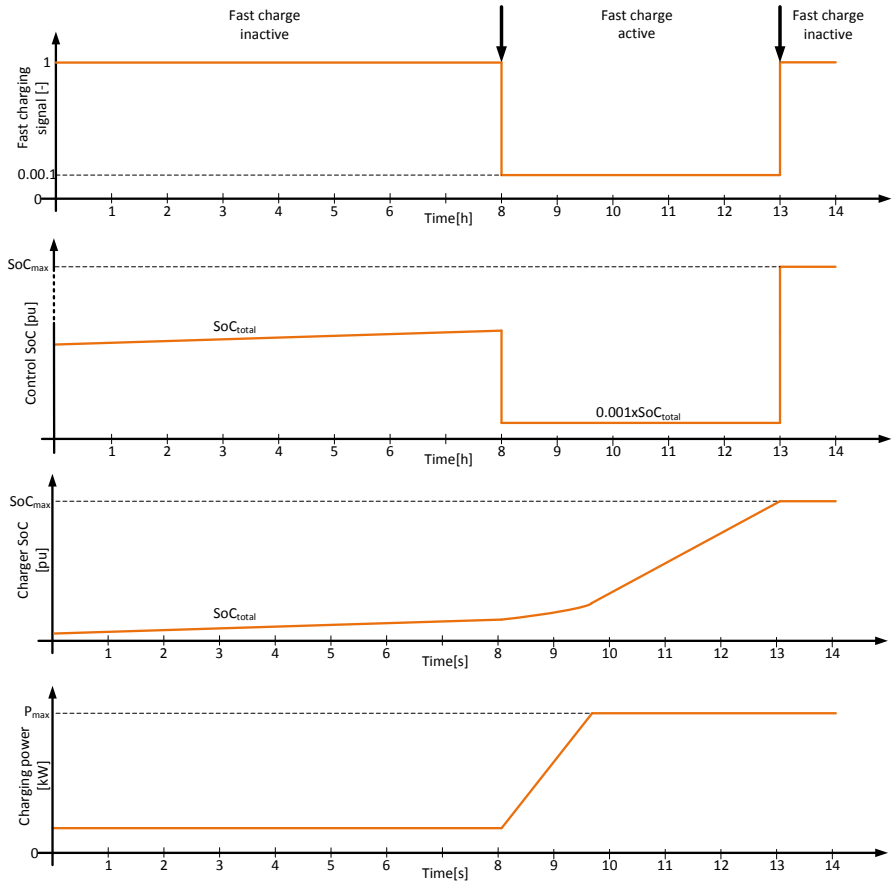

Figure 5.10: Fast charging process

The manipulated $SoC_{control}$ is sent to the sub-system controller as a very low SoC. The sub-system controller reacts by increasing the charging power. The figure consists of four plots, where first plot shows the value of the fast charging factor, SOC_{fc}. The second plot shows $SOC_{control}$ seen by the sub-system control. The third plot depicts the real SoC of the battery seen by the EV charger. The last plot illustrates the charging power.

It is assumed that the battery has started charging with power defined by the regular sub-system algorithm until 08:00. At 08:00 the car owner decides to enable fast charging. Instantaneously $SOC_{control}$ is decreased. The control therefore detects a very low SoC of the battery and increases the power up to rated charger power or up to the point where a grid violating occurs. The high charging power is present until the battery is fully charged. As the battery is fully charged the fast charging signal is reset and $SOC_{control}$ returns to the original value which means that the priorities of the sub-system controller is no longer affected by the fast charging request.

Fig. 5.11 shows an example of the fast charging. In the upper plot no fast charging is requested. In the lower plot EV#3 activates fast charging around 13:00 and is prioritized for more power than the rest of the EVs.

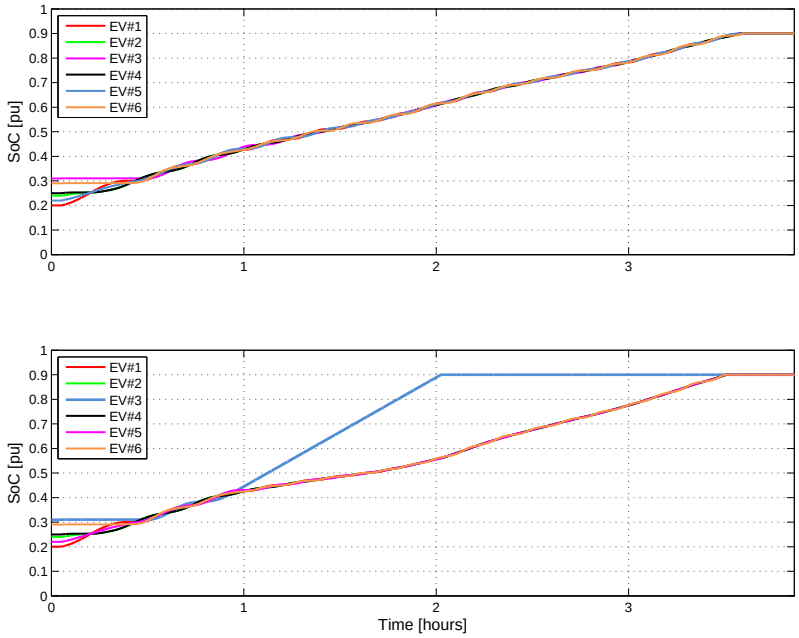

Figure 5.11: Practical example of the fast charging control

Till now the overall functionality of the model has been presented. The coming sub-sections will go into detail with with the actual implementation along with a presentation of some of the technical parameters used within the models.

5.3.1 Batteries

The most common EV storage unit is an electrochemical battery which converts electrical energy into chemical energy and vice versa. As the battery is a crucial component of the EV representation in DSL, a short literature review, along with a comparison of modeling approaches is presented in this sub-section. The battery parameters and battery model layout are specified and presented after the

review.

One of the most popular types of rechargeable batteries used in the automotive industry is the lithium-ion battery which is also known as li-ion [42]. The reason behind choosing li-ion batteries is their high energy density, relatively high output voltage, long life cycle as well as having a small memory effect [43]. Furthermore, [22] compares three recently developed battery technologies. Namely, the lead-acid battery, lithium-ion battery and nickel-metal battery and conclude that only the li-ion battery is viable for supplying electrical vehicles.

The highly advanced electrochemical phenomena which occur inside li-ion batteries are not simple to describe by chemical laws. They are even more complex to describe purely mathematically. Hence, a plenty of research has focused upon finding a proper representation of the phenomena using simplified relations. The research is focussed on finding a reasonable compromise between phenomena complexity and modeling possibilities. In other words, the research is trying to represent the most relevant battery properties with simplicity in mind.

Different approaches allow for representing the battery behaviour by chemical, electrical or mathematical laws. Three common representations are reported in literature [44] as:

- Electrochemical
- Analytical
- Electrical

The article provides a detailed review of different battery representations with respect to their specific purpose. One solution is the so-called electrochemical model. The electrochemical model consists of a highly complex structure, frequently used to analyse transient behaviour, optimize internal parameters and tune the performance. The analytical approach is yet another possibility. However, this technique is regarded as a low accurate which poorly illustrates the dynamic processes (charging/discharging) if at all. The most common approach is a model based on an electrical circuit representation. It captures a majority of the detailed parameters which are not included into the analytical model and does not contain highly complex structure as the electrochemical approach. As a consequence, it is relatively easy to implement and does not require high computation power. Moreover, a battery represented by electrical components i.e. voltage source, resistors, capacitors etc. is easier to understand and implement into electrical circuits simulators.

The electrical models are subdivided with respect to the applied law:

- Thevenin
- Impedance
- Runtime - based on approach

According to [42], the impedance representation, which only requires modest computational power is well suited for long term simulations. The impedance model is able to capture a variety of different properties including the non-linear behaviour of the open circuit voltage (V_{OC}) with respect to the state of charge (SoC). The SoC represents the current state of energy stored in the battery. The open circuit voltage is the voltage measured at the battery terminals while no external circuit connected. The SoC-V_{OC} characteristic uncovers the main drawback of li-ion batteries which is the highly non-linear dependency between the two presented parameters. However, the non-linear behaviour is

more visible when the battery energy is completely depleted or completely charged. Therefore, in practical applications, the non-linear sections of the SoC-V_{OC} characteristic as utilizing the full capacity range of the batteries equals having a high degradation ratio [45]. It is recommended not to discharge li-ion batteries below 0.2 [pu] SoC and charge above 0.9 [pu]. Fig. 5.12 shows an example of the non-linear SoC-V_{OC} relationship for a single li-ion cell [44]. According to the figure, the non-linear part of the characteristic is outside the practical operational range and is therefore presumed to be neglect-able in long term analysis.

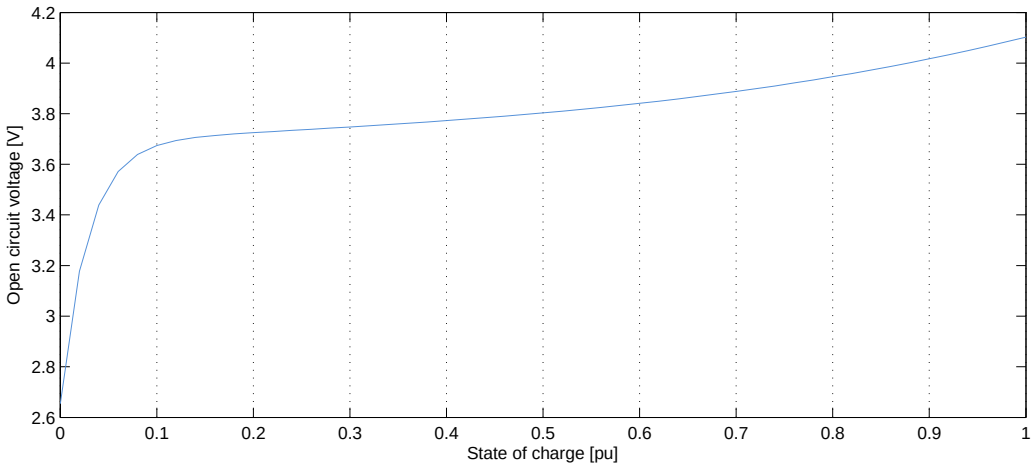

Figure 5.12: V-SoC characteristic for a single li-ion cell

Fig. 5.13 presents the simplified impedance model of a li-ion battery proposed by [44]. In the article the resistive and capacitive components are constant within the assumed operational range of 0.2 < SoC < 0.9 [pu]. The transient components C_P and R_P primarily show their behaviour in the range of 0 < SoC < 0.2 [pu]. Hence, for long term simulations and while only utilizing 0.2 < SoC < 0.9, the battery model can be simplified into only two components. The capacitor, C_U, which represents the usable battery capacitance and the resistor, R_S, which allows for defining charging and discharging losses. In literature, R_s, is usually defined as the round trip efficiency which for li-ion batteries used for EV applications is estimated to be 98.6% [46].

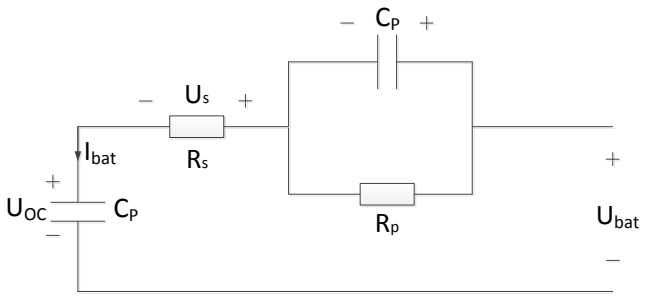

Figure 5.13: Electric circuit representation of a li-ion battery [44]

where,
U_{OC}: Open circuit battery voltage
U_{bat}: Battery terminals voltage
R_s: Series resistance
R_p: Transient resistance
C_p: Transient capacitance

C_u: Usable capacitance
U_s: Voltage drop

It has been chosen to equip all EVs with a li-ion battery package of 24kWh. This decision is based upon [33] which lists EVs currently available on the Danish market. The EVs currently are equipped with battery packages ranging between 10-24(50) kWh. As the battery packages are only expected to be larger in the future, the largest battery has been chosen.

Fig. 5.14 represents the battery model. The model of the battery is based upon the simplified impedance circuit. The input signal, P_{batt}, refers to the charging power received from the charger. This power must be reduced due to the battery losses as well as normalized from hours to secends. An average efficiency of the charging process of li-ion batteries is estimated to be 99.3% [46]. Eq. 5.19 shows the calculation of the gain ,K_{batt}.

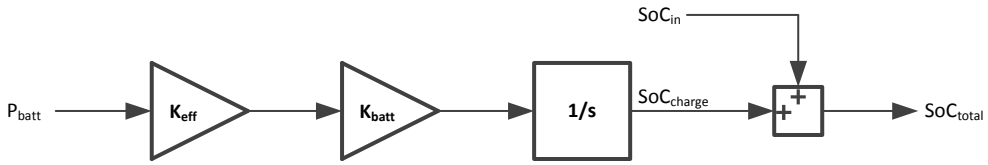

Figure 5.14: Representation of the battery block

$$K_{batt} = E_{batt} \cdot K_N \Rightarrow \quad [-] \quad (5.19)$$

$$K_{batt} = 24 \cdot \frac{1}{3600} = 1.157 \cdot 10^{-5} \quad [-]$$

where,
E_{batt}: Battery capacity [kWh]
K_N: Normalization factor [h/s]

Eq. 5.20 shows the full charging power transformation.

$$SOC_{total} = SOC_{in} + \frac{K_{eff} \cdot K_{batt} \int P_{batt}(t)\ dt}{SOC_{max}} \quad [\text{pu}] \quad (5.20)$$

where,
SOC_{total}: Actual battery SoC [pu]
SOC_{in}: Battery SoC initial value [pu]
SOC_{max}: Battery maximum SoC [kWh]
K_{eff}: Battery efficiency [-]
K_{batt}: Battery integration gain [-]
$P_{batt}(t)$: Power received from the charger [kW]

Due to battery degradation, the operational range of the battery will be limited to stay within 0.2-0.9 pu.

5.3.2 Charger

In literature, there are many different battery chargers qualified for EV applications. Due to [47] and the project assumption of using a 11kW rated charger power charger, only 3 phase variable power

units are taken into account. A short review allowed to find many different types of chargers which would qualify for use in this project. The main task of the charger model is to convert the square wave input signal to a power signal and scale it properly. To do so, a simple representation using a single integration block is expected to meet the demand of the tasks.

The model is represented by a simple integration block, efficiency gain as well as a normalization factor from hours to seconds. The efficiency gain will allow to distinguish between input power and output power. Typical efficiency factors for recently developed EV charger applications have been analysed and compared by [48]. New types of 12kW, 3 phase EV chargers are expected to operate with an efficiency between 98% and 99%. Therefore, the efficiency has been assumed to be 98%. The model represented by the layout shown in Fig. 5.15

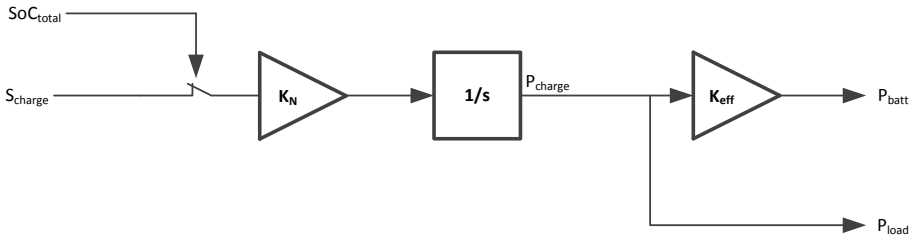

Figure 5.15: Charger block representation

5.4 Sub-system controllers

The sub-system control strategy has been designed and developed in order to control the EV charging process by having constant control of the charging power with respect to LV grid constrains. It is a middle layer control in the full control structure. Fig. 5.16 shows a flowchart of the sub-system control algorithm which controls up to 6 EVs. The control operates in a loop which continuously checks the status of the charging power of the plugged-in EVs, SoC of the EVs as well as grid constrains across the controlled sub-system. The sub-system controller does not directly affect the heat pumps, as all heat pump control takes place in the actual HP control unit. The sub-system only makes the lowest voltage measured in the sub-system available to the HPs.

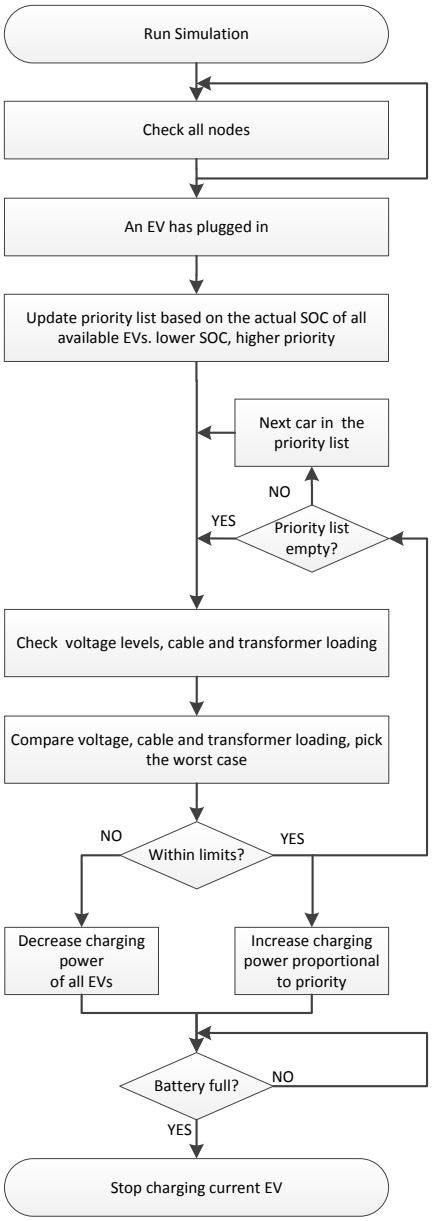

Figure 5.16: EV charging control

The algorithm constantly checks the current number of EVs plugged-in. The plugged-in units are prioritized with respect to their current state of charge. The unit with the lowest SoC is given the

highest rank on the priority list. If two units are plugged-in at the same moment, both start charging no matter their SoC. If one of the EVs have a higher SoC than the other, this EV will have its charging power decreased through time. Similarly, the EV with a lesser SoC will have its power increased with time. The manipulation is based upon their rank on the priority list. A high rank means that an EV will increase its charging power very fast, a lesser rank less fast and a low rank will have its charging power reduced. The manipulation occurs continuously and priorities shift due to changing SoCs, EVs connecting and voltage levels changing. The power consumption will keep increasing until a grid violation is detected, decrease a bit followed by a small increase and the loop goes on. None of the grid components are allowed to violate the presumed limitations (node voltages/cable current/ transformer power) which means that the total charging power is increasing until the weakest component reaches its limit. If the limit is crossed, the charging power of all EVs connected in the sub-system decreases with some slope until the weakest component returns back to its proper status. Following the return back to the proper status, the charging power of each individual EV is increased with a slope proportional to its rank on the priority list. In case two batteries have identical SoC, the average charging power is equal for both.

The functionality of the sub-system controller is explained by a simplified example shown in Fig. 5.17. Two EVs are connected at time, T=0. The figure is divided to the three following graphs:

- Graph a - shows the charger input signal S_{charge}
- Graph b - shows the simplified charging power P_{batt}
- Graph c - shows the simplified state of charge SoC

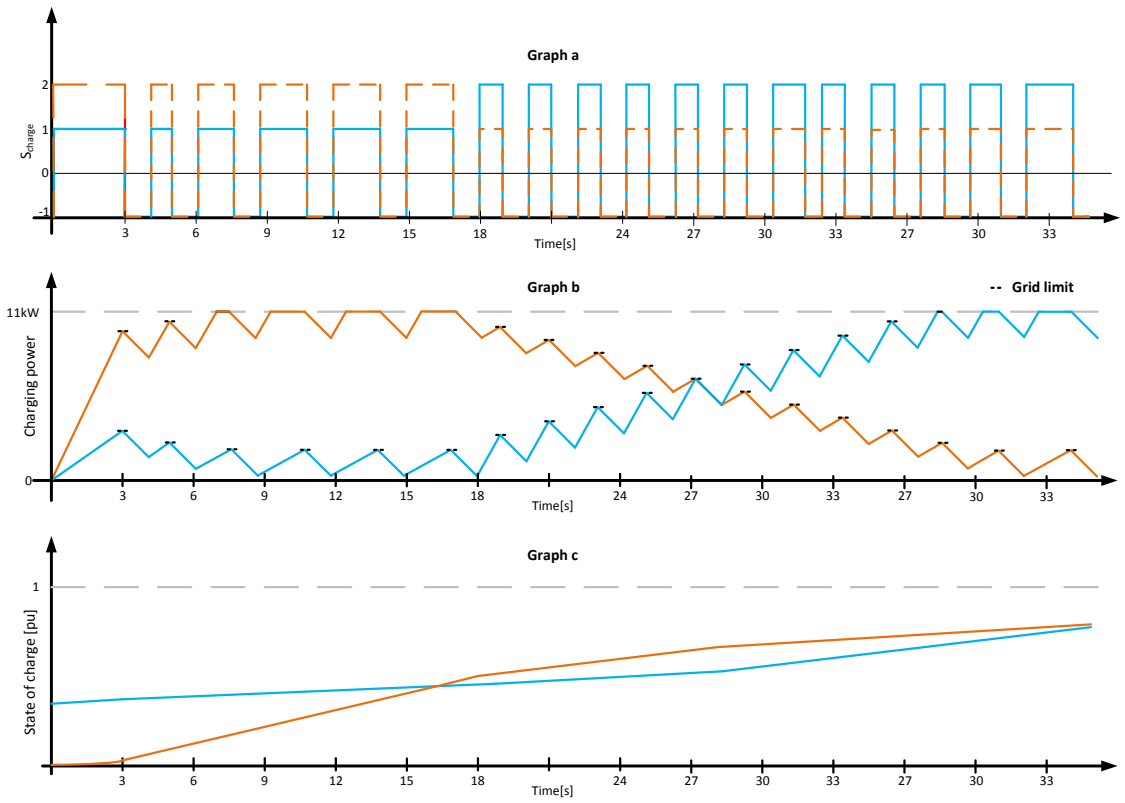

Figure 5.17: Fundamental principles of the sub-system controller

A few key points:

- The EV chargers are presumed to contain voltage meters at their input terminals
- The lower voltage limit is 0.94 pu
- The orange graphs represent EV1 and the blue represent EV2

On Graph b at time T=0, none of the EVs are charging. Graph c shows that the SoC is different for both EVs. EV2 is storing more energy than EV1. Therefore, EV1 is located higher on the priority list than EV2. As a consequence, EV1 is receiving the input signal, S_{charge}, with a higher amplitude after T=0s (see Graph a). As shown previously in Fig. 5.15, the charging power, P_{batt}, is obtained by integration of the input signal S_{charge}. The signal S_{charge} for the orange EV has two times the amplitude of the other EV. Hence, the charging power for the orange EV is increasing two times faster until T=3s. At T=3s, one of the EVs measure a voltage violation. In such a situation both chargers must decrease the charging power until the identified node recovers. Therefore, within this time, both signals S_{charge} are equal to 1. In the example, the proper voltage has been achieved at T=4s. Time T=4s indicates the end of the first "control cycle". This means that the S_{charge} would stay unaltered if nothing would change. The charging power for both EVs are at the levels they are designed to be at.

An important aspect of the control is the decreasing slope of the charging power. This slope must be equal for both units during every cycle. This means that the negative amplitude of S_{charge} must be equal for all connected EVs. For different decreasing slopes the algorithm does not work properly, if at all.

At time T=5s, the voltage at one of the EV terminals is violated again. As before, both control signals immediately drop down to -1 and consequently both charging powers drop down with the same slope. After a voltage level gets back into the acceptable range, the procedure starts over again. In the third cycle, at time T=7s, the power of EV1 reaches its maximum power of 11kW and from this moment the charger connected to EV1 is charging with the maximum constant power P_{bat} = 11kW. The entire procedure repeats continuously until T=16s. At this time the SoC of EV1 becomes equal to the SoC of EV2 (see Graph c). This causes a change in the priority list and from this point the average power of the blue EV is increasing and the orange EV is decreasing.

Fig. 5.18 presents original signals from the DSL simulation. The figure only shows the behaviour of one of the EVs connected in the sub-system. It is seen that the charging power almost does not fluctuate (see Fig. 5.18, middle plot).

Fig. 5.18 shows another aspect of the control strategy. The amplitude of the control signal S_{charge} varies with respect to the first position on the priority list, dropping down to the second position after 9430s. This is seen as the reduction in amplitude of S_{charge}. Even as it receives a lesser priority, the EV remains charging with 11kW. This is because the duty cycle, is high enough, for the signal to be positive for longer than it is negative. The duty cycle is adjusted according to the grid limit. The sub-system therefore is capable of supplying at least 2 EVs with maximum power at this time. The power begins decreasing after 9580s when the battery SoC is so high, that it is bumped to the third position on the priority list. The amplitude and duty cycle now becomes so low that the power decreases. This example shows how the EVs are able to make sure that maximum grid utilization is obtained.
Fig. 5.19 shows a fictitious example of the behaviour of 5 EVs in a sub-system. The sub-system controller attempts to utilize the maximum grid capacity with respect to the minimum voltage limit of 0.94 pu. The EVs 5, 4, 3 and 1 are connected to the grid at t=30 minutes. EV 5 and 4 have the lowest SOC which means they get the highest priority and get charged the fastest. As they are charged faster,

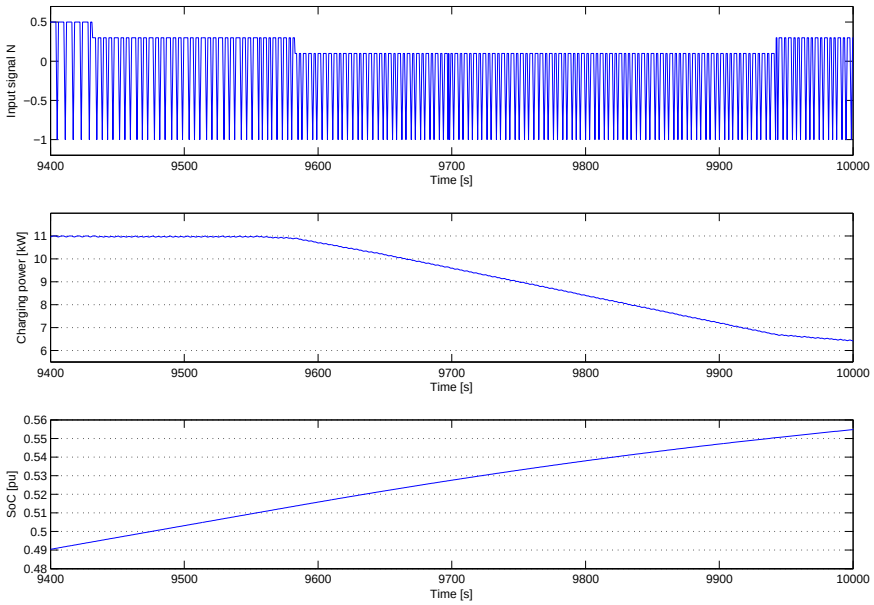

Figure 5.18: EV charger signals

at some point their SoC become higher than EV 3, which means that the priorities shift. At time t=2.5 hour, EV 2 connects to the grid with a SOC of zero, therefore receiving the highest priority. This is seen very clearly in the charging power. As EV 2 connects, the charging power of the four already connected EVs is reduced. This effect is seen at the lower plot of the figure.

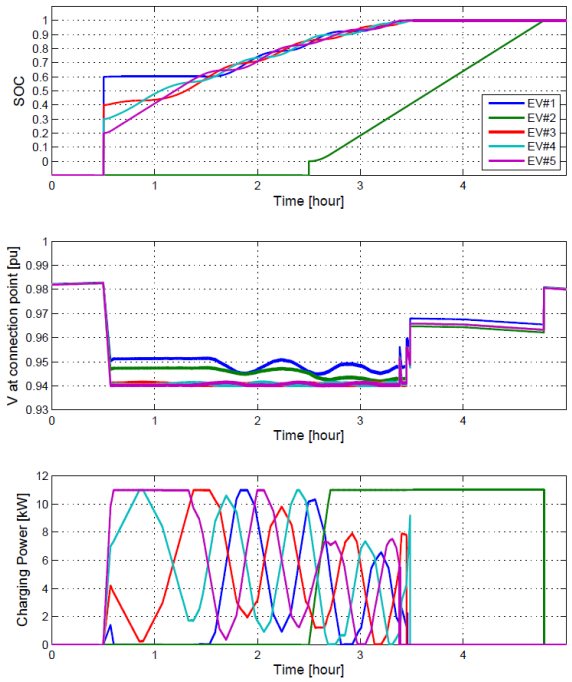

Figure 5.19: 6 EVs example

5.5 Grid Control

The "grid control" is the top layer control strategy of the grid utilization control. In practice this layer is responsible for dividing the total full capacity between the sub-systems in order to equalize the charging time of EVs connected in different sub-systems. By doing so, all EVs of the grid will assist in improving conditions if voltage violations occur even if present in other sub-systems than where the EVs are connected. The grid control has a higher relevance in grids with large differences between the relative strength of the feeders.

As an example, assume that a typical LV grid supplies households, EVs and HPs through 4 feeders. Feeder 1, 2 and 3 are very strong and may possibly supply the double amount of the current load without violating any grid constrains. Feeder 4 is much weaker, and only able supply the actual load by going straight to the voltage level limit. When the voltage levels are very close to the limits, the EV plant/sub-system control will only allow for limited power for charging the EVs. Additionally, HP units will operate in emergency mode which may cause even higher average consumption than during normal operation (see section 5.2). Consequently, some of EV or HP owners located at the end of the weak feeder may complain because of high electricity bills caused by HPs operating constantly in emergency mode or not fully charged EVs even after pressing the fast charging button.

In order to prevent such situations, the top layer control limits the power in some of the strong sub-systems to increase the overall grid voltage, so that the weaker sub-systems can utilize more power. The concept is shown in Fig. 5.20. The grid control receives the average energy value from each sub-system. By limiting the EV power consumption in the sub-systems with the highest state of energy, it is improving the operational conditions in the sub-systems with the lowest state of energy. Only the EVs are directly affected by the grid control operation. Moreover, it is only possible to regulate the EV power down.

Eq. 5.21 presents the calculation of the mean value energy in a specific sub-system.

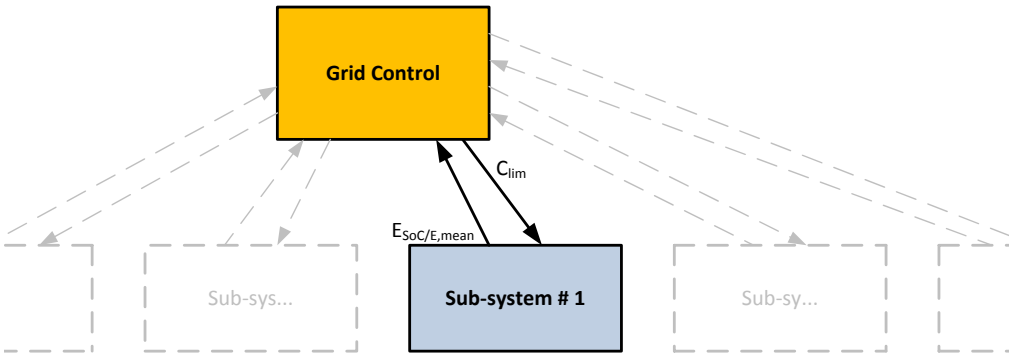

Figure 5.20: Grid control structure

The mean value state of energy is calculated as follows:

$$E_{SoC/E,mean}(x) = \frac{\sum_{n=1}^{k} SoE_{HP} + \sum_{n=1}^{l} SoC_{EV}}{k+l} \quad \text{[pu]} \quad (5.21)$$

where,
$E_{SoC/E,mean}(x)$: Mean value state of energy of sub-system x [pu]
SoE_{HP}: HP state of energy [pu]

SoC_{EV}: EV state of charge [pu]
k: Number of HPs in the sub-system [-]
l: Number of EVs in the sub-system [-]

The EV power is regulated by the feedback signal C_{lim} which is proportional to the difference between the sub-system with the lowest SoE and the considered sub-system. Eq. 5.22 shows the calculation of C_{lim}.

$$C_{lim}(x) = -0.013\ (E_{SoC/E,mean}(x) - SoE_{low}) \quad [-] \quad (5.22)$$

where,
$C_{lim}(x)$: Power limitation factor for sub-system x [pu]
SoE_{low}: Lowest mean value state of energy [pu]

The dependency between the SoE difference and $C_{lim}(x)$ is graphically illustrated by Fig. 5.21. The linear dependency can altered by tuning the constant present in Eq. 5.22. The current value have through limited testing (in LV-II) presented a good trade-off between equality and grid utilization. By extensive testing the parameter could most likely be tuned for more optimal performance. Perhaps by implementing a non-linear characteristic or making the parameter dependent of for instance the lowest voltage level measured in the sub-systems.

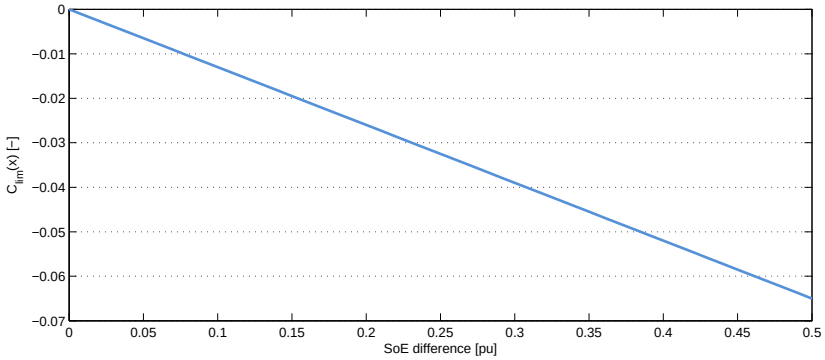

Figure 5.21: Power limitation function

The limitation signal is sent back to the considered sub-system where it is added to the lowest voltage seen by the subsystem control. By doing so the sub-system control reacts as if the lowest voltage has decreased by $C_{lim}(x)$ and therefore reduces the consumption of the EVs. Eq. 5.23 shows this relation. By adding $C_{lim}(x)$, the voltage seen by subsystem control, V_{lim}, reaches the assumed limit of 0.94 pu faster even though the measured voltage is far from the limits. This forces the sub-system control to limit EV consumption.

$$V_{lim}(x) = V_{low} + C_{lim}(x) \quad [\text{pu}] \quad (5.23)$$

where,
$C_{lim}(x)$: Power limitation factor applied to sub-system x [-]
V_{low}: The lowest measured voltage in the sub-system [pu]
$V_{lim}(x)$: The voltage seen by the controller of sub-system x [-]

By implementation of the grid control it is possible to keep the state of energy of the sub-systems relatively close. Examples of the functionality of the grid control is to be found in the in section 5.7, where various case studies are performed.

5.6 Case Studies

This section contains the case studies made in order to verify the control applied to the heats pumps and electric vehicles. The section contains three sub-sections followed by a discussion of the gained results.

The HP thermal consumption is applied according to what is presented in sub-section 3.3.2, the EV driving patterns according to section 3.4 and the ambient temperature for summer and winter as follows:

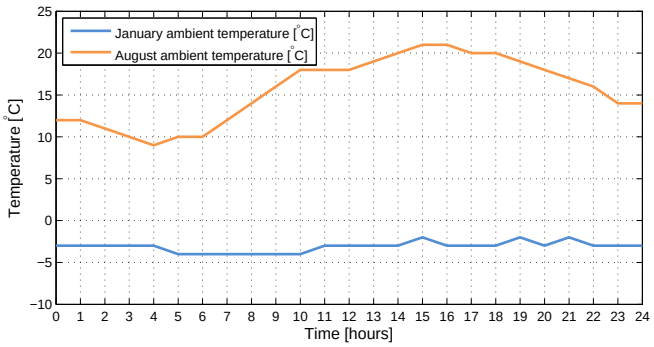

Figure 5.22: Ambient temperatures for Aug 11th and Jan 22nd

The placement of the sub-systems for both LV grids and the units per sub-system, which have been distributed randomly across the grids, are to be found in appendix A.5.

All simulations have been pre-initialized for 7 hours. This means that the actual simulations run for 31 hours instead of 24. Only the last 24 hours are presented.

The pre-initialization is performed since that starting the simulations at 00:00 would cause all EVs to start charging from midnight which is not realistic. Similarly, all HPs would be turned off at midnight since they all start with some energy in their water tanks. The HPs need to run for some time in order to randomize their behaviour. The HP initial energy has been randomized in the range 0.2 - 1 pu.

The case studies will be highly dominated by winter scenarios as this will test the control to its fullest, since the grids naturally will be heavier loaded. Only the first sub-section contains summer studies, which are performed to give a wider understanding of the grid behaviour in the seasons.

The first sub-section contains the results gained by completely removing the grid limitations of the models as well as removing the 0.2 pu dead-band of the heat pumps reserved for emergency voltage control. By doing this the units will consume power as needed. These scenarios are performed to have a reference for the studies with active control.

The second sub-section presents the results obtained by switching unit and sub-system control on.

The third sub-section presents the grid control case studies.

5.6.1 No Control

This section presents scenarios where the units are not controlled. This has the effect that the units will consume power without any concern for the grid limits.

Fig. 5.23 shows the results of the "no control" case study for LV-I summer and winter. The upper plot represents summer and the lower plot represents winter. The orange graphs represent the lowest voltage recorded in sub-system 4, which is the weakest sub-system of LV-I. The blue graphs represent the lowest voltage recorded in sub-system 7/8, which is the strongest sub-system of LV-I. The relative strength of the sub-systems have been decided based upon the results gained in the steady state analysis.

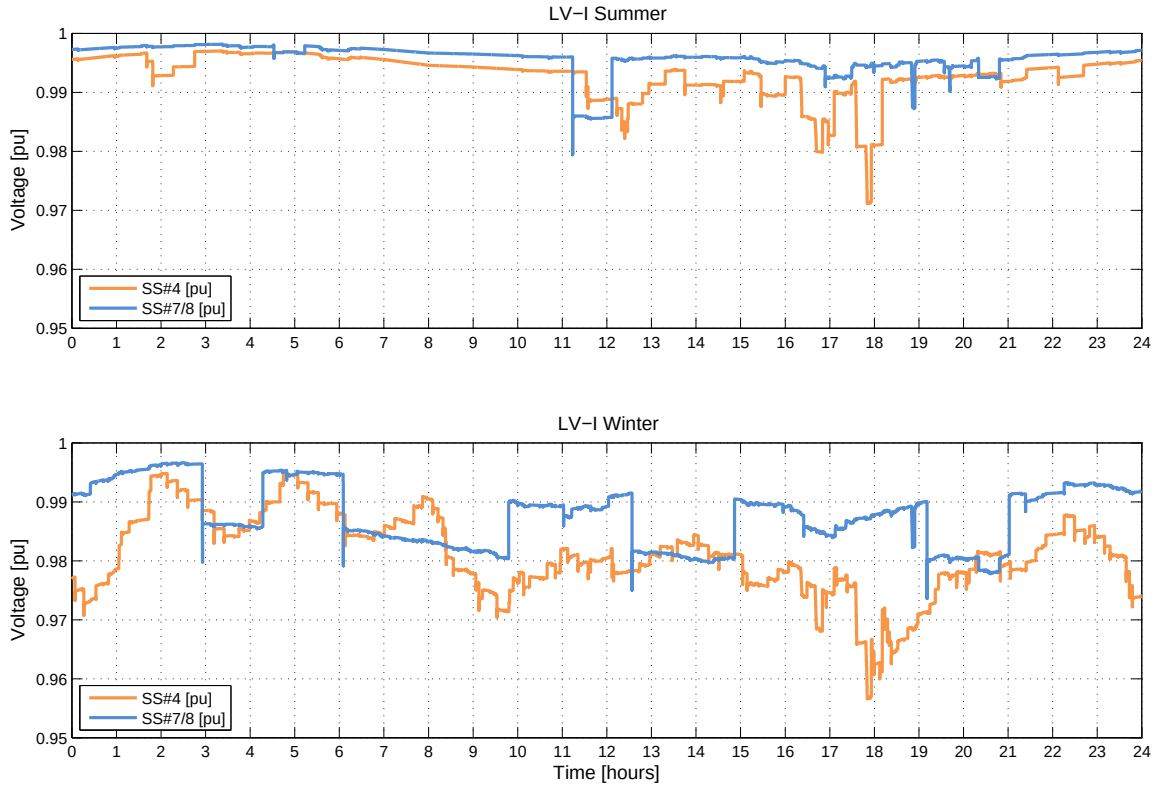

Figure 5.23: LV-I, No Control - Feeder voltage

The plot shows that due to the high strength of LV-I, no grid violations occur even when the units are allowed to consume as they please. It is visible that the voltage is affected by the EVs connecting around 17:00 both during summer and winter.

The results show that sub-system four is only weak when compared to the other sub-systems of LV-I. The relative strength of sub-system 4 is high. As the weakest and strongest sub-systems has been investigated it is presumed that the voltage levels of the remaining sub-systems will be in-between these.

Fig. 5.24 shows the same scenario for LV-II as the one just applied to LV-I. The grid violation parameters for the control has been shut off and the dead-band of the HPs has been reset to function between 0-1 pu. A winter and a summer scenario is presented. The orange graphs represent the lowest voltage recorded in sub-system 6A, which is the weakest sub-system of LV-II. The blue graphs represent the

lowest voltage recorded in sub-system 3A, which is the strongest sub-system of LV-II.

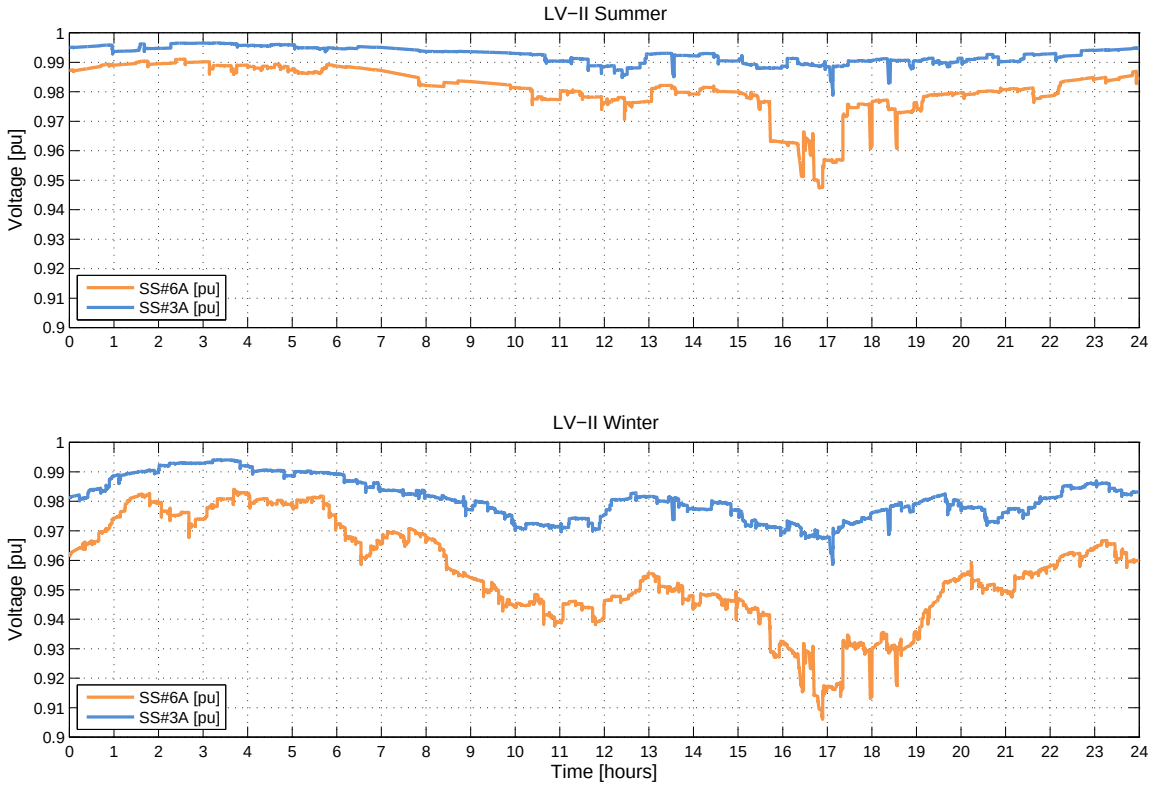

Figure 5.24: LV-II, No Control - Feeder voltage

The study of LV-II shows that the grid is able to support the non-controlled units only during summer where all sub-systems are expected to stay above the voltage level of 0.94 pu.

The winter scenario shows that the non-controlled units push the voltage level of sub-system 6A way below the limit of 0.94 pu as the EVs connect during the afternoon. The sub-system is just 0.005 pu above the grid code limit of EN 50160 [9] which is considered to be very low. It is clear to see that it would be beneficial if some of the load can be shifted from the time period of 16:00 to 19:00 to other times of day.

The winter scenarios of the weak and sub-systems of both LV grids will be used as references in the following case studies of the performance of the control with grid limits activated as well as the HP emergency control activated.

5.6.2 Sub-system Control

The case studies performed in this sub-section presents the functionality of the controlled units without the top-layer grid control active. Therefore, it is expected that the voltage levels will improve from the non-controlled scenario. Only winter cases will be presented and only for the weakest feeders as these challenge the control the most.

Fig. 5.25 shows the power consumption measured at the transformer of LV-II for a winter case without control and compares it to the one where the sub-system control is active. The upper plot depicts the transformer power of the two scenarios and the lower depicts the voltage level of sub-system 6A which is the weakest sub-system of LV-II. The blue graphs depicts no control and the orange control.

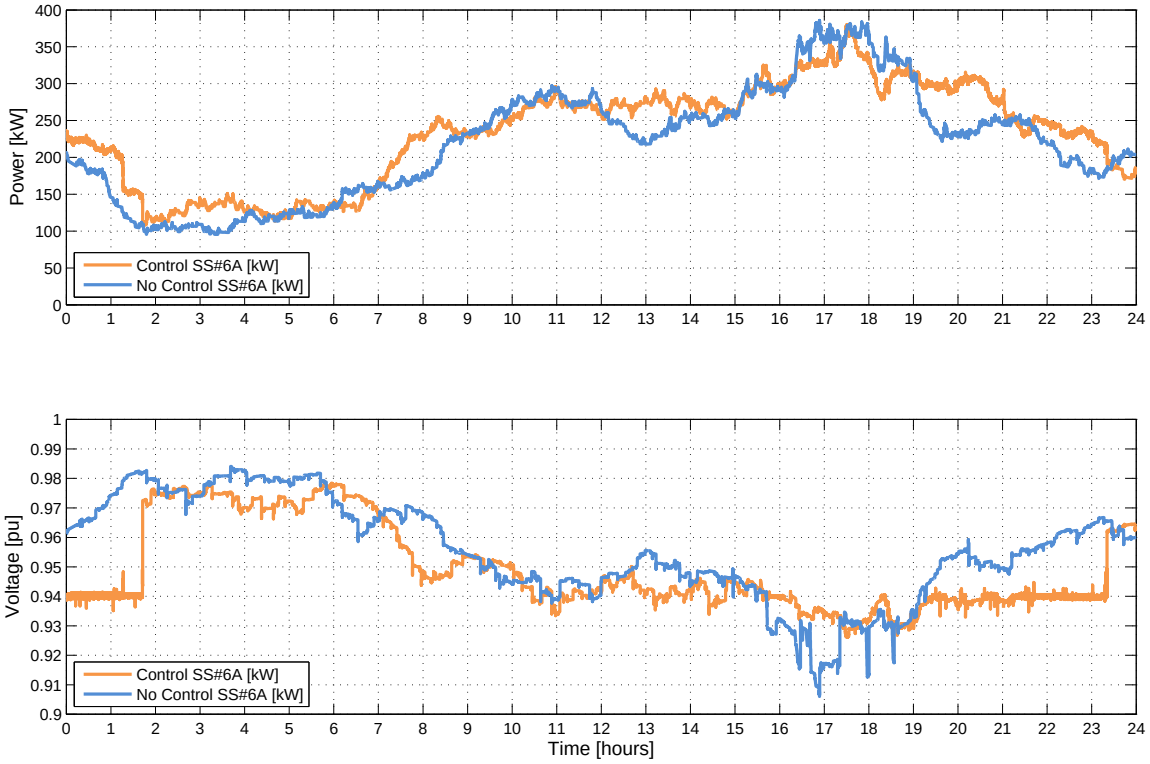

Figure 5.25: LV-II, Winter - Control without the top layer - Power and voltages

The figure clearly shows that the voltage improves as the control is applied. The worst voltage measured without control is ≈0.905 pu and with control ≈0.925 which is a relatively large improvement. In general the power plot shows the general tendency that the consumption of power is increased at times where the the grid allows for higher loading and decreases when the voltage limits are violated.

At the voltage plot it is seen that with control, the EVs that arrived home the day before, are still charging. They are charging all the way to the limit of 0.94 pu. At some point the EVs are fully charged to SoC = 0.9 pu, and the voltage floats freely near the level it had without control. Around 8:00 when people are awake and the household consumption increases, the voltage of the sub-system decreases. As no EVs are connected and the voltage is not severe enough for the HPs to apply emergency control, nothing much happens until the EVs begin connecting at 16:00. At this point the charging of the EVs begin. The no-controlled EVs all charged with full power as they arrived which caused the rather massive voltage drop at 17:00. The controlled units highly improve this. The EV consumption is completely shut down when the voltage is below 0.94 pu. The voltage drop seen in the controlled case is therefore due to household consumption and HP consumption. The HPs enter emergency operation

around 16:30 and helps keep the voltage drop close to 0.94 pu for some time. The length of the voltage drop is unfortunately so long, that the HPs start consuming again while the voltage is below 0.94 pu. The HP emergency control is better suited for short high amplitude voltage issues, especially during winter, where they need to consume rather often.

The heat pump emergency operation is presented for the previous case in Fig. 5.6.2. The upper plot represents the dead-band manipulation off all heat pumps connected in sub-system 6A and the lower plot the lowest voltage level of the sub-system.

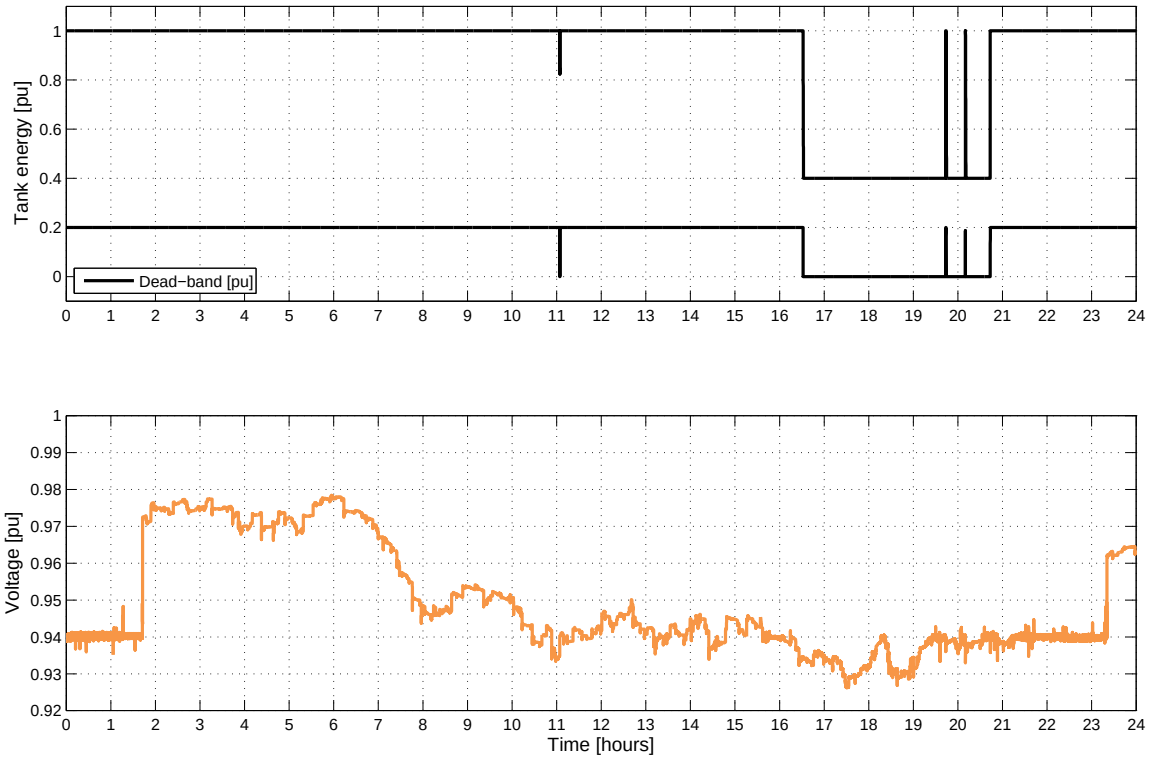

Figure 5.26: LV-II, Winter - Control without the top layer - HP emergency control

The figure shows that the EV emergency control is active during the winter day in the weakest feeder. At 11:00 a voltage drop occurs. The voltage drop has a value of 0.935 pu. As the heat pumps are equipped with an adaptive delay, it takes roughly 10 minutes before they react. It is seen that the voltage improves during the operation, which is the exact idea behind the control approach. Between 16:00 and 17:00 the voltage yet again drops below 0.94 pu. The HPs react again, but are this time not able to increase the voltage sufficiently. This means that the HPs operate in emergency mode for roughly four hours. The heat pumps are heavily loaded by the thermal demand which means that they are not able to extend the consumption for the full four hours. As such, the HPs do not assist in active voltage improvement during the 16:00-21:00 period. The HPs are better suited for fast steep voltage drops during winter.

Fig 5.27 shows the same scenario as the one just presented for LV-II, for LV-I.

This case study shows that LV-I's weakest feeder, even during winter time, is able to support 50% HPs and 25% HPs even without control. This means that LV-I in its current state will is ready for 2025. As no voltage limits are crossed, cable- or transformer loading exceeded the control is inactive for the

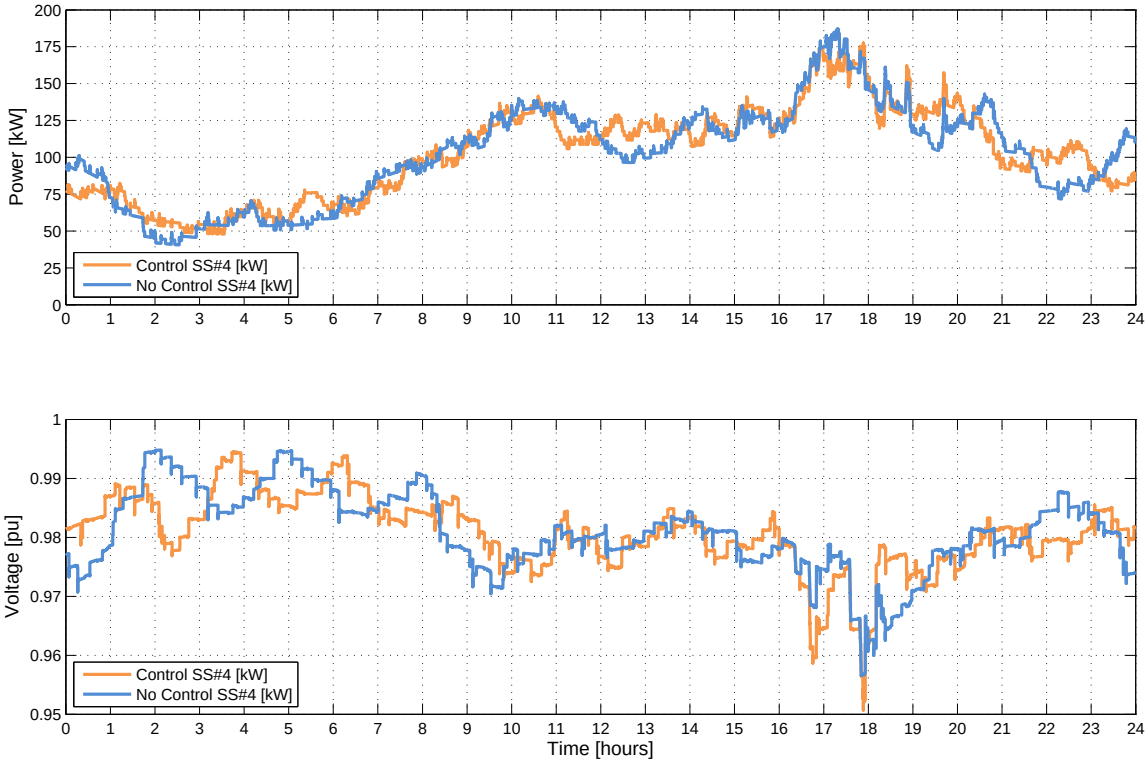

Figure 5.27: LV-I, Winter - Control without the top layer - Power and voltages

whole study case.

An interesting side effect of implementing the control in a grid as strong as LV-I is the fact that the energy supply of the heat pumps is effectively lowered as 0.2 pu of the tank is reserved for voltage emergencies. The effective tank size is limited which means that the HP will run more often. The voltage emergencies are most likely not going to happen due to internal events in the LV grid, but depending of what occurs in the external grid, the emergency control could at some times be useful anyway.

5.6.3 Full Control

The full control scenarios, as the name implies, present the full implementation of the introduced control strategy. As the previous study cases have shown that LV-I is so strong that all units are able to charge with maximum power at all times, the grid control will only be presented for LV-II during winter.

Fig. 5.28 compares the sub-system control performance to the full control performance. The plot is divided into three parts. The two upper graphs represent the average energy of the units of the nine sub-systems. The orange and blue lines, which have very low average SoE between 16:00 and 22:00 represent sub-system 6A (orange) and sub-system 6B (blue). The lower part shows the lowest voltage level measured in sub-system 6A.

The case study shows that the full control further increases the voltage level of the weak sub-system 6A. This is done by limiting the EV power consumptions in the stronger sub-systems.

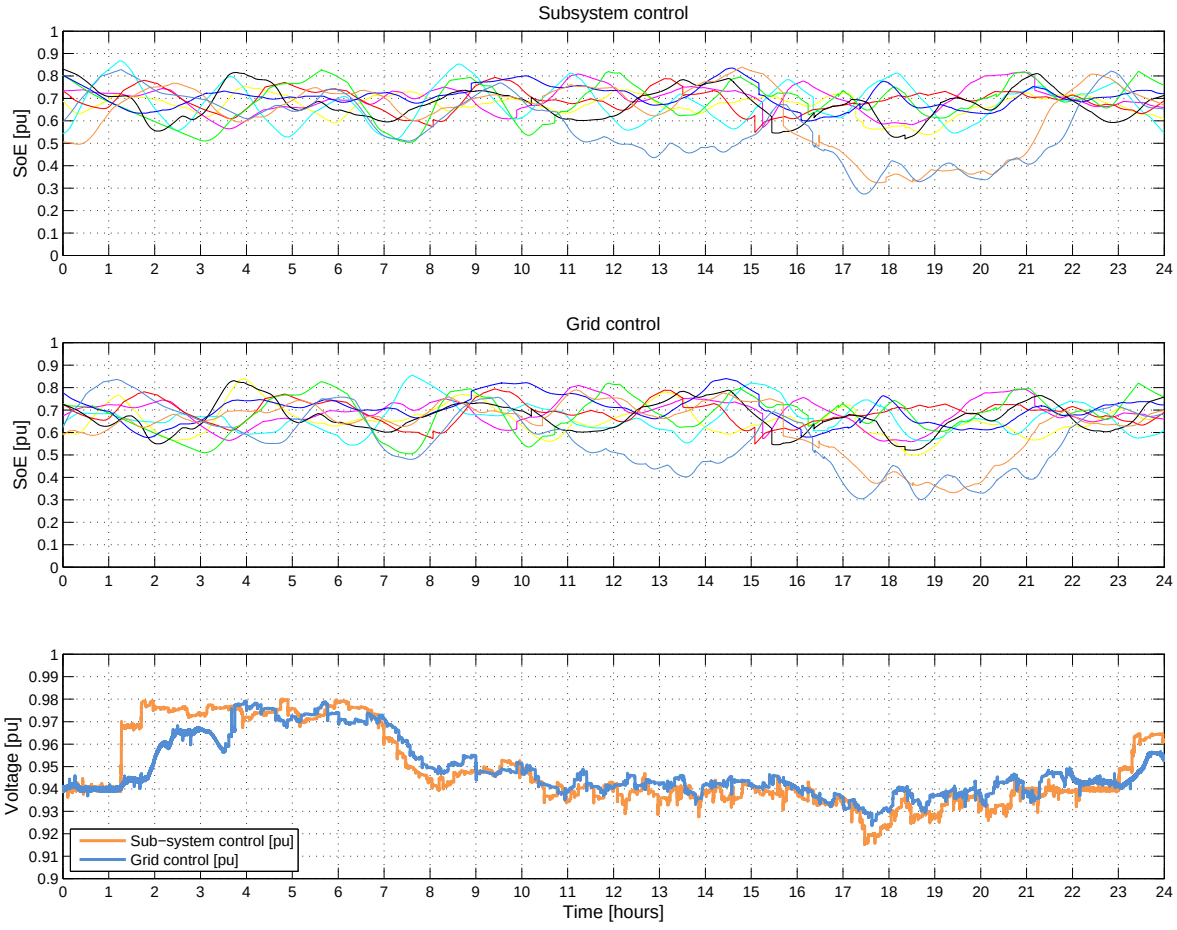

Figure 5.28: LV-II, Winter - Comparison between sub-system control only and full control - Overview of behaviour

The figure shows that the lowest voltage recorded improves by almost 0.01 pu with the grid control turned on. Due to the adaptive power consumption of the electric vehicles, the EVs in weak sub-systems are forced not to consume at times where the voltage drops below 0.94 pu. This has the consequence that the average energy per unit in the sub-system will fall behind the average state of energy of the stronger sub-systems. Without the grid control, the EVs of strong sub-systems will con-

tinue consuming even if the voltage level of the weaker sub-systems drop below 0.94 pu. This means that the EVs of the strong sub-systems actively contribute to the poor voltage conditions of the weaker sub-systems. The grid control forces the EVs of the stronger sub-systems to react to the poor conditions in the weaker sub-systems by limiting the power consumption. The effect of the grid control clearly shows in Fig. 5.28 The total EV consumption is effectively shifted from the highly congested 16-21 period to late evening and night.

Fig. 5.29 shows the power consumption of the full control compared to only sub-system control. The plot is divided into four sections. The upper one shows the lowest voltage of sub-system 6A. the second section shows the transformer load. The third and fourth the EV power consumption with only sub-system control and full control.

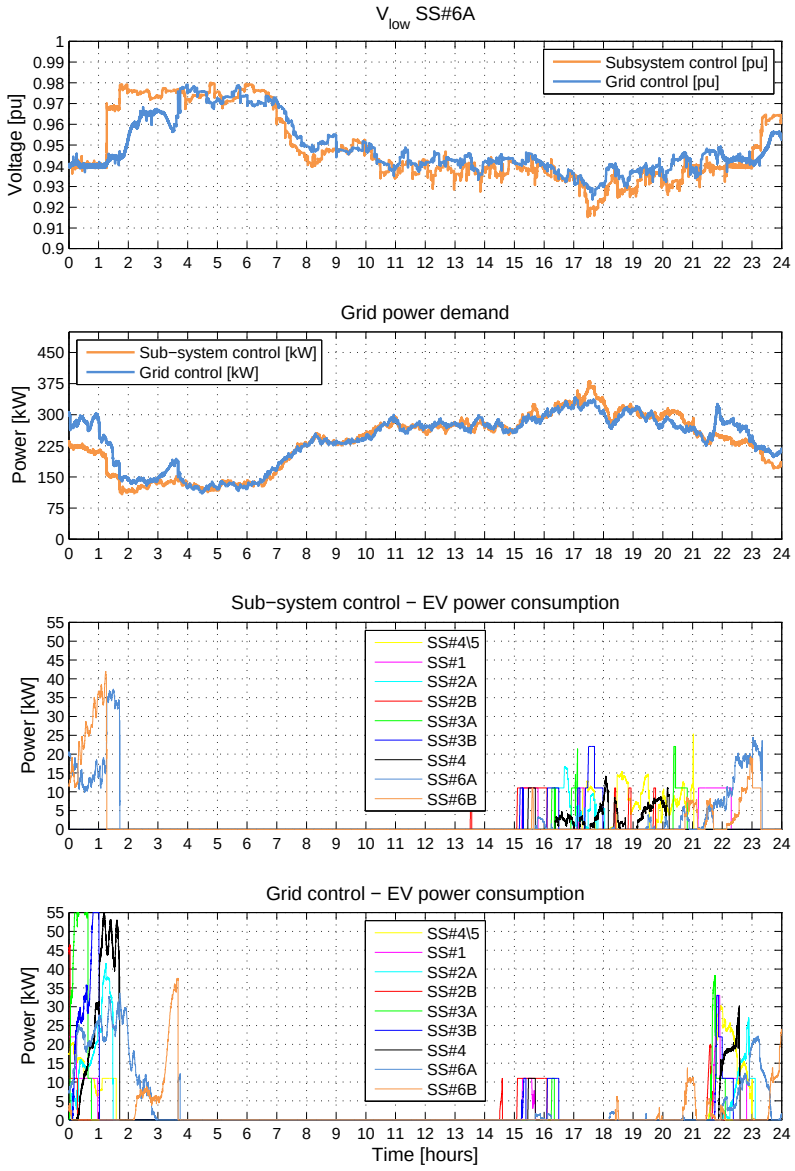

Figure 5.29: LV-II, Winter - Comparison between sub-system control only and full control - EV power consumption

The two lower sections clearly shows the functionality of the grid control. When the voltage of the weaker sub-systems drops during the highly congested period between 16:00 and 21:00 the grid control ensures that most EVs are not allowed to charge within the period effectively increasing the volt-

age level. As the voltage levels improve as the household consumption decreases, the EVs are yet again allowed to charge.

5.7 Discussion

This section presents a short overview of the result obtained by doing the case studies presented in the previous section.

The case studies without control shows that, as expected, the strength of LV-I is relatively high which makes is a poor candidate for a control approach which optimises voltage conditions. LV-I in its current state would most likely be able to handle the extra load from the units in 2025 without undergoing any major improvements.

LV-II on the other hand is much weaker. Therefore, it is a good candidate for the implementation of the control strategy. The case studies have shown that without control, the units add so much consumption at unfortunate times, that the weaker feeders almost cross the voltage limits of EN 50160.

Fig. 5.30 presents an overview of the voltage recorded in sub-system 6A under the influence of different levels of control.

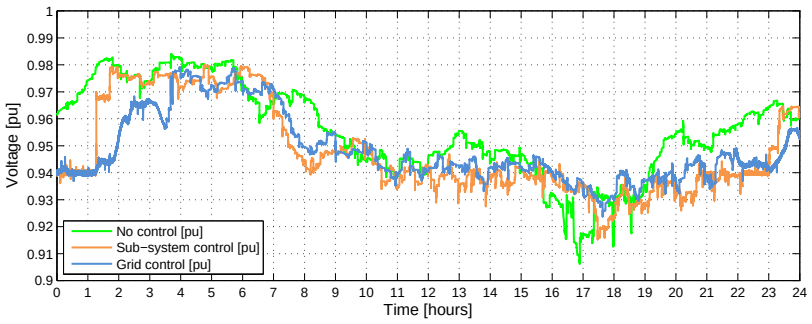

Figure 5.30: Voltage comparison under the influence of different levels of control - Sub-system 6A

Each layer of control improves the voltage some by utilizing the flexibility offered by the units. The heat pumps have presented better voltage improvement functionality during short voltage drops.

The top layer grid control has presented the ability to be able to further increase the voltage of the weaker feeders. The grid control has been tuned very aggressively in the case studies presented in order to emphasise its functionality. For practical applications this might not be the best approach. Limiting the power consumption by 1kW in a strong feeder does not grant 1kW extra capacity in a weak feeder. Therefore the ratio between limitation and improvement by the applied is not ideal. Applying the grid control for practical applications would therefore need to finely tuned in order to meet some specific demands.

6 Flexibility Control

This chapter contains the flexibility control implemented in the models. The flexibility control is not a isolated application. It works in parallel with the dynamic control structure presented in chapter 5.

The flexibility control is designed for the aggregator to be able to provide balancing services to the TSO. The regulating power needed by the TSO in order to balance the frequency has been described in section 2.3, page 13.

Section 2.3 describes that the regulating power can be divided into three separate groups which have various properties, such as rules for when and how they are activated as well as for how long. The flexibility control implemented in this project is not targeted specifically for any of the three groups. The approach is based on the idea, that the aggregator will enter into an agreement with the TSO, where the aggregator is paid somewhat proportionally to the flexibility possible to offer.

The control has been designed for a scenario where the TSO is able to send a signal to the grid controller (via the aggregator), requesting a specific consumption of the grid, which the controller will attempt to match by manipulating the unit operation. The control design will treat the HPs and EVs differently as they offer different possibilities and limitations. They will be working in parallel towards the same goal which is to track the power request signal.

The heat pump flexibility control will be able to track the signal in steps of ±3.1kW by turning on-/off single units. Overly aggressive control of the HPs will cause the heat pumps to become increasingly less responsive to the control as well as lowering the heat pump system average energy supply.

The EVs will be able to adapt the power consumption continuously to match the signal, but is dependent of the amount of EVs connected which determines the maximum amplitude of the consumption. Furthermore, the SoC of the EVs connected will determine for how long it is possible to track the signal.

The primary purpose is not only to implement an approach possible of acting flexible "by command", but also to investigate how flexible it is possible to act while respecting consumer comfort and grid limitations.

It is not possible to define flexibility as being one specific quality. The investigations carried out will look into flexibility in terms of the following items:

- How does the lenght of a request influence the flexibility?
- How does the time of day affect the possibility of acting flexible?
- How does the seasons affect the possibility of acting flexible?

The chapter starts out with an overview of the whole system where the items concerning the flexibility control are highlighted.

In the second section the specific modelling of the heat pump flexibility control is presented followed by the EV modelling in section three.

The last section contains the case studies performed to investigate the bullets presented previously.

6.1 Overview

This section presents an overview of the flexibility control. As stated in the chapter introduction, the TSO will request a specific consumption of the LV grid as whole via the aggregator. The aggregator will send a request signal to the grid controller which will try to match the consumption to the request.

Fig. 6.1 represents an overview of the whole system (dynamic control included). The signals and parameters relevant to the dynamic control has been greyed out.

As seen, the grid controller is receiving two new signals. The $P_{request}$-signal represents the tracking signal which is requested via the TSO. The idea behind the signal is that the aggregator, which is controlling the units in a lot of different LV grids, will receive the "full" request and then based upon capacity, divide the request between the grids. The P_{actual}-signal represents the power measured at the transformer terminals.

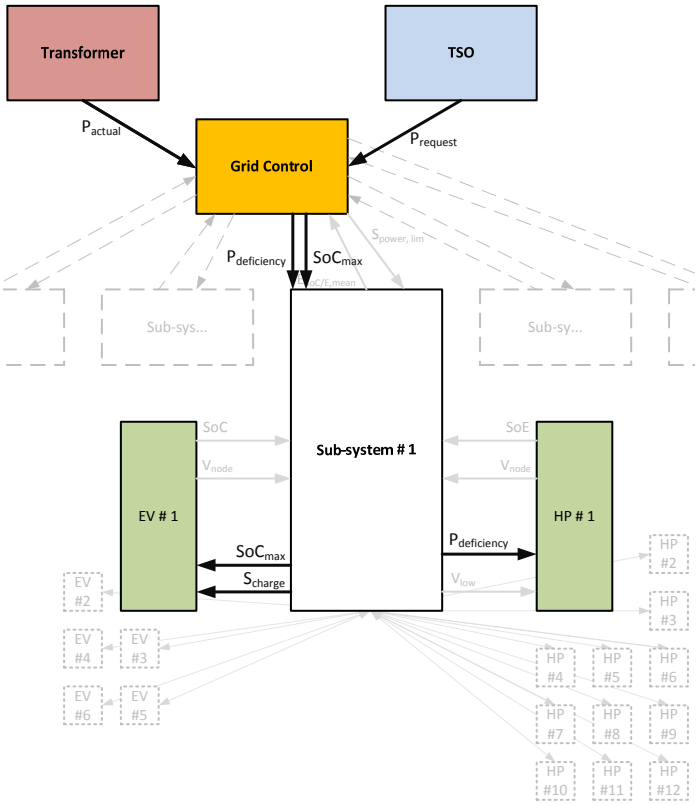

Figure 6.1: Flexibility control - Simplified overview

Based on the two new inputs, the *Grid Control* calculates the difference between request and actual consumption. The difference has been named $P_{deficiency}$ and determines the operation of the flexibility control completely.

The heat pumps track the deficiency signal by control of the dead-band. If more or less power is required the lower- or upper limit is manipulated until the power is within ±3.5kW. The heat pumps are therefore allowed to produce a limited tracking error. The control will stay passive if the error is within the acceptable range.

The EVs will track the signal continuously which means that they react to the slightest mismatch between the requested amount of power and the actual amount of power.

The power deficiency is defined as:

$$P_{deficiency} = P_{actual} - P_{request} \quad \text{[kW]} \quad (6.1)$$

where,
$P_{deficiency}$: Power deficiency in the grid [kW]
P_{actual}: Power measured at the transformer terminals [kW]
$P_{request}$: Power requested by the TSO via the aggregator [kW]

Fig. 6.2 represents a graphical representation of Eq. 6.1.

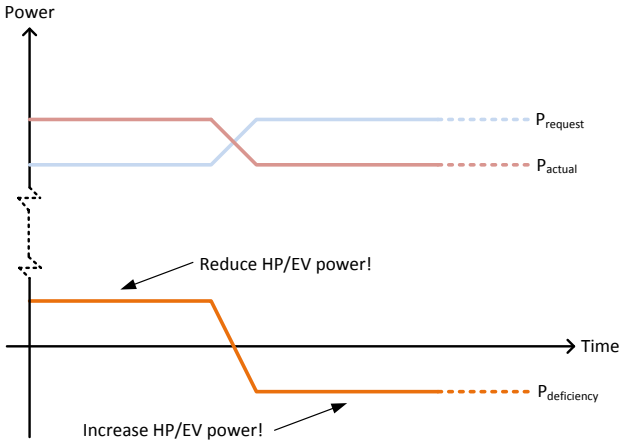

Figure 6.2: Example of the power deficiency presented in Eq. 6.1

6.2 Heat Pump Flexibility

As previously mentioned, the flexibility control is applied as working in parallel with the dynamic control. The HP dynamic emergency control presented in chapter 5, has a higher priority than the flexibility control. This means that if a severe voltage issue occurs while the system is tracking a specific request, the emergency dead-band control will overrule the control described within this section.

The heat pump plant overview presented in Fig. 5.2 has been extended to include the deficiency signal generated by the top layer *Grid Control*. The sub-system controller has no real influence on the HP flexibility operation. In regards to the flexibility control, the sub-system controller merely serves as a link in-between, relaying the deficiency signal and lowest voltage to the various HPs of the sub-system.

Fig. 6.3 shows the extended HP control block for the flexibility control.

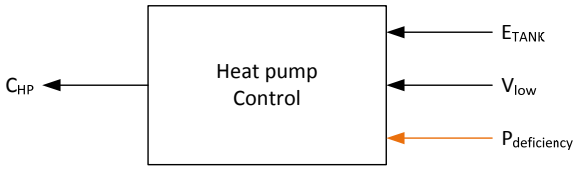

Figure 6.3: HP Control block including the tracking signal

The HP flexibility control has been designed to force the heat pumps in strong sub-systems to turn on units more aggressively than heat pumps in weaker sub-systems in case of a negative deficiency. Likewise, in case of a positive deficiency, the HPs in weak sub-systems will more aggressively turn off units than HPs in strong sub-systems.

This approach has the side-effect that the overall tracking by the HPs will be slower as not all units will act as fast as possible. This side-effect of the control is not necessarily seen as being very negative. Heat pumps naturally require to be controlled smoothly in order not to reduce the overall energy supply of the HP-system.

The HP dead-band control applied to control the flexibility operation of a single HP is described by Eq. 6.2 and Eq. 6.3. First, the control of the lower band which performs the turn-on operation is presented.

$$\begin{aligned} &\text{if} \quad P_{deficiency} < -3.5kW \quad && K_{Fmin}(t) = K_{AF,min}(v) \\ &\text{else} && K_{Fmin}(t) = -\infty \end{aligned}$$

$$E_{min} = \int K_{Fmin}(t)\ \mathrm{dt}\ , \quad 0.2 \leq E_{min} \leq 0.55 \qquad \text{[pu]} \quad (6.2)$$

where,
$K_{Fmin}(t)$: Integration factor [-]
$K_{AF,min}(v)$: Variable dependent upon the V_{low} input [-]
E_{min}: Lower limit of the regular ON-/OFF control [pu]

The $K_{AF,min}(v)$ parameter is dependent upon the lowest voltage of the system. The parameter controls fast the lower band is increased when additional power is needed. The model reads the value of

$K_{AF,min}(v)$ from an array.

The control of the upper band controls how aggressively the control turns off units. The upper-band control acts opposite to the lower band. It tries to turn off units faster in weak feeders and turn off slower in strong feeders. The control of the upper band looks as follows:

$$\begin{aligned} &\text{if} \quad P_{deficiency} > 3.5kW \quad && K_{Fmax}(t) = -K_{AF,max}(v) \\ &\text{else} && K_{Fmax}(t) = \infty \end{aligned}$$

$$E_{max} = \int K_{Fmax}(t)\ \mathrm{dt}\ , \quad 0.65 \leq E_{max} \leq 1 \qquad \text{[pu]} \quad (6.3)$$

where,
$K_{Fmax}(t)$: Integration factor [-]
$K_{AF,max}(v)$: Variable dependent upon the V_{low} input [-]
E_{max}: Upper limit of the regular ON-/OFF control [pu]

The $K_{AF,min}(v)$ and $K_{AF,max}(v)$ parameters are highly influential to the performance of the flexibility control. The tuning of these parameters has been an interesting task to perform. If they are tuned too lightly the heat pumps will not be able to track the deficiency signal very closely. If the heat pumps operate too aggressively their average energy supply is lower since turning on and off frequently, which also in the long term is not healthy for the induction motor.

The control allows for a tracking error of ±3.5kW, which in total is 7kW. This value has been chosen since the HPs employ soft-starters. A HP starting up will for one second consume 6.2kW. As such, the dead-band allows for the HP operation with soft starters. If the dead-band did not include space for the soft-starter, the HPs could start an avalanche of units turning on and off, since a heat pump turning on could cross the upper tracking band which would the turn of another HP.

The flexibility control will at some point of time wear itself out. For some amount of time, the heat pumps will be able to track the request, but as the the requested electric consumption most likely will not match the thermal demand, at some point the mismatch will cause the tank to be full or empty. If the tank is full at a time where more power is requested, increasing the lower band will have no effect on the consumption. The same would apply for an empty tank and a request for less power. The effect of this phenomena would have limited effect for the overall tracking capabilities of the grid as whole if occurring for a single heat pump. Unfortunately, if the tracking request is extended in time,as time grows the side-effect will occur at more and more HPs making the control unable to track a request.

The more aggressive the $K_{AF,min}(v)$ and $K_{AF,max}(v)$ parameters are tuned, the faster the control will wear itself out.

The settings of the parameters is depicted in Fig. 6.4. The figure shows the two factors plotted versus the lowest voltage recorded in the sub-system. The orange curve represents $K_{AF,max}(v)$ which controls the upper band (turn-off band). The blue curve represents $K_{AF,min}(v)$ which controls the lower band (turn-on band).

It is seen that they differ through the voltage range of 0.9 - 1 pu according to the design approach described throughout the section.

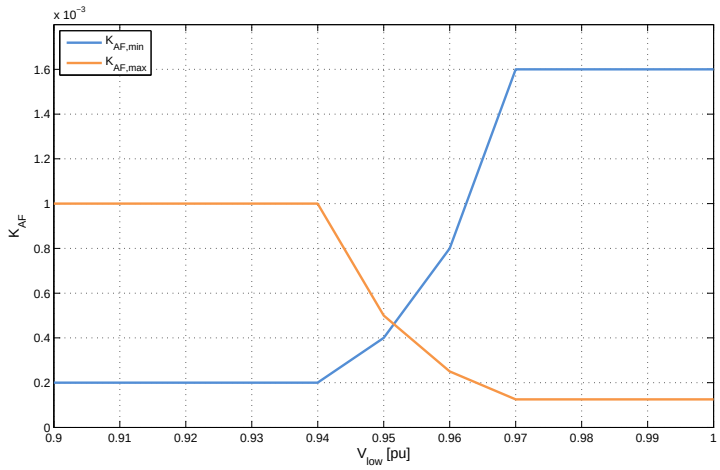

Figure 6.4: Setting of the flexibility integration factors

Fig. 6.5 shows a randomly chosen example of the HP flexibility control. The operation of the heat pumps of two sub-systems, a weak and a strong, are shown. The plot is divided into three sub-plots. The upper plot depicts the deficiency signal and the dead-band of the HP control.

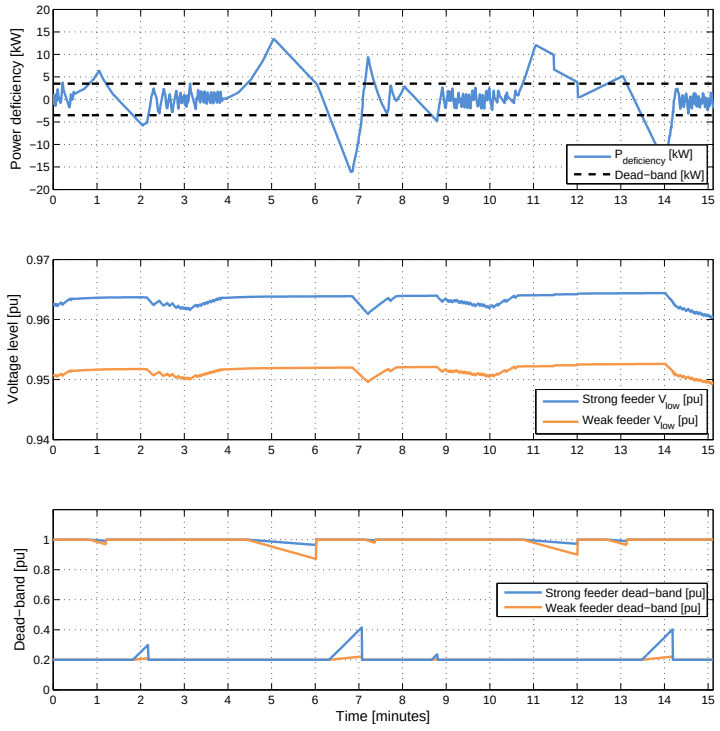

Figure 6.5: Example: Heat pump flexibility control functionality

The middle plot shows the lowest voltage level recorded in the two sub-systems which controls the integration factors according to Fig. 6.4. The lower plot shows the product of the control, namely the HP dead-band manipulation. As seen, the control increases the lower limit when more power is requested and reduces the upper limit when less power is requested. According to Fig. 6.4 the heat pumps react differently due to the different voltage levels in the sub-systems.

6.3 Electric Vehicle Flexibility

The EVs are well suited for this type of control, as their power consumption unlike the HPs, can be varied. The idea behind the EV control is similar to the one applied for the dynamic top layer control. The dynamic top layer control limits the power consumption of EVs in certain sub-systems.

The sub-system control applied previously automatically tries to utilize all free capacity in a sub-system while prioritizing the EVs with lower SoC. This approach will not be changed in the flexibility control. Therefore, the maximum possible consumption of the EVs is obtained by applying no limitations of the standard control.

As such, the flexibility control needs to be able to gradually limit the power consumption to match the deficiency signal. As such, the control applied needs to be able to fully limit the standard control to match the lowest possible request and do nothing in order to match the highest possible request.

There are two major limitations of the EV flexibility. First of all, if a low amount of EVs are available in the grid, the flexibility will be limited. This scenario could occur during the working hours of a regular weekday where many people are at work. The second limitation is that very little flexibility is available if most of the EVs in the grid are fully charged. This could occur since most EVs are arriving back at the household during late afternoon and the charging begins. After some time the majority of the EVs will be charged. Ideal flexibility conditions are therefore when the EVs are available and not fully charged.

The first limitation cannot be circumvented as this only relies on the EV user preferences. The second can be bypassed in the contract between aggregator and EV owner. Basically, it would be beneficial to the flexibility operation if the EVs were only charged to the SoC they need, which in most cases does not imply a fully charged battery. As presented in section 3.4 a lot of the EV owners will be driving less than 40km/day corresponding to roughly 6kWh (or 0.25 pu) of the battery capacity. The owners driving a short daily distance therefore do not necessarily need a fully charged battery to meet their demands. Some of these owners could most likely be convinced to allow the aggregator to keep some battery capacity as reserve, if this would cause a reduction of the monthly fee.

The EV batteries are not allowed to be discharged past 0.2 pu since it would reduce the battery life time. An EV owner driving an average distance of less than 40km/day would therefore ideally need a capacity of 0.45 pu when leaving the household in the morning. As many factors influence the capacity needed, some additional capacity would need to be added before the time of leaving in real life.

In order to lower the modelling complexity it has been decided to limit the the regular charging to a maximum of 0.7 pu for all EVs in the LV grids during normal operation. If some flexibility demand is required, the upper limit is increased to the battery maximum of 0.9 pu. Therefore, 0.2 pu has been put in reserve for the flexibility control. If an EV owner know that he/she needs to drive for a longer distance than usual the user can request fast charging (see section 5.3) which overwrites the upper limit of 0.7 pu. The activation of a fast charging request would add to the EV user monthly fee.

As introduced previously, the EV flexibility control takes place at the top level control, the *Grid Control*. The regular grid control, presented in chapter 5, is turned off when a request is active. Basically the flexibility is prioritized over equality when a request is active.

The setting of the maximum allowable SoC is presented in Eq. 6.4.

$$\begin{aligned} &\text{if} \quad P_{request} \neq 0 \quad SoC_{max} = 0.9 && \text{[pu]} \quad (6.4)\\ &\text{else} \qquad\qquad\ \ SoC_{max} = 0.7 && \text{[pu]} \end{aligned}$$

Eq. 6.4 therefore helps ensuring that at least some capacity is available for tracking throughout the daily cycle. This statement requires that some EVs are connected in the grid of course. Even with the implementation of Eq. 6.4, times where EVs are available in the grid, but no flexibility is possible can occur. If a high demand tracking period occurs, many EVs will be charged closely to the true limit of 0.9 pu. If relatively shortly after the first tracking period ended, another tracking response is requested by the TSO, most EVs will be fully charged, and their flexibility very limited.

The EV flexibility control overrules the equality control of the *Grid Control* block, but uses the same parameter, namely C_{lim}, to limit the power consumption of all EVs connected in the grid. The manipulation of C_{lim} in order to meet the tracking demands is presened in Eq. 6.5.

$$\begin{aligned} &\text{if} \quad P_{deficiency} > 0 \quad K_f(t) = -K_t \\ &\text{else} \qquad\qquad\ \ K_f(t) = K_t \end{aligned}$$

$$C_{lim} = \int K_f(t)\ \mathrm{dt}\ , \quad -0.045 \leq C_{lim} \leq 0 \qquad [-] \quad (6.5)$$

where,
$K_f(t)$: Integration factor [-]
K_t: Integration gain - determines how aggressive the control behaves [-]
C_{lim}: Factor which manipulates the behavior of the sub-system controller [-]

The sub-system controller will control (limit) the power according to $V_{low} = V_{low} + C_{lim}$.

Fig. 6.6 shows a randomly chosen section of time where the flexibility control is active.

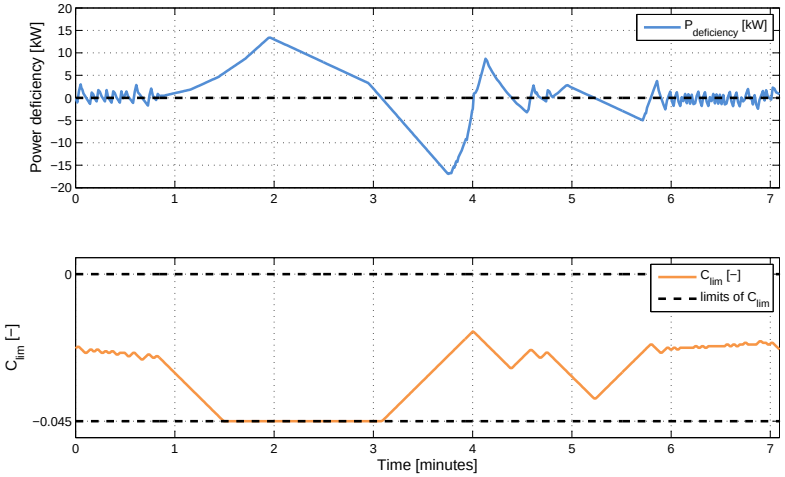

Figure 6.6: EV flexibility control example

The EV flexibility control implementation is simple. The actual operation though, is relatively complex, as it adopts the behaviour of the sub-system control. The control therefore respects the priorities of the EVs connected in the sub-systems. As such, the control will during a high power request charge

the units with lower SoC the fastest while respecting the voltage (cable- and transformer) limits of the grid.

Fig. 6.6 represents the EV flexibility control. The plot is as seen divided into a lower and an upper part. The upper part represents the power deficiency signal which when positive implies the demand for a reduction of power and vice-versa. The lower section represents C_{lim} which can limit the power consumption of the EVs.

As seen, the control acts as soon as $P_{deficiency} \neq 0$. This means that the EV control will continuously try to adapt to the changing conditions such as varying household power consumption, heat pumps turning on or off as well as a changing power request from the TSO.

The value of the control parameter C_{lim}, is limited between 0 and -0.045. A value of 0 makes the sub-system controllers act unlimited which ensures that they, due to their configuration, will maximize the power consumption of the EVs. If the lower limit of C_{lim} = -0.045 is reached the sub-system controller will act as if the lowest voltage of the sub-system is 0.045 pu lower than the measured value. As the lowest voltage of a sub-system decreases below 0.94 pu, the charging of EVs will be stopped.

At Fig. 6.6 it is seen that the controller at some point tries to stop all EV consumption.

The case studies presented during the next sub-section will test the response of the EV and HP flexibility control.

6.4 Case Studies

This section contains and presents the case studies performed in order to investigate the performance of the flexibility control.

The case studies use the same input data as the case studies performed in section 5.7. This means that the HP thermal consumption is applied according to what is presented in sub-section 3.3.2, the EV driving patterns according to section 3.4 and the ambient temperature for summer and winter as follows:

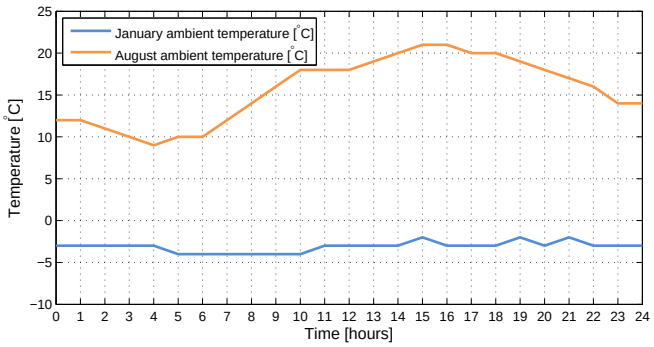

Figure 6.7: Ambient temperatures for Aug 11th and Jan 22nd

The placement of the sub-systems for both LV grids are to be found in appendix A.5.

In total, five different case studies will be presented. Three studies for LV-II, all during a winter scenario as well as two studies for LV-I during a summer scenario.

The request is applied either at 12:00→ or at 20:00→ for all cases. Due to the driving patterns implemented very few EVs will be connected in the grid during midday. Therefore, the midday studies reflect the HP flexibility (only) as well as the minimum flexibility of the grid as whole. Most EVs arrive back at their respective households between 16:00 and 19:00.

The summer scenarios carried out in LV-I are of interest since the HP operation is highly seasonal dependent. As the thermal demand during summer is almost non-existent as well as the COP being higher, the HPs will consume power for less time, less frequently. Therefore, the control applied is expected to show a limited effect during summer. The HPs are assumed to have close to no flexibility. The LV-I case studies will show how impaired the HPs are.

Table 6.1 presents the five case studies carried out in order to assess the performance of the flexibility control.

Case	Grid	Day	Time	Length	Request	Amplitude
1	LV-II	Jan 22^{nd}	12:00	3hr	Constant	110%
2	LV-II	Jan 22^{nd}	20:00	3hr	Varying	85-135%
3	LV-II	Jan 22^{nd}	20:00	3hr	Constant	125%
4	LV-I	Aug 11^{th}	12:00	3hr	Constant	100%
5	LV-I	Aug 11^{th}	20:00	3hr	Constant	200%

Table 6.1: Flexibility case studies

The amplitude parameter in the table refers to the relative difference between a scenario without flexibility and the flexibility case in question. The amplitude of the no-flexibility scenario has been taken as the average consumption over the three hours which all the tests run for.
Fig. 6.8 presents the case studies performed in the grid LV-II. The constant tracking request might seem simple to track and rather dull but even as the request is constant a lot of other values are changing in time such as:

- Household consumption
- Thermal demand
- Ambient temperature
- EV consumption
- HP consumption

As these parameters are changing in time, the control needs to actively regulate up-/down in order to match the constant demand. Such an operation therefore challenges the control. Furthermore it is easy to see if (when) the control fails as time increases. The three hour testing is expected to challenge the flexibility of the units quite some.

The case with a varying request is included to investigate how fast the control is able to adapt to a fluctuating demand.

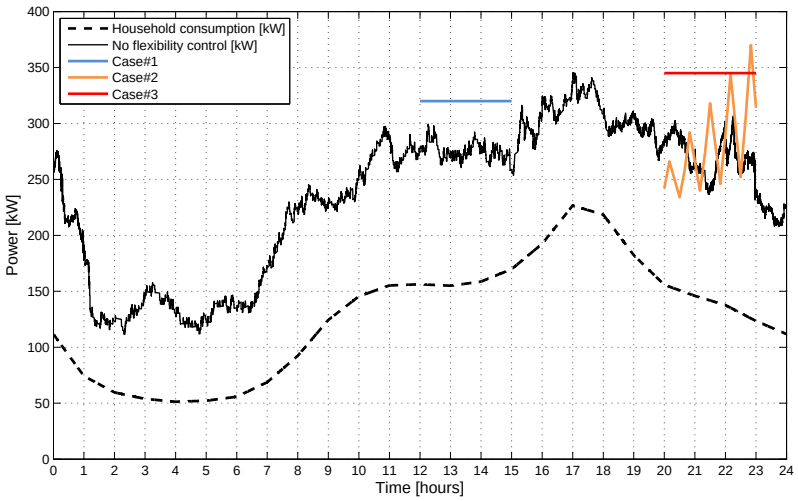

Figure 6.8: LV-II - Winter - flexibility case studies

The models have been pre-initialized for 7 hours as was done in chapter 5 as well.

Fig. 6.9 presents the case studies performed in LV-I during a summer scenario. As seen, the household consumption during summer is relatively low. The consumption from the units is very low as well. At point the unit-consumption is completely non-existing. The heat pumps has a higher energy supply as the COP is higher during summer which means that they have a higher "charging" energy supply. They therefore fill the tank relatively fast. The high energy supply combined with a very low thermal demand has the consequence that the heat pumps will consume power very seldom during summer.

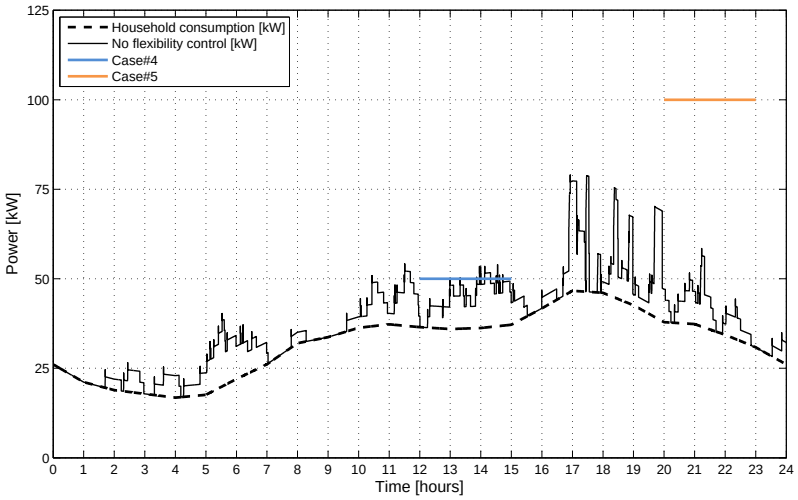

Figure 6.9: LV-I - Summer - flexibility case studies

The LV-I midday case study is expected to show that the consumption is somewhat uncontrollable as only heat pumps are available. The EV operation and control will more or less completely determine the success of the evening study.

6.4.1 Case 1

This sub-section presents the first case study. The grid-control of LV-II will January 22^{nd} at 12:00 receive a constant tracking request of 320kW (110% of the three hour mean value without any request) present for three hours. This scenario will primarily represent the HP operation as close to no EVs are connected in the grid.

Fig. 6.10 presents an overview of the performance of the flexibility control for case 1. The figure is divided into an upper- and a lower part. The upper part shows the consumption if no tracking was requested (black dashed curve), the tracking request (orange curve) and the response of the grid (blue curve).

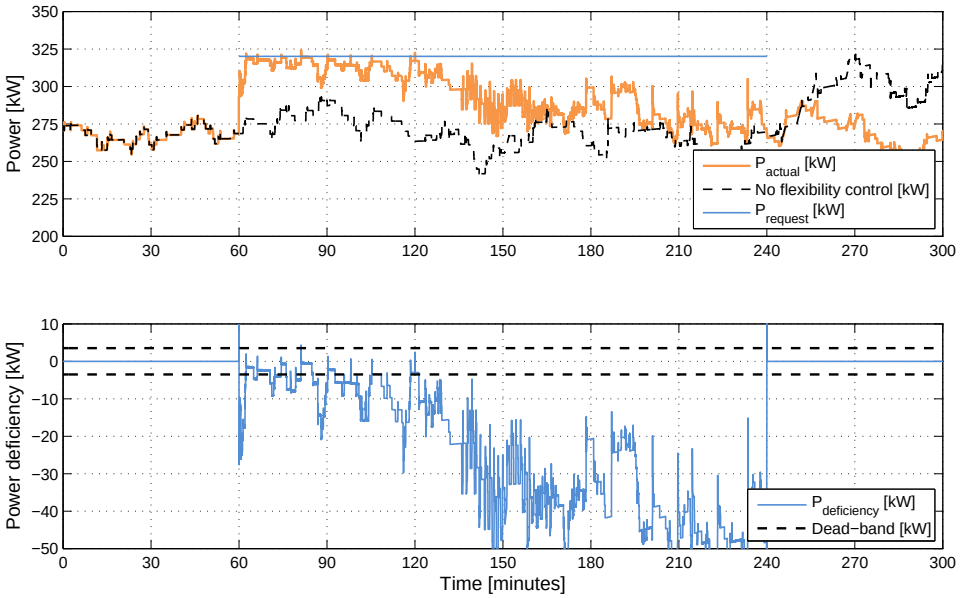

Figure 6.10: Case study 1 - Overview of performance

Fig. 6.10 clearly shows that the units are not able to track the signal for the three hours. The units possible to act on the request is highly dominated by HPs.

First of all the units under-shoot the target of 325kW for approximately 5 minutes. This is due to the setting of the HP flexibility control. The HP flexibility control is not allowed to act very aggressively as described earlier, which is the cause of the mismatch. The control could be tuned to act more aggressively if desired which would cause the period with under-shoot to be limited some. The under-shoot would always be present to some degree though.

The extra demand of 50kW related to the normal operation has the effect that additionally ≈16 HPs need to be turned on "artificially". The control is able to stay above a value of -10kW for roughly 25 minutes after which the tracking becomes worse and worse. After 60 minutes the tracking has broken down which causes the consumption to float freely.

The reason behind this is that the control of the lower band at some point renders unable to turn on additional units. At the very start of the tracking request, the various heat pump controllers increase their lower band according the lowest voltage level received by the grid controller. As the controllers keep receiving a negative deficiency signal they keep increasing the lower band until the maximum has been reached. At this point all heat pumps are either turned on or are not within the energy band

of 0.2-0.55 pu. Therefore, the controllers have no possibility to further increase the power consumption.

This effect is depicted in Fig. 6.11. The upper section of the figure represents the deficiency signal and the lower graph the dead-band settings for all HPs connected in sub-system 3B.

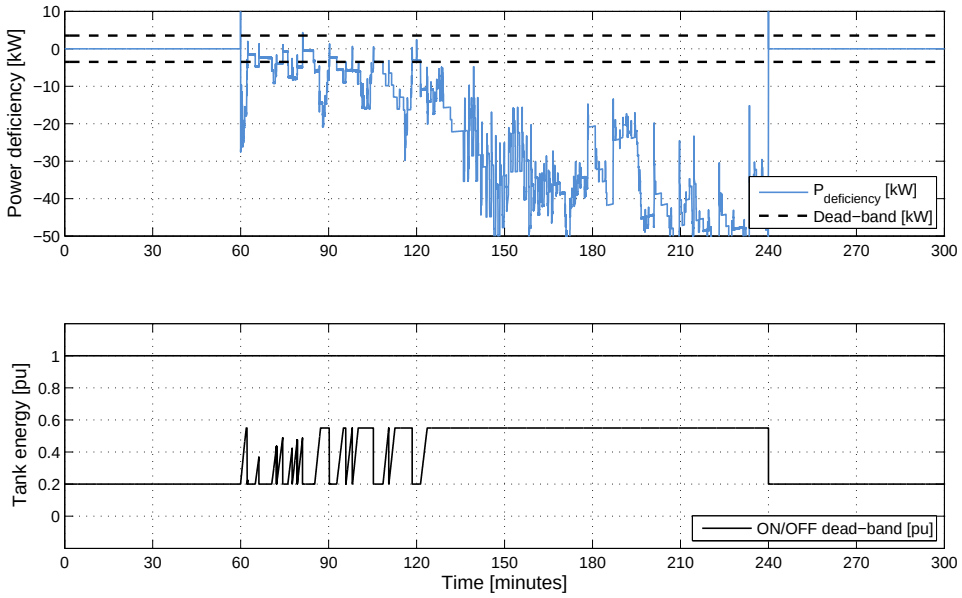

Figure 6.11: Case 1 - Flexibility control operation

The figure shows that the control acts as soon as the deficiency appears. After roughly 5 minutes, the deficiency is within the limits of ±3.5kW and the lower band resets. As time grows and the deficiency increases, the control tries to turn on units increasingly aggressive. After approximately an hour the control renders unable to track the request as the maximum limit for the lower band is kept constant.

An unintended side-effect of the control appears after the first hour. As the flexibility control keeps trying to increase the consumption, the lower band is kept at its maximum for two hours. For this time period the effective tank size is therefore reduced from 0.8 pu to 0.55 pu. This has the effect that the HPs will turn on and off more frequently, decreasing their average energy supply.

To negate this effect, the HP flexibility control should be able to detect that the HP system has become uncontrollable and reset the band(s). Due to time constraints, such a function has not been implemented.

6.4.2 Case 2

This sub-section presents the second case study. The grid-control of LV-II will January 22^{nd} at 20:00 receive a fluctuating tracking request of 242-370kW (85-135% of the three hour mean value without any request) present for three hours. The request fluctuates more heavily as time grows. This scenario represents the combined operation of both types of units. Most of the EVs are connected in the grid which means that good conditions for flexible operation are present. The tracking request will force the flexibility control to up- and down regulate rather aggressively to meet the demand.

Fig. 6.12 presents an overview of the performance during the second scenario.

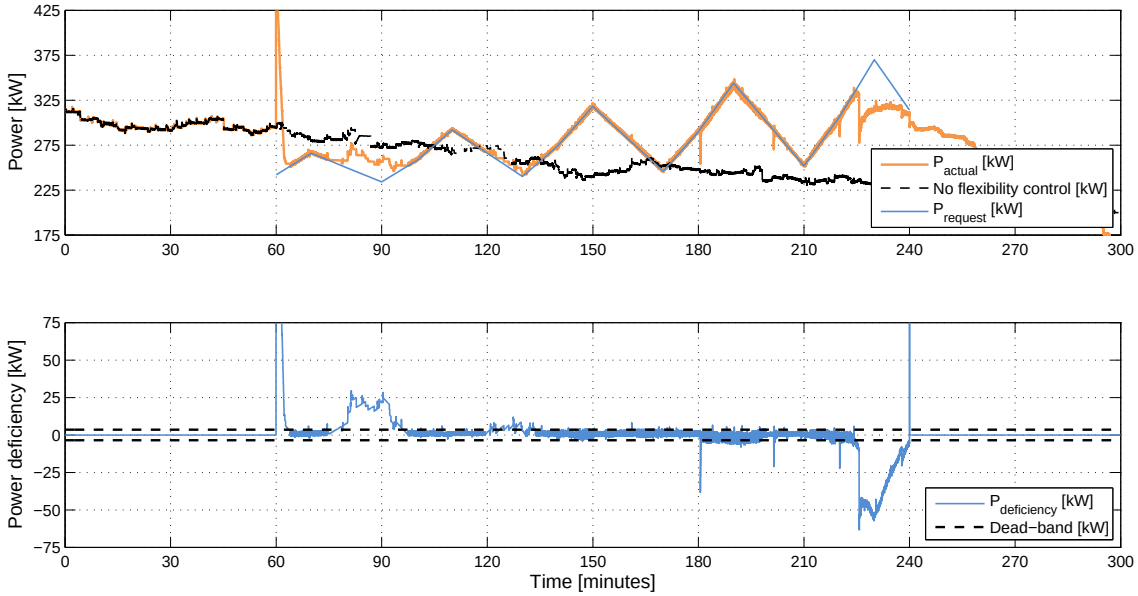

Figure 6.12: Case study 2 - Overview of performance

As seen, the overall tracking of the request looks rather good.

As the request begins, a massive overshoot of 350kW (not visible on the graph) is present for a few seconds after which it decays rather fast. This undesirable effect is due to the flexibility control in combination with the sub-system control. As the tracking request begins, the EVs are allowed to utilize the upper 0.2pu of the battery capacity. The switch from 0.7 - 0.9 pu happens instantaneously (1 step-size). As approximately 40 EVs are at this point of time connected in the grid, they all try to consume maximum power to utilize the grid to its maximum. The sub-system control is designed to increase power, check the grid status and then act according to the status of the grid. The controller therefore detects no issues, increases EV consumption, detects a voltage violation and decreases EV consumption some. This process goes on until the voltage and power consumption is within the desired ranges.

When the request begins most sub-systems have voltage levels above the limit of 0.94 pu, which has the consequence that the sub-system controllers will increase the power in order to estimate the power consumption which will utilize the feeder to its fullest (increase the power til V=0.94 pu). At current time, the EV control is possible to increase the power from 0-11kW in one step (1 second). Multiple solutions are possible to implement to reduce this effect. The most obvious being adding a limit for how fast the EVs are able to change their power consumption. The level at current time is approximately ±11kW/second. By reducing this parameter the tracking response would be affected as well, making the response of the EVs slower. Another possibility would be to let the sub-system controller apply the request delayed for each sub-system. For instance sub-system 1 would receive the request at t=0, sub-system 2 at t=1 etc.. This approach would limit the overshoot to 66kW per subsystem. A combination of various approaches would most likely offer the least overshoot while not limiting the EV tracking response too much. Possibly other solutions are viable to investigate, but due to time constraint neither the solution presented nor others have been implemented or tested.

Fig. 6.13 presents the manipulation of the HP dead-band for heat pumps connected in feeder 3B (strongest feeder) as well as the manipulation of the power limiting parameter, C_{lim}, of the EVs.
As seen the HPs are controlled much less aggressive than the EVs. First of all, the EVs are able to track

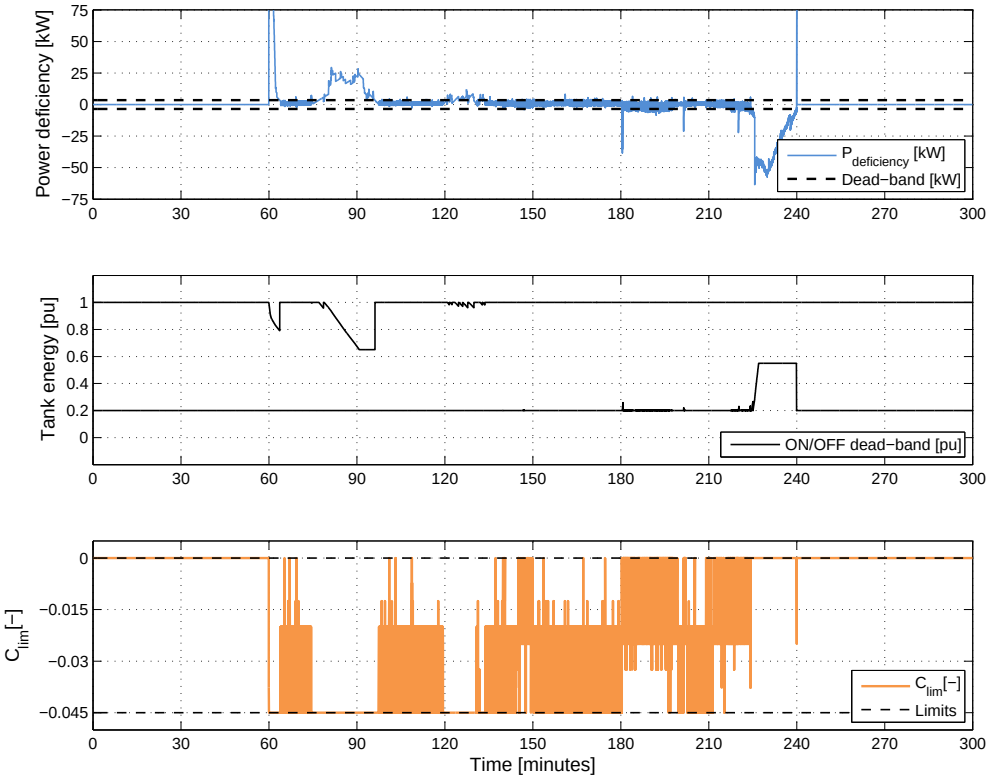

Figure 6.13: Case 2 - Flexibility control operation

the request very closely which causes the heat pumps to act passively as they only track a deficiency greater than ±3.5kW. The HPs comes into play when larger deficiencies occur. This phenomena is not a mistake, its based upon the decision that the HPs should be controlled gently. Through extensive testing the operational dead-band as the aggressiveness of the HP operation could be tuned in order to find the most appropriate trade-off between tracking response and the desire to tend the heat pump average energy supply. The heat pumps therefore only assist the EV tracking rather than acting overly aggressive.

20 minutes after the request begins, the units overshoot their target by ≈25kW. At this time the request is close to 50kW less than under normal operation conditions. It is seen, that C_{lim} is at its minimum value, which has the effect that the EV consumption is shut completely off. The HPs control attempt to shut off as many units as possible, but are not able to keep up with the decreasing request.

At times 180, 200 and 220 minutes brief under-shoots of -50kW to -20kW occurs. These are due to the EV batteries of various sub-systems being completely charged (SOC = 0.9pu). This phenomena is depicted in Fig. 6.14. The lower part of the figure represents the sum of the EV consumption of sub-system 2A, 3A and 3B.
As seen, the EV power tracks the requested amount of power pretty closely until two hours have passed. At this time the EVs of the various sub-systems start to become fully charged. The plot shows that the EVs of sub-system 3A are charged faster than the EVs of sub-system 2A (except for one EV arriving late with low SoC) which are charged faster than the EVs of sub-system 3B. The reason for this simply is the voltage levels in the three sub-systems. The worst voltage level of sub-system 3A is higher than the worst voltage level in the two other feeders. Therefore, as the EV plant/sub-system control allows for the EVs of sub-system 3A to charge with a higher power than the control of the two other sub-systems. The flexibility control applies C_{lim} equally to all sub-systems.

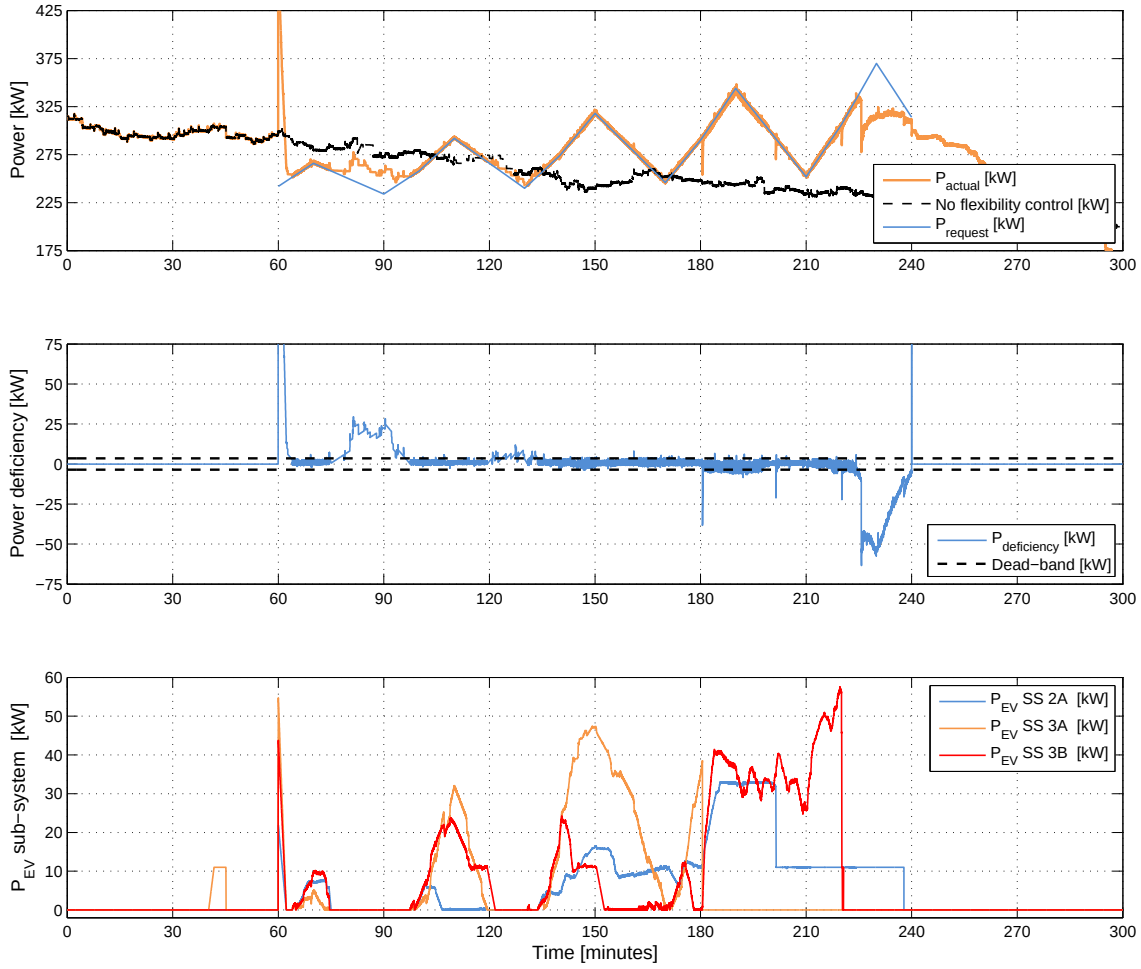

Figure 6.14: Case 2 - EV power consumption

As the sub-system control tries to charge the EVs according to priority, the EVs ideally are fully charged at the exact same moment of time. This is exactly what happens at 180 minutes. All EVs of sub-system 3A are fully charged at the same time. As the power consumption from the EVs of sub-system 3A stops instantaneously, the flexibility control increases C_{lim} to increase the power consumption of the other sub-systems. This effect is clearly seen in Fig. 6.14 as sub-system 2A and 3B ramps up their consumption swiftly.

Yet again the control shows some challenges. As the consumption of the sub-systems is lost instantaneous as the EVs become fully charged, the tracking response is affected. The results therefore show that a ramp-down of the EV consumption needs to be implemented. This would be rather simple to implement as a linear reduction of the charging power as the EV batteries are close to full. Due to time constraints this approach has not been implemented.

6.4.3 Case 3

This sub-section presents the third case study. The grid-control of LV-II will January 22^{nd} at 20:00 receive a constant tracking request of 345kW (125% of the three hour mean value without any request) present for three hours. This scenario resembles *Case 2* and represents the combined operation of both types of units. Most of the EVs are connected in the grid. This tracking request will show for how

long the flexibility control is able to force the units to "over-consume".

Fig. 6.15 presents an overview of the performance of the flexibility control for case 3.

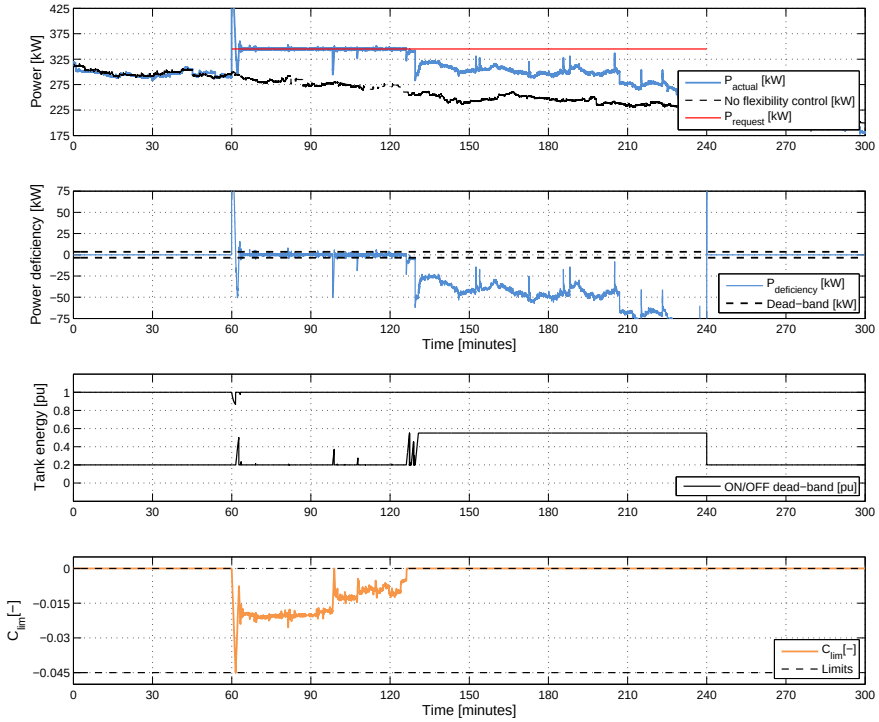

Figure 6.15: Case 3 - Overview of performance

As seen, the units are able to track the request very closely for one hour after which the deficiency becomes very high. The figure shows the behaviour of the control which hints to what occurs while the tracking request is active.

First of all, the overshoot as the request begins is present yet again due to reasons explained in the previous case study. Interestingly it is to see that a rather large under-shoot now is present following the overshoot. The reason behind this is the simple nature of the C_{lim} control. C_{lim} needs some time to adopt to the constant request which is shown in the figure as the fluctuating behaviour seen as the request starts. Ideally C_{lim} would decrease directly to the value of -0.017 without any fluctuations.

The control stops being able to track after approximately one hour. At this point, the HP control is at its limit and the EVs are completely unlimited. Therefore the control cannot affect additional units.

Fig. 6.16 shows a detailed view of what happens with the tracking. The figure shows the deficiency signal along with the EV power consumption of the four strongest sub-systems followed by the EV consumption of the five weakest sub-systems.
The figure clearly show that the strength of the various sub-systems affect the tracking capabilities of the grid as whole. The middle section shows that as long as the batteries of the strongest sub-systems are not fully charged, the flexibility possible to offer is rather high. As stronger sub-systems become inactive one by one the tracking capability decreases. The possibility to track the request completely dissipates after approximately 70 minutes where the batteries of the remaining strong sub-system drops down to the charging of a single EV.

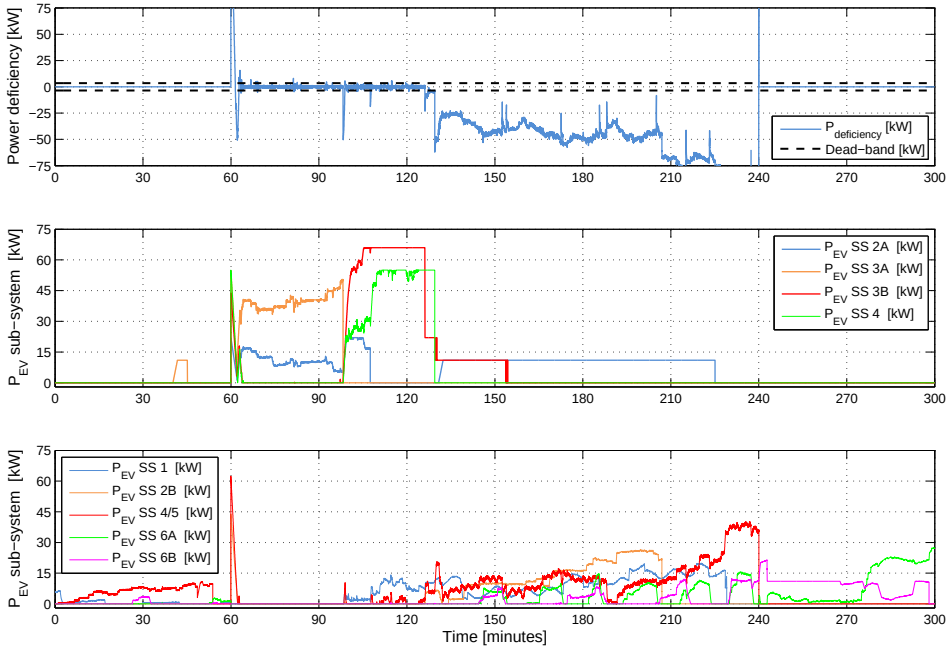

Figure 6.16: Case 3 - EV power consumption

At this point C_{lim} does not limit the EV charging at all. Even tough the EV charging is not artificially limited, the remaining five sub-systems with EVs not fully charged, are not capable of consuming the requested power. The reason behind this that the voltage drops of the five weakest feeders limits the possibility to increase the power additionally. A rough estimate would show that the tracking of the signal would have been possible for more than two hours if the strength of the five weakest sub-systems would have been similar to the four strongest.

6.4.4 Case 4

This sub-section presents the fourth case study. The grid-control of LV-I will August 11^{th} at 12:00 receive a constant tracking request of 50kW (100% of the three hour mean value without any request) present for three hours. This scenario represents a section of time where the grid flexibility is expected to be at its lowest. Close to no EVs are connected in the grid. The HPs will have a high energy supply combined with a low request. This makes the possible consumption of the heat pumps very low.

Fig. 6.17 shows an overview of the performance of the flexibility control during case study 4.
This case study applies a very gentle tracking request as close to no EVs are connected in the grid combined with the fact that the HPs are not well suited for providing flexibility during summer.

The heat pumps are actually able to track the request for the full duration of three hours. The deficiency is more or less kept within ±5kW for the full duration. The plot shows the manipulation of the dead-band for sub-system 1 along with the HPs' tank energy levels. It is seen that as soon as the request occurs, the lower band is increased to match the higher request. In sub-system 1, this has the effect that two HPs turn on. The manipulation of the lower band during time looks as if it has no effect. This is not the case since the manipulation takes place in all the sub-systems which causes HPs in some of the other sub-systems to turn on.

If the request would have been a bit higher or present for a longer time, the HPs would not have been able to match the request. As the heat pumps are fully "charged", it takes quite some time for

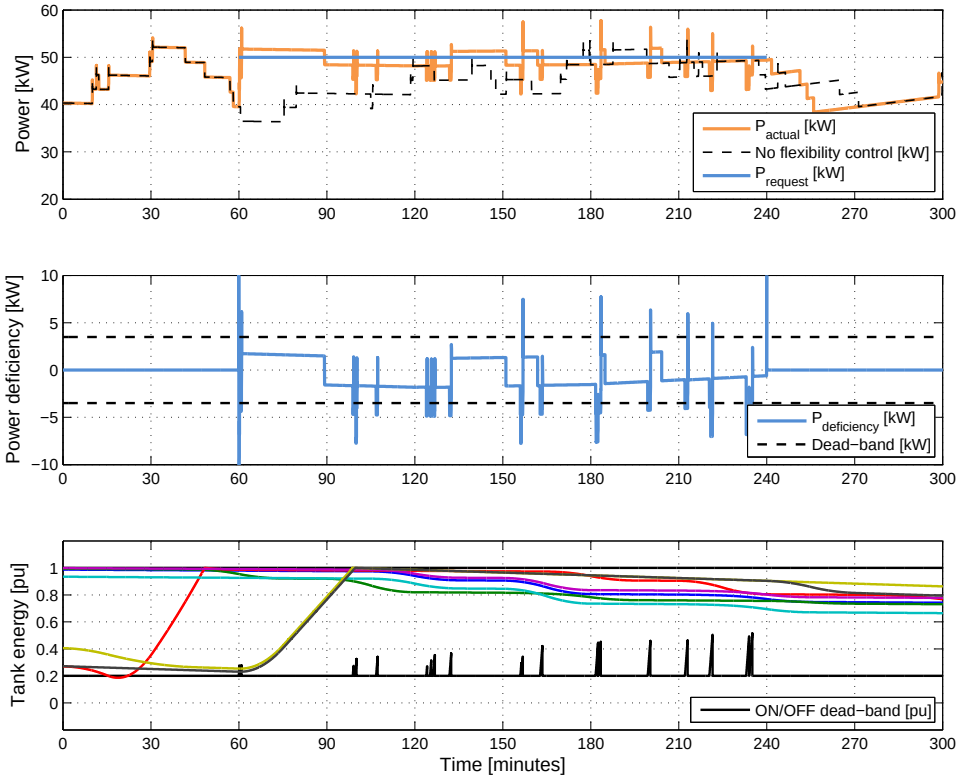

Figure 6.17: Case 4 - Overview of performance

the energy to decrease since the thermal demand is very low. If the HP tank energy is above a value of 0.55 pu, the lower band manipulation is not able to turn on additional units. It is seen that this scenario is rather close to happen as the request ends. At the last lower band manipulation, the value is almost at 0.55 pu.

6.4.5 Case 5

This sub-section presents the fifth case study. The grid-control of LV-I will August 11^{th} at 20:00 receive a constant tracking request of 100kW (200% of the three hour mean value without any request) present for three hours. This scenario presents a section of time where the heat pumps are expected to contribute with close to no flexibility. As such, this case will look into the possible flexibility of the EVs more or less alone.

Fig. 6.18 shows an overview of the performance of the flexibility control behaviour during case 5. The request applied is seen as being rather ambitious as it doubles the normal consumption. Yet again, the over-shoot and spikes appear which causes and possible solutions have been presented previously.

It is seen that the control track the signal very closely for more than an hour. The relative flexibility of the units is rather high and the best of the five case studies. The reason for this is not that the units perform better than during the other studies. As this case is performed in LV-I, the EVs have very good operating conditions. This shows as all EVs being able to fully charge from 0.7 - 0.9 pu in just under 90 minutes. As a comparison, the EVs of LV-II utilized the full 3 hours, and some EVs even needed charging after the request period ended.

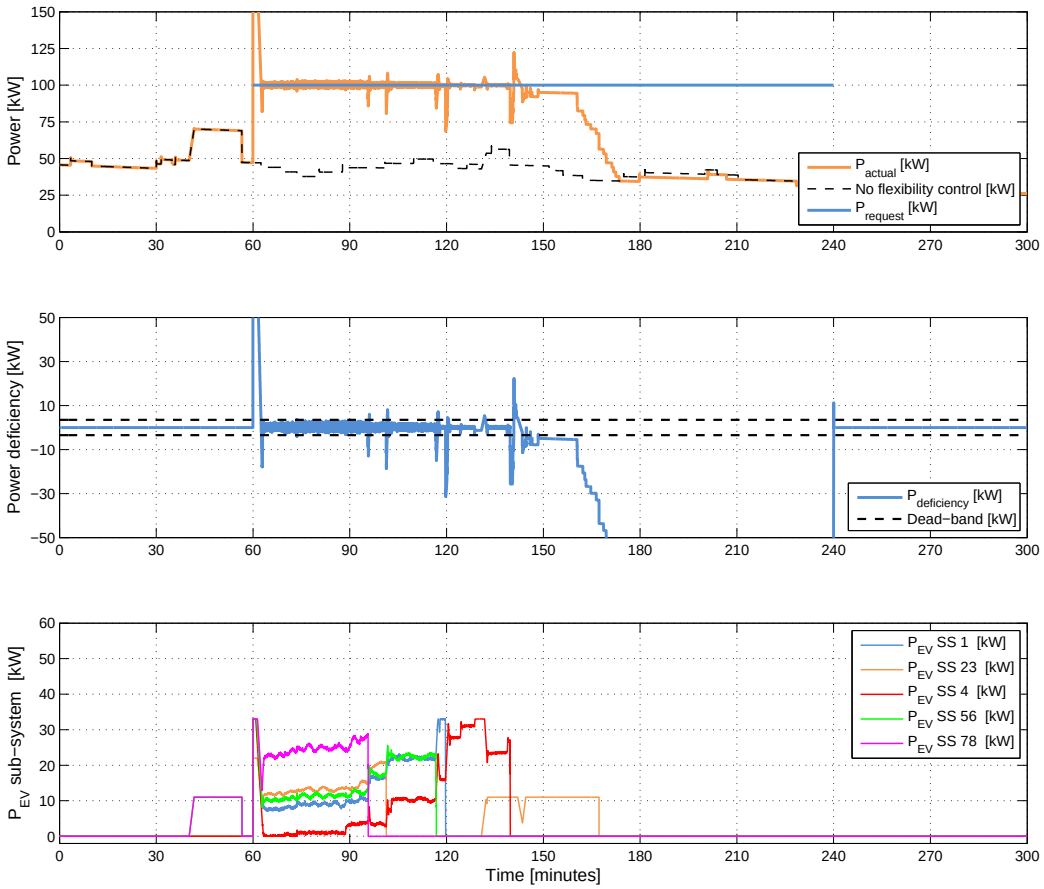

Figure 6.18: Case 5 - Overview of performance

As LV-I is a strong grid, the request could most likely be increased by quite some before the tracking would be impossible. The voltage levels are so high that most (probably all) EVs would be able to charge with the full 11kW simultaneously. As roughly 20 EVs are connected in the grid, their combined consumption therefore could add up close to 220kW. By increasing the power the time for which tracking is possible would be limited though.

6.5 Discussion

The case studies have shown that the flexibility control makes possible to track a request fairly decent in general.

The EVs show better properties for tracking than the HPs since they offer the possibility to continuously alter their consumption between 0 and 11kW. Their primary limitation is that there are times where very few will be connected in the grid. This means that only at some instances of time the good properties of the EV tracking can be utilized. The EV flexibility is also highly affected by their point of connection. If connected at a weak node, their flexibility will be rather limited, as they will only be allowed by the internal settings of the control to charge with rather low power. In order to ensure that EVs are even able to act flexible, some of the battery capacity must be reserved for flexible operation. The EV flexibility therefore is a product of the strength of the connection node, amount of reserved capacity and time of day.

The case studies have shown that the HPs are able to track a request. The performance of the HP flexibility is a trade-off between the desire not to control the units too aggressively and the demand for flexibility. At times where the HPs and EVs track together, the EVs will track a request so closely that the HP control does not sense if up- or down regulation is needed. This has the unfortunate effect, that at times where both types units are tracking together the EV flexibility will be used up after which the HP flexibility control takes over. The reason behind this is the fact that the HP control utilizes a margin of allowable error, and the EVs do not.

The case studies have shed light on various unexpected issues within the control design. Most of these issues are expected to be solvable and possible solutions have been presented as the issues presented themselves.

7 Conclusions

This master's thesis has investigated the effects of implementing a high penetration of heat pumps and electric vehicles in the future Danish LV grids.

Two Danish LV grids, a relatively strong (LV-I) and a relatively weak (LV-II), have been implemented in DIgSILENT PowerFactory. The grids have been equipped with time-dependent consumption for each individual household in order to determine the daily hourly loading of the grids during summer and winter. Heat pumps of 3.1kW and electric vehicles chargers of 11kW have been implemented one by one in both LV grids, in the ratio 2:1, until grid violations occur. The connection point of the individual units have been decided by use of one of three implementation algorithms, each designed to assess specific scenarios. By use of the algorithms, strong and weak points in both LV grids have been identified. It has been determined how many units the LV grids are able to run simultaneously during worst case and realistic conditions. The studies show that the voltage levels in the grids are the primary limitation when assessing how many units each grid is able to adopt. LV-II have key weak points highly limiting for how many units it is able to adopt.

Dynamic models of the electric vehicles and heat pumps have been developed and implemented in DIgSILENT PowerFactory's DSL environment in order to further investigate the impact these units have on the future LV grids. As the first part of the project concluded that the voltage level of both LV grids is the defining limiting factor for the amount of units possible to implement, the control design for the units has been designed in order to assist the voltage level. Three levels of control have been designed, ranging from unit control to sub-system control to the top level grid control. The heat pump model has been equipped with an emergency voltage function which utilizes an adaptive delay to determine when to operate. The electric vehicle control is performed at the sub-system level of the control. The sub-system controller is designed in order to prioritize the charging of electric vehicles with lower than average state of charge. The charging of the electric vehicles respects the voltage limit of the grids by adapting the power consumption to the current grid status. The top layer grid control has been designed in order to equalize the charging conditions of the electric vehicles across the grids. Case studies show that the control design makes possible to utilize the flexibility offered by the units, to shift power consumption from highly congested periods to less loaded periods, whereby the voltage levels of the grids improve substantially.

The project includes the design of a control strategy implemented at the (top layer) grid control, which overrules the equalization control, and enables the aggregator to provide balancing services to the TSO. The flexibility control is capable of limiting the power consumption of the electric vehicles which makes possible to adapt the overall electric vehicle consumption to track a requested power consumption. The heat pumps have been equipped with a flexibility control design which manipulates the regular dead-band control in order to track a requested amount of power. Case studies show that the time of day, time of year as well as the strength of a specific LV grid influences the possibility to track a requested amount of power. Seen from a general perspective, the control design enables

the units to provide balancing services with a fairly low tracking error.

8 Future Work

The project carried out presents opportunities for improvements within the work carried out. For instance various parameters already implemented in the models are possible to tune to optimise the performance of the current models.

The investigation of the impact the units have on power quality would be an interesting topic to investigate. In order to do so, the current models would need to be updated to be able to reflect short term transient behaviour. Unbalanced loading would fit into this investigation as well.

Varies unexpected issues have been discovered during the investigations of the case studies. For the majority of the issues, possible solution approaches have been proposed. These solutions would need to be implemented and tested.

The current models only include one kind of heat pump and one kind of electric vehicle. Implementation of a multiple of different kinds and types of units would make possible to produce more refined and realistic results. The implementation of a heat pump possible of varying its compressor speed would be a natural further step in the heat pump modelling.

At current time it has not been decided how the units communicate or what happens if communication breaks down. As this would be very important for practical applications, therefore an investigation looking into the possibilities of adding redundancies in the models would increase the value of the project. While doing so, it would be obvious to look into the communication and amount of data which would be needed in the future.

The project has investigated the possibility to enable the aggregator to provide balancing services to the TSO. The next step could be investigating the possibility to interact with the balancing market (Elbas) as well. This would most likely involve some sort of short-term prediction based upon the energy stored in the units of the grid. The models in their current state would most likely be well suited for this extra functionality. A very interesting topic would be how the balancing request from TSO would interact with the desire to provide flexibility services to the balancing market.

The incorporation of long term prediction, planning when it would be economically feasible to consume power bought at the spot market, would make possible to optimise consumption based upon the possible savings (/earnings) while interacting with multiple markets simultaneously.

The vehicle-to-grid concept would be interesting to incorporate into the existing flexibility structure as it would radically improve the flexibility possible to offer. A natural part of a V2G implementation would include a literature review making possible to assess battery degradation and optimise the V2G usage hereafter.

Another unit of interest to implement would be PV panels as the EVs and HPs could most likely store some of the energy produced by these units.

I

APPENDIX

A Appendix A

A.1 Maximum Grid Utilization - Summer cases

This section of the appendix shows the results of the maximum grid utilization study during summer for LV-I and LV-II. The study has been presented in sub-section 4.4.3 at page 62.

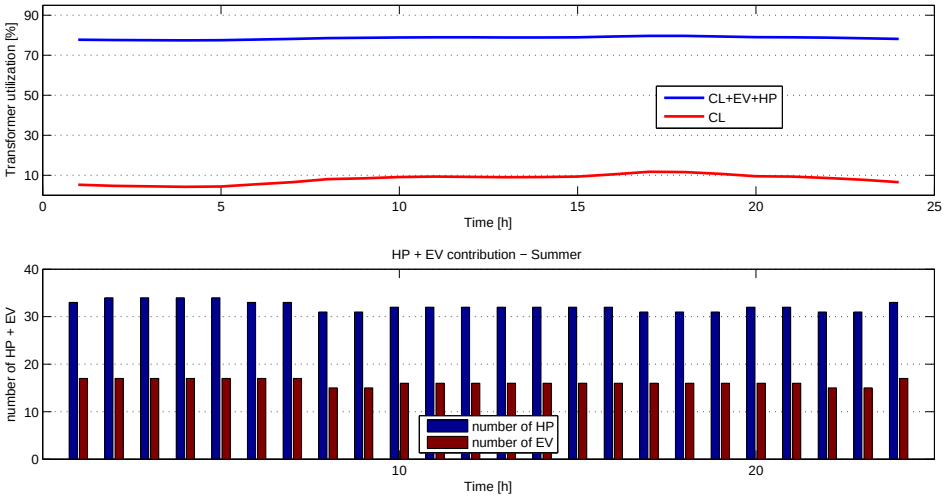

Figure A.1: Maximum grid utilization: LV-I - Summer - Uniform algorithm

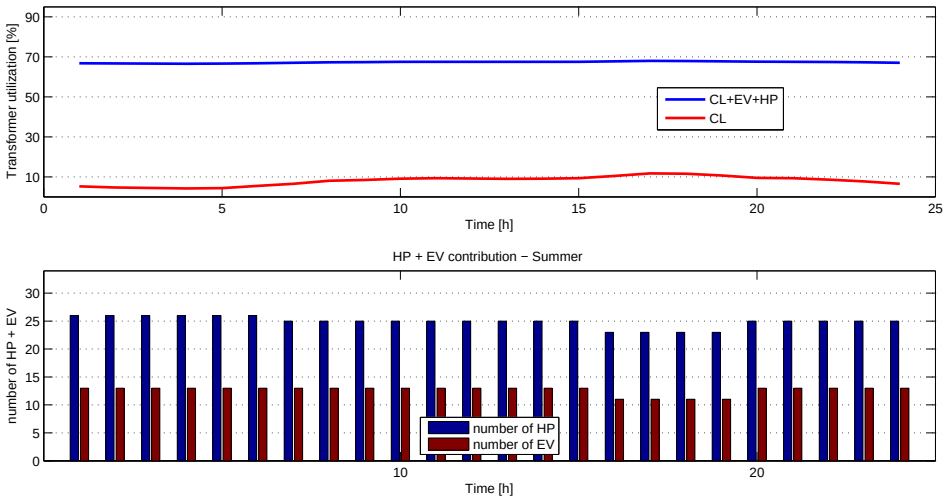

Figure A.2: Maximum grid utilization: LV-I - Summer - Adverse algorithm

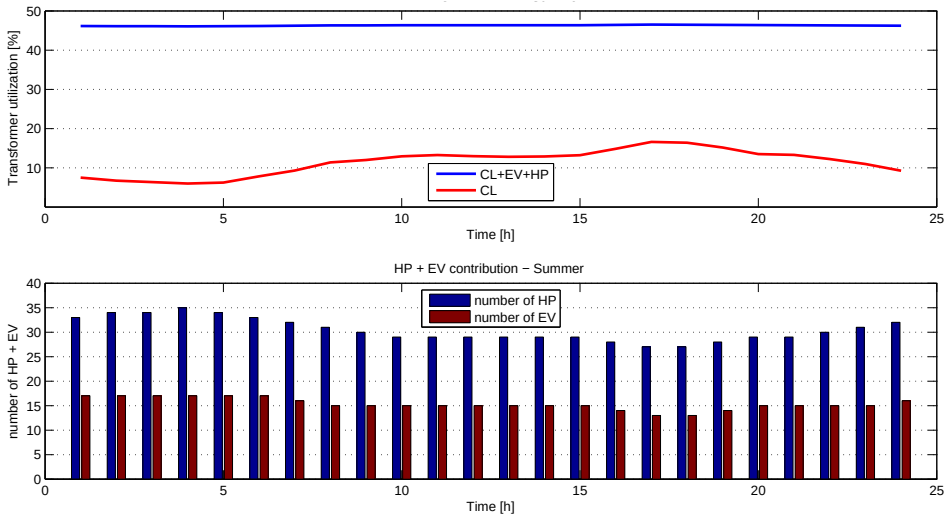

Figure A.3: Maximum grid utilization: LV-II, tie-points closed - Summer - Uniform algorithm

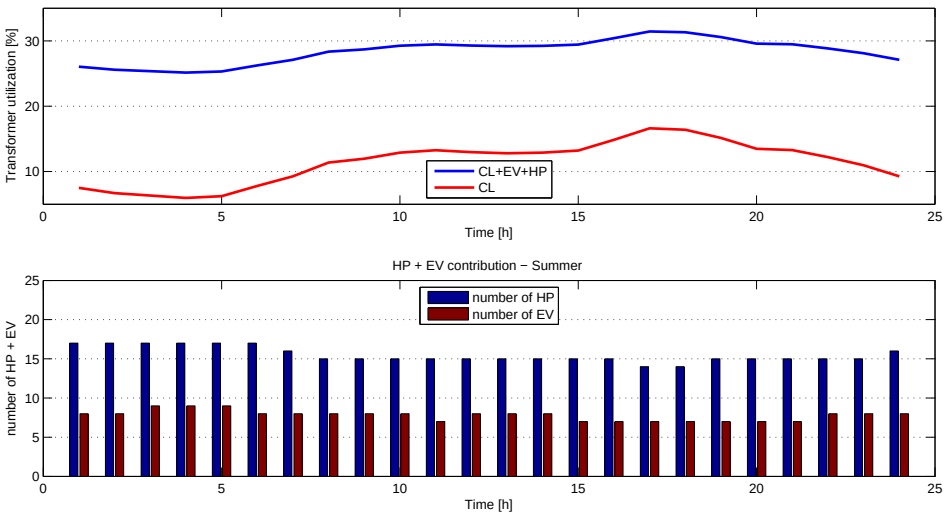

Figure A.4: Maximum grid utilization: LV-II, tie-points closed - Summer - Adverse algorithm

A.2 EV Driving Patterns

This section consists of two subsections. Sub-section A.2.1contains a MATLAB script has been used to create driving patterns, laboriously described in section 3.4, page 40). Sub-section **??** contains histograms that allowed to compare Normal, Kernel, Gamma, Weibull distribution functions to the Original distribution. To the naked eye the Kernel distribution looks to be the most suitable and adequate to further investigation.

A.2.1 Driving pattern MATLAB script

```
% Driving patterns
clear all; clc; close all
% DTU data histogram construction
% input vector
% k=[0.2531 0.1240 0.0993 0.0680 0.0501 0.0422 0.0304 0.0222 0.0196 0.0132 0.0301 0.0212 ...
    0.0109 0.0056 0.0031 0.0023 0.0015 0.0008 0.0008 0.0007 0.0004 0.0002 0.0002 0.0001];
% d=[0 10 20 30 40 50 60 70 80 90 100 150 200 250 300 350 400 450 500 600 700 800 900 1000];
k=[0.4531 0.1240 0.0993 0.0680 0.0501 0.0422 0.0304 0.0222 0.0196 0.0132 0.0301 0.0212 ...
    0.0109];% Distance input data taken from DTU
d=[0 10 20 30 40 50 60 70 80 90 100 150 200];% distance input data taken from DTU



% Distance pattern estimation
%input data
k=[0.4531 0.1240 0.0993 0.0680 0.0501 0.0422 0.0304 0.0222 0.0196 0.0132 0.0301 0.0212 ...
    0.0109];
d=[0 10 20 30 40 50 60 70 80 90 100 150 200];% data from dtu paper

%Prepare the data based on original distance grah
k2=100*k;
bar(d,k2)

z=0;
j=0;
for j=j+j+1:(length(d)-1)
    i=0;
    for i=i+1:k2(j)
        z=z+1;
        M(z)=d(j);
    end
end
 hist(M,100)   % show the histogram of the distance data
S=20000; % assumed total number of samples
k2=round(S*k);
j=0;
z=0;
for j=j+1:(length(d)-1)
    i=0;
for i=1:k2(j)
    xa=d(j);
    xb=d(j+1);
    z=z+1;

    M(z)=xa+(xb-xa)*rand(1,1);% matrix with all the data fitting to the original graph in the...
        paper
```

```
43  end
44  end
45  % prepare the energy demand after the day
46  %energy per 1km
47  Eu=0.15;% energy in kwh per 1 km
48  Nev=100;% number of utilised EVs
49  In=Data3(1:Nev);% define number of patterns
50  Eev=In*Eu;%energy demand per 1 car matrix of a New cars
51  B=24; %Battery sizes??????????????????????????????????????
52  Soc=0.7-Eev/B;% i substract from the max charging value =0.7
53
54  % distribution functions fitting and comparison
55  %Original signal
56  v=var(M);
57  m=mean(M);
58  O(1,:)=[m v];
59  N=M/200;%define N which keeps values between 0 and 1, some distribuions require that (go to ↩
        pu)
60  %listing all the considered distributions by format char that i can substitute then in random↩
        function
61   P={'Original' 'beta' 'BirnbaumSaunders' 'Exponential' 'Gamma' 'InverseGaussian' 'Kernel' '↩
        Logistic' 'Loglogistic' 'Lognormal' 'Nakagami' 'Normal' 'Rayleigh' 'tLocationScale' '↩
        Weibull'}';
62  %P={'Original' 'Normal' 'Gamma' 'Weibull' 'Kernel' }';% prepared for the report
63  i=1;
64  for i=i+1:length(P)
65  %Beta distribution
66  %P=char('beta', 'binominal');
67  % P=['beta      '; 'binominal'];
68  c=[P(i)];
69  c=char(c);
70  k=fitdist(N',c);
71  Beta=random(k,20000,1);
72
73  bet=Beta*200;% come back to the absolute values
74  M2(:,i-1)=bet;
75  v=var(bet);
76  m=mean(bet);
77  O(i,:)=[m v];% build the comparison list
78
79  end
80
81  % cut out data above 200km because of battery capacity limit
82  j=0;
83  for j=j+1:1
84    i=0;
85    z=0;
86    for i=i+1:length(M2)
87        if M2(i,j)<=200 & M2(i,j)>0
88            z=z+1;
89            M3(z,1)=M2(i,j);
90
91        else
92
93        end
94    end
95
96  end
97  j=1;
98  for j=j+1:2
99    i=0;
```

```
  z=0;
  for i=i+1:length(M2)
      if M2(i,j)<=200 & M2(i,j)>0
          z=z+1;
          M4(z,j)=M2(i,j);

      else

      end
  end

end
j=2;
for j=j+1:3
  i=0;
  z=0;
  for i=i+1:length(M2)
      if M2(i,j)<=200 & M2(i,j)>0
          z=z+1;
          M5(z,j)=M2(i,j);

      else

      end
  end

end
j=3;
for j=j+1:4
  i=0;
  z=0;
  for i=i+1:length(M2)
      if M2(i,j)<=200 & M2(i,j)>0
          z=z+1;
          M6(z,1)=M2(i,j);

      else

      end
  end

end
% Distance Histogram preparation
subplot(5,1,1)
 [nb,xb]=hist(M,200);
     bh=bar(xb,nb);
     set(bh,'facecolor',blu);
     xlabel('Driving Distance [km]')
       ylabel('Number of Samples')
          title('Original distribution')
     axis([ 0 200 0 1000])
set(gca,'YGrid', 'on')% set only horizontal grid lines, gca means get current axes!!!!!!!!!! ↩
    it is a command!!!!!!!!
 set(gca,'YTick',0:200:1200);
 % set(gca,'XTick',0:12:1200);


% Leaving, coming distribution generating graph DTU
a=[100 100 100 100 99.9 99.29 97.3 94.95 96.4 97.1 96.85 96.9 96.85 96.8 95.95 94.4 94.35 ↩
    95.65 97 98.05 98.7 98.74 98.9 99.2]% availability input data from DTU
% Availability estimation leaving/coming back
```

```
 AvL=random('normal',8,1.5,100,1);%  prepare 100 differente patterns with mean valu 8
 AvC=random('normal',17,1.5,100,1);%  prepare 100 differente
 patterns with mean valu 17
% keep leaving and coming realistic, include av speed 50 km i am chacking if the cars are abe↩
     to leave and come if not leaving time is shifting until i find the proper time
i=0;
k=0;z=0;
for i=i+1:length(Soc)
if   AvL(i)+(Data2(i)/50+4)< AvC(i)% checking if car is able to drive the distancre
     M(1,i)=Soc(i);
     M(2,i)=AvL(i);
     M(3,i)=AvC(i);
      else
     k=k+1;
     AvC(i)= AvL(i)+(Data2(i)/50+4);%if not add a delay
      M(1,i)=Soc(i);
     M(2,i)=AvL(i);
     M(3,i)=AvC(i);
 end
    if Data2(i)==0% check if car is drivin, if not add very long late leaving time/longer ↩
        than 24h
         z=z+1;
     N(1,i)=M(1,i);
     N(2,i)=50;
     N(3,i)=55;

    else% if not keep normal distance value

     N(1,i)=M(1,i);
     N(2,i)=M(2,i);
     N(3,i)=M(3,i);

    end
end

N(4,:)=Data2;% adding total distance to final data matrix
N(5,:)=Eev;% adding energy demand to final data matrix
 subplot(2,1,1)
 bar(N(4,:))
 subplot(2,1,2)
 bar(N(3,:))
hold on
 bar(N(2,:),'red')
hold off

N=N';%final outut matrix

xlswrite('Intro_data3',N);
%
at this point i know who is coming and leaving i have saved the mtrix N with all the dta ↩
    included
%
```

A.2.2 Distribution function comparison

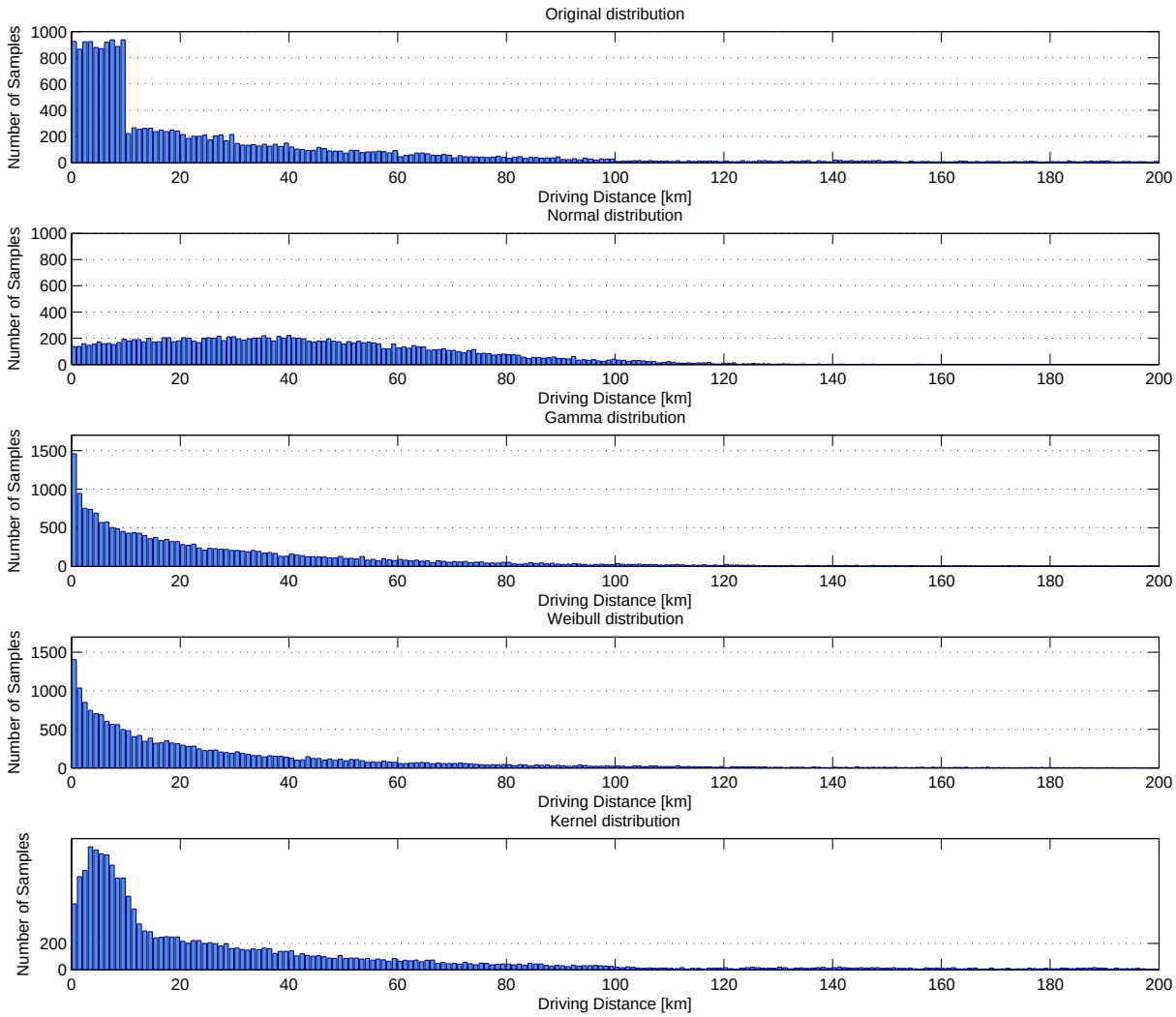

Figure A.5: Comparison of distribution functions

A.3 DSL Models

This section shows screenshots of the DSL models an adds a few comments to each one. In order to actually understand how the models work and interact it is recommended that the complete model is loaded from the CD. In oder to do so an unlimited license for DIgSILENT PowerFactory is needed. The models will be presented for LV-II only, but only slight differences between LV-I and LV-II exist. Most of the models presented are used a multiple of times in the full models.

The "HP plant 300/500" (Common model) represents the the heat pump plant equations which describe the heat pump behaviour.

HP Plant 300/500:

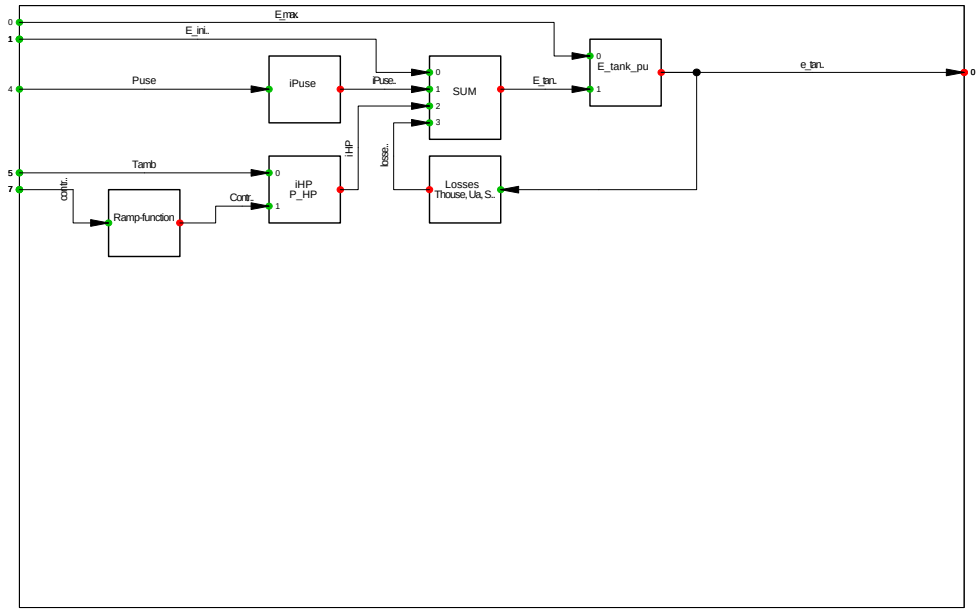

The "3 HPs" (Composite model) connect 3 HP plants with inputs and outputs.

3 HPs:

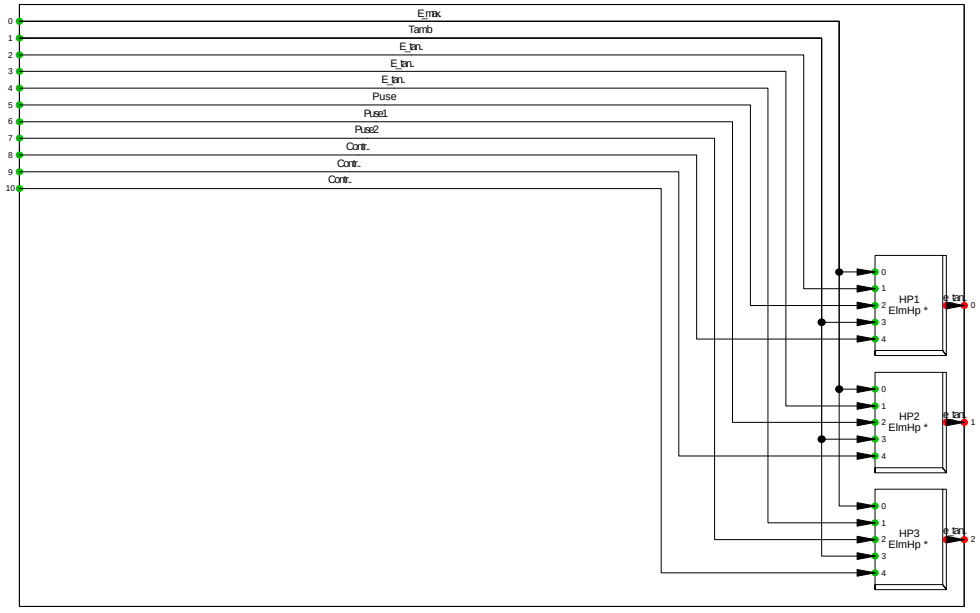

The "12 HPs" (Composite model) connect 12 HP plants with inputs from the input ElmFiles and outputs to upper layers.

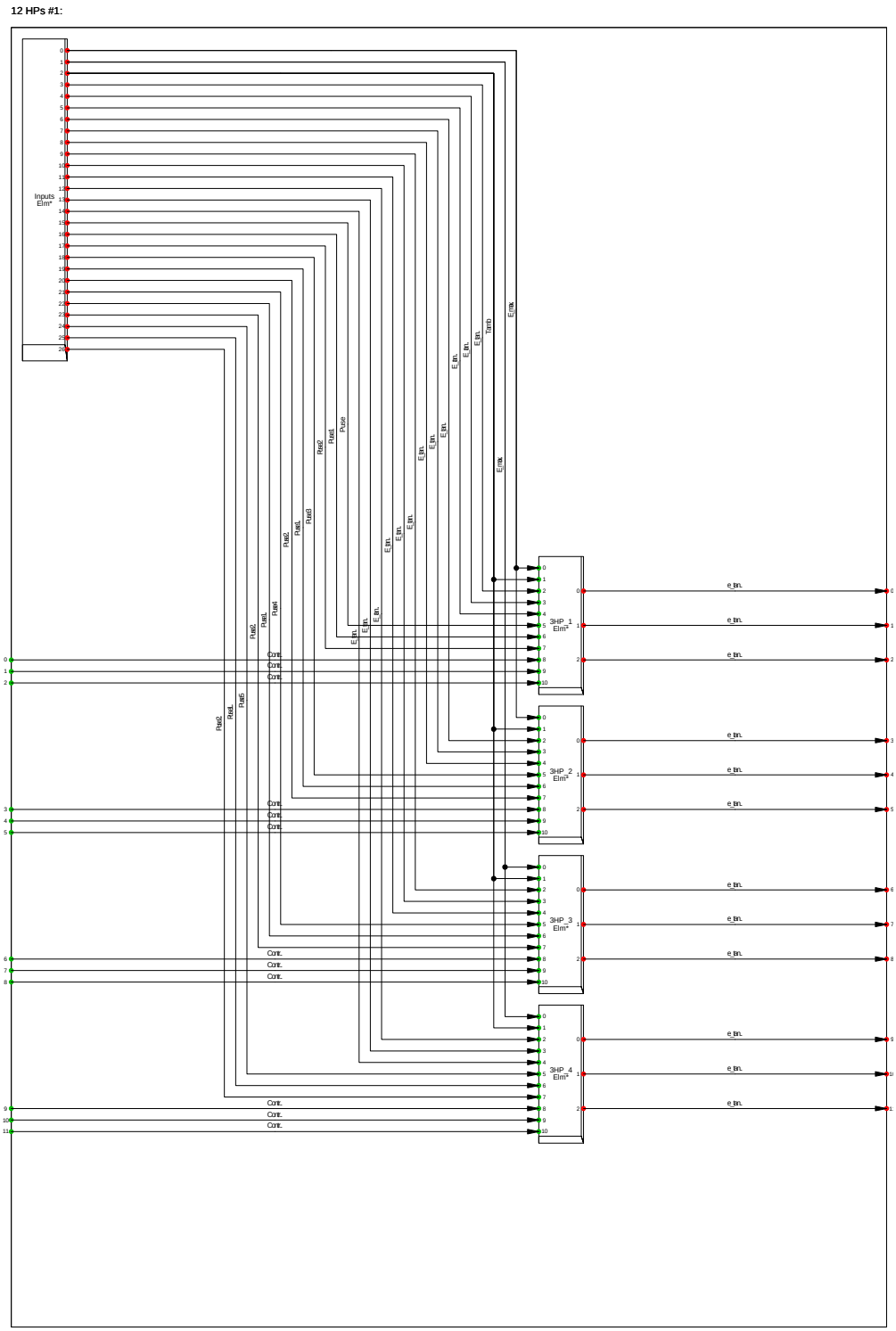

The "HP Inputs" (Common model) loads inputs from .txt files.

HP_Inputs:

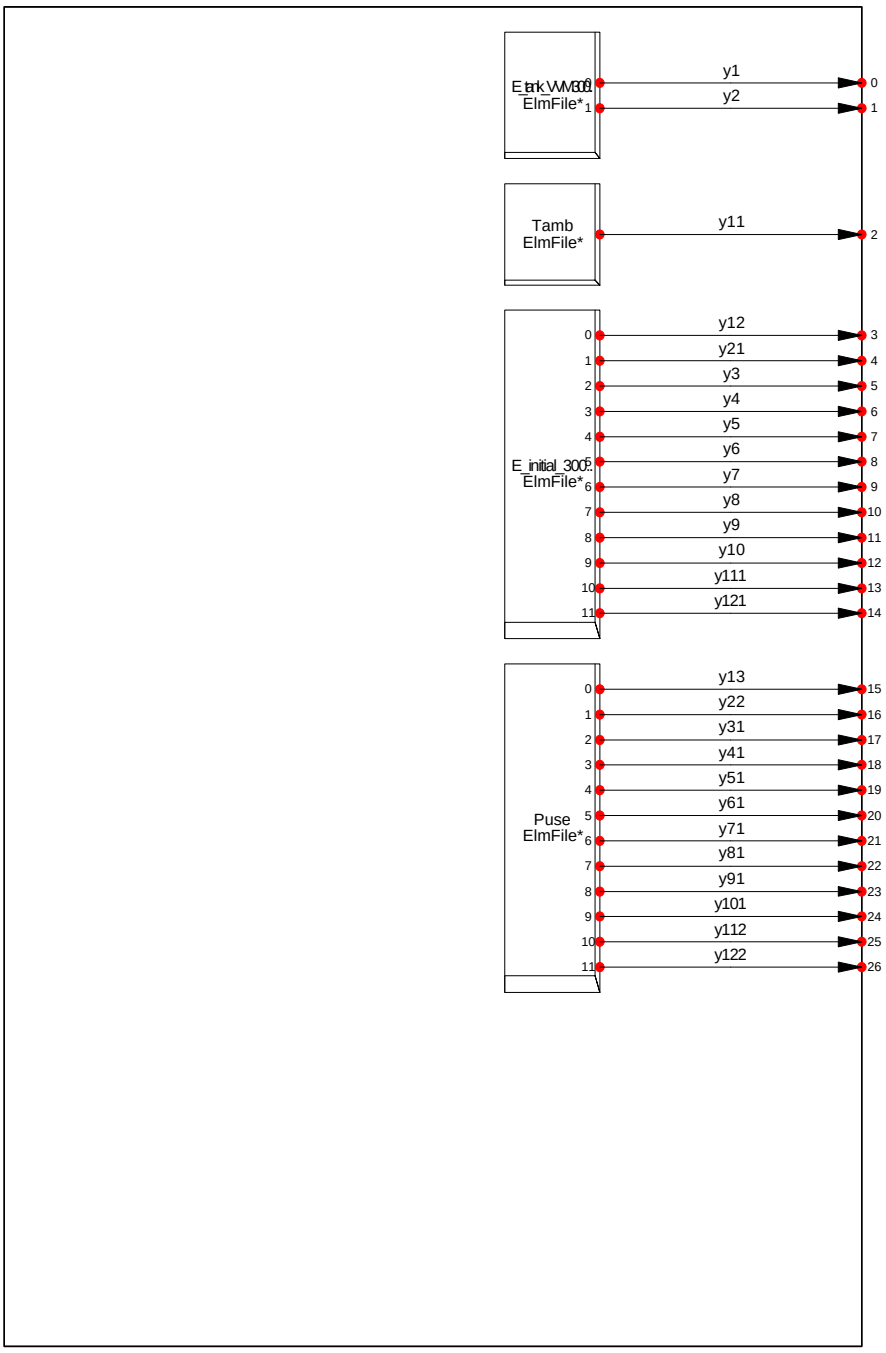

The "12 HPs TOP" (Composite model) connects the 12 HPs with the control string and output-power string. It also receives the deficiency signal for the flexibility control and redirects it to the control string.

12 HPs TOP:

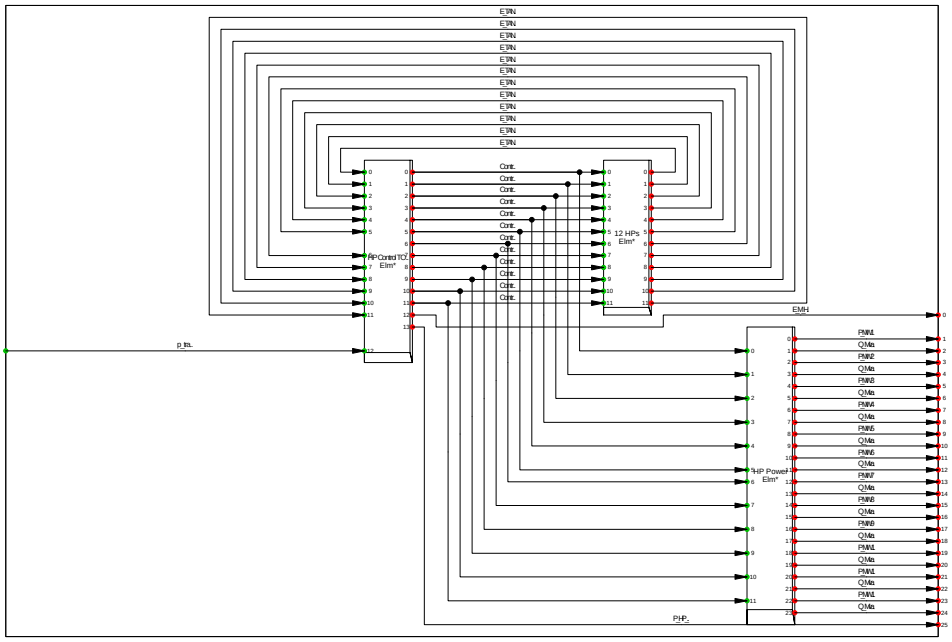

The "HP Control TOP" (Composite model) connects the tank energy of all HPs, sends it to the control common model along with the measured voltage levels at the HP connection nodes. It outputs the HP ON-/OFF signals. It also outputs mean value energy of the HPs.

HP Control TOP:

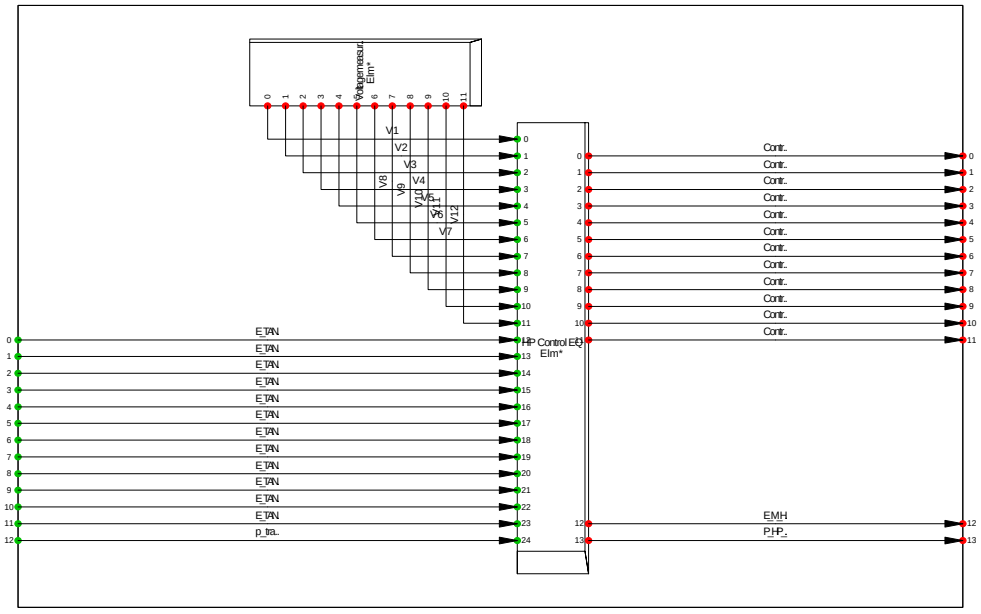

The "HP Control EQ" (Common model) contains all control od the HPs. ON-/OFF control, emergency voltage control and flexibility control. It controls a maximum of 12 HPs corresponding to a sub-system.

HP Control EQ:

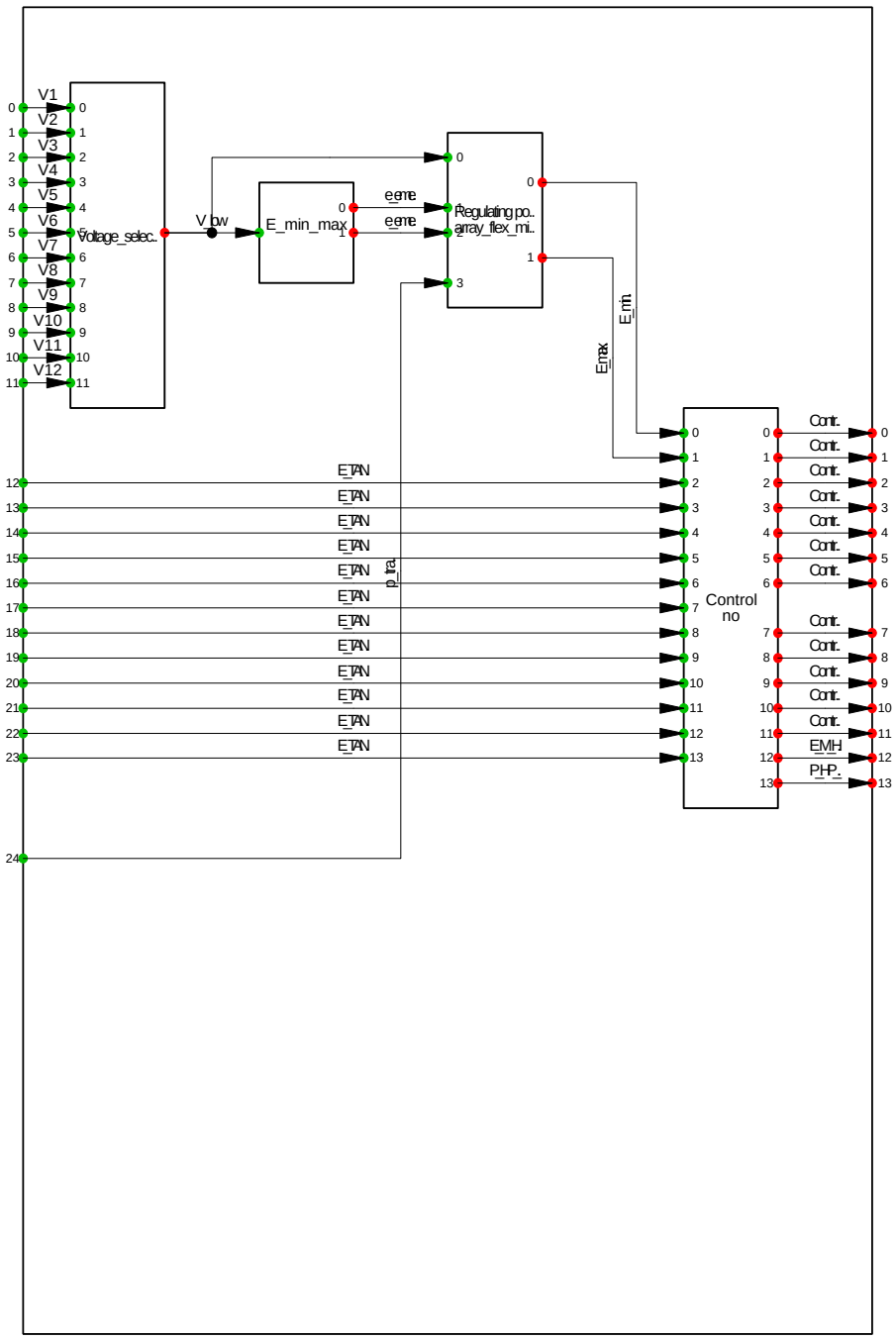

The "12 HPs to grid" (Composite model) is a layer on top of the "12 HPs TOP" which connects the 12 HPs to loads in the grid. The power consumption is sent to the loads here. This model is connected to the "Control Grid top" model which is shown later.

12 HPs to grid:

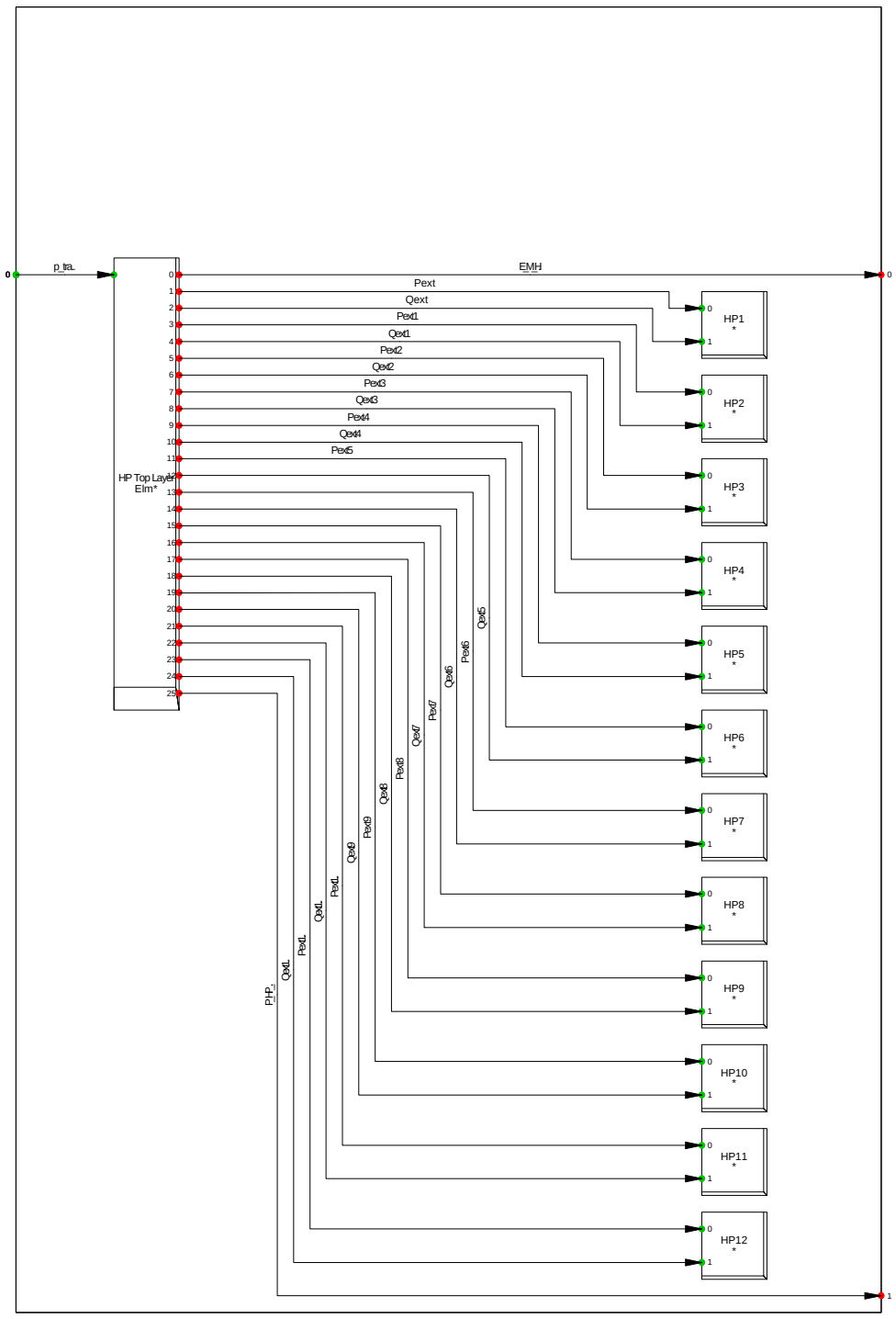

The "12 HPs Power" (Common model) computes the HP power consumption, P and Q as well as contains the equations for the soft-starter characteristic.

12 HP Power:

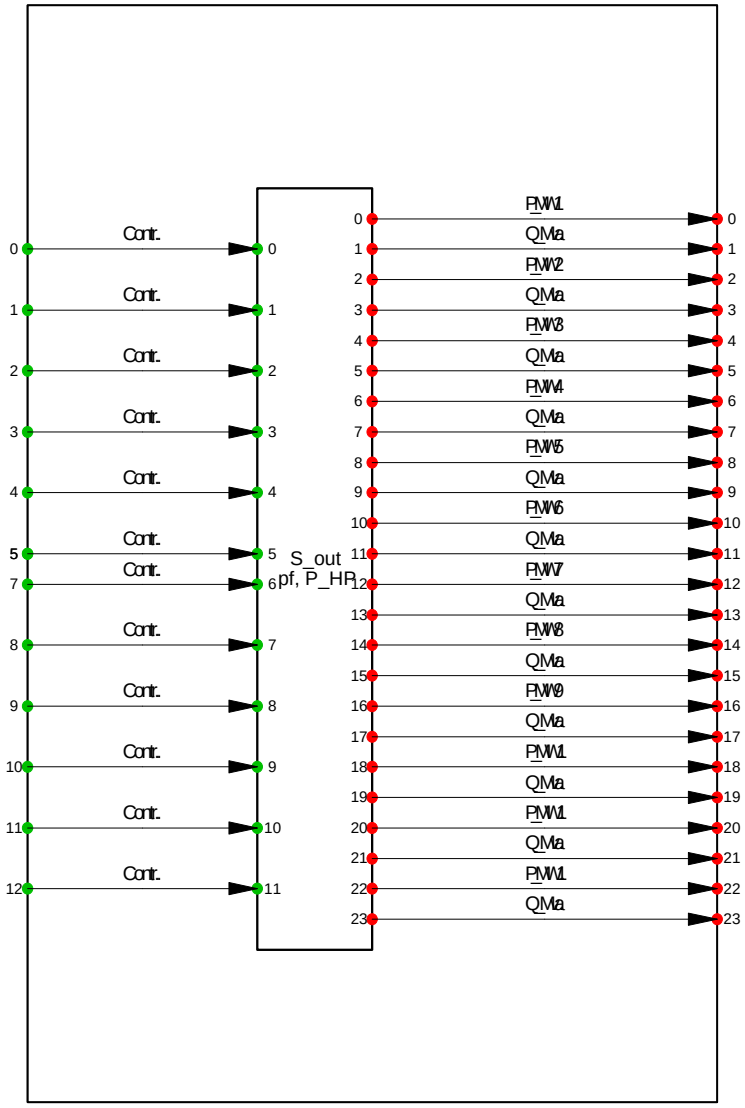

The "Charger v3" (Common model) represents the behaviour of the EV charger.

Charger v3:

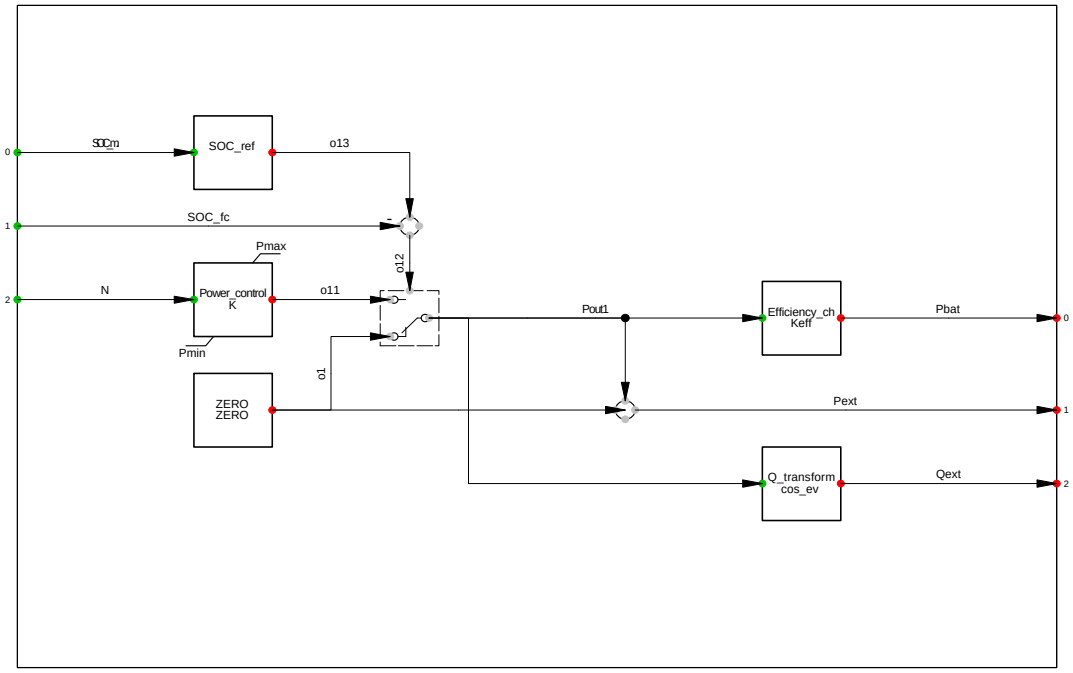

The "Battery" (Common model) represents the behaviour of the EV battery.

battery:

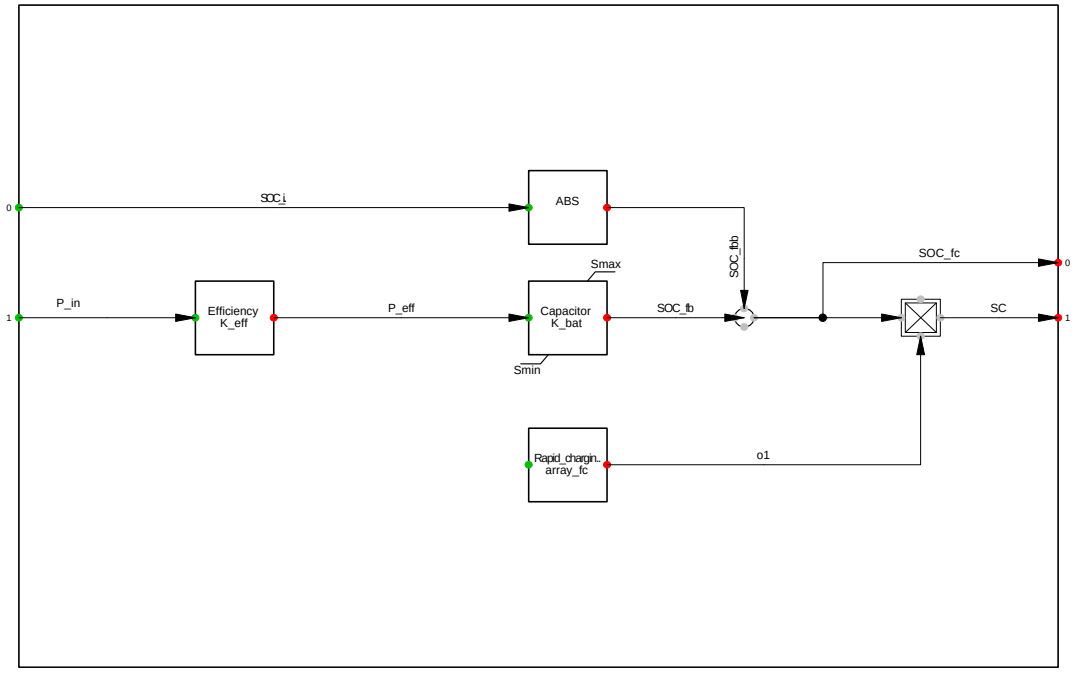

The "3 EVs" (Composite model) connects 3 batteries, 3 chargers, input SoC, grid load and input charging signal (S_{charge} = N)

3 EVs:

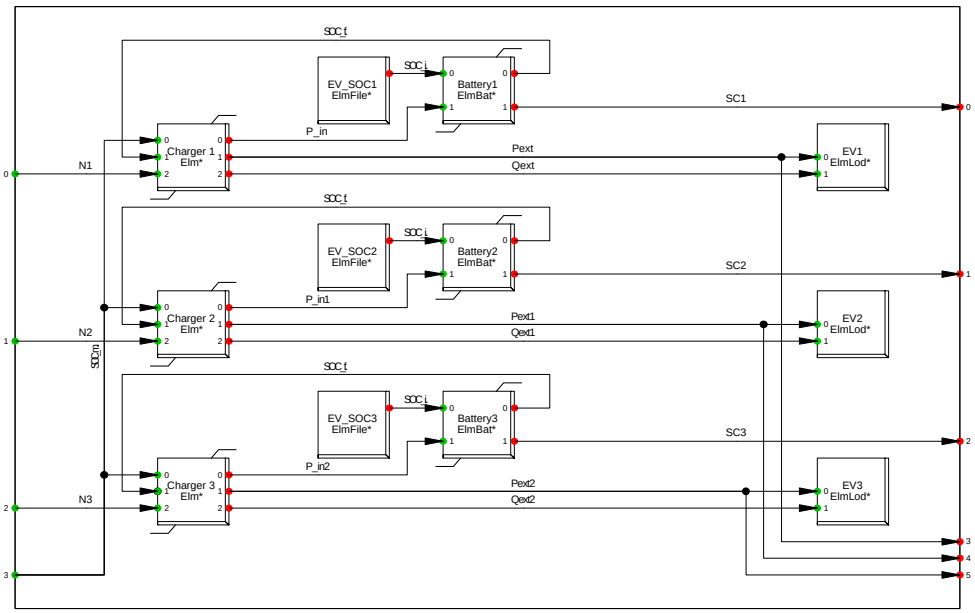

The "Charging system" (Composite model) connects 2 timer 3 EVs.

Charging_system:

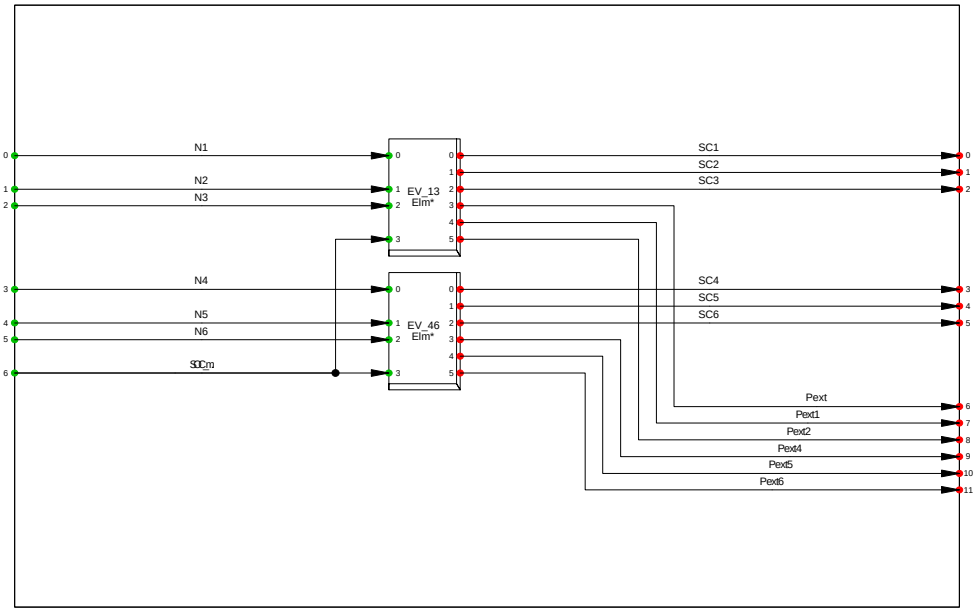

The "Sub EV Controller" (Composite model)represents the EV-half of a sub-system. It connects all functionalities of the EVs excluding the grid control.

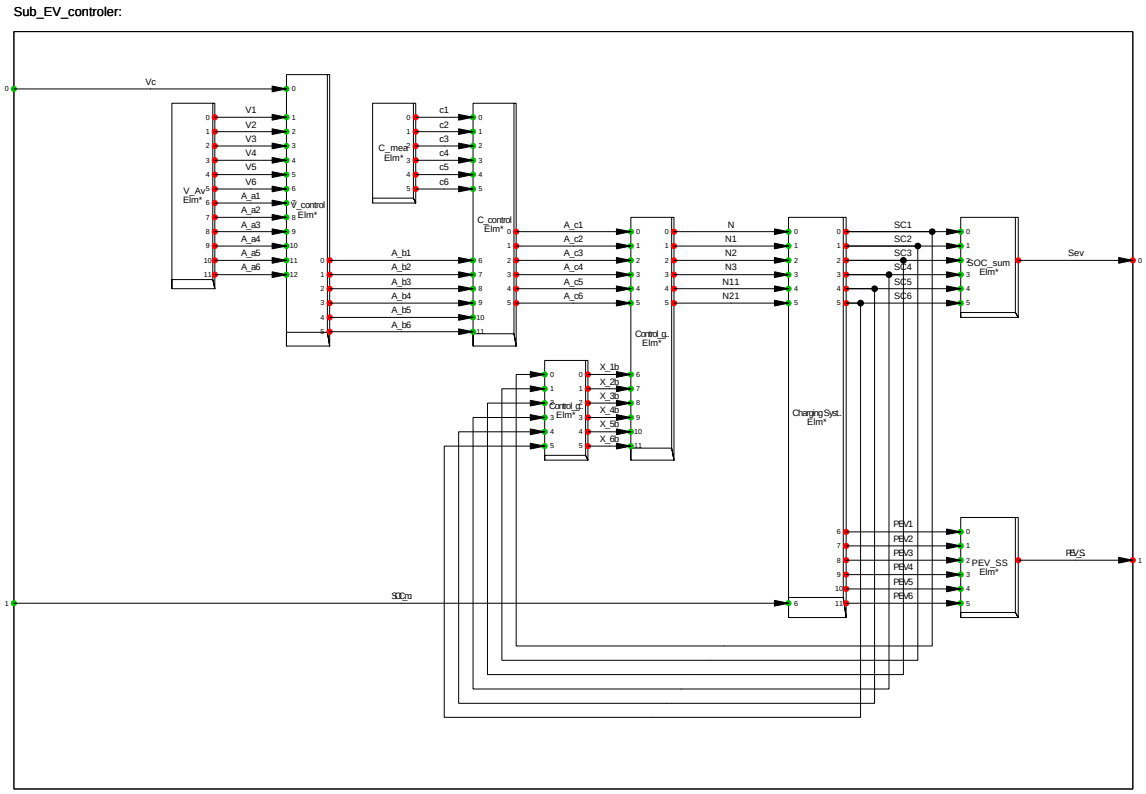

The next block is called "Control Gen X" (Common model) and has been cut out weirdly since it was presented on A1 paper in DIgSILENT. The signals to the right are output from the block, the the left are inputs to the block. Control Gen X defines the amplitude of the charging signal based upon the priority list also defined in the block.

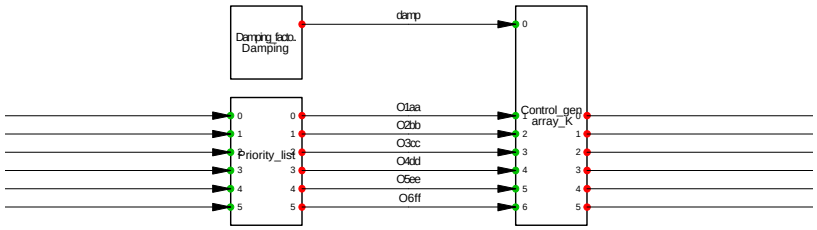

The "C mea" (Common model) block measures the current at the cable connected from the cable box at the household.

C_mea:

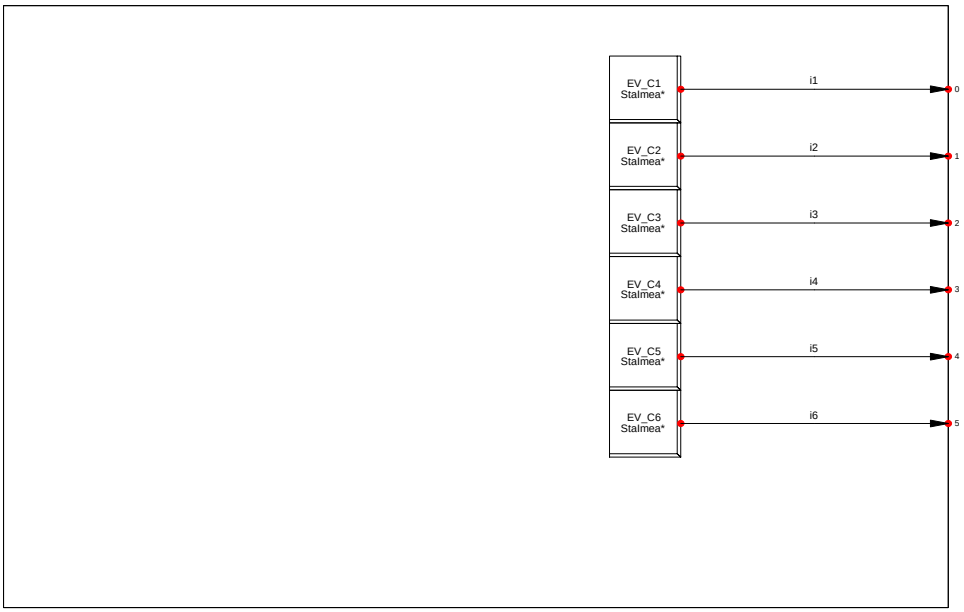

The "V AV" (Common model) measures the voltages at the connection nodes of the EVs as well as reads if the EV is connected or not from ElmFiles.

V_Av:

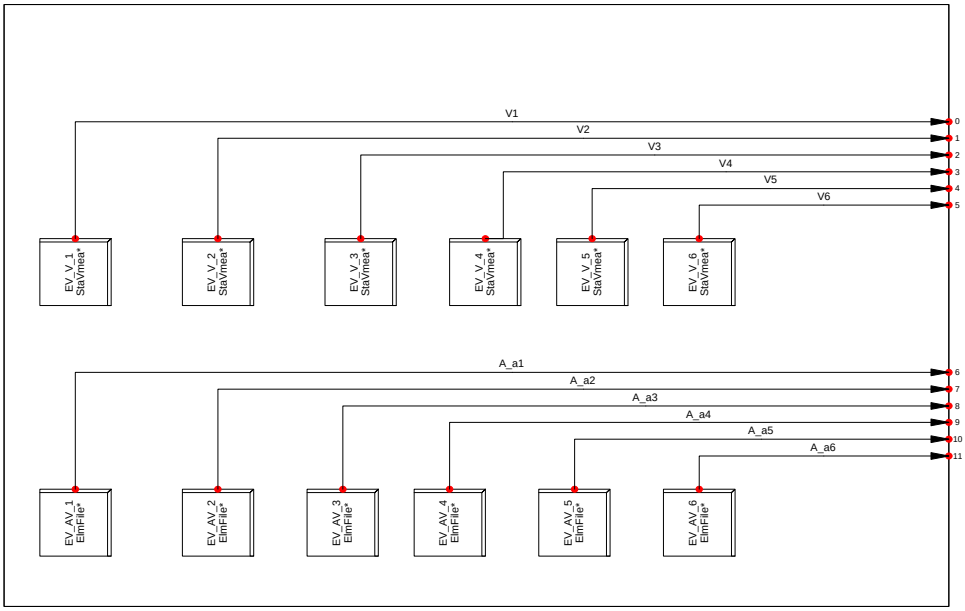

The "C control" (Common model) performs the duty cycle limitation of the EV S_{charge} signal if an overload of the cables to the cable box is detected.

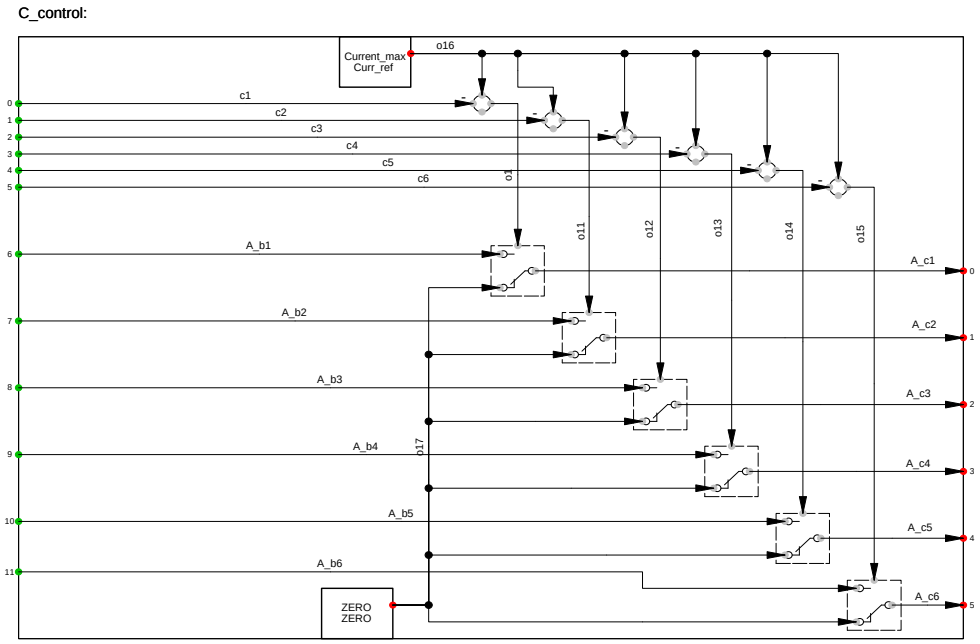

The "Control gen N" (Common model) combines the duty cycle and amplitude manipulation to create the final S_{charge} sent to the individual chargers.

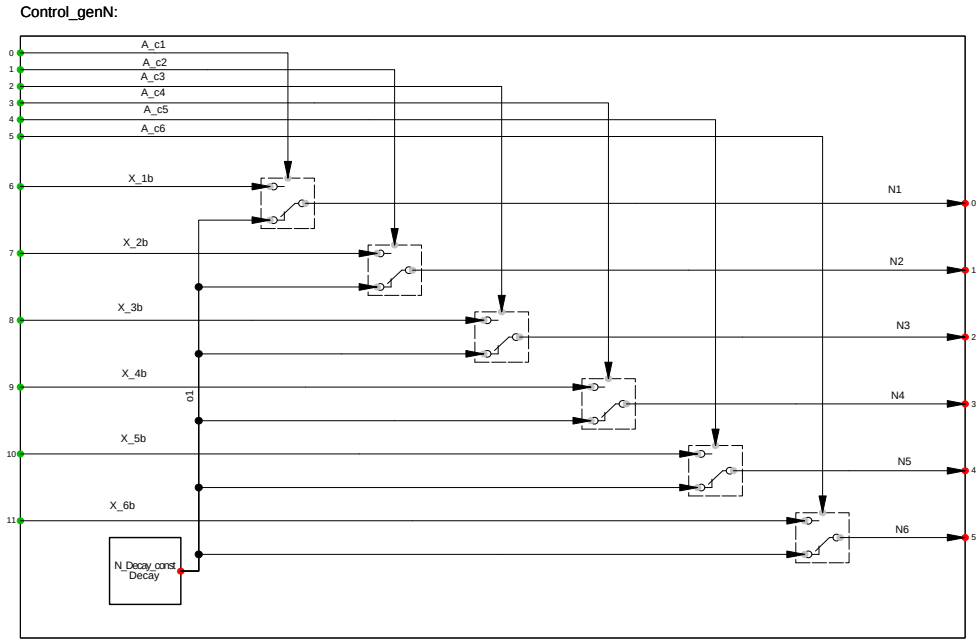

The "PEV SS" (Common model) computes the total power consumption of the EVs connected in a sub-system.

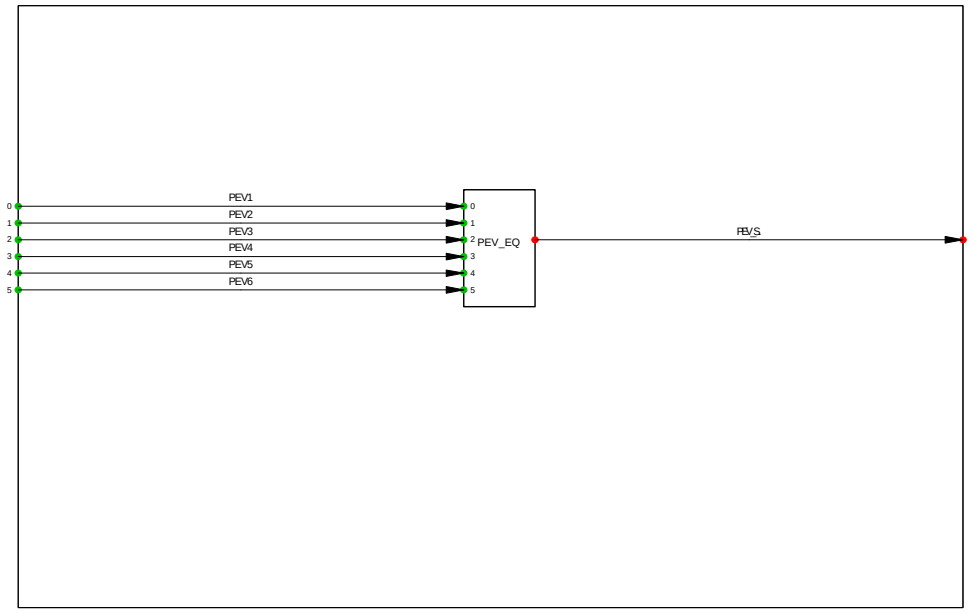

The "V Control" (Common model) manipulates the duty cycle of S_{charge} if a voltage limit is crossed.

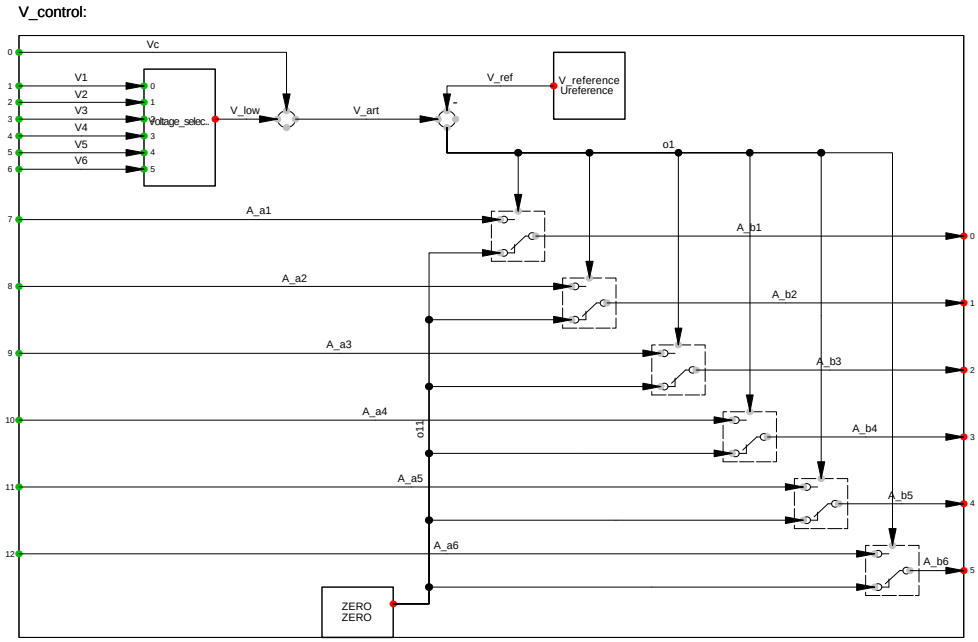

The "Control Grid Top" (Composite model) connects the sub-systems to the flexibility control and equalization control.

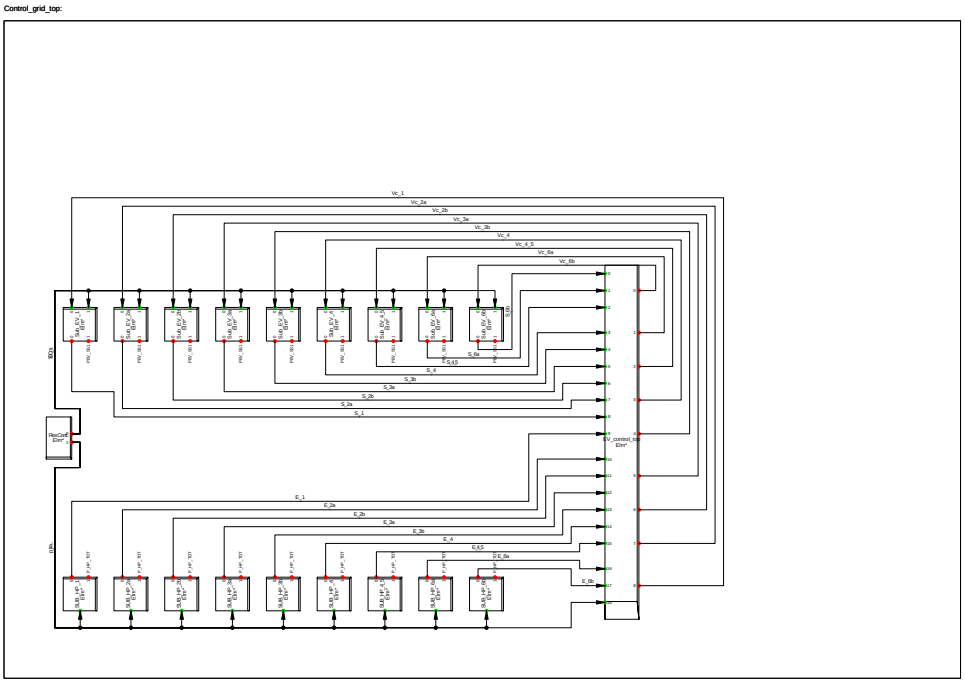

The "GC Flex Top" (Composite model) reads the TSO/aggregator power request from an ElmFile and computes the power deficiency which is sent to the sub-systems. It also controls SoCmax.

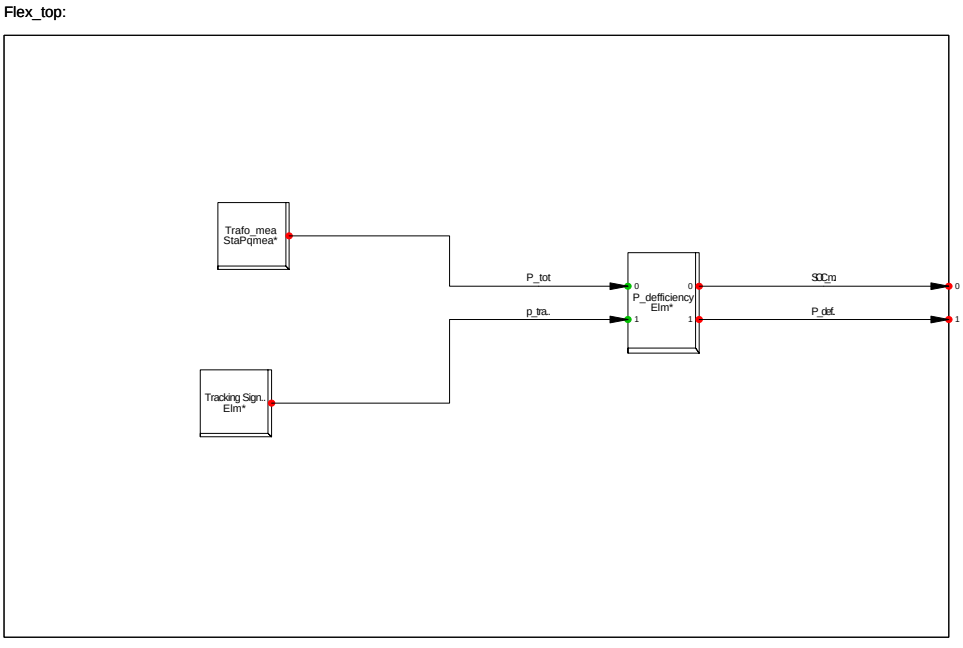

The "EV control top" computes the power limitation factor specific for each individual sub-system for the equalization control and the overall power limitation factor for the flexibility control.

EV_control_top_L2:

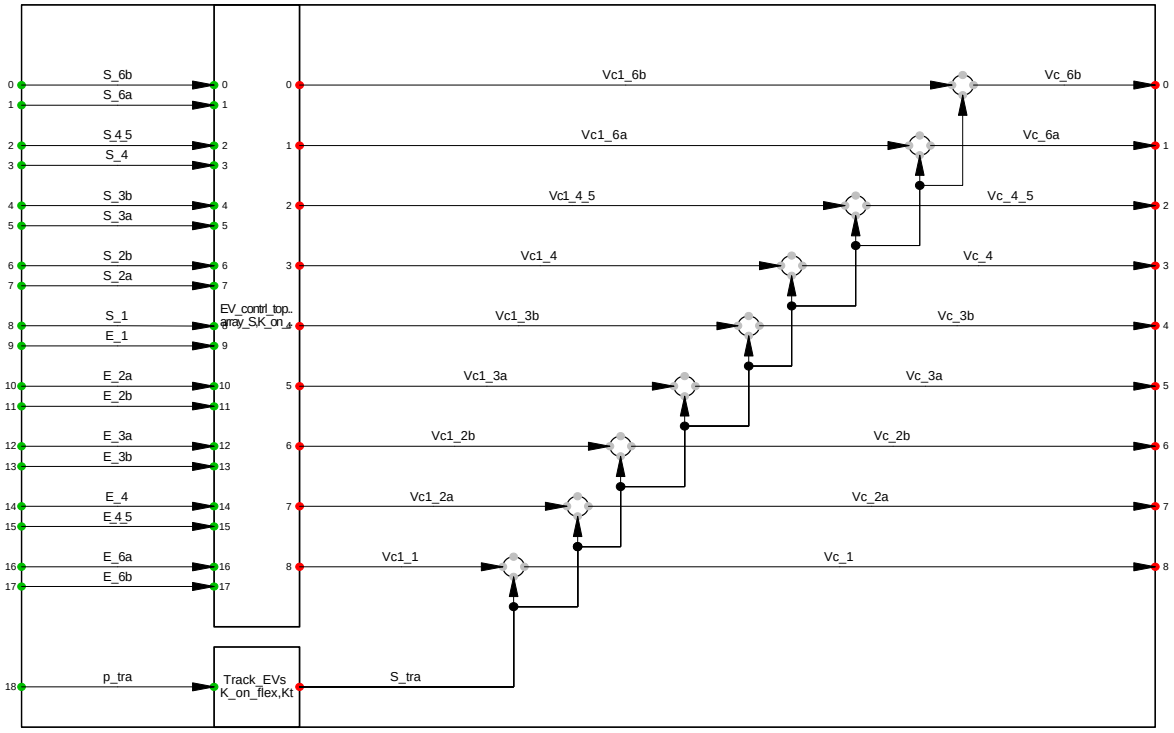

The figure below shows an overview from DIgSILENT which shows a tiny section of the composite and DSL-models from LV-II.

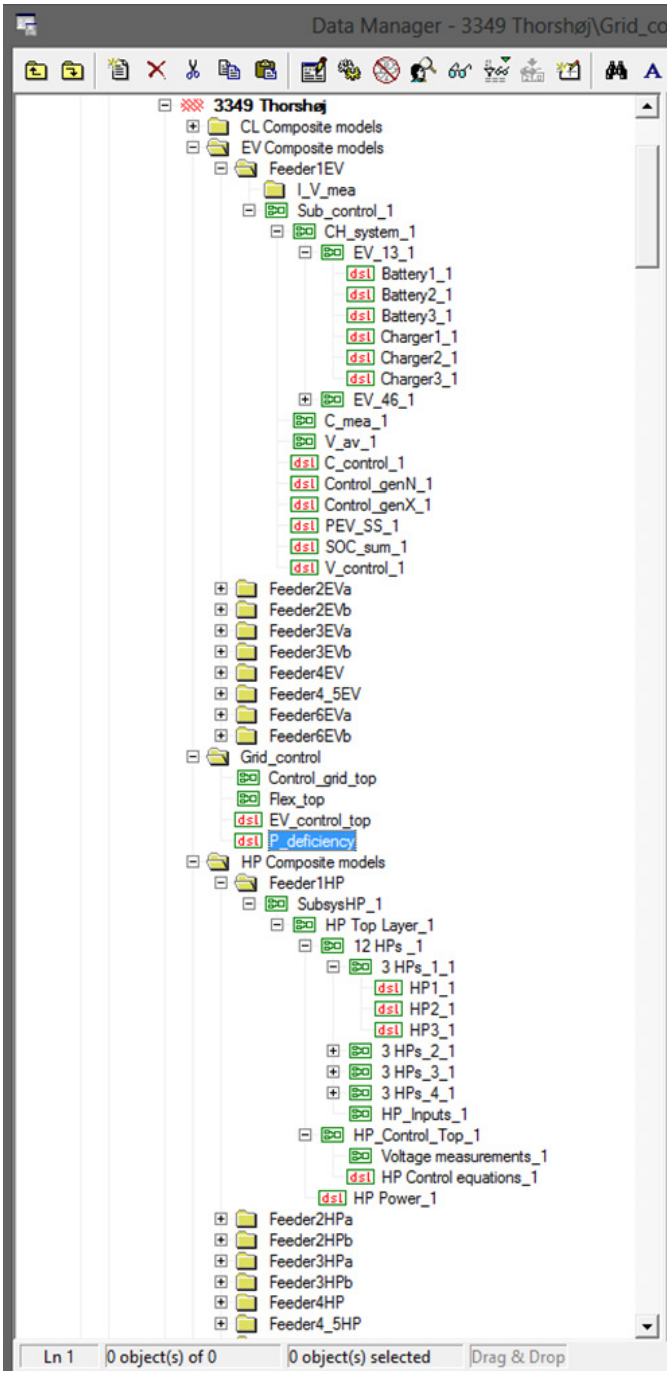

A.4 Sub-systems

Below the placements of the sub-systems of LV-I and LV-II are found.

A.5 Units per sub-system

Sub-system	Households	HPs	EVs
1	15	8	4
2/3	18	10	4
4	20	10	5
5/6	18	9	5
7/8	13	7	3
All	**84**	**44**	**21**

Table A.1: Sub-systems of LV-I

Sub-system	Households	HPs	EVs
1	20	10	5
2A	17	10	3
2B	16	9	4
3A	17	8	5
3B	12	5	6
4	24	12	5
4/5	21	11	6
6A	21	9	6
6B	18	9	5
All	**166**	**83**	**45**

Table A.2: Sub-systems of LV-II

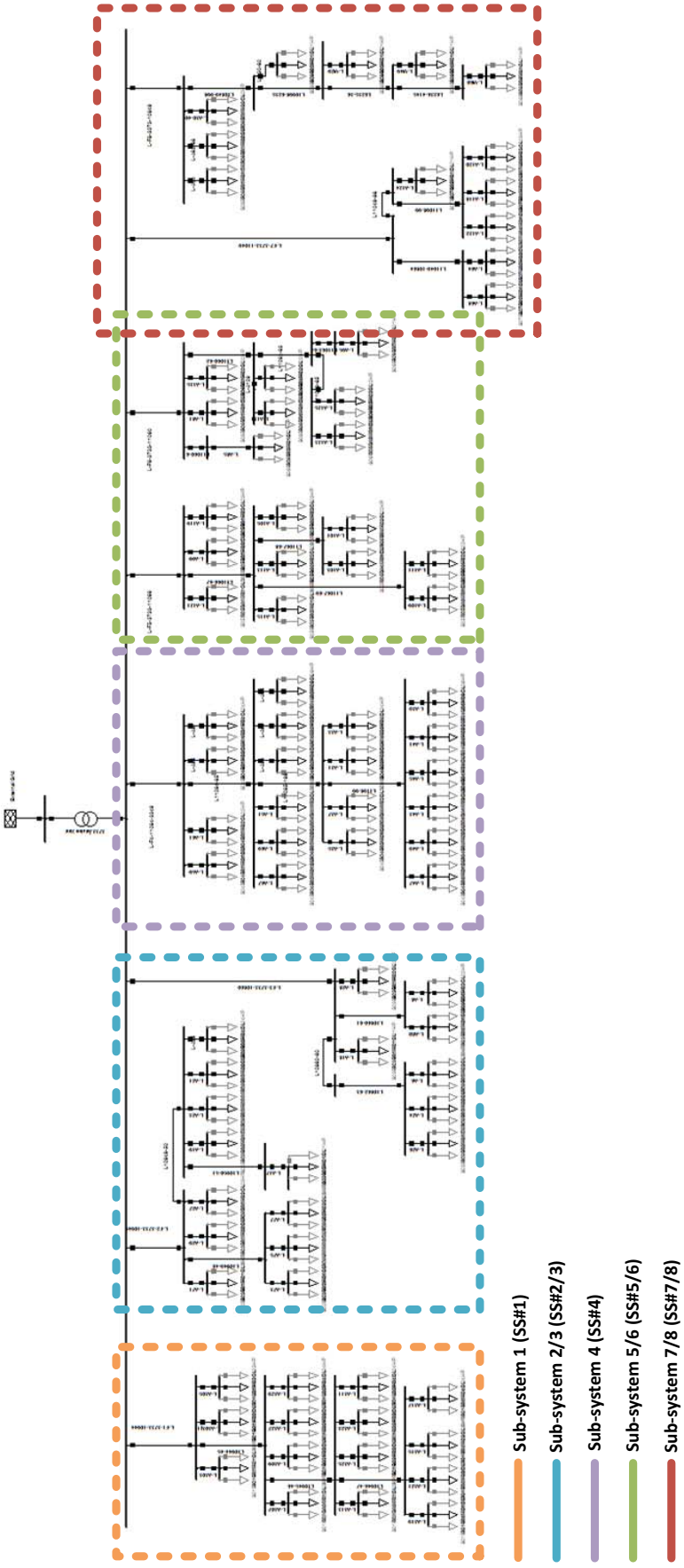

Figure A.6: Sub-system placement LV-I

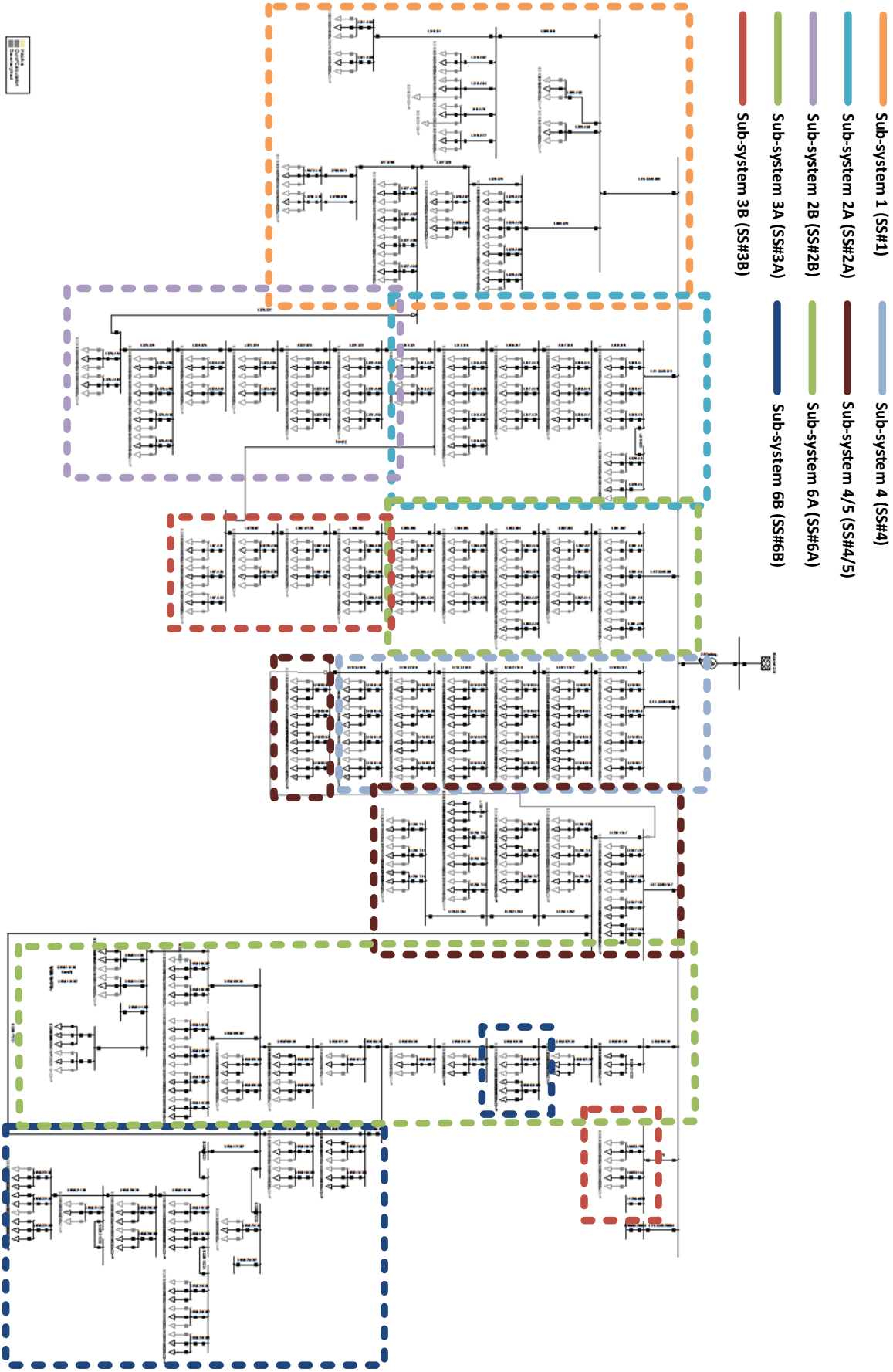

Figure A.7: Sub-system placement LV-II

B Nomenclature

CHP	Combined heat and power
CL	Common load
COP	Coefficient of function
DSL	DIgSILENT Simulation Language
DSO	Distribution system operator
EV	Electric vehicle
HP	Heat pump
LDF	Load factor
LV	Low voltage
LV-I	Low voltage grid number 1
LV-II	Low voltage grid number 2
RMS	A DIgSILENT Simulation Tool
SoC	State of charge
SoE	State of energy
TSO	Transmission system operator
V2G	Vehicle to grid

C Bibliography

[1] Energy Ministry of Climate and Building. Energistrategi 2050 - fra kul, olie og gas til groen energi, February 2011.

[2] Energy Ministry of Climate and Building. Accelerating green energy towards 2020, March 2012.

[3] Trine Madsen Engel. Optimal udnyttelse af el-distributionsnettet - metoder til anvendelse af restkapacitet til fleksibelt forbrug. Master's thesis, Risoe DTU, 2011.

[4] Energinet.dk. Effektiv anvendelse af vindkraftbaseret el i danmark - samspil mellem vindkraft, varmepumper og elbiler, March 2009.

[5] Energinet.dk and Danish Energy Association. Smart grid in denmark 2.0, October 2012.

[6] Energinet.dk. Webpage, February 2013. URL `http://energinet.dk/EN/OM-OS/Om-virksomheden/Sider/default.aspx`.

[7] Energinet.dk. Systemplan 2012, November 2012.

[8] Energinet.dk. Smart grid i danmark - bilagsrapport, .

[9] Henryk Markiewicz and Antoni Klajn. Power quality application guide - voltage disturbances standard en 50160 voltage characteristics in public distribution systems. Wroclaw University of Technology, July 2004.

[10] The Danish Energy Agency. Webpage, March 2013. URL `http://www.ens.dk/da-DK/Info/TalOgKort/Statistik_og_noegletal/Oversigt_over_energisektoren/Stamdataregister_vindmoeller/Documents/Oversigtstabeller_UK-DK.xls`.

[11] Energinet.dk. Smart grid i danmark, .

[12] Nord Pool Spot. Nord pool spot europes leading power markets, Jan 2013.

[13] Energinet.dk. Energinet.dk's strategi for systemydelser, May 2011.

[14] P. Palensky. Demand side management: Demand response, intelligent energy systems, and smart loads. *IEEE Trans. on Industrial Informatics*, Vol. 7, No. 3, 2011.

[15] Danfoss. Webpage. URL `http://www.consumers.heatpumps.danfoss.co.uk/Content/6331D020-EDA6-4468-8E2A-168FFED6B9EC_MNU17538742_SIT776.html`.

[16] M. Akmal. Impact of high penetration of heat pumps on low voltage distribution networks. *Paper accepted for presentation at the 2011 IEEE Trondheim PowerTech*, 2011.

[17] J. Curtiss Fox. A voltage flicker suppression device for residential air conditioners and heat pumps. *14th International Conference on Harmonics and Quality of Power (ICHQP)*, 2010.

[18] Georgios Papaefthymiou. Potential of heat pumps for demand side management and wind power integration in the german electricity market. *IEEE Transactions On Sustainable Energy, Vol. 3, No. 4*, October 2012.

[19] Luther Dow. A novel approach for evaluating the impact of electric vehicles on the power distribution system. *Power and Energy Society General Meeting, 2010 IEEE*, 2010.

[20] Jayakrishnan R. Pillai. Integration of electric vehicles in low voltage danish distribution grids. *Power and Energy Society General Meeting, 2012 IEEE*, July 2012.

[21] Sekyung Han. Development of an optimal vehicle-to-grid aggregator for frequency regulation. *IEEE Transactions On Smart Grid, Vol. 1, No. 1*, June 2010.

[22] Z. Chengke. Modeling of the cost of ev battery wear due to v2g application in power systems. *IEEE Transactions On Energy Conversion, Vol. 26, No. 4*, 26:10, December 2011.

[23] International Energy Agency (IEA). Prospects for large-scale energy storage in decarbonised power grids. 2009.

[24] Andres H. Foosnes. Report: Wp2.7 grid codes and regulation related to evs. *project EDISON*, 2011.

[25] Olivier Sidler. Dsm: major findings of an end-use metering campaign in 400 households of four european countries. *ECEEE*, 2003.

[26] Anders Risum Korsgaard. *Design and Control of Household CHP Fuel Cell System*. PhD thesis, Aalborg University, 2006.

[27] D. L. Nickel and H. R. Braunstein. Distribution transformer loss evaluation: Ii - load characteristics and system cost parameters. *IEEE Transactions on Power Apparatus and Systems*, PAS-100, No. 2:14, February 1981.

[28] Peter Vinter. Using continuous state estimation in grid planning. *CIRED 20th International Conference on Electricity Distribution*, 2009.

[29] SINTEF Energy Research. Energy efficiency and load curve impacts of commercial development in competitive market. *EFFLCOM project*, 2003.

[30] Anders R. Korsgaard. Design and control of household chp fuel cell system. Master's thesis, AAU, IET, 2007.

[31] Qiuwei Wu. Driving pattern analysis for electric vehicle (ev) grid integration study. *Innovative Smart Grid Technologies Conference Europe (ISGT Europe)*, pages 1–6, 2010.

[32] J. Waddell. Impact of plug in electric vehicles on manitoba hydro's distribution system. *Proc. IEEE Electrical Power and Energy Conference*, Oct 2011.

[33] Dansk Elbilkomite, April 2012. URL `http://www.danskelbilkomite.dk/Elbil_salg.htm`.

[34] A. M. Ihbal. Identifying the nature of domestic load profile from a single household electricity consumption measurements. 2011.

[35] I. Richardson. Domestic electricity use: A high-resolution energy demand model. 2010.

[36] Dan Schillinger. Variable speed technology improves power factor, boost grid reliability [commercial report, danfoss]. 2011.

[37] Taisuke Masuta. Modeling of a number of heat pump water heaters as control equipment for load frequency control in power systems. *PowerTech, 2011 IEEE Trondheim*, 2011.

[38] NIBE. Installatoerhaandbog - nibe f2026 - luft-/vandvarmepumpe.

[39] Voelund Varmeteknik. Varmtvandsbeholder - vvm 300, .

[40] Voelund Varmeteknik. Varmtvandsbeholder - vvm 500, .

[41] Yang Chen. Effsys2 - project report, co2 heat pumps for the swedish market - test and analysis of the sanyo eco-cute heat pump modified for swedish conditions. Year N/A.

[42] Long Lam. A practical circuit-based model for li-ion battery cells in ellectric vehicle applications. *Telecommunications Energy Conference (INTELEC)*, 33:1–9, 2011.

[43] Walter van Schalkwijk. *Advances in lithium-Ion batteries*. Palo Alto, Calif. Library, 2002.

[44] Min Chen. Accurate electrical battery model capable of predicting runtime and i-v performance. *IEEE TRANSACTIONS ON ENERGY CONVERSION,*, 21:1–8, 2006.

[45] J. Heinzmann. Charged 2020. Presentation, July 2010.

[46] Davide Andrea. *Battery management systems for large Lithium-ion battery packs*. Artech House, 2010.

[47] Murat Y. Review of battery charger topologies, charging power levels and infrastructure for plug-in electric and hybrid vehicles. *Power Electronics*, 28:2151 – 2169, May 2013.

[48] Soeiro T. Three-phase high power factor mains interface concepts for electric vehicle battery charging systems. *Applied Power Electronics Conference and Exposition*, 27, 2012.